ABSTRACT

Structure-Activity Relationships and Thermodynamics of Combretastatin A-4 and A-1 Derivatives as Potential Inhibitors of Tubulin Polymerization

Benon E. Mugabe, M.Sc.

Mentor: Mary L. Trawick, Ph.D.

Inhibition of tubulin polymerization has been identified as a significant characteristic of potential anticancer agents. Tubulin is a heterodimeric protein of α and β polypepetide chains, each with a molecular weight of 50kDa and is the biochemical target for several clinically used anticancer drugs. Tubulin was purified from calf brain by a method that uses a series of selective polymerizations induced by a temperature jump in the presence of GTP followed by cold depolymerization. Protein purity was determined by SDS-PAGE and the ability of tubulin to polymerize into microtubules. As part of a program to identify vascular disrupting agents (VDAs), we have determined the effect of more than 78 combretastatin A-4 and A-1 analogs on tubulin polymerization. Combretastatin analogs with substitutions in both the trimethoxyphenyl and phenolic rings were analyzed. These included bromo, chloro, fluoro, mono and di-nitro, di-amino and di-amino hydrochloride, serinamides, serinamide hydrochloride salts of CA-4 and CA-1 derivatives many of which showed good antitubulin activities (IC_{50} = 1.1 – 3.0μM) which were comparable to those of CA-1 and CA-4. Generally, water soluble

combretastatin phosphate salts analyzed did not show significant inhibitory activity on tubulin polymerization.

Our research also explored the application of isothermal titration calorimetry in determining the thermodynamic parameters of binding of CA-1, CA-4 and some of their derivatives. Microcalorimetric studies of the interactions between tubulin and combretastatin analogs were designed to directly determine the enthalpy, binding affinity and the number of binding sites involved upon interaction. We have defined the various thermodynamic signatures that characterize interaction of these compounds with tubulin. All tubulin-combretastatin analog interactions were exothermic and showed favorable free energies and binding affinity constants ($0.1 - 9.8 \times 10^5$ M^{-1}). The binding affinity constants, stoichiometry, and the thermodynamic signatures suggested hydrogen bonding and hydrophobic contacts for the stronger binding interactions between CA-1 and its analogs which were both enthalpy and entropy driven whereas 2,3 di-amino CA-1 and others showed low binding constants, with evidence of conformational changes upon binding.

Structure-Activity Relationships and Thermodynamics of Combretastatin A-4 and A-1 Derivatives as Potential Inhibitors of Tubulin Polymerization

by

Benon E. Mugabe, M.Sc.

A Dissertation

Approved by the Department of Chemistry and Biochemistry

Marianna A. Busch, Ph.D., Chairperson

Submitted to the Graduate Faculty of
Baylor University in Partial Fulfillment of the
Requirements for the Degree
of
Doctor of Philosophy

Approved by the Dissertation Committee

Mary L. Trawick, Ph.D., Chairperson

Kevin G. Pinney, Ph.D.

Robert R. Kane, Ph.D.

Carlos E. Manzanares, Ph.D.

Bryan W. Brooks, Ph.D.

Accepted by the Graduate School
December 2005

J. Larry Lyon, Ph.D., Dean

TABLE OF CONTENTS

LIST OF FIGURES

LIST OF TABLES

LIST OF ABBREVIATIONS

α	Alpha
Ala, A	Alanine
ANS	Anilinonaphthalene 8-sulfonate
Arg, R	Arginine
Asn, N	Asparagine
Asp, D	Aspartic acid
ATP	Adenosine triphosphate
β	Beta
BisANS	4,4'-Bis (1-anilinonaphthalene 8-sulfonate)
°C	Degree Celsius
CA-1	Combretastatin A-1
CA-1P	Combretastatin A-1 diphosphate
CA-4	Combretastatin A-4
CA-4P	Combretastatin A-4 phosphate
CA-4G	Combretastatin A-4 glucuronide
Cal	Calorie(s)
CSC	Calorimetric science cooperation
2-CTC	2-Chloroacetyl-3-demethylthiocolchicine
3-CTC	3-Chloroacetyl-3-demethylthiocolchicine
Col	Colchicine

Cys, C	Cysteine
DAMA-colchicine	*N*-deacetyl-*N*-(2-mercaptoacetyl)-colchicine
DMSO	Dimethylsulfoxide
DMXAA	5,6-dimethylxanthenone-4-acetic acid
DTT	Dithiothreitol
EDTA	Ethylenediamine tetra acetic acid disodium salt
EGTA	Ethylene glycol-bis(β-aminoethyl ether)-*N,N,N',N'*- tetra acetic acid
FAA	Flavone acetic acid
ΔG	Change in Gibb's free energy
GAPs	GTPase activating proteins
GDIs	Guanosine diphosphate exchange inhibitors
GDP	Guanosine diphosphate
GMPCPP	Guanylyl-(α,β)-methylene-diphosphonate
GEFs	Guanosine diphosphate exchange factor
Gln, Q	Glutamine
Glu, E	Glutamic acid
Gly, G	Glycine
gm	Gram(s)
GPCR	G-protein coupled receptor
GTP	Guanosine triphosphate
h	Hour(s)
H	Hydrogen
His, H	Histidine

HPLC	High performance liquid chromatography
ΔH	Change in enthalpy
IC_{50}	Concentration of the analog that inhibits tubulin polymerization in the reaction mixture by 50%
Ile, I	Isoleucine
ITC	Isothermal titration calorimetry
J	Joules
K	Kelvin
K_a	Association constant
K_b	Binding affinity
$K_{b,obs}$	Observed binding affinity
kDa	Kilodaltons
kcal	Kilocalorie(s)
KJ	Kilojoule(s)
LDS	Lithium salt of dodecyl sulfate
Leu, L	Leucine
Lys, K	Lysine
µ	Micro
µM	Micromolar
µW	Microwatts
µJ	Microjoules
m	Milli
M	Moles per liter
MAPs	Microtubule associated protein(s)

MCAK	Mitotic centromere – associated kinesis
MDC	2-Methoxy-5-(2,4-dimethoxyphenyl)-2,4,6-cycloheptatrien-1-one
MDR	Multidrug resistance
MES	2-(*N*-Morpholino)ethanesulfonic acid
Met, M	Methionine
$MgCl_2.6H_20$	Magnesium chloride (hydrated)
MLC	Myosin light chain
MLC-P	Phosphorylated myosin light chain
mmol	Millimole(s)
MTC	2-Methoxy-5-(2,3,4-trimethoxyphenyl)-2,4,6-cycloheptatrien-1-one
MTOCs	Microtubule organizing centers
N	Molar binding stoichiometry
OX16C	CA-1 diphosphate dipotassium
OXi-4503	CA-1 diphosphate
PAGE	Polyacrylamide gel electrophoresis
PEM	PIPES-EGTA-$MgCl_2$ buffer
Phe, F	Phenylalanine
pH	-Log (hydrogen ion concentration)
PIPES	Piperazine-*N,N'*-bis(2-ethanesulfonic acid)
Pro, P	Proline
Q_i	Cumulative heat
QSAR	Quantitative structure-activity relationships
R	Gas constant

RH	Relative humidity
rpm	Revolutions per minute
RTK	Receptor tyrosine kinase
ΔS	Change in entropy
SAPK2	Stress-activated protein kinase 2
SBDD	Structure-based drug design
SDS	Sodium dodecyl sulfate (lauryl sulfate)
SLD	Stathmin-like domain
SE	Standard error
sec	Seconds
T	Temperature
TBAs	Tubulin binding agent(s)
Thr, T	Threonine
TKB	2,3,4-Trimethoxy-4'-acetyl-1,1-biphenyl
TMB	2,3,4,4'-Tetramethoxy-1,1'-biphenyl
TNF-α	Tumor necrosis factor-alpha
Trp, W	Tryptophan
Tyr, Y	Tyrosine
UV	Ultraviolet
Val, V	Valine
VDA	Vascular disrupting agent(s)
VEGF	Vascular endothelial growth factor
VTAs	Vascular targeting agent(s)

ACKNOWLEDGMENTS

Blessed be the Lord who is good and always causes us to triumph. I wish to thank Dr. Mary Lynn Trawick for giving me the opportunity, accepting and allowing me to carry out my research work in her laboratory. Thank you Dr. Trawick for introducing me to the protein tubulin and the art of perseverance when I had to purify it. You were there when I needed your help and what a wonderful journey it has been. Thank you for your constant professional advice and encouragement.

To Dr. Carlos E. Manzanares, Director of Graduate Studies, thank you for accepting my application and opening the door for me to study at Baylor University. Thank you for giving me a teaching assistantship through which I have been fully supported and for the Dole Fellowship that has greatly enabled me to finish the preparation of my dissertation in time.

I wish to thank my dissertation committee members, Dr. Kevin Pinney, Dr. Robert Kane, Dr. Carlos Manzanares and Dr. Bryan Brooks for reviewing my dissertation. I thank Drs. Charles Garner, Kevin Pinney and Robert Kane for your leadership in synthesizing the combretastatin analogs and for giving me the opportunity to analyze them. Thanks to every student who was involved in synthesizing them, and for patiently waiting for the results.

I want to thank Nancy Kallus, Barbara Rauls, Adonna Cook, Virginia Hynek and Andrea Johnson for all the special assistance you accorded me when I was in need. Nancy, thank you for giving me a familiarization tour of Waco and making settling down

easier. Barbara, thank you for the fax you helped me send that was timely. It helped unlock another chapter in my life.

To members of Dr. Trawick's research group, a big thank you. I wish to thank Scott Studerus for the initial work you did in tubulin research and for training me to take over from where you stopped. Tom Guu, thank you for being so dear to me and for introducing me to Joy FM. Sam, Milenka, Maryuri, Frank, thanks for making biochemistry research fun.

I wish to thank Baylor University and the Department of Chemistry and Biochemistry, all my Professors and staff, for assimilating me into the graduate program and into Baylor's great community. For all the support you have given me, I will forever be grateful. I also wish to thank Oxigene Inc and Baylor University Research Committee for supporting my research. Thanks to H&B Packing of Waco for providing the calf brains.

I wish to thank members of the Christian Life Fellowship for your prayers and for keeping the faith. My Pastor Robert Nelson and Sister Cindy, the moment I visited your church, I knew that surely God was in that place and yet I had not been aware of it. To my friends Ronnie and Allison Stephens, there is no greater love than this; that a man should stand surety for a stranger. Thank you for sponsoring my family for a greater destiny. To all members of the International Believers' Christian Fellowship of Waco, I say thank you. I would never forget to thank Dr. Okani and Sister Eunice. You were so good to me and for that may God bless you big. Geoffrey, Sarah, and Obat, thank you for being great friends. Elder Nkoyo, thank you for your music which still echoes in my ears.

I wish to thank my dear wife Sheila A. Mugabe for being my support. Surely a wife of noble character, who can find? You are worth more than rubies to me. Your great works for our household will always bring you praise. I wish to thank my sons Aaron and Elijah who have always inspired and caused me to smile. My mother Hope Rwendeire, thank you for loving me, for praying for me and for all your steadfastness. John, Joviah, Beatrice, Esther, Magret, Reuben and Franco, thank you for being part of my family. To my daddy Bernard Rwendire (the late), thank you for showing me the way to be a man.

Not unto me but to El-Shaddai, the Lord God Almighty, be all the glory, honor and praise. You have been my joy, my hope, my confidence and my firm foundation. You made a way for me where there seemed to be no way. You made a way in the desert and streams to flow in a wasteland. You have been my sun and shield and my exceeding great reward. You told me that you would never leave me nor forsake me. You have always been a pillar of cloud to guide me during the day and a pillar of fire to give me light during the night. Thank you Jesus Christ, for I knew I could depend on you. You have done for me exceedingly, abundantly, above and beyond my highest prayers. Blessed is the man who trusts in you.

DEDICATION

Unto El-Shaddai, the Lord God Almighty,

Who has been my Shepherd all my life to this day;

Whose angel has always delivered me from all harm;

And on whose mighty right hand I have always leaned.

CHAPTER ONE

Structure-Activity Relationships and Thermodynamics of Combretastatin A-4 and A-1 Derivatives as Potential Inhibitors of Tubulin Polymerization

Introduction

According to the American Cancer Society, in the United States during the year 2005, an estimated 1,372,920 new cases of cancer will be diagnosed and an estimated 570, 280 people will die of cancer which is 25% of the cause of all deaths (www.cancer.org). Traditional methods of fighting cancer such as chemotherapy or radiation therapy are usually targeted at the various affected cancer cells with varying degrees of success. Vascular disrupting strategies however seek to affect the tumor vasculature, thereby removing critical nutritional support. In 2003, the United States government through the FDA granted fast track designation for combretastatin A-4 disodium phosphate (CA-4P), one of the first vascular disrupting agents to advance to phase II trials, in the treatment of anaplastic thyroid cancer (ATC).

Dr. Trawick's Research Laboratory and Collaborators at the Center for Drug Discovery, Department of Chemistry and Biochemistry, Baylor University, Waco, Texas, have been involved in investigating the role of vascular targeting as a possible approach for cancer therapy. This strategy has been accomplished through the design and synthesis of combretastatin analogs, compounds that are known to induce damage to the tumor vasculature. Tubulin is the major component of microtubules which are crucial in the maintenance of the form and shape of endothelial cells that line tumor vasculature. The main purpose of this research was to explore the structure-activity relationships of the

interactions of combretastatin analogs with tubulin by determining the extent of tubulin polymerization as a first step in elucidating the potency of these analogs as vascular disrupting agents. The other objective was to explore the use of isothermal titration calorimetry in determining the thermodynamics of the interactions of these combretastatin analogs with tubulin. We have evaluated more than 78 new Combretastatin A-1 and A-4 analogs as potential inhibitors of tubulin polymerization and more than 50% of the newly synthesized combretastatin analogs have shown high potency as antitubulin inhibitors. This biological evaluation has included nitrogen substituted combretastatin analogs containing nitro, amine, hydrochloride salt, and serinamide salt functionality as well as mono and dichloro substituted analogs in both the trimethoxyphenyl and the phenolic rings of combretastatin A-1 and A-4. Preclinical development trials on the soluble combretastatin A-4 and A-1 phosphate prodrugs are so far encouraging. The target audience for this research is the scientific world which includes the national and international health care professionals, the research oncologists, physicians who are involved in cancer research and treatment, as well as the cancer patients.

Tubulin protein is a major target of anticancer molecules, and therefore inhibitors of polymerization of tubulin into microtubules have attracted great attention as antitumor agents for cancer chemotherapy. Numerous laboratories have been involved in the synthesis and biological evaluation of compounds that either inhibit or stabilize formation of microtubules. Most of these compounds have been structurally designed to mimic and bind at the tubulin binding sites of several naturally occurring compounds such as taxol®, vinblastine, colchicine, and combretastatin A-4 and A-1.

Chapter Two of this dissertation presents work on purification of tubulin from calf brains, a protocol that is based on the procedure first reported by Hamel and Lin's laboratory. The three day procedure involved a series of tubulin polymerization and depolymerization steps, conditions that were easily achieved during ultracentrifugation. The purified tubulin was subjected to sodium dodecyl sulfate - polyacrylamide gel electrophoresis in order to ascertain its purity. Pure tubulin was used throughout the course of this study. Chapter two also reports in detail the bioanalytical evaluation of structure-activity relationships of combretastatin A-1 and A-4 analogs with various modifications in the A and B-rings as inhibitors of tubulin polymerization. The new analogs included bromo, chloro and fluoro CA-4 and CA-1 derivatives as well as mono and di-chloro substituted CA-4 and CA-1 derivatives. A tri-fluorinated CA-1 was also evaluated. The effects of mono and di-nitro, di-amino and di-amino hydrochloride CA-4 and CA-1 salts on tubulin polymerization are discussed. The effects of serinamide combretastatin analogs on tubulin polymerization are presented. The antitubulin effects of CA-4 and CA-1 serinamide hydrochloride salts were also analyzed and the findings are presented. The antitubulin effect of replacement of the methoxy group on position 4 with a methyl group on the phenolic ring was evaluated and is hereby reported. The prodrug CA-4P is already undergoing phase two clinical trials. We report on a bioanalytical method developed to evaluate the effect of its equally effective counterpart prodrug CA-1P on tubulin polymerization and to study its stability under different temperature and relative humidity conditions. Results on the effect of a CA-4P metabolic product on tubulin polymerization are also reported. A number of combretastatin A-1

and A-4 analogs containing salient functional modifications on both the A and B rings were confirmed as excellent inhibitors of tubulin polymerization.

Chapter Three of this dissertation reports on the investigation of the thermodynamics of the interactions of some of these CA-1 and CA-4 analogs with tubulin. Although structure–based drug design through molecular modeling can be used to predict quantitative structure-activity relationships as discussed in chapter two, this approach lacks the thermodynamic data that are required to verify the models involved. In addition, during drug development, very fast and important decisions have to be made especially in cases where the lead compounds are exhibiting similar structure activity relationships. Knowledge of the thermodynamic characteristics of these compounds helps the researcher in determining and pursuing analogs that exhibit favorable enthalpic, entropic characteristics as well as high binding affinities. This type of data is currently lacking for a majority of compounds that have been highlighted as potential tubulin polymerization inhibitors and ultimately anticancer agents. For the first time, we report on the use of isothermal titration calorimetry in elucidating the thermodynamic properties of some selected combretastatin analogs as inhibitors of tubulin polymerization. We report the various thermodynamic signatures observed during the interaction of CA-1, CA-4, colchicine, and several combretastatin analogs. Their binding affinities and the enthalpic and entropic contributions to the interactions between the tubulin and the analogs are discussed. Binding reactions that involve good hydrogen bonding, hydrophobic interactions or a combination of the two, as well as conformational changes and the number of binding sites on the tubulin heterodimer involved in the interactions are discussed.

CHAPTER TWO

Structure-Activity Relationships of Combretastatin A-4 and A-1 Derivatives as Potential Inhibitors of Tubulin Polymerization

Introduction

Tubulin is the building block of microtubules which are a main component of the mammalian cytoskeleton. They have many important activities especially cell motility, transportation of cellular materials, shape and polarity of the cell and are involved in mitosis. Microtubules are polymers of tubulin and they basically consist of structures that are built from αβ-tubulin heterodimers. Microtubules have a diameter of approximately 24 nm and their lengths vary from micrometers to millimeters. They are core cylinders, made up of 13 protofilaments of αβ-tubulin subunits arranged into a cylindrical structure. Dynamic instability of microtubules is controlled by interaction with other proteins. For example, during the prophase of mitosis, microtubules grow out from the centrosome (Zheng, 2004, Desai *&* Mitchison, 1997). During this process, when a microtubule binds to a chromosome, it becomes stabilized.

Also microtubule associated proteins (MAPs) bind to microtubules, a process that is also regulated by both phosphorylation and dephosphorylation processes. This is usually achieved through growth factor signal pathways that activate protein kinases that catalyze phosphorylation of tubulin-binding domains of MAPs. Thus phosphorylation can lead to the detachment of MAPs from microtubules. Microtubules are nucleated and organized by the microtubule organizing centers and these include the centrosomes and basal bodies. Microtubules are capable of growing and shrinking by the addition or

removal of tubulin from the plus end. Microtubules tend to interact with other proteins in the cell and these proteins are known to regulate microtubule activities. Proteins that interact with tubulin in the microtubule have been subdivided into several major categories depending on their functions and activities. These include microtubule associated proteins, microtubule motors proteins and other heterogeneous proteins (Mandelkow *et al*., 1995). Microtubule associated proteins are structural proteins that bind, stabilize and promote the formation of microtubules. Some MAPS have been characterized, especially those isolated through a series of polymerization and depolymerization steps. They include MAP1, MAP2, MAP4 and the tau proteins. Type I MAPs which are found in axons and dendrites of nerve cells and in some non-neural cells, have several repeats of the sequence KKEX (Lys-Lys-Glu-X) that binds to negatively charged tubulin domains. Type II MAPs (MAP4 & Tau) are also found in axons, dendrites and normal cells. They have 3-4 repeats of an 18-residue sequence that binds tubulin (Mandelkow *et al*., 1995).

A lot of studies have been accomplished about the major constituents of microtubules, microtubules, microfilament and intermediate filaments. Microtubule motors proteins are known to interact transiently with microtubules and are generally associated with their interaction with the microtubule–organizing sites such as the centrosomes or kinetochores (Olmsted, 1986). These proteins are known to cause movement along the microtubules through chemical energy from ATP hydrolysis. There are other proteins that are found associated with microtubules and they include the glycolytic enzymes, kinase enzymes (e.g. protein kinase A), biosynthetic enzymes, end

binding proteins, proteins that mediate microtubule-actin interactions, proteins that link to membrane receptors (e.g. G-proteins) and ribonucleoproteins (Mandelkow *et al*., 1995).

Vascular targeting is increasingly being recognized as an effective new method of fighting against cancer and ocular diseases. Combretastatin A-4 (CA-4P) prodrug developed by Oxigene Inc., has already demonstrated promising results in Phase I clinical trials and has now progressed into later stages of Phase I and Phase II trials. Combretastatin A-1 phosphate (CA-1P), also referred to as OXI-4503, which is more potent than CA-4P, is also undergoing rapid development as a possible vascular targeting agent (Hill *et al*., 2002; Tozer *et al.,* 2005). Tumor vasculature is an attractive target for cancer therapy because the provision of oxygen and nutrients by a single vessel supports the survival of many tumor cells. There are two distinct therapeutic strategies that interfere with the tumor endothelium. Antiangiogenesis interferes with formation of new blood vessels whereas vascular targeting destroys already formed neovasculature of actively growing tumors. Although there are differences between the two strategies, including their administration schedules, individual agents can possess both antiangiogenic and antivascular characteristics (Kanthou *et al*., 2004).

The combretastatins are structurally related to the ancient tubulin-binding agent colchicine, and are themselves tubulin binding, microtubule depolymerizing agents. Colchicine was recognized as having vascular damaging effects as early as the 1930s (Boyland and Boyland, 1937; Seed *et al*., 1940). However, because of its high toxicity, it has been excluded from clinical development. Numerous combretastatin analogs have been synthesized by various laboratories and several compounds have shown tremendous inhibitory effects on the polymerization of tubulin into microtubules (Aleksandrzak *et al*.,

1998, Ohsumi *et al.,* 1998, Pettit *et al*., 1998). The Aventis compound AVE8062, formerly the Ajinomoto Co. Inc compound; AC7700 is one of those vascular distrupting agents that have shown necrosis effects on tumor cells (Nihei *et al.,* 1999, Hori *et al*., 2001). Also, compounds 5,6-dimethylxanthenone-4-acetic acid (DMXAA) and flavone acetic acid (FAA) are two of a series of drugs that have several antivascular actions, including the induction of cytokines. Although CA-4P, CA-1P and similar compounds have been categorized as vascular-disrupting agents (VDAs), their effects as tubulin-binding drugs are not always specific for endothelial cells. Depolymerization of tubulin inhibits spindle formation in dividing cells and proliferation although some tumor cell types are more sensitive to the CA-4P than endothelial cells (Tozer *et al*., 2005). By interfering with the normal microtubule polymerization / depolymerization process, vascular targeting agents also cause mitotic arrest of eukaryotic cells especially in tumor cells (Wang *et al*., 2002).

Compounds that interact with tubulin are heterogeneous in nature and structure (Bacher *et al*., 2001). Because of diversity in the synthetic nature, potent *in vitro* and *in vivo* antitumoral activity and efficacy against multidrug-resistance (MDR) tumors, antitubulin agents have significant potential in cancer therapy. Characterization of structure activity relationships of synthetic anticancer agents is very important as it sets the stage for further clinical development of specific prodrugs in tumor cell and cell-free systems.

Background

Tubulin Structure

Tubulin is the main structural subunit of microtubules (Nogales *et al.*, 1998, 2000; Hyams and Llyod, 1994). It is a heterodimeric protein of two 50kDa polypeptides designated α and β (Little and Seehans, 1998) and is the biochemical target for several clinically used in anticancer drugs (Jordan *et al.*, 1998; Luduena and Roach, 1991). The core of each tubulin protein contains two β-sheets of 6 and 4 strands, flanked by 12 α-helices (Nogales *et al.,* 1998, 2000)(Figure 2.1). Each monomer is very compact, but can be divided into three functional domains namely; the amino-terminal domain containing the nucleotide-binding region, an intermediate domain containing the Taxol-binding site, and the carboxyl-terminal domain, which probably constitutes the binding surface for motor proteins.

The N-terminal domain which consists of amino acid residues 1 – 206 is formed by alternate β-strands (S1-S6) and helices (H1-H6). The nucleotide binding domain is formed by each of the loops that connect each strand and helix (T1-T6) and the amino terminal end of the core helix (H7) (Nogales *et al.*, 1998). Another domain is formed by three helices (H8-H10) and several sheets (S7-S10). The third domain which is the carboxyl terminus region is created by two antiparallel helices (H11 and H12) that cross over to the N-terminal and the nucleotide binding domain. The nucleotide binding site on the α-subunit is located within the interface between the α,β dimer (Nogales, 2000). The interaction between domains is very tight such that the effects that nucleotides, drugs and other proteins in the cell have on tubulin are firmly linked. Also each monomer binds a guanine nucleotide, which is non exchangeable when it is bound in the α protein, or N

site, and exchangeable when it is bound in the β subunit, or the E site (Nogales *et al.*, 1998). Both α-tubulin and β-tubulin bind one GTP. Whereas α-tubulin binds irreversibly to GTP and can not hydrolyze it, β-tubulin hydrolyzes GTP to GDP and P_i and can exchange GTP for GDP. Each tubulin monomer contains about 450 amino acids (Downing, 2000) and both share about 40% amino acid sequence identity and both

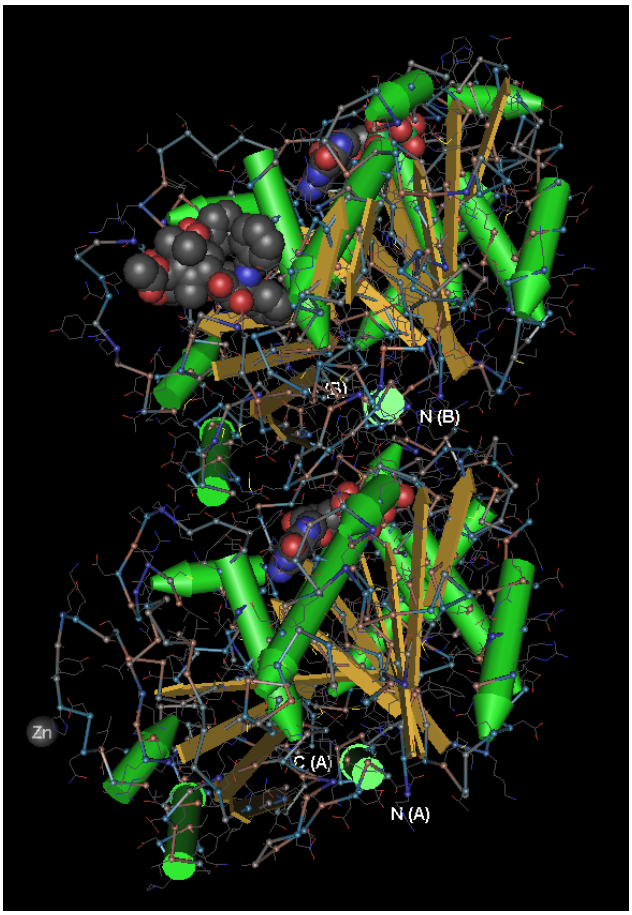

Figure 2.1. Refined Electron Crystallography Structure of α,β-Heterodimer from Zinc-Induced Sheets Stabilized with Taxol® showing the protein backbone and the amino acid residue side chains. α-Tubulin with bound GTP (bottom) and β-tubulin (top) containing GDP and Taxol®. (All heterogens are in Space Fill). The α-helices and β-sheets are colored green and yellow respectively (Nogales *et al.*, 1998, 2000). Illustration was drawn using Cn3D 4.1 by Benon Mugabe.

undergo a variety of post translational modifications such as phosphorylation, acetylation, detyrosination and glutamylation (Luduena, R.F 1998; Verdier-Pinard *et al.*, 2003; Jayaram and Haley, 1994; Shivanna *et al.*, 1993). By using yeast genetics in making several yeast mutant tubulins in which altered GTPase activity is paralleled by altered dynamic instability, Davis *et al.,* (1994) demonstrated that microtubule stability is closely linked to GTP binding and hydrolysis.

Microtubule Structure

Microtubules are composed of 13 linear protofilaments, each of which is composed of alternating α,β-tubulin subunits (Figure 2.2). These protofilaments interact laterally to form a cylinder with an external diameter of around 24nm, an internal bore of around 15nm and each protofilament has an intrinsic polarity. One end of the microtubule, the minus end, which is slow growing, is ringed with α-tubulin and the other, the plus end which is fast growing, is ringed with β-tubulin. The microtubule wall consists of α/β tubulin heterodimers which are connected to each other by longitudinal bonds connected to dimers in protofilaments and lateral bonds connecting to dimers in adjacent protofilaments.

The protofilaments inside microtubules are straight and parallel to their axis. Usually there are 13 protofilaments in microtubules although microtubules with 10-16 protofilaments have also been observed (Erickson, 1974). In a fully formed microtubule, a line of subunits forms a shallow helix that meets the third subunit up when it has completed the circuit of 13 protofilaments. This is referred to as a 3-start helix, because it is always important to start three independent helices to cover all the subunits. The

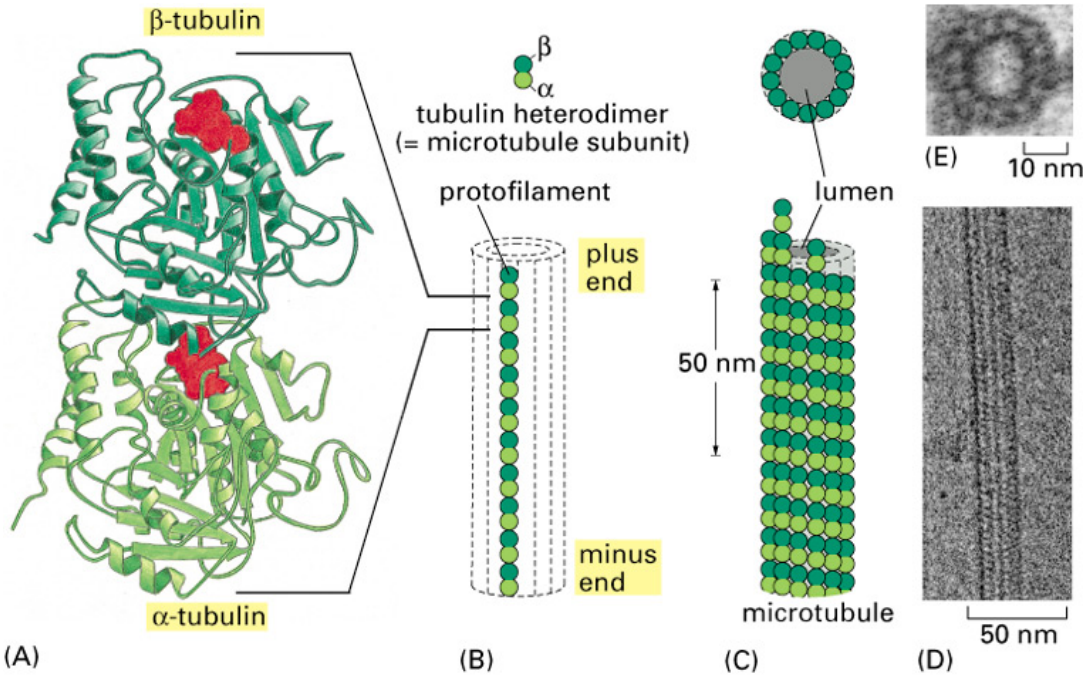

Figure 2.2. The Structure of Microtubules. (A) αβ-tubulin heterodimer. (B) A structure of a microtubule showing a single protofilament composed of tubulin heterodimers which are the microtubule subunits. (C) A 13 protofilament microtubule showing a theoretical A-type lattice. (D) and (E) Cryoelectron microscopy of a fully formed microtubule and its lumen respectively. From *http://www.ncbi.nlm.nih.gov* (Molecular Biology of the Cell, 4th edition).

microtubule helix appears left-handed (Erickson, 1974; Mandelkow *et al.*, 1986). Associated with these microtubules are a number of proteins known as microtubule associated proteins (MAPs), each with a mass of between 125 - 350 kDa depending on species. Although the purpose of these MAPs is still unclear, microtubules form faster in their presence and the MAPs also appear to protect the microtubule from agents which induce depolymerization such as low temperature and Ca^{2+} ions (Jordan *et al.*, 1998).

Microtubule Dynamic Instability

Microtubule assembly starts with a slow, kinetically disfavored nucleation phase that involves the assembly of several αβ-tubulin dimers into a small microtubule (Zheng, 2004). Upon successful nucleation of microtubules, the process is followed by a microtubule elongation phase which is much faster than the nucleation phase. In this phase, the microtubule dynamic structures undergo an intrinsic dynamic behavior in which they are constantly assembled and dissembled. Observations from microtubules formed from purified tubulin have led to the description of microtubule dynamic instability using four parameters. These include the rates of growth (polymerization) and shrinkage (depolymerization) and the frequencies of catastrophe which is the transition from polymerization to depolymerization controlled by catastrophins, and rescue which is the transition from depolymerization to polymerization (Zheng, 2004, Desai *et al*., 1997) (Figure 2.3).

During polymerization, GTP-tubulin subunits are continuously added to the end of the microtubule. During or shortly after addition of domers in this polymerization process, the tubulins in the subunits hydrolyze their bound GTP releasing a molecule of inorganic phosphate. In vitro, the growth rate of a microtubule is a function of the concentration of the amount of free tubulin dimers present. During depolymerization, GDP-tubulin subunits and oligomers are released from the microtubule ends at a very rapid rate. However, it has also been shown that the frequency of catastrophe seems to decrease with increasing levels of tubulin since catastrophe takes place at a lower speed than rescue (Walker *et al*., 1988).

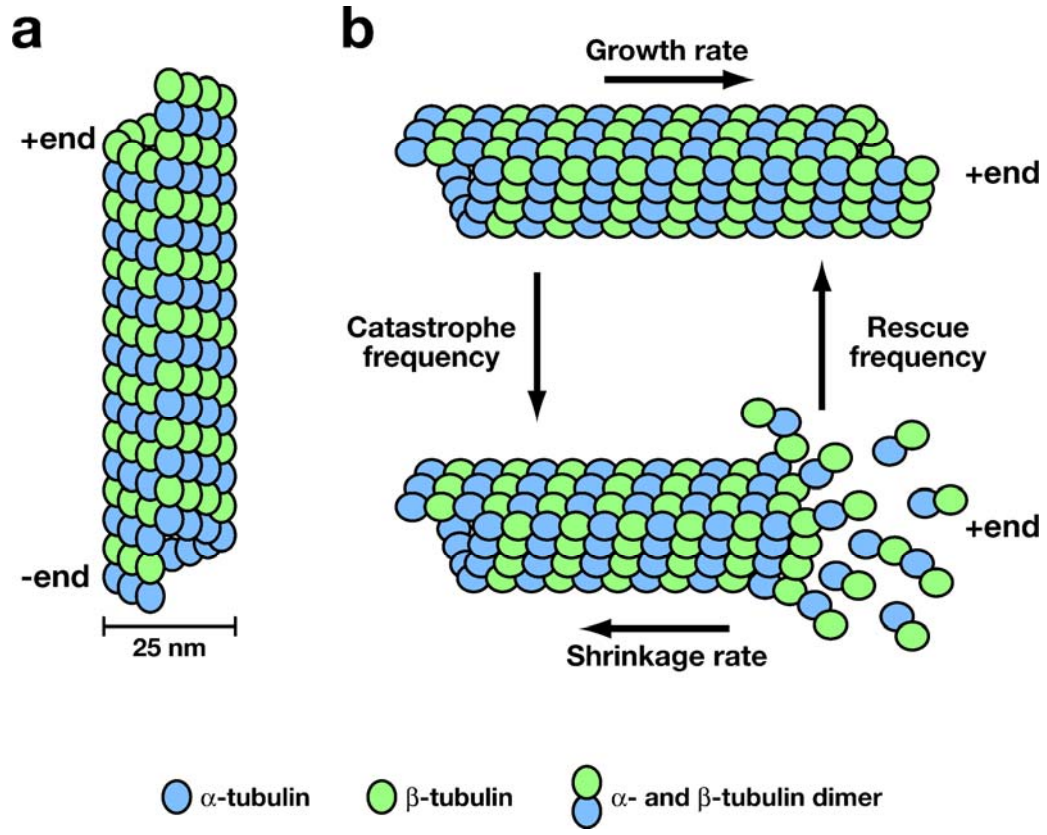

Figure 2.3. Microtubule Structure and Dynamic Instability. (A) A side view representation of a microtubule consisting of α,β-tubulin subunits assembled in a head to tail fashion. (B) Microtubule dynamic instability showing the dynamic behavior of microtubules characterized by the rates of growth and shrinkage and the frequencies of catastrophe and rescue (Reproduced with permission from Zheng, 2004).

General Mechanism Underlying Microtubule Dynamic Instability

Microtubule dynamic instability is maintained through the hydrolysis of GTP bound to β-tubulin at the exchangeable site during polymerization and the resulting GDP at the E-site does not exchange as long as the β-tubulin remains on the microtubule (David-Pfeuty *et al*., 1977; MacNeal *et al*., 1978; Desai *et al*., 1998). However, upon depolymerization, the released tubulin subunits can exchange GDP on the E-site for GTP, thus starting another round of polymerization. Similarly, α-tubulin binds GTP; however

this GTP is bound in a non-exchangeable manner at the N-site, buried in the protein where it is not hydrolysable during polymerization (Spiegelman *et al*., 1977).

Microtubules use energy from GTP hydrolysis to maintain their dynamic instability but they never reach a steady state. Activation of β-tubulin GTPase occurs upon addition of a tubulin heterodimer to a microtubule and through the direct binding of the adjacent α-tubulin to the GTP. When GMPCPP, a nonhydrolyzable analog of GTP within the course of many experiments was used for the *in vitro* tubulin polymerization studies, the normal P-O-P linkage between the β-tubulin and the γ phosphate in this analog was not hydrolyzed by tubulin. Indeed, normal tubulin polymerization occurred which confirmed that the free energy of hydrolysis was not required during polymerization (Hyman *et al*., 1992). Microtubules formed with GMPCPP were structurally more rigid than those from GTP, depolymerized slowly and they did not exhibit dynamic instability. These characteristics suggested that the main role of GTP hydrolysis was to destabilize the microtubule lattice by creating GDP-bound subunits that make weaker intersubunit contacts, leading to increased depolymerization (Caplow *et al*., 1994).

Structural Basis of Microtubule Dynamic Instability

Microtubule dynamics and the geometry of the intersubunit bonds in the microtubule lattice have been studied by electron microscopy. Whereas in microtubules protofilaments are usually straight, microtubule depolymerization leads to curved protofilament oligomers. It has been hypothesized that the major driving force during microtubule depolymerization is the curling of these protofilaments (Mandelkow *et al.,* 1985, 1988, 1991). Indeed the existence of curled oligomers during microtubule

depolymerization has been confirmed by cryoelectron microscopy and X-ray scattering studies. It was noted that divalent ions tend to stabilize these curved protofilament oligomers which enhances protofilament peeling and increases the depolymerization rate at the microtubule depolymerizing ends (Tran *et al*., 1997). Following these finding, they postulated that polymerization at the plus end first leads to formation of a flat sheet like structure which then closes to form the cylindrical microtubule structure. It was also proposed that the closing of the sheet stays behind the plus-end where tubulin subunits are being added and depolymerization is triggered when the closing tubular structure catches up with the polymerizing end of the microtubule. The closing was presumed to be along the seam in the lattice (Chretien *et al*., 1995; Desai *et al*., 1997). They proposed that the microtubule sheet may represent a structural cap that stabilizes a polymerizing microtubule although this was just a correlation.

Regulation of Microtubule Nucleation and Polymerization

Microtubule nucleation and polymerization in cells are coordinated and regulated by microtubule organizing centers. In the cell during interphase, the centrosome which is a major microtubule organizing center, is found adjacent to the nucleus and is involved in nucleating microtubules that extend into the cell periphery with their dynamic plus ends (Zheng, 2004). Numerous microtubule binding proteins in the cell have been found to modulate microtubule dynamic instability in order to achieve highly dynamic and relatively stable microtubules. Intracellular small guanosine triphosphate binding proteins (GTPases) are involved in the regulation of microtubules in spindle assembly, cell polarization, cell motility and asymmetric cell division (Zheng, 2004). The major players in cell polarization and in providing active signals that regulate the reorganization

of the microtubules in the cytoskeleton are the Rho GTPases. The Rho family is a member of the Ras superfamily with numerous protein members such as the Rho, Rac and Cdc42. These GTPases have diverse regulatory functions in actin and microtubule cytoskeletons, gene transcription, and in the progression of the cell cycle (Etienne-Manneville *et al*., 2002).

The guanosine diphosphate exchange inhibitors (GDIs) extract Rho proteins from the membrane thus allowing Rho to cycle between the active GTP-bound form and the inactive GDP-bound form (Figure 2.4). Both forms are regulated by Rho (guanosine diphosphate exchange factors (GEFs) which catalyze the formation of Rho GTP, Rho GTPase activating proteins (GAPs) which catalyze the hydrolysis of RhoA GTP and Rho GDIs which regulate the cycling of Rho between the membrane and the cytoplasm. The activation of Rho is mainly mediated by Rho GEFs (Zheng, 2004). Rac and Cdc42 are also known to regulate microtubule stability by targeting microtubule regulators. The signaling by Rac and CDc42 has been implicated in the regulation of microtubule dynamics through p21-activated kinases which are serine/threonine kinases (Kuntziger *et al*., 2001; Bokoch, 2003). Both Rac and Cdc42 are able to bind p21-activated kinases which may lead to the disruption of the dimerization state of the kinase followed by a series of conformational changes that rearrange the kinase domain into an active site. Thus it is known that stimulating cultured cells with epithelial growth factor leads to phosphorylation of the serine 16 of the microtubule destabilizer, Stathmin/Op18, and since serine 16 phosphorylation prevents stathmin/Op18 from binding and destabilizing

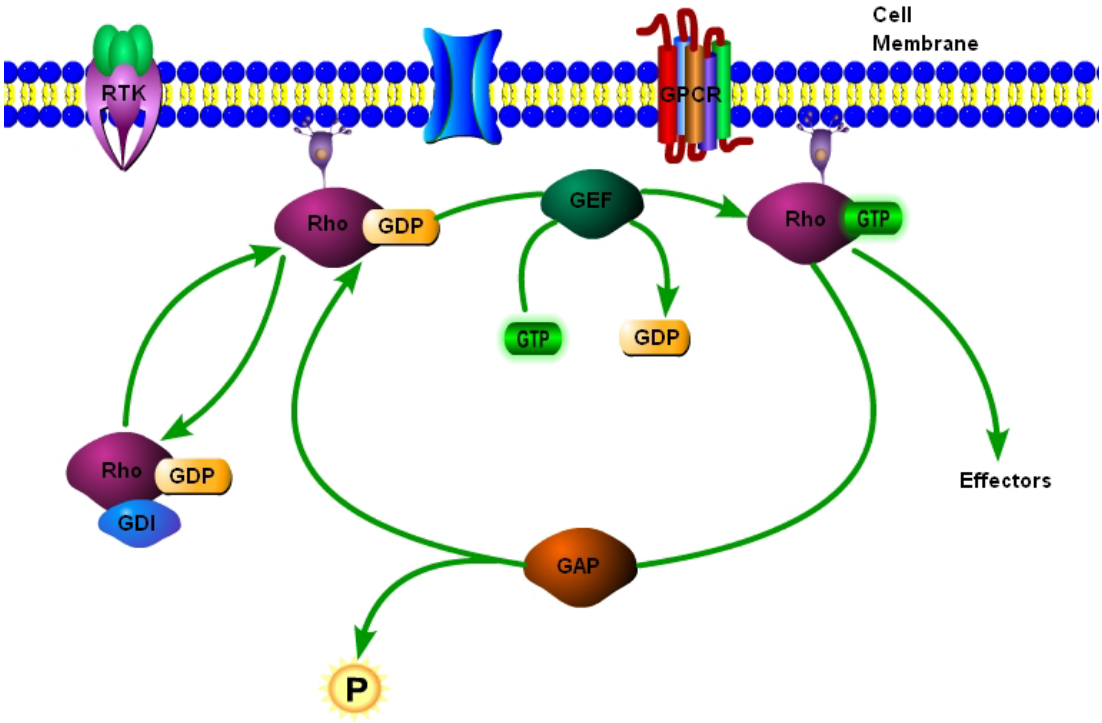

Figure 2.4. Proteins that Regulate the Rho GTPase Cycle (Zheng, 2004). Redrawn using Pathway Builder Tool 1.0 by Benon E. Mugabe.

microtubules, Rac and Cdc42 mediated p21-activated kinase activation may cause microtubule stabilization (Daub *et al*., 2001). Ran GTPase, another member of the Ras family of monomeric G proteins is located in the interphase nucleus. The main function of Ran GTPase is the regulation and nucleocytoplasmic trafficking of macromolecules during interphase (Weis, 2002). Ran GAP1, the only Ran GTPase activating protein is located in the cytoplasm and the only GEF for Ran, thus for RCC1 is found in the nucleus. Ran is also known to be involved in the control of the assembly of the mitotic spindle and nuclear envelop (Quimby *et al*., 2003), mitotic checkpoint (Yamaguchi *et al.,* 2003) and DNA replication (Arnaoutov *et al*., 2003). Heterotrimeric G-proteins, which are known to have α, β, and γ- subunits consist of many family members that regulate numerous downstream effectors in receptor mediated signaling.

Microtubule Associated Protein (MAPs)

Attempts to identify MAPs high have led to enormous investigations into the biochemical constituents of microtubules and their role in the cytoskeletal system. Although efforts to isolate the mitotic spindle have sometimes proved unsuccessful, major breakthroughs have been made in isolation and identification of MAPs (Kuriyama *et al*, 1984). The discovery that microtubules could be assembled *in vitro* from mammalian brain tissue extracts was very fundamental in trying to identify protein components that were associated with microtubules (Borisy *et al*., 1975).

Since then, high molecular weight MAPs that constantly form projections from the surface of microtubules have been resolved and characterized into several major components; MAP1 (300-350 kDa) and MAP2 (270 kDa) (Sloboda *et al*., 1975). In 1975, Weingarten and coworkers were also able to isolate the protein tau which was found to consist of several polypeptide chains with molecular weights between 55 and 68kDa. These proteins are required for assembly of tubulin subunits into the microtubules and they also stabilize the assembled microtubules. Some MAPs are usually found cross-linked to other adjacent microtubules and are even involved in linking microtubules to other membranes and intermediate filaments. Therefore, MAPs are proteins that constantly interact with microtubules by stabilizing or destabilizing them. Some MAPs also mediate the interaction of microtubules with other proteins in the cell.

Microtubule Destabilizing Proteins

Some proteins associated with microtubules have been found to induce microtubule depolymerization by binding to tubulin dimers and thereby increasing the

rate of catastrophe. Catastrophe-promoting proteins known as catastrophins, which are destabilizing proteins, promote catastrophe by disintegrating microtubules. This is achieved through various mechanisms that include severing the microtubules and generating new ends that lack a GTP cap, promotion of the hydrolysis of GTP and thereby eliminating the stabilizing GTP cap and finally inducing a conformational change in tubulin that destabilizes the microtubule structure. All this is dependent upon the induction of GTP hydrolysis at the microtubule plus ends (Howell *et al.,* 1999).

Op18/stathmin is a microtubule destabilizing protein that usually increases in abundance in some cancer cells. Op18/stathmin, the main protein known to induce depolymerization of microtubules, is itself regulated through the cell cycle by phosphorylation (Lawler, 1998). Other kinase-like proteins have recently been characterized and these include XKCM1 and XKIF2. XKCM1 is a member of the MCAK subfamily of kinesin motor proteins. This microtubule destabilizing effect of XKCM1 is itself antagonized by Protein XMAP215. The phosphorylation of XMAP215 at the beginning of mitosis results in increased microtubule instability as microtubules disassemble and tubulin dimers form the mitotic spindle. These proteins are very important microtubule depolymerizers and are required for the formation and maintenance of the mitotic spindle. They are known to act enzymatically causing rapid microtubule disassembly, and hydrolysis of ATP is required to separate them from the depolymerized tubulin dimers (Walczak *et al*., 1996). The mechanism under which these proteins bind differentially to the microtubule plus and minus ends has not yet been elucidated.

Microtubule Stabilizing Proteins

Several structural MAPs have been known to stabilize microtubules, inhibiting their depolymerization and are themselves regulated by phosphorylation. The exact sequence in tubulin by which MAPs bind tubulin is still a subject of debate (Nogales, 2000). Several serine-threonine kinases have been identified and these kinase enzymes have are known to regulate microtubule affinity by phosphorylating the tubulin binding domain of MAPs, causing their detachment and enhancement of dynamic instability (Drewes *et al*., 1998).

Proteins of the MAPs family have been well studied and they include the neuronal MAP2, MAP4 and tau, which participate in determining the structure of different parts of nerve cells. These proteins share a conserved C-terminal microtubule-binding domain and covalent cross-linking experiments have shown that tau binds both α and β-tubulin subunits at two different sites (Chau *et al.,* 1998). They are also known to share the variable N-terminal domains which project outwards and interact with other proteins.

Tau and MAP2 are known to stabilize microtubules by binding at the Taxol binding site on tubulin. Cells can regulate their microtubule dynamics and behavior by altering the concentrations of different MAPs (Nogales, 2000; Vaillant *et al*., 1998). XMAP215, which is a highly conserved MAP with a molecular weight of 215 kDa, has been shown to stabilize the plus ends of microtubules, thus preventing catastrophe (Ainsztein *et al*., 1994).

The Role of Actin in the Cytoskeleton

The cytoskeleton is an extensive array of filaments that give the cell its shape and the ability to move. It is responsible for the arrangement and internal motions within the organelles of living systems. The cytosol is a highly organized gel whose composition varies significantly throughout the cell (Voet and Voet, 1995). Microfilaments which are about 90 Å in diameter fibers, consist of the protein actin and like microtubules, they have a mechanically supportive function. Both actin and microtubules are intrinsically polar because their subunits have an asymmetric conformation. By interacting with protein myosin, microfilaments form contractile assemblies that are responsible for intracellular movement. Actin and myosin are the major protein components in the muscle.

Another major component of the cytoskeleton is the intermediate filaments which are non polar and symmetric protein fibers with about 100 to 150Å in diameter. They have a load bearing function. Protein keratin forms a major portion of the net work of intermediate filaments that are found in the skin. *In vitro*, actin is monomeric at low temperatures, low ionic strength and alkaline pH. However under physiological conditions, G-actin polymerizes in a process that is catalyzed by the hydrolysis of ATP. Therefore actin is an ATPase that binds ATP and is buried deep in the cleft of the protein, orientated in such a way that it faces the minus end of the polymer. There are several differences in the two ends of the polymer where by the plus end exhibits high rates of polymerization and depolymerization than the minus end (Kabsch & Vandekerckhove, 1997).

In vivo, microfilament polymerization and depolymerization are influenced by actin binding proteins. Profilin, a 16kDa protein, is known to bind G-actin in a 1:1 profilactin complex thus preventing actin polymerization (Voet and Voet, 1995). Profilin is also known to bind a large number of phospholipids and in so doing allows the polymerization of actin to be concentrated in the cellular cortex.

At physiologically actin levels, a high percentage of the monomeric actin binds spontaneously into F-actin, thus preventing monomeric actin from binding thymosin. Competition with profilin for the binding of G-actin is known to occur which assists in the exchange of ADP to ATP and in allowing addition of the actin monomers on the growing end (Remedios, *et al*., 2003). ATP accelerates actin polymerization through the activation of G-actin and preferential addition to a particular end of the growing actin filament. ATP eventually gets hydrolyzed but only after polymerization has occurred. Thus there is a critical concentration of G-actin at which activated monomer actin units are added predominantly but not exclusively to the preferred end of the filament at the same rate that monomer units dissociate from the opposite end of the filament. Under these conditions there is neither growth nor shrinkage but the filament is able to maintain a constant length through this treadmilling phenomenon as its component units are translocated from one end of the actin filament to the other (Carlier, 1998; Voet and Voet, 1995).

Anticancer Agents and Tubulin Polymerization

Because of their importance in mitosis and cell division, microtubules are an important target for anticancer drugs (Jordan and Wilson, 1998; Giannakakou *et al.*, 2000). These anticancer agents which bind in widely different regions on tubulin can

have dramatic effects on the dynamics of the microtubule and thus on the health and viability of the cell (Downing, 2000; Pinney *et al*., 2000) (Figure 2.5). The primary

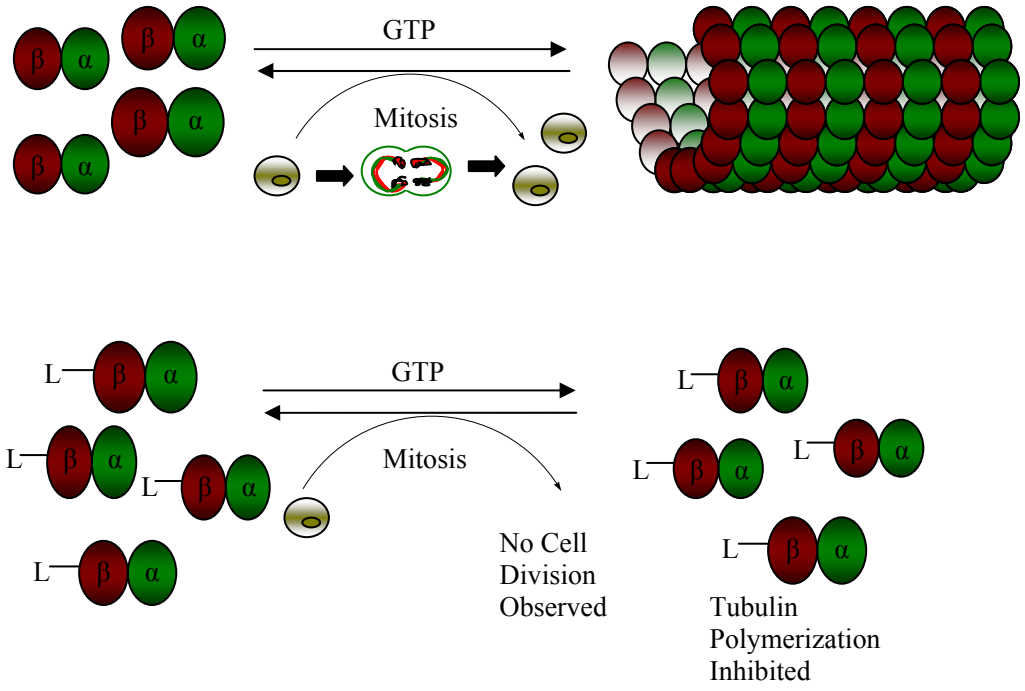

Figure 2.5. Normal Tubulin Polymerization in Cell Division (above); Disruption of Tubulin Polymerization by an Anti-Tubulin Agent (below)(Kevin G. Pinney *et al*., 2000).

target for binding of all these ligands so far identified is β-tubulin, and thus it has a very important role as a regulator of microtubule dynamics. These drugs have been classified into four major groups according to their binding sites on tubulin. They include those that bind at the colchicine site, those that bind at the Taxol site and those that bind at the vinblastine site. This is illustrated in Figure 2.6 where (T) is Taxol site; (C) represents the Colchicine site; (B) is the Benzimidazole site; (V) is the Vinca domain; (E) and (N) represent GDP and GTP at the exchangeable and nonexchangable sites respectively (Downing, 2000).

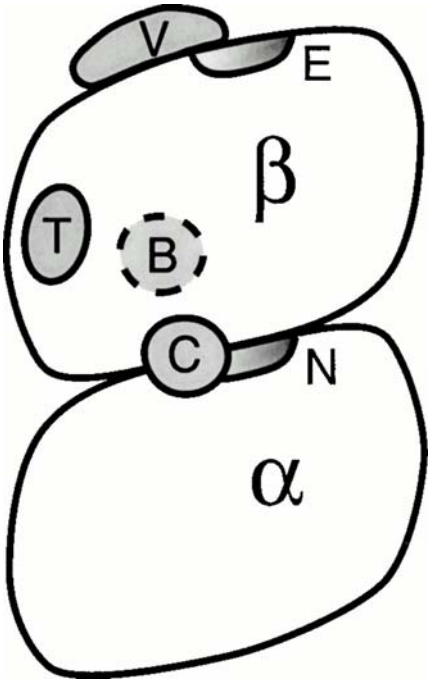

Figure 2.6. A Representation of Positions of Ligand Binding Sites on αβ-Tubulin Heterodimer (Downing, 2000).

Also, these drugs have been characterized into two major classes according to their function. They include those that inhibit microtubule assembly (colchicine, combretastatin and vinblastine families) and those that promote microtubule assembly and stabilization (Taxol family) (Hamel, 1996) (Figure 2.7).

Colchicine inhibits microtubule formation and at higher concentrations, it disrupts microtubules. Colchicine is known to interact with β- tubulin. The colchicine binding site together with a model of the colchicine orientation in tubulin has been proposed (Uppuluri *et al*., 1993). Also cross linking has been observed between the A-ring of colchicine and Cys356 of β-tubulin (Bai *et al*., 1996; Downing, 2000). Some of the compounds in the colchicine family with modifications in both the A and C rings that are known to bind with tubulin and inhibit tubulin polymerization are shown in figure 2.8.

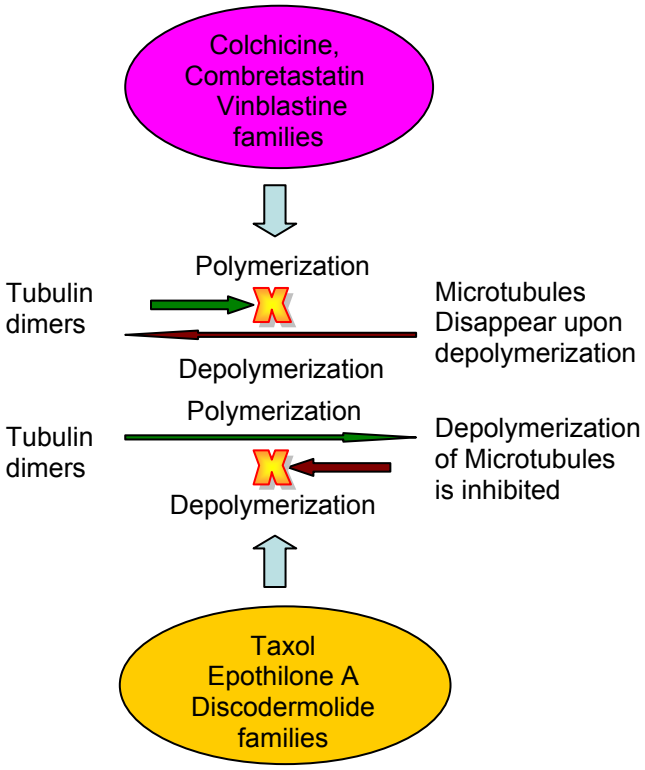

Figure 2.7. The Effect of Various Ligand Families on Microtubule Assembly.

Colchicine Binding Site

The identification of the colchicine binding site on tubulin has eluded scientists for decades. Small ligands have been used in trying to define their binding sites through induction of covalent interactions between tubulin and the specific ligands. The use of direct photoaffinity labeling has yielded some useful information regarding the likely binding pocket for colchicine at the interface of both α and β-tubulin monomers (Uppuluri *et al.,* 1998). Using 3-chloroacetyl-3-demethylthiocolchicine (3CTC), a competitive inhibitor of colchicine for the colchicine binding site on tubulin, Bai (1996) and coworkers were able to determine the location of this important binding site. In this

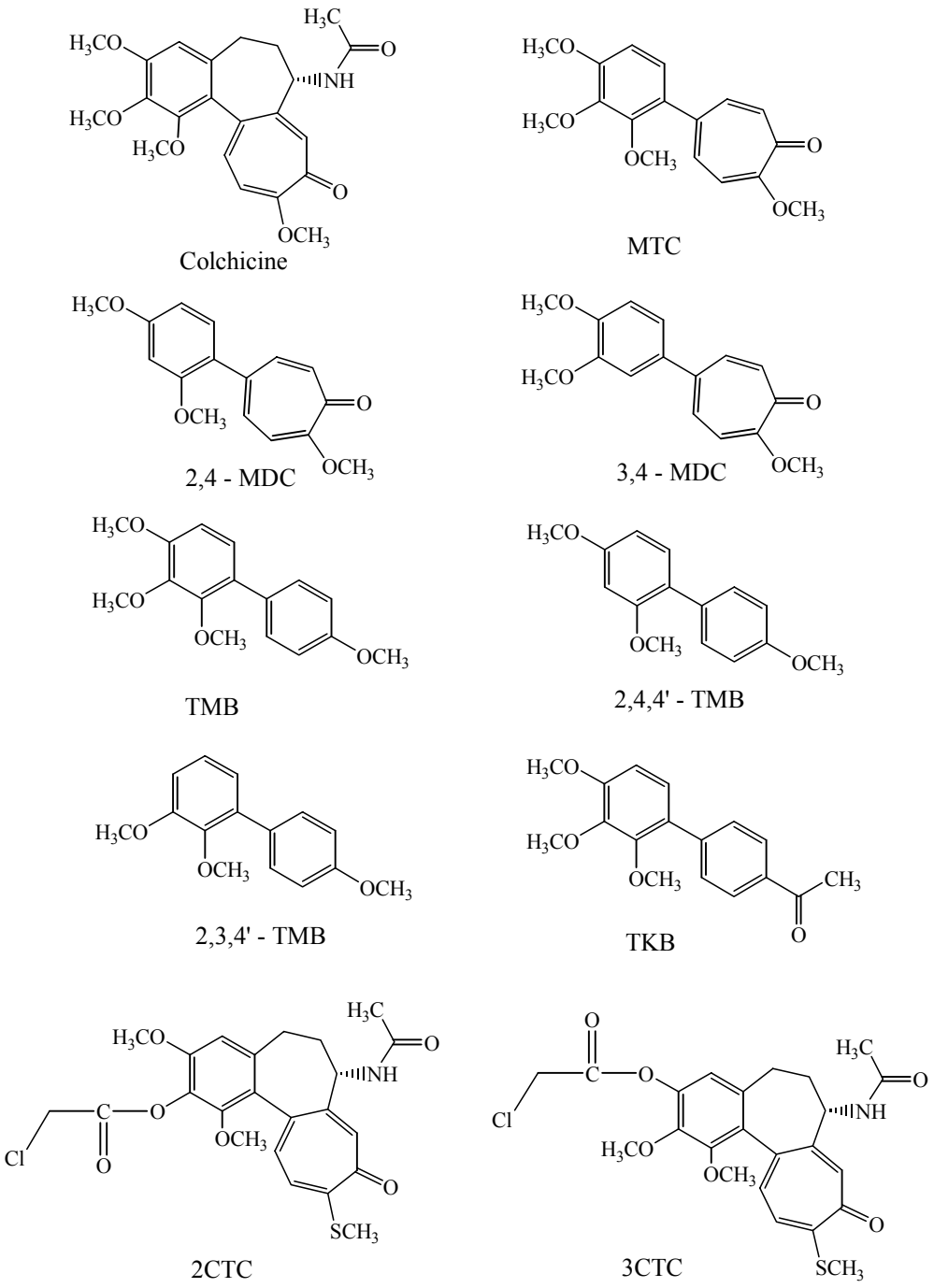

Figure 2.8. Structures of Colchicine and Biphenyl Analogs (Andreu *et al*., 1998).

experiment, 3-chloroacetyl-3-demethylthiocolchicine was reacted with tubulin, digesting with enzymes and the resultant products were isolated and amino acid sequence of the radiolabeled peptides was determined. They found that covalent interaction had occurred

between the tubulin and the [^{14}C] 3CTC specifically at the 354 cysteine amino acid residue. The sequences of isolated radiolabeled peptides showed that at least 90% of the covalent interaction was at cysteine 354.

From this observation, they postulated that the C-3 oxygen atom of colchicine analogs usually lies within 3 Å of the sulfur atom of cysteine 354 and that the trimethoxyphenyl ring (ring A) of colchicine lies between cysteine 354 and cysteine 239. This conclusion was reached based on the already known distance of 9 Å between the two residues (Bai *et al*., 1996). They also concluded that the colchicine tropolone moiety could be located between the peptide region containing the cysteine 239 residue and the amino terminal region of the β-tubulin monomer. This was confirmed by the labeling patterns observed from photoactivation experiments of tubulin – colchicine complexes. The binding of colchicine to tubulin is well illustrated in figure 2.9. Upon interaction, a colchicine-induced conformational change is known to affect the distal domain of the α-subunit (Cys295, Cys305, Cys315 and Cys316) (Chaudhuri A. R *et al.*, 2000). Fluorescence resonance transfer (FRET) has also been used to elucidate the distance between the colchicine and the Taxol binding sites which has been found to be about 17 Å (Han *et al*., 1998). The side chains of amino acid residues are very important for ligand-protein binding and overall interaction. Using an automated docking methodology through grid search and thereafter performing manual refining on the coordinates of the docked complex, Pal and coworkers were able to identify a likely binding site of colchicine on tubulin (Pal *et al*., 2001). Starting with initial coordinates around Cys356β, the binding site of colchicine identified was found close to the His37β, and several

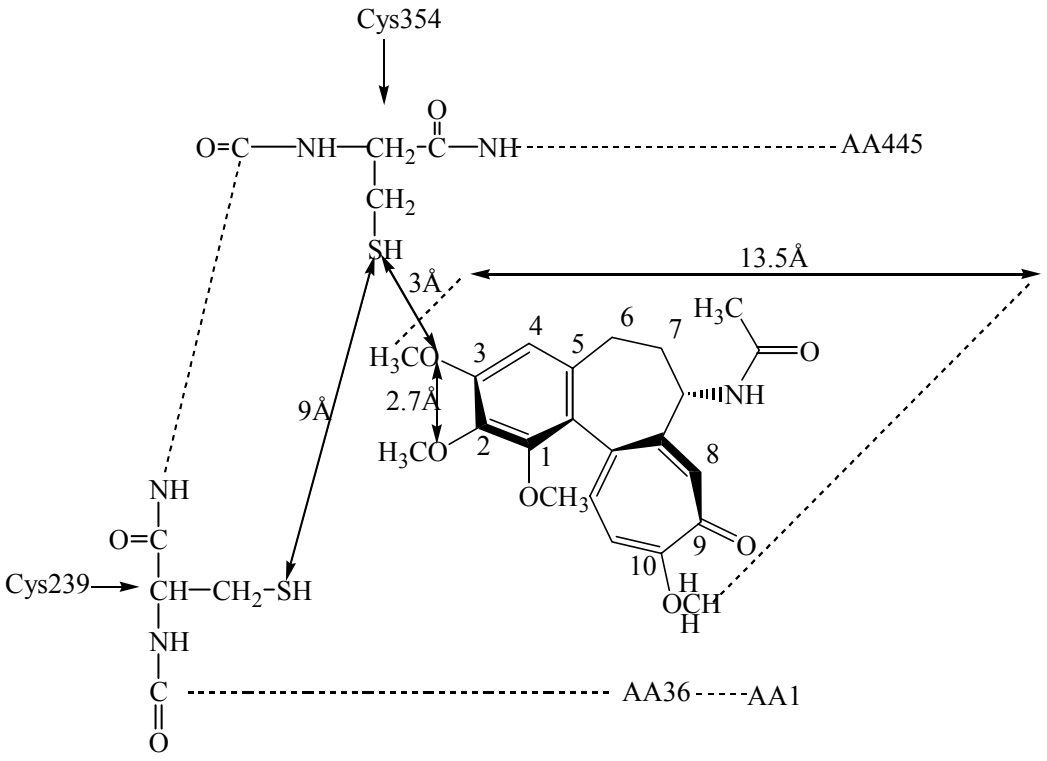

Figure 2.9. A Diagrammatic Representation of the Proposed Interaction of Colchicine with Tubulin (Bai *et al*., 1996).

isoenergetic colchicine orientations were observed. The colchicine process revealed an initial fast and reversible component, followed by a tighter binding and quasi-irreversibility. The docking site is a hydrophobic patch surrounded by a network of hydrogen bonds. They observed that the bulk of the molecule was associated with β-tubulin subunit and the side group to the ring B of colchicine forms hydrogen bonds with the α-tubulin subunit. In particular, the acetamide group on ring B made a hydrogen bond contact with the main chain atoms of Gly81α. They showed that His37β made a stacking contact primarily with the A-ring of colchicine. The trimethoxyphenyl ring (ring A) is in close proximity to Cys356β (Pal *et al*., 2001, Bai *et al.,* 1996). Through competitive studies with radio- labeled colchicine, CA-1 and CA-4 are known to bind on

this same colchicine binding site, information on the specific interactions and non-covalent bonding that exists between amino acids and combretastatin analog functional groups upon binding is still lacking.

Molecular Interaction of Colchicine and Tubulin with Stathmin-Like Domain Complex

A 3.5 Å resolution structure of tubulin with colchicine and a stathmin like domain complex has been studied in order to obtain insight into the regulation of microtubule dynamic instability (Ravelli *et al*., 2004). Ravelli and coworkers showed that colchicine binds to tubulin at a location where curved tubulin is unable to give the microtubule its normal straight structure. In the complex, it was found that the RB3-SLD adopts a hook-like structure that enables it to accommodate the two bound tubulin dimers (Figure 2.10).

The RB3-SLD consists of three domains that include an N-terminal cap, a variable linker and a helical carboxy-terminal domain (Maucuer *et al*., 1993). Serine 16 which is conserved in the stathmin family and is activated by phosphorylation during signal transduction lies in the sharp turn of the β-hairpin of the N-terminal cap domain. It is believed that its phosphorylation inhibits the formation of the right conformation of the N-terminal cap. Since the residues of the tubulin interacting with the N-terminal cap constantly mediate the longitudinal contacts between heterodimers assembled in microtubule protofilaments, the SLD can sterically hinder the addition of an α,β-heterodimer at the plus end of microtubules via the N-terminal cap domain while also maintaining a curvature via its C-terminal helical domain.

During microtubule dynamic instability, a kinetic barrier has to be maintained between the straight and curved tubulin structures H6 and H7 loops together with T5 are known to contribute to the formation of this barrier. Shrinkage of one protofilament

induces a destabilization of the nearest one whose immediate domains it interacts with, by allowing it to curve. The curvature formed leads to additional loss of both longitudinal and lateral energy since longitudinal interactions are extensively reduced in curved microtubules than in straight ones. This leads to microtubule disassembly and

Figure 2.10. Structure of Tubulin-DAMA-Colchicine:RB3-SLD Complex. (Ravelli *et al.*, 2004). From *http://www.ncbi.nlm.nih.gov*; drawn using Cn3D - 4.1 by Benon Mugabe.

increased rate of tubulin depolymerization. Also it has been postulated that GTP regulation of microtubule dynamic instability involves the binding of GTP to β tubulin which leads to a conformational change that locks H7 helix in its straight tubulin structure through interactions with the N-terminus (Lowe & Amos, 1998). Lateral interactions in microtubules also double lock the H7 helix through contacts at the C-terminus with the intermediate domain. Upon GTP hydrolysis, the first lock is loosened resulting in the microtubule maintaining its straight structure because of the lateral interactions. However, the microtubule can easily curve and depolymerize automatically upon the loss of these interactions.

The structure of tubulin-podophyllotoxin-RB3-SLD has also been determined at 4.2 Å and it has been shown that podophyllotoxin competitively binds at the colchicine site (Wilson *et al*., 1974; Ravelli *et al*., 2004). When colchicine was replaced by *N*-deacetyl-*N*-(2-mercaptoacetyl)-colchicine (DAMA-colchicine), the location of the *N*-acetyl group was established and the orientation of the colchicine molecule was defined (Figure 2.11). Ravelli and coworkers were able to show that the colchicine site is embedded in the intermediate domain of β-tubulin and is surrounded by the S8 and S9 strands, loop T7, H7 and H8 helices as well as loop T5 of the neighboring α-subunit. Previously it has been revealed that colchicine analogs with substitutions at the ring A methoxy positions are crosslinked with Cysβ241 (Bai *et al*., 2000). One important future of colchicine binding to tubulin is the movement of the T7 loop and H8 helix which creates room for the binding of colchicine. Nogales and coworkers (1999) have established that microtubule dynamic instability requires both longitudinal and lateral interactions between tubulin subunits as well the M loops of straight tubulin which are

central to lateral interactions. When colchicine bound tubulin is added to the plus end of the microtubule, no lateral contacts are established between the complex and the newly formed protofilament because of partial displacement of the M loop. This is due to failure in adopting the straight tubulin conformation as this would result in steric

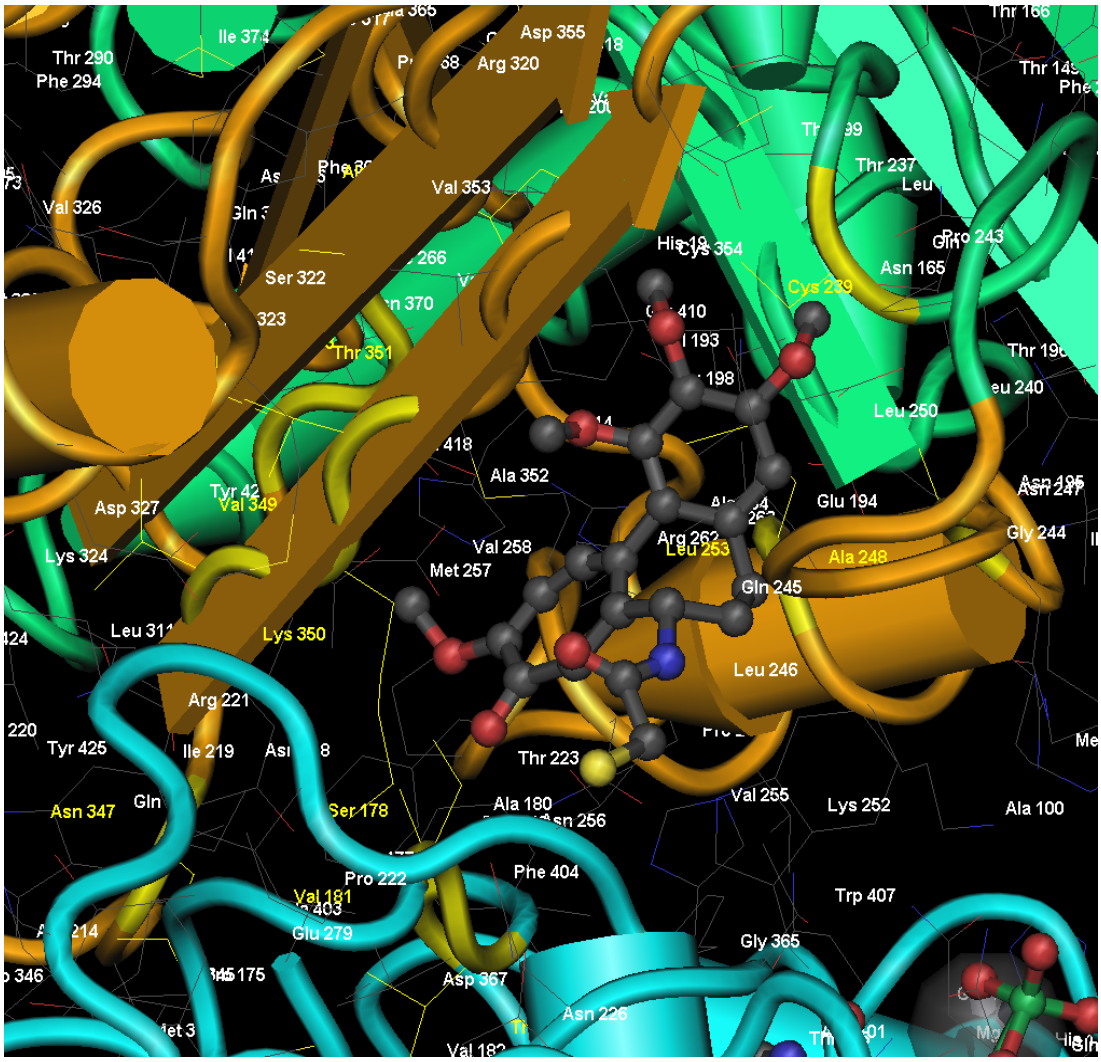

Figure 2.11. Structure of a Ternary Tubulin–DAMA-Colchicine:RB3-SLD Complex (Ravelli *et al.*, 2004). Amino acid residues within 3.5 Å distance from DAMA-Colchicine are shown in yellow. From *http://www.ncbi.nlm.nih.gov*; drawn and labeled using Cn3D - 4.1 by Benon Mugabe.

hindrance between the colchicine and the α-subunit. The body of the microtubule is preserved as long as loss in lateral contacts is minimized (Ravelli *et al*., 2004).

Vascular Targeting

This is a method of cancer treatment that is designed to target newly formed abnormal tumor blood vessels, rather than the established blood vessels found in healthy tissue, resulting in fewer side effects in the oncology setting than conventional disease treatments such as radiation and chemotherapy. The inherent differences between blood vessels constituting tumors and those associated with normal tissues have provided a variety of unique targets for the design of potent therapeutics (Siemann, 2002). Therapeutic vascular targeting has been concentrated on anti-angiogenic approaches, which aim to prevent the neovascularization processes in tumors, whereas antivascular (vascular targeting) approaches, using vascular disrupting agents (VDAs), aim to cause the rapid and selective shutdown of the established tumor vasculature, leading to secondary tumor-cell death.

VDAs are designed to address the complete spectrum of solid tumors, whereas other approaches, which directly target tumor cells, require the development of different drugs for varying types of solid tumors. Since VDAs are designed to target endothelial cells associated with new blood vessel formation, drug resistant mutations are unlikely to occur. The tumor endothelium is usually the main target of cancer therapy by VDAs. The destruction of already formed neovasculature of actively growing tumors is now at the center of anticancer drug discovery (Hahnfeldt *et al.,* 1999; Schweigerer, 1995). The ability of vascular targeting agents to selectively target newly formed or abnormal blood vessels makes them suited for cancer chemotherapy and certain ocular diseases.

Tumor Vasculature

Solid malignant tumors are characterized by uncontrolled neoplastic cell division. The tumor vasculature is usually different from the normal vasculature. Tumor blood vessels are immature and have poorly developed walls which are characterized by a discontinuous endothelial-cell lining. Common characteristics of vessels constituting the tumor microcirculation are dilated and elongated shapes, blind ends and abrupt changes in diameter and vascular compression (Hill *et al*., 1995). On the other hand, the endothelial cells are often irregularly shaped, forming an uneven luminal layer, with loose interconnections and focal intercellular openings. These features contribute to a high intrinsic vascular permeability to macromolecules (Jain, 1987; DvoraK *et al.,* 1991).

Vascular Disrupting Agents (VDAs)

Vascular Disrupting agents (VDAs) are molecules that attack the established blood vessels of a solid tumor and inhibit the flow of blood through it. By inhibiting blood flow to the tumor, they prevent the transportation of both oxygen and nutrients to it, hence VDAs are lethal to tumor cells. Earlier cancer therapies such as the deliberate induction of bacterial infections in cancer patients partly relied on damage to tumor blood vessel network for their therapeutic efficacy (Starnes, 1992). However, in 1923, Wolgum suggested that thrombosis in blood vessels could lead to tumor regression. It has been found that large numbers of neoplastic cells naturally depend on endothelial cells for their nutritional support. It was then postulated that damaging the tumor endothelium could have a lethal impact on cell survival and growth (Denekamp, 1984, 1993). The general mechanism by which VDAs destroy tumors is through blockage of blood vessels. They take advantage of the differences in tumor and normal tissue blood vessels to directly and

selectively damage the endothelia of tumors. Once a VDA binds to its target, endothelial cells of the tumor blood vessels begin to round up and necrosis is initiated. However, it is important to note that VDAs do not prevent the formation of new blood vessels. There are two major types of VDAs that are currently being developed for cancer treatment; ligand-directed and small molecule VDAs (Siemann, 2002).

Ligand-Directed and Small Molecule VDAs

Ligand-directed VDAs use antibodies, growth factors and peptides to selectively target toxins, pro-coagulants and pro-apaptotic effectors specifically to tumor endothelium. The main aim of the ligand-directed approach is to make use of VDAs that bind selectively to components of tumor blood vessels thereby targeting the only the agents that destroy those blood vessels. In this approach, ligand-directed VDAs consist of targeting and effector groups that are linked together through bonding. The targeting moiety is usually an antibody or a peptide directed against a marker that is selectively up-regulated on tumor *versus* normal tissue endothelial cells (Thorpe, 2004). Small molecule VDAs do not specifically localize to the tumor endothelium but are known to exploit the tremendous differences between tumor and normal endothelial cells in order to induce selective vascular dysfunction (Chaplin *et al*., 2002; Thorpe *et al*., 2003). These differences in tumor compared with normal tissue endothelial cells include their increased proliferation, easy permeability and reliance on the tubulin cytoskeleton to maintain shape. Gene therapy is a powerful tool in the fight against cancer. Since the endothelial cells are in contact with the blood circulation, they are the best target for this approach.

Several approaches that have been explored include the use of endothelial cell-specific promoter elements and vectors with restricted cellular tropisms (Modlich *et al*., 2000, Trepel *et al*., 2000). There are several potentially specific neovascular targets for antibodies and these include extracellular matrix components such as fibronectin, endothelial – specific markers such as VEGF receptor, and tumor endothelial-associated cell surface markers such as anionic phospholipids. Thus, ligand-based VDAs use a targeting ligand to achieve selectivity of binding to tumor vasculature. Another approach is targeting specific endothelial cell receptors with toxic fusion proteins. Since VEGF receptors are typically over expressed in the endothelium of tumor vasculature while they are almost absent in the vascular endothelium of normal tissues, such receptors are normally good targets for therapeutic strategies aimed at inhibiting tumor vascularization (Veenendaal *et al*., 2002). The two types are usually grouped together because they both cause acute vascular collapse in tumors, which leads to massive central necrosis. There are currently two classes of small molecule agents that can induce extensive hemorrhagic necrosis in tumors as a result of vascular collapse and these include tubulin binding agents (TBAs) and flavonoids such as flavone acetic acid (FAA) and its analogs.

Tubulin Binding Agents

Small molecule VDAs that have reached phase II clinical trials include Combretastatin A-4 disodium phosphate (CA-4P), CA-1P and the CA-4 derivative AVE8062A and the phosphate prodrug of N-acetylcolchinol (ZD6126) all of which rapidly induce large reductions in vasculature volume, extensive tumor necrosis and loss of viable tumor cells (Blakey *et al.,* 2002; Siemann *et al*., 2002). Within minutes of exposure to these tubulin binding agents, microtubules of proliferating endothelial cells in

tumor blood vessels show damage. Colchicine, a potent tubulin binding agent, is too toxic for clinical use. Its damaging hemorrhage and extensive necrosis effects on tumor vasculature have been know since the 1930s (Seed *et al.,* 1940; Ludford *et al.,* 1948). ZD6126, a phosphate prodrug of N-acetylcolchinol rapidly induces large reduction effects in vascular volume, tumor necrosis and tremendous decrease in number of viable tumor cells (Blakey *et al*., 2002; Siemann *et al*., 2002). The potent VDAs vincristine and vinblastine have also shown profound tumor damaging vascular effects by binding at the tubulin heterodimer (Baguley *et al.,* 1991; Hill *et al.,* 1993).

Combretastatins

Combretastatins belong to a new series of therapeutic compounds known as vascular disrupting agents (VDAs) (Figure 2.12). Combretastatins drastically reduce blood flow in tumors as shown in preclinical animal models. The combretastatins have a mode of action different from angiogenesis inhibitors in that they are designed to disrupt already formed tumor vasculature as opposed to angiogenesis inhibitors which prevent the growth of new blood tumor blood vessels. The combretastatins were first isolated by Pettit and coworkers in 1982 from the South African Cape Bushwillow tree *Combretum caffrum* (Lin *et al.,* 1988). A series of many natural compounds and synthetic products have been isolated and characterized as Combretastatin A-1, A-2 and A-4. The Combretastatin A series is characterized by a trimethoxyphenyl ring (ring A) connected to the methoxyphenolic ring (ring B) through an ethene bridge. The combretastatin B series have their two phenyl rings separated by an ethane bridge. The combretastatin C series are similar to CA-1 but the rings are featured as a tricyclic core.

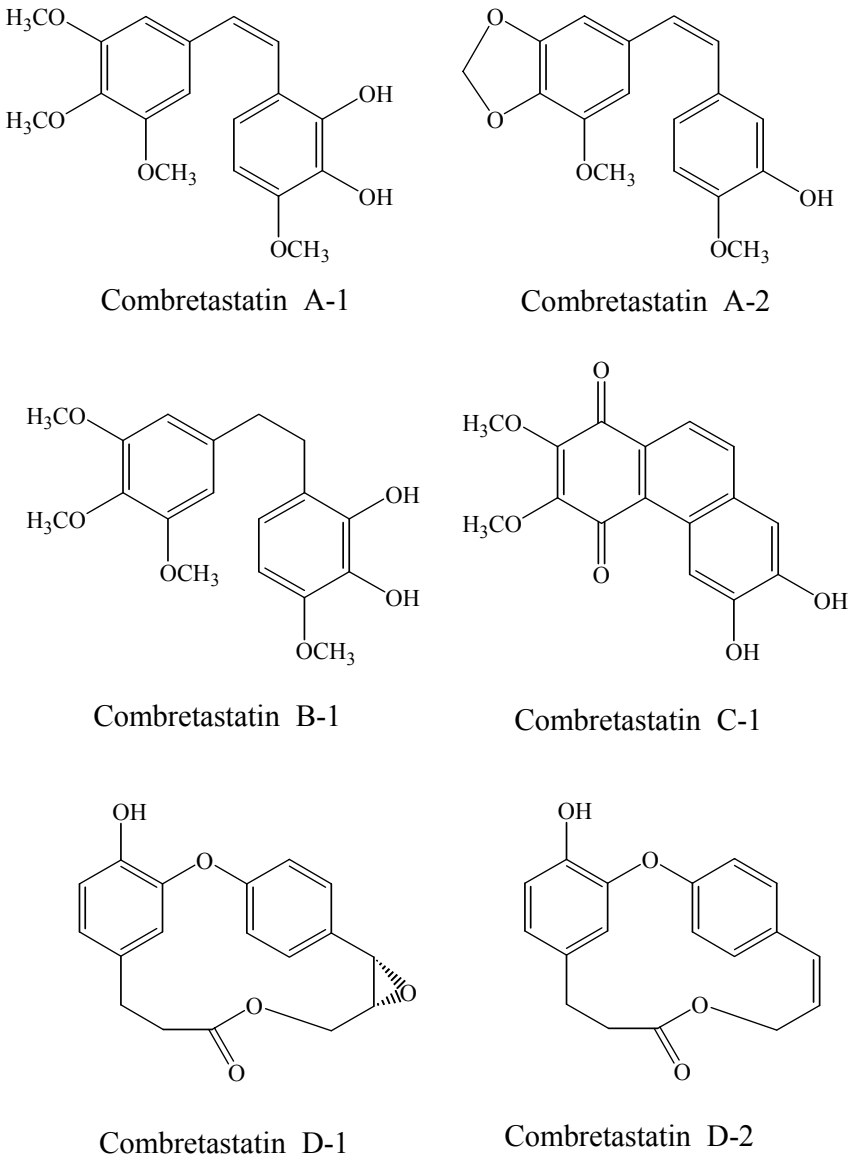

Figure 2.12. Structures of a Series of Combretastatin Compounds (Lin *et al.,* 1988).

The combretastatin D series consists of an ether linage connecting the two aryl rings through a macrocyclic lactone. Combretastatin A-4 is the most active of 17 isolated compounds against a number of tumor cells and its development has commenced rapidly since the synthesis of a more soluble combretastatin A-4 disodium-phosphate salt (Pettit *et al.,* 1995).

Metabolism of Combretastatin Analogs

Within minutes of administration, CA-4-P or CA-1-P is rapidly cleaved to CA-4 or CA-1 by the action of endogenous non-specific phosphatase enzymes with the release of CA-4 or CA-1 and a phosphate group (Pettit *et al*., 1995). The released combretastatin molecule is believed to bind tubulin at the colchicine-binding site. Another CA-4 derivative, AVE8062, which is a CA-4 serine prodrug, is cleaved by amino peptidases which break down the peptide bond releasing the CA-4 and the serine moiety to form the active drug (Hori *et al*., 1999; Nihei *et al*., 1999; Hori *et al.,* 2002). Pharmacokinetic analysis using HPLC has shown that CA-4 disodium phosphate upon dephosphorylation, releases CA-4 which binds glucuronic acid forming CA-4 glucuronide (CA-4G) as the main metabolic product which is then cleared from the body through urination (Stevenson *et al*., 2003).

Flavonoids

The development of a series of flavonoid compounds that includes FAA and DMXAA (Figure 2.13) started with the discovery that FAA, which was previously found to have unexpectedly high anti-tumor action in murine models, induced acute hemorrhagic necrosis of established subcutaneous murine colon tumors. Additional experiments showed that FAA caused a selective shutdown of tumor blood flow (Smith *et al*., 1987, Evelholch *et al*., 1988), Hill *et al*., 1989), and Zwi *et al*., 1989). FAA has been shown to induce hemorrhagic necrosis similar to that induced by TNF-α. This observation pointed to a similarity in the mechanisms of both FAA and TNF-α (Ching *et al*., 1994 and Philpott *et al*., 1995).

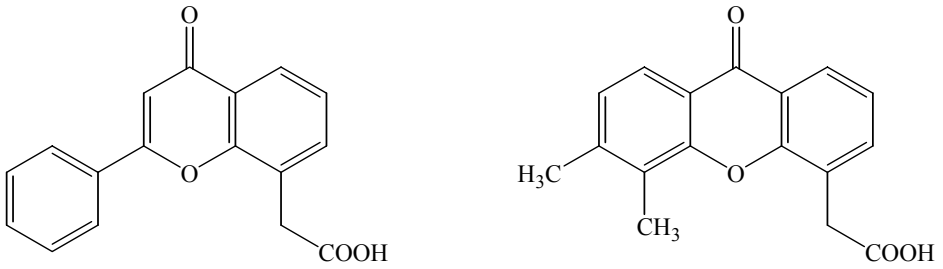

FAA DMXAA

Figure 2.13. Structures of Flavone Acetic Acid and 5,6-Dimethylxanthenone-4-Acetic Acid.

The Ching group and Philpott and coworkers were able to show role of TNF-α in flavone antitumor activity through the ability of antibodies to TNF-α to inhibit FAA-induced vascular collapse. Since tumor necrosis can be induced by clamping or ligation of the tumor-supplying blood vessels, or even by killing the mouse and maintaining the tumor at body temperature, the induction of tumor necrosis following treatment indicates cytotoxicity as a result of restricted blood flow (Denekamp *et al*., 1983; Zwi *et al*., 1989). The most promising flavone derivative; 5,6-dimethyl xanthenone-4 acetic acid (DMXAA), is currently undergoing clinical trial evaluation in combination with cytotoxic therapy, for the treatment of various malignancies by Cancer Research United Kingdom. FAA is also active and can easily be modified for synthesis of other potential derivatives. DMXAA which has emerged from this programme is 16 times more dose-potent than FAA (Baguley, 2003).

Tubulin Polymerization Strategy

Tubulin polymerization in endothelial cells can be inhibited, which results in rapid occlusion of the tumor vasculature, leading to vasculature shutdown (Hori K *et al*.,

1999, Nihei Y *et al*., 1999). The modulation of tubulin polymerization has been implicated as an important approach in pursuit of anti-tumor agents (Wilson & Jordan, 1995). Combretastatin A-4 and A-1 (figure 2.14) and numerous anti-mitotic compounds have been shown to have inhibitory activity to microtubule assembly (tubulin polymerization) by binding to the colchicine binding site. Although Taxol, epothilone and discodermolide (Figure 2.15) act as antimitotic drugs, they work through a different mechanism in that they stabilize microtubules and thus promote tubulin polymerization. However, the binding effects of many new combretastatin analogs on tubulin and the dynamics of the structural effects and conformational changes involved have not been elucidated.

The abundance of literature on colchicine and CA-4 has allowed synthesis of chemically modified CA-4 derivatives. Combretastatin A-4 (Lin *et al*., 1988; Hamel, 1988), podophyllotoxin (Jardin, 1980) and steganacin (Zavala *et al*.,(1980); Van der Eycken *et al*.,(1989) are some of the natural products that are known to bind to the same binding site as colchicine and their synthetic analogs inhibit tubulin polymerization (Sackett, 2002) (figures 2.15 & 2.16). Ligands binding in the colchicine binding site of tubulin represent an array of antimitotic agents that inhibit cancer cell proliferation. CA-4 ((*Z*)-1-(3-hydroxy,4-methoxyphenyl)-2-(3,4,5-trimethoxy phenyl)ethene), which was first isolated by Lin *et al*.,(1988), was found to be a potent cytotoxic agent that is active against multi-drug resistance cancer cells and is a powerful inhibitor of tubulin polymerization. Combretastatin A-4 is also able to elicit irreversible vascular shutdown within solid tumors, leaving normal vasculature intact (Gaukroger *et al.*, 2001).

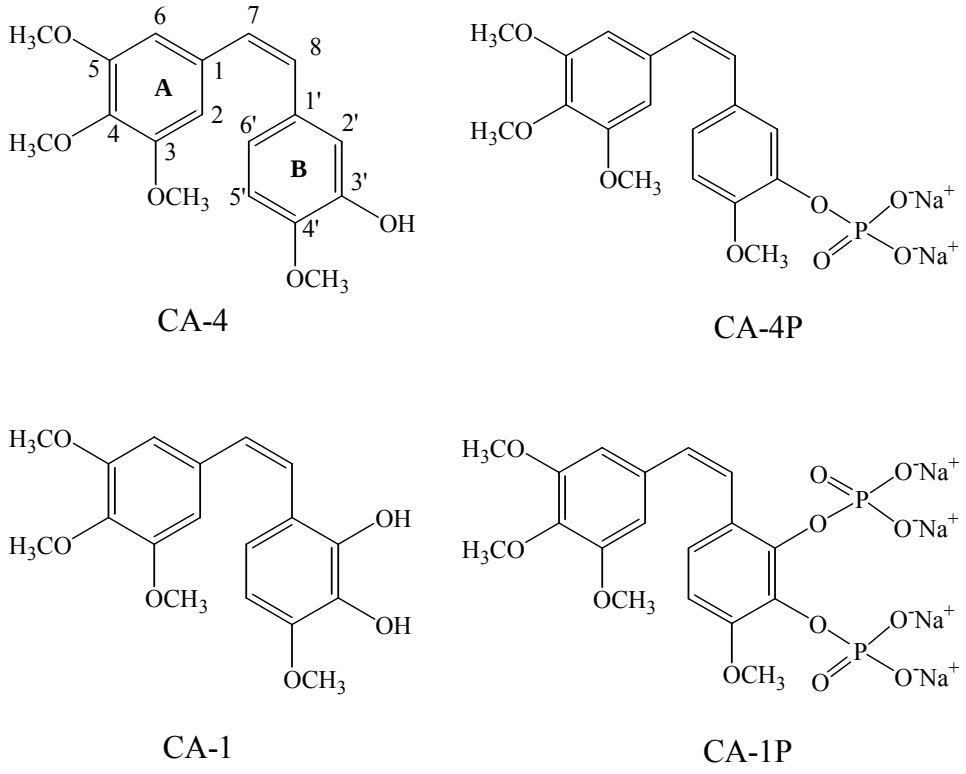

Figure 2.14. Structures of Combretastatin A-4 and A-1 and their Soluble Phosphate Salts.

Mechanism of Vascular Disruption

VDAs are known to cause rapid and selective shutdown of blood flow in tumors. CA-1 and CA-4 disodium phosphate are currently in preclinical and clinical development. In endothelial cells in culture, CA-4 causes fast re-organization of the actin cytoskeleton, which is mediated by disorganization of the tubulin cytoskeleton. An increase in vascular permeability is a key component of the mechanisms that lead to the shutdown of tumor blood flow by both classes of drugs (Hill *et al*., 1989; Rustin *et al*., 2003).

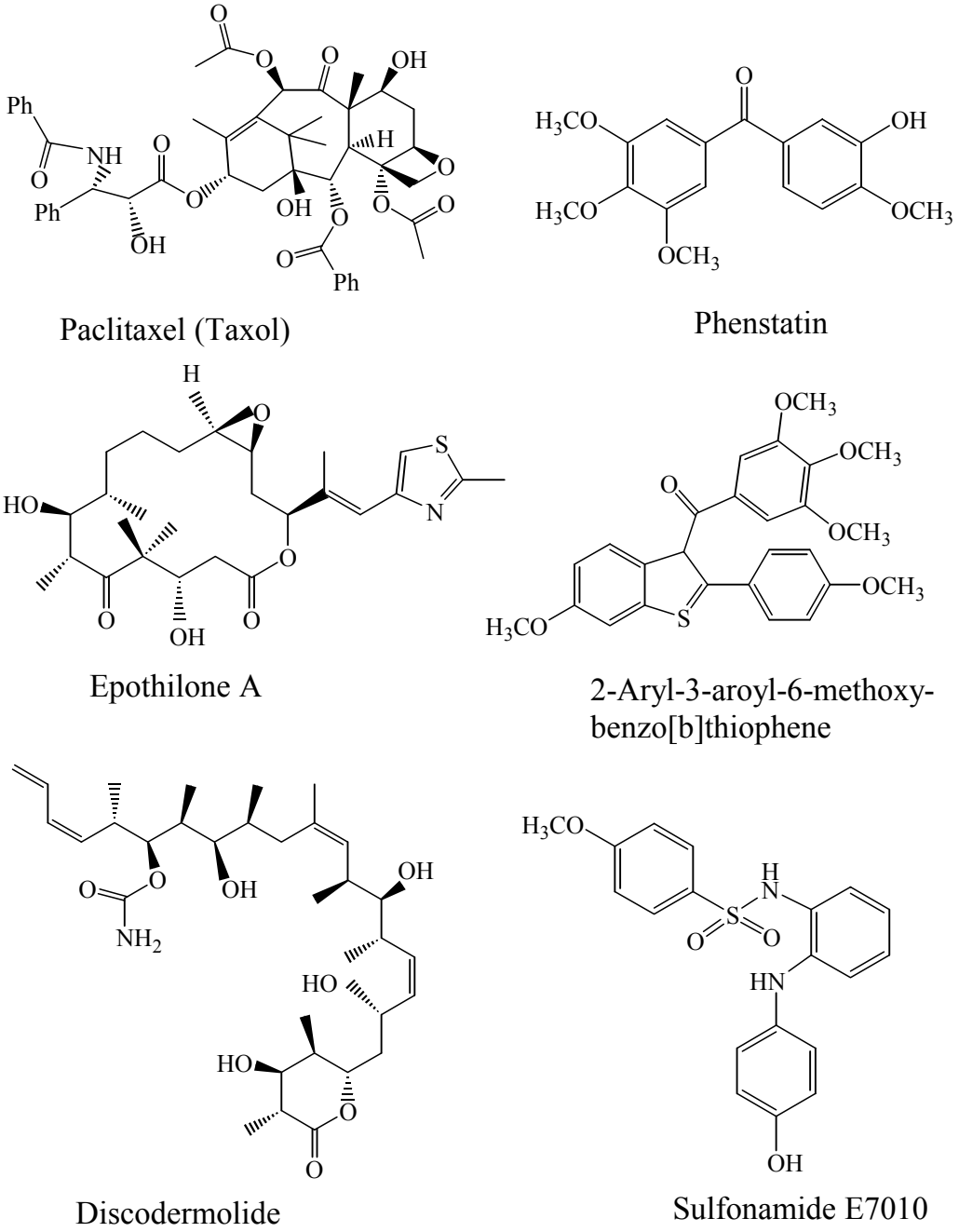

Figure 2.15. Some Natural and Synthetic Antimitotic Compounds that bind to Tubulin (Von Angerer, E., 2000; Pettit, G.R., *et al.,* 1998; Pinney, K.G. *et al.,* 1999, Hamel, E., 1999).

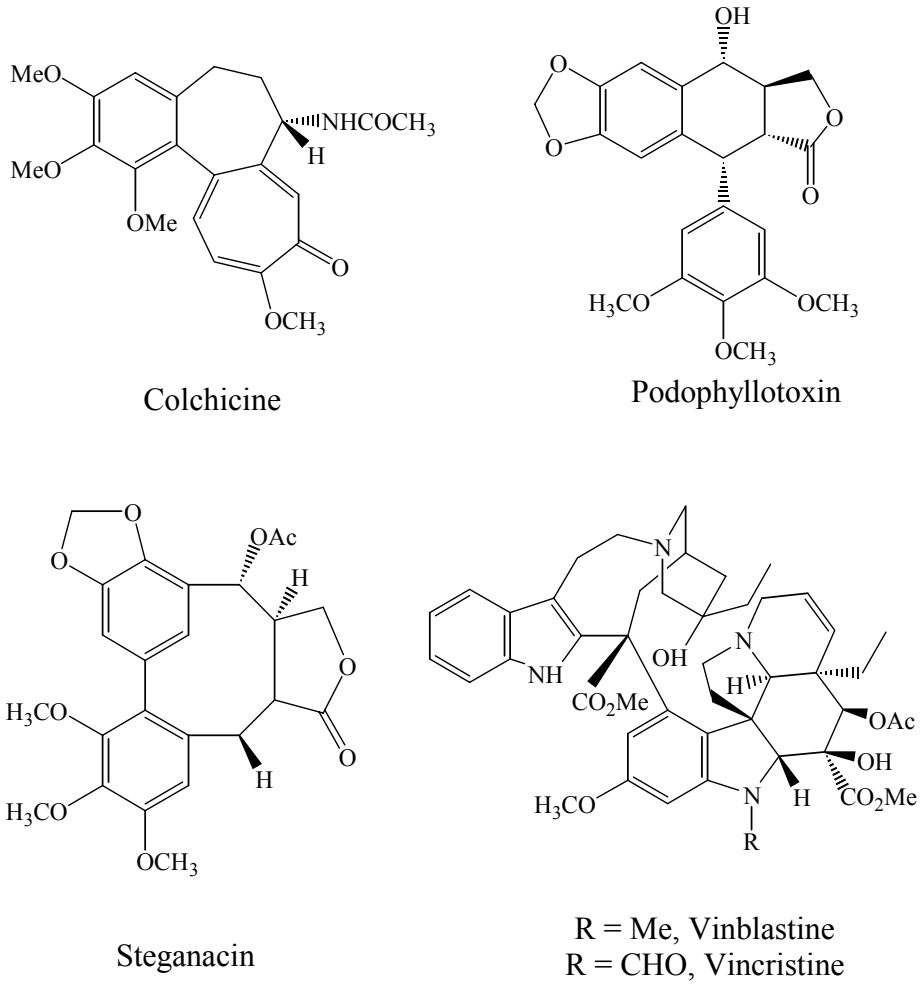

Figure 2.16. Structures of Some Compounds that Bind at the Colchicine Site on Tubulin (Lin *et al*., 1988; Hamel, 1988; Jardin, 1980; Zavala *et al*.,(1980); Van der Eycken *et al*.,(1989).

The basis for the susceptibility of the tumor vasculature to the VDAs that are currently in preclinical and clinical development is still unclear. However, it has been discovered that within various tumor types, increased susceptibility correlates with increased permeability of tumor vasculature (Nihei *et al*., 1999). Figure 2.17 shows the proposed effect of VDAs on endothelial cells, blood flow, and tumors. In (A), the tumor cells (blue) receive oxygen and nutrients through neovessel formed by a network of

endothelial cells. These endothelial cells are largely dependent on the tubulin cytoskeleton to maintain their shape. Mature endothelial cells depend on both on tubulin and actin. In (B), as the VDA enters the endothelial cells, it induces tubulin depolymerization, leading to the breakdown of cytoskeleton. Soon, endothelial cells start losing shape and begin rounding up, blocking the blood vessel and causing a reduction in blood flow. The tumor cells furthest from the neovessel become increasingly hypoxic (purple). The tubulin cytoskeleton continues degenerating in (C), causing the affected

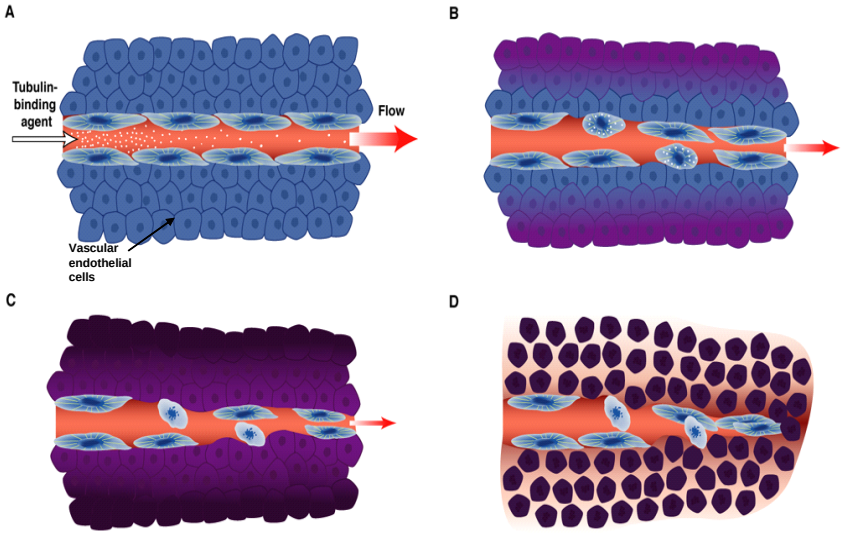

Figure 2.17. Proposed Molecular Mechanism of Action of Tubulin Binding Agents (Reproduced with permission from Siemann, D.W., 2002).

endothelial cells to break off and die, leading to more blockage of the only channel through the tumor. The blood vessels undergo necrosis as more tumor cells continue to die. Finally in (D), there is complete blood flow shutdown as the blood vessel is lost, causing necrosis of the tumor cells leading to the death of the tumor (Siemann, 2002).

Purpose of this Research

As a first step in the development of vascular disrupting agents, quantitative comparisons between new synthesized compounds and the already developed ones usually referred to as standards is very crucial. The purpose of this study was to characterize interactions of all newly synthesized combretastatin analogs with tubulin using the tubulin binding assay so as to provide a comprehensive overview of their effect on tubulin polymerization. A series of more than 78 combretastatin A-4 and A-1 analogs synthesized by Drs. Charles M. Garner, Robert R. Kane and Kevin G. Pinney (faculty members in the Department of Chemistry and Biochemistry at Baylor University) were assayed for their abilities to inhibit tubulin polymerization as part of a program to define the structure activity relationships between the substitutions on the combretastatin aryl ring systems and tubulin binding.

Structure-activity relationship analysis of the combretastatins has shown that the *cis* configuration of the stilbene unit is the most important factor for inhibition of cancer cell growth (Cushman *et al.*, 1992 and 1992). *E*- stilbenes show a dramatic decrease in their inhibitory effects on cancer cell growth and tubulin polymerization when compared to their corresponding *Z*-isomers, and in some cases the *cis* isomer is 10,000 times more potent than the *trans* isomer (Gaukroger *et al*., 2001).

The majority of studies on tubulin have been done using bovine brain tubulin. This is because calf brain tissue is the most abundant source of microtubules (Mandelkow *et al*., 1995). Tubulin is a labile molecule that converts from its αβ-tubulin microtubule polymerized state to a depolymerizing state within hours when place on ice. The tubulin extinction coefficient was 1.2 L $g^{-1}cm^{-1}$ at 278 nm (Harrison *et al.*, 1976) and 0.65 L g^{-1}

cm^{-1} at 255 nm respectively whereas the extinction coefficient for GTP was 12.17 x 10^3 and 7.66 x 10^3 M^{-1} cm^{-1} at 255 and 278 nm respectively. The molecular weight of the α,β-tubulin heterodimer was assumed to be 100 kDa.

Materials and Methods

General Section

All solutions were prepared with ultrapure water that had been filtered through a Corning 0.22 micron vacuum filter purchased from VWR. All chemicals and reagents were purchased from Sigma-Aldrich chemical company, USB chemicals, Acros chemicals and Fisher Scientific and were used as purchased. Hamilton syringes and needles used in serial dilutions and polymerization studies were obtained from Fisher Scientific. They were thoroughly cleaned in DMSO 99% before and after use. Polypropylene micro centrifuge tubes were used in all serial dilutions. All inhibition studies were carried out on an Agilent 8453 UV Spectrophotometer equipped with kinetics program software. UV micro quartz cuvettes were obtained from Starna Cells and were always cleaned with distilled water and dried with a jet of compressed nitrogen gas before and after use. All incubation steps were carried out on a Thermolyne type 16500 dry heater controlled at 30°C. The Neslab RTE 111M microprocessor controlled external circulating water bath and Lauda RM-6 external circulating water bath were programmed by scrolling through their active programs. Both water baths were equipped with Nalgene 550 silicone tubings and value plastic polypropylene reducers and tubing clamps. Laboratory grade ethylene glycol from Fisher Scientific was used to keep the baths at constant temperatures. ITC Hastelloy-C Cell Assemblies complete with cells

were purchased from Calorimetry Sciences Corporation and were always cleaned with distilled water and flashed with a stream of compressed nitrogen before use.

Preparation of Solution A

Solution A consisting of MES (0.1M) pH 6.4, EGTA (1mM), EDTA (0.1mM), $MgCl_2$, (1.0mM), 2-mercaptoethanol (1.0mM) and GTP (0.1mM) was prepared as follows. MES (acid component) (7.675 g, 0.036 moles) and MES (basic component) (13.9 g, 0.064 moles) were dissolved in ultra filtered water and the solution made up to 1.0 L. EGTA (0.3804 g, 1.0 mmol) and EDTA (37.2 mg, 0.1 mmol) were weighed and added to this MES buffer making stock solution A. Also $MgCl_2.6H_2O$ (0.2033 g, 1.0 mmol), was added to the buffer making stock solution A. On the day of each tubulin purification, to 35 mL of stock solution A was added 35 µL of 0.1M GTP for a final concentration of 0.1mM. Also (35 µL) of 2-mercaptoethanol (0.039 g, 1.0M) was added to solution A (35 mL) for a final concentration of 1.0mM.

Preparation of 10X Solution A

10X Solution A consisting of MES (1.0M) pH 6.4, EGTA (10mM), EDTA (1mM), $MgCl_2$ (10mM), 2-Mercaptoethanol (10.0mM), GTP (3.0mM) and ATP (0.01M) was prepared as follows. MES (acid component) (7.675 g, 0 .036 moles) and MES (basic component) (13.9 g, 0.064 moles) were dissolved in ultra distilled water (100mL). EGTA (0.3804 g, 1.0 mmol), EDTA (37.2 mg, 0.1 mmol), and $MgCl_2.6H_2O$ (0.2033 g, 1.0 mmol) were weighed and added to the buffer. ATP, GTP and 2-mercaptoethanol were added to the MES buffer on the day of tubulin preparation. To 5.0 mL of this stock solution A was added ATP (27.5 mg, 1.0 mmol), GTP (7.9 mg, 0.3 mmol) and 50 µL of 2-mercapto-ethanol (10.0 mM).

Preparation of Solution A + 4M Glycerol (0.5 L)

MES (acid component) (7.675 g, 0.036 moles) and MES (basic component) (13.9 g, 0.064 moles), pH 6.4 containing EGTA (0.19 g), EDTA (0.0186 g), $MgCl_2.6H_2O$ (0.10165 g), were mixed in 0.1 L of ultrapure water. To 50 mL of this stock solution was added Glycerol (d = 1.25 g/ml) (147.0 mL, 4.0M), 0.5 mL of 2-mercaptoethanol (1.0M) and 0.5 mL of GTP (100mM). All the compounds were dissolved in the MES solution and then made up to 500 mL with ultrapure water. The mixture was stirred thoroughly and after mixing, the solution was decanted into a plastic nalgene ware buffer bottle for storage until use. 2-Mercaptoethanol (0.5 mL, 1.0M) was prepared by transferring 35.0 µL it into a plastic micro centrifuge vial and adding water (0.465 mL), giving 0.5 mL of the solution. GTP (0.02616 g, 100.0 mmol) was dissolved in water (0.5 mL). Both GTP and 2-mercaptoethanol were added to the final solution (0.5 L) on the day of tubulin purification giving GTP (0.1mM) and 2-mercaptoethanol (0.1mM) respectively.

Preparation of Saline Solution (0.8% w/v):

Sodium chloride (8.0 g) was dissolved in ultrapure water (1.0 L) and stored in a refrigerator. This was used to keep the calf brains sterile while in transit from the slaughterhouse to the cold room in the purification laboratory.

Preparation of Glutamate (2.0M), pH 6.6

L-glutamic acid, sodium salt monohydrate (37.43 g) (USB chemicals) was dissolved in ultrapure filtered water (100 ml). The pH was adjusted to 6.6 by adding HCl (1.0M) dropwise while stirring and taking the pH readings on a Corning pH meter which had previously been calibrated with calibration buffers. For a glutamate (1.0M) solution, 10 ml of the stock (2.0M) were mixed with ultrapure water (10 ml). All solutions were

prepared with ultrapure deionized water which had been filtered through a corning 0.22 micron vacuum filter.

Preparation of GTP (0.1M)

Guanosine-5-triphosphate (13.075 mg) was dissolved in 250 µl of deionized water giving GTP (0.1M) solution. For inhibition of tubulin polymerization experiments, 50 µl of this GTP stock solution was dissolved in 450 µl of ultrapure deionized water giving a GTP (10.0mM) solution. Fresh GTP solution was prepared daily and was chilled on ice before running the polymerization experiments.

Dimethylsulfoxide (DMSO) 99.9%

Dry pure dimethylsulfoxide was used as solvent for combretastatin analogs whereas CA-1 and CA-4 diphosphate and aminohydrochloride salts were dissolved in water. However in some instances, the salts used were dissolved in DMSO especially for analog samples with low water solubility properties. The final concentration of DMSO in the reaction mixture was 4.0% v/v.

Preparation of CA-1 and CA-4 Ligand Solutions

Combretastatin A-1 and A-4 ligands were weighted using a Mettler Toledo AX microbalance with a readability of 0.01 mg. The ligands were dissolved in either dry pure DMSO (99.9%) or deionized water, giving 0.1M stock solutions. 10 µl of each combretastatin analog (0.1M) was then made to 1000 µl using DMSO or deionized water giving 1.0 mmol ligand solutions. 8 µl of each ligand solution (1.0 mmol) was added to the polymerization reaction mixture containing 184 µl of tubulin (1.0 mg/ml) in sodium glutamate (1.0M) and 8 µl of GTP (10mM) giving a total final volume of 200 µl. The

concentration of the ligand in this final reaction mixture was 40μM. The effect of this inhibitor concentration (40μM) on tubulin polymerization was investigated for each inhibitor. No further analysis was done on analogs that did not inhibit tubulin polymerization at this concentration. Those that did inhibit tubulin polymerization, 6-8 serial dilutions were carried out giving analog concentrations ranging from 1000 - 12.5 μM in DMSO. (8.0 μl) of each of these solutions gave a final concentration of 40 – 0.5 μM in a total volume of 200 μl.

CA-1 Diphosphate Dipotassium (OX16C) Samples

CA-1 diphosphate dipotassium samples which had previous been kept under controlled temperature and relative humidity conditions (25°C/60%RH and 40°C/75%RH), were analyzed for their effect on tubulin polymerization. As per the batch record of the CA-1P finished product manufactured samples, tromethamine (0.1M) had been used as a buffer before lyophilization of the samples. In addition, anhydrous lactose (50 mg/ml) had been used as the bulking agent. These prodrug samples had been formulated in lactose buffer and then freeze dried. Three samples in each set were analyzed in duplicate for their effect on tubulin polymerization. Each sample vial contained approximately 20 mg of CA-1P. A total of 14.0845 ml of water was used to dissolve the contents of each vial giving concentrations of 2.5 mmolar solutions. This amount of water was carefully delivered into the vials using a 10.0 ml sterile syringe. A standard pure sample of CA-1 was also provided by Oxigene Inc.

Tubulin Purification

Tubulin was purified from calf brain according to the method described by Hamel and Lin (1984)(Figure 2.18). The night before tubulin purification, the Ti-45 rotor and waring blender were cooled in a refrigerator. Fresh, warm bovine calf brains were received from the slaughterhouse and transported in approximately 0.5 L of ice-cold isotonic (0.8%) saline solution. In the cold room, blood vessels, meninges, blood clots, brain stems were removed by blotting the brain surface with paper towels, leaving only the gray and white matter. The brain sample was weighed and rinsed with more 0.8% saline.

The brain sample was homogenized in a precooled Waring blender at top speed for one minute in 0.75 mL/g of 4°C Solution A (0.1M MES pH 6.4, 1mM EGTA, 1mM $MgCl_2$, 1mM 2-mercaptoethanol, 0.1mM EDTA, 0.1mM GTP) containing 4M glycerol. Approximately 300 gm and 650 gm of brain tissue were used for one and two batch tubulin purification respectively. This amount of brain produced about 500 – 800 ml of homogenate and 150 – 320 ml of supernatant after centrifugation. The homogenate was aliquoted into six 70 ml polycarbonate centrifuge bottles and centrifuged using a precooled Ti-45 rotor and Beckman Coulter UltraCentrifuge at 2°C at 32,000 rpm for 1 hour. The cold Ti-45 rotor was then warmed with 80°C at water until its temperature had been raised to 37°C. The centrifuge was also warmed to 37°C.

The accumulated supernatant (156 ml) from single batch was then placed into a wide mouth jar and ATP (85.97 mg, 1.0 mmol) and GTP (24.49 mg, 0.3 mmol) were added. While incubating first batch, a second batch of brain homogenate was prepared and centrifuged at 2ºC as described previously. The resultant supernatant was pooled

together with that from the first batch, warmed to 37°C in a water bath, then incubated for 40 minutes, and then centrifuged at 37°C at 32,000 rpm for 1 hour. The supernatant (1.0 ml) was saved and labeled as first warm supernatant. Both the rotor and centrifuge were then cooled to 2°C.

Using disposable calibrated plastic pipettes to transfer the first warm pellet into Potter Elvehjem homogenizer, the first warm pellet was homogenized in a cold Potter-Elvehjem tissue homogenizer in 12 ml of 4°C solution A (cold depolymerization), starting with 0.5 ml in each tube. After homogenizing, the suspension was kept on ice for 30 minutes, and then centrifuged using precooled 10 ml centrifuge tubes and adapters in a Ti-45 rotor at 2°C for 30 minutes at 24,000 rpm. The cold pellet was then homogenized in 6 mL of 4°C solution A. The 2°C centrifugation and homogenization (with pellet in up to 8 ml solution A on the final extraction in order to have at least 35 mL after adding the glycerol in the next step), was repeated and then one more centrifugation at 2°C for 30 minutes at 24,000 rpm was done. Tubulin was expected to be in the cold supernatant. Using sterile pasteur pipettes, the supernatant was removed from the small tubes, pooled, and the cold pellet was collected and frozen at -70°C as MAPS.

To each 10 ml of pooled supernatant (approximately 27.5 ml by now for double batch) was added 12.1 ml of pure glycerol (4M), and 1.375 mL of the 10X MES buffer containing MES 1.0M, (pH 6.4), EGTA 10.0mM, $MgCl_2$ 10.0mM, 2-mercaptoethanol 10mM, and EDTA 1.0mM to maintain the concentrations of these components. In addition, ultra pure water (0.275 ml) was added to each 10 ml combined supernatant. Also, ATP (15.1 mg, 1 mmol) and GTP (4.32 mg, 0.3 mmol) were added for final concentrations of 1.0mM and 0.3mM respectively.

The rotor, adaptors and centrifuge were again warmed to 37°C. The mixture was incubated while stirring at 37°C for 1 hour (tubulin polymerization). The mixture was centrifuged at 37°C for 1 hour at 32,000 rpm. The rotor, adaptors and centrifuge were again cooled to 2°C. This warm supernatant (1.0 ml) was saved as second warm supernatant. The pellet was homogenized in 13.0 mL of solution A and the suspension was left on ice for 30 minutes. The suspension was centrifuged at 2°C for 30 minutes at 24,000 rpm. The cold pellet was set aside as MAP 1. The 16.1 ml of combined cold supernatant from this centrifugation which contained two-cycle microtubule protein was frozen in liquid nitrogen, and then stored overnight in a –70° freezer. This was the end of the first day.

High - Mes Tubulin Polymerization

On the second day, about 16.1 ml of the combined cold supernatant was thawed in a water bath to 25°C. The rotor, adaptors and centrifuge were warmed to 37°C. To this two-cycle microtubule protein was added 0.1M GTP (161 μL,) and 0.2M DTT (161 μL,) giving a final concentration of 1.0 mM GTP and 2.0 mM DTT respectively. Also solid, neutral basic MES (4.544 gm) and acid MES (0.71 gm) were added, giving 1.36M final concentration basic component and 0.242M acid component respectively. The mixture was incubated at 37°C for 1 hour and then centrifuged at 37°C for 1 hour at 39,000 rpm. The rotor adaptors and centrifuge were cooled to 2°C with ice. While maintaining the temperature at 37°C, the high MES supernatant was decanted, flash frozen in liquid nitrogen and then kept at -70°C. The pellet was homogenized in 8 ml of cold 1.0M sodium glutamate. The homogenate was left on ice for 2 hours, and then centrifuged at

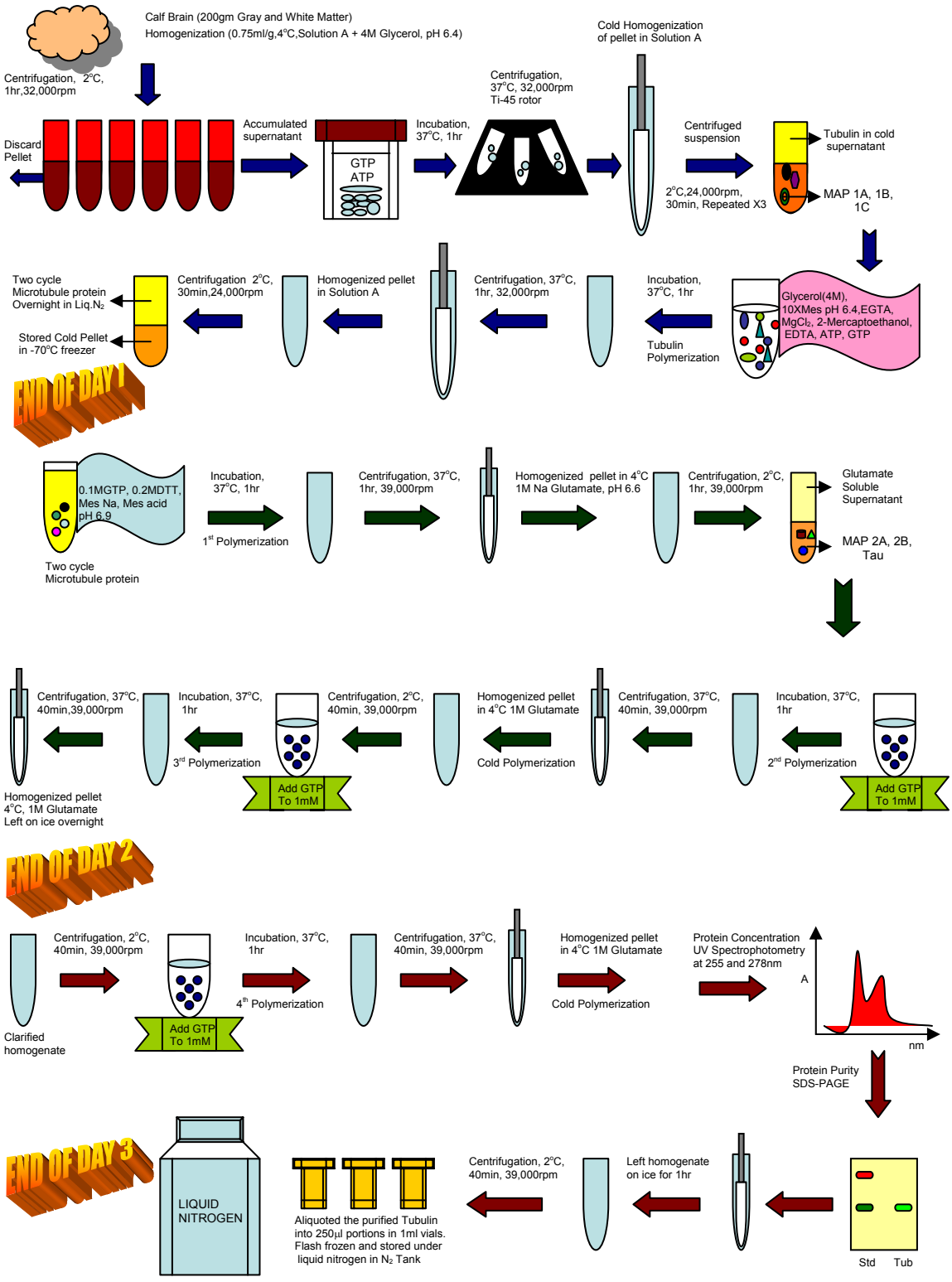

Figure 2.18. Tubulin Purification from Calf Brain. Purification Protocol was based on the procedure described by Hamel and Lin (1984). Drawn by Benon E. Mugabe, 2005.

2°C for 1 hour at 39,000 rpm. The rotor, adaptors and centrifuge were warmed to 37°C. The cold pellet (MAP 2), was kept in the freezer for future analysis.

Purification of the Tubulin Glutamate – Soluble Component

To the cold sodium glutamate soluble supernatant (6.0 ml) was added 0.1M GTP (60 μL) to a final GTP concentration of 1mM and incubated at 37°C for 1 hour (this was second polymerization and the solution turned milky in less than 5 minutes). The suspension was then centrifuged at 37°C for 40 minutes at 39,000 rpm. The rotor and centrifuge were then cooled to 2°C. While maintaining temperature of 37°C, the supernatant was decanted and stored. The pellet was homogenized in a cold Potter-Elvehjem tissue homogenizer in 4 ml of 4°C 1.0M glutamate (cold depolymerization), left on ice for 1 hour and the homogenate was clarified with a 40-minute 2°C centrifugation at 39,000 rpm. The pellet was saved in the freezer. The rotor, adaptors and centrifuge were warmed to 37°C. GTP (60 μL, 1.0 mmol) was added to the supernatant, the tube was rinsed with 0.5 ml of 1.0M glutamate and the mixture was incubated for 1 hour at 37°C (tubulin polymerization). A 40-minute 37°C centrifugation was done to recover polymerized tubulin (third polymerization). The pellet was homogenized in 4.5 ml of 4°C 1.0M glutamate, and left on ice overnight. This marked the end of day 2.

On the third day, the homogenate was clarified with a 40 minute 2°C centrifugation at 39,000 rpm. Once again, the pellet was saved. The rotor, adaptor and centrifuge were warmed to 37°C. 45 μl of GTP (0.1M) were added to the supernatant to bring it to 1.0mM GTP. A fourth tubulin polymerization was performed by incubating

the suspension for 1 hour at 37°C, and then recovering the tubulin with a 40 minutes 37°C 39,000 rpm centrifugation. The pellet was then homogenized in about 4.0 ml of 1.0M sodium glutamate at 4°C, giving a final concentration of about 9.55 mg/ml. The exact amount of 1.0M sodium glutamate added was determined after performing protein estimation by UV spectrophotometry. The homogenate was left on ice for 1 hour, and then, the combined homogenate was clarified as before with a 40-minute 2°C 39,000 rpm centrifugation. Another tubulin concentration determination was carried out to determine the exact final concentration of tubulin. The purified tubulin supernatant was then aliquoted, flash frozen and stored in liquid nitrogen in vials each containing about 2.5 mg of tubulin for polymerization assays and others containing 3.1 mg of tubulin for ITC experiments. The procedure used in this study was for research laboratory scale (about 4 - 5 brains per tubulin preparation) that yielded between 0.05 - 0.1 grams of purified tubulin per purification.

Determination of Tubulin Purity by SDS-PAGE

Tubulin purity was determined by SDS-PAGE and by its ability to polymerize. Following the SDS-PAGE protocol described by invitrogen, electrophoresis was performed on NuPAGE novex bis-tris gels using the XCell *Surelock*^{TM} mini-cell. To 40 µl of tubulin (10µM) was added 10 µL of NuPAGE® LDS sample buffer (4x) and 30 µL of deionized water giving a total volume of 80 µL. The mixture was centrifuged for 1 minute in a tabletop eppendorf centrifuge at 4.0^{o}C and was then heated at 70^{o}C for 10 minutes. 10 µL of both the tubulin mixture and the MultiMark multi-colored standard were loaded to the 12% precasted mini-gel. The upper and lower® buffer chambers of the electrophoretic tank were filled with 200 and 600 ml 1x NuPAGE® LDS running buffer

respectively. The gel was run at 200V constant for 35 minutes (Mes buffer) with a current of 100-125 mA/gel. The gels were stained using the SimplyBlue^{TM} SafeStain Microwave protocol for staining NuPAGE Gels. In this method, the gel was placed in 100 ml of ultrapure water and microwaved on high (950-1100 watts) for 1 minute. After shaking the gel on an orbital shaker, the water was discarded and the process was repeated twice. SimplyBlue^{TM} SafeStain (30.0 ml) was added and the gels were microwaved on high, then shaken on an orbital shaker for 10 minutes and the stain was discarded. The gels were then washed in 100 ml ultrapure water on an orbital shaker for 10 minutes. 20% NaCl (20 ml) was added and the gels were again shaken on an orbital shaker for 10 minutes. Protein bands with different mobilities were visualized against a protein standard consisting of 9 multi-colored protein bands in the range of 4 – 185 kDa using white light on a UV-illuminator. The gels were placed in ziplock polyethene bags and scanned using Photoshop 7.0 software.

Determination of Tubulin Concentration

Tubulin concentration was determined by two-component analysis (Barbier *et al.*, 1996) using U.V spectrophotometry and the absorption was measured at 278 and 255 nm and at the following extinction coefficients: for tubulin, 1.2 L $g^{-1}cm^{-1}$ at 278 nm (Harrison *et al.*, 1976) and 0.65 L g^{-1} cm^{-1} at 255 nm; for GTP, 7.66 x 10^3 and 12.17 x 10^3 M^{-1} cm^{-1} at 278 and 255 nm respectively. Using a Hamilton syringe, three 20 μL aliquots of the purified tubulin were diluted in a ratio of 1:20, by adding 380 μL of 1.0M glutamate solution. A 1:40 dilution of each of these protein solutions was made by taking 150 μL of the 1:20 dilution and adding 150 μl of 1.0M glutamate solution giving a final dilution factor of 40. The UV Spectrophotometer was blanked using 200 μL of cold

1.0M glutamate solution. Using the UV Spectrophotometer and 250 μL quartz cuvettes in a thermostated cuvette holder and a Lauda water bath at 8^{o}C to prevent polymerization of tubulin, the absorbance of each protein solution (200 μL) was measured at fixed wave lengths (255 and 278 nm) (Figure 2.2). A stream of nitrogen gas was held above the cuvette holder to remove any condensation that may occur on the sides of the cuvettes. Tubulin concentration was determined by using the following simultaneous equation:

$$\text{Absorbance at 278 nm} = 1.20X + 7.66Y$$

$$\text{Absorbance at 255 nm} = 0.65X + 12.17Y$$

Where : X = Concentration of Tubulin in mg/ml in the diluted sample; and

Y= Concentration of GTP in mg/ml in the diluted sample.

Inhibition of Tubulin Polymerization

Tubulin polymerization was induced in the presence of an organic acid (sodium glutamate) and GTP by a temperature jump to 30 ^{o}C according to the method of Verdier-Pinard *et al.*, (1998). Polymerization was followed turbidimetrically at 350 nm using a kinetics program in an Agilent 8453 spectrophotometer equipped with UV-visible ChemStation software, a jacketed cell holder, a Lauda RM-6 external circulating water bath and a Neslab TTE 111M microprocessor controlled external circulating water bath. Ethylene glycol (25 % v/v) in water was used as the cooling agent in both water baths. Figure 2.19 shows a summary of the protocol for the inhibition of tubulin polymerization. Purified tubulin (10.0 mg/ml) was removed from liquid nitrogen and thawed on ice for about 30 minutes. This stock tubulin was diluted to a concentration of 1.0 -1.2 mg/ml using 1.0 M sodium glutamate, pH 6.6. To ice chilled tubulin (1.0 mg/ml) in 1.0 M sodium glutamate, pH 6.6 (10μM) at 0 °C was added pure DMSO (4 % v/v final

concentration) for the control or 2.5 – 1000 μM of the analog to be analyzed in DMSO or in deionized water (DI), giving a final concentration of 0.1 – 40.0 μM of the analog in a total volume of 200 μl of reaction mixture. The mixture was incubated at 30 °C for 15 minutes on a Thermolyne type 16500 dry block heater in order to allow the analog to interact with tubulin and was then placed on ice at 0°C for another 15 minutes. 8 μl of 10 mM GTP (final concentration of 0.4 mM), was added to the reaction mixture on ice, mixed, and immediately transferred into a pre-cooled 250 μl micro quartz cuvette. A stream of nitrogen was used to prevent any condensation on the cuvette. The baseline was established at 350 nm at 0 °C and after 100 seconds, polymerization was initiated by a temperature jump to 30 °C. After 1500 seconds, the water bath was switched to the cold one at 0 °C to induce depolymerization. Turbidity (Absorbance) readings were recorded every 10 seconds.

Oxi-4503 Bioanalytical Method Development

The purpose of these experiments was threefold. First, the main aim of the experiment was to determine the effect of CA-1 diphosphate dipotassium (OX16C) (100 μM) on tubulin polymerization. Secondly, the effect of CA-1 diphosphate dipotassium (OX16C) (100 μM) in presence of CA-1 (1.0. 2.0, 2.5 and 5.0 μM) on tubulin polymerization was determined. Thirdly, the effect of controlled temperature and relative humidity (RH) conditions on the stability of CA-1 diphosphate dipotassium prodrug was evaluated. Tubulin polymerization was induced in the presence of an organic acid (sodium glutamate) and GTP by a temperature jump to 30^{o}C according to the method of Verdier-Pinard *et al*., (1998). Polymerization was followed turbidimetrically at 350 nm using a kinetics program on an Agilent 8453

spectrophotometer equipped with UV-visible ChemStation software, a jacketed cell holder, a Lauda RM-6 external circulating water bath and a Neslab TTE 111M microprocessor controlled external circulating water bath. CA-1 diphosphate dipotassium (20 mg, 2.5 mmol) was dissolved in distilled water (14.0845 ml). 8.0 µl of this solution gave a final concentration of 100µM in a 200 µl reaction mixture.

To ice chilled tubulin (1.0 mg/ml) (184.0 ml) in 1.0 M sodium glutamate, pH 6.6, was added pure distilled water (8.0 µl) for the control or (8.0 µl) solution of CA-1 diphosphate dipotassium (2.5 mmoles) giving a final concentration of 100.0 µM or solutions of CA-1 diphosphate dipotassium (2.5 mmol) containing CA-1 (25.0, 50, 62.5 and 125.0 µM in DMSO), (8.0 µl) giving a final concentration of 100.0 µM (OX16C) containing 1.0, 2.0, 2.5 and 5.0 µM in a total volume of 200 µl of reaction mixture respectively. To CA-1 diphosphate dipotassium samples which had previous been kept under controlled temperature and relative humidity conditions (25°C/60%RH and 40°C/75%RH), a total of 14.0845 ml of water was used to dissolve the contents of each vial giving concentrations of 2.5 mM solutions. This amount of water was carefully delivered into the vials using a 10.0 ml sterile syringe. 8 µl of each of these solutions were added to tubulin as described above. The various mixtures were incubated at 30°C on a Thermolyne type 16500 dry block heater for 15 minutes and cooled at 0°C on ice for 15 minutes. An aliquot of 10 mM GTP (final concentration of 0.4 mM), was added to the reaction mixture on ice, mixed, and immediately transferred into a pre-cooled 250 µl micro quartz cuvette. A stream of nitrogen was used to prevent any condensation on the cuvette. The baseline was established at 350 nm at 0°C and after 100 seconds,

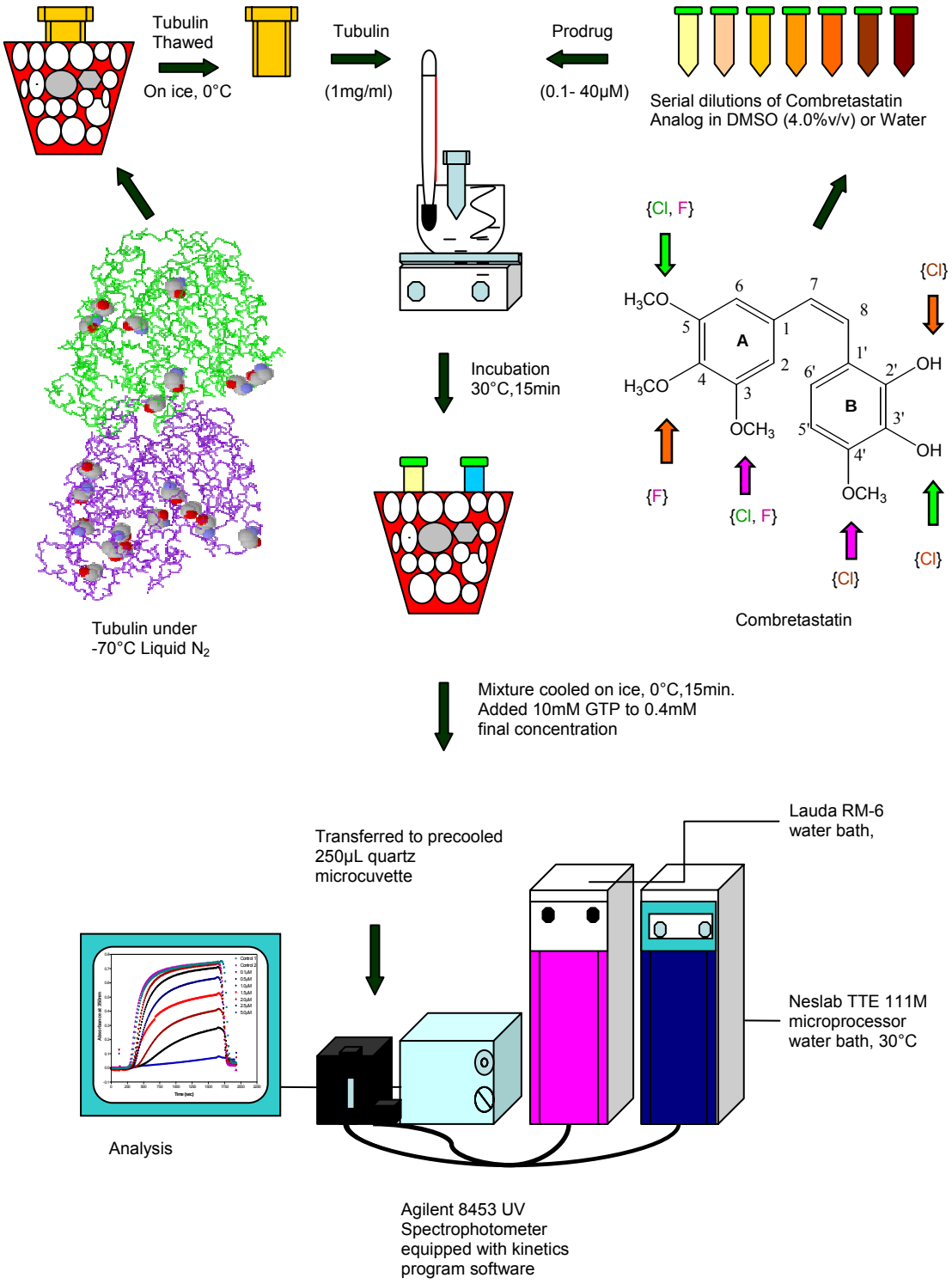

Figure 2.19. Determination of IC_{50} values of Combretastatin Analogs. Drawn by Benon E. Mugabe.

polymerization was initiated by a temperature jump to 30°C. After 1500 seconds, the cold water bath at 0 °C was used to induce depolymerization. Turbidity (Absorbance) readings were recorded after every 10 seconds.

Data Analysis

The absorbances at 350 nm representing the extent of tubulin polymerization in each reaction mixture for every compound were plotted against time in seconds. Data analysis was performed by nonlinear regression analysis using the Prism software (GraphPad). IC_{50}, Hillslopes, R^2 and log IC_{50} values of the various analogs were determined from plots of percent polymerization against log concentration of the combretastatin analogs using the following one site competition equation:

$$Y = Y_B + \frac{(Y_T - Y_B)}{1 + 10^{(X\text{-}LogIC_{50})Hillslope}}$$

Where: X = Log concentration of the binding ligand, Y = Percent polymerization, Y_B = percent polymerization at the bottom plateau, Y_T = percent polymerization at the top plateau. IC_{50} was the X value obtained when tubulin polymerization was halfway between Y_T and Y_B. It was the concentration of the analog that inhibited tubulin polymerization in the reaction mixture by 50 % (IC_{50} value).

The variable Hillslope describes the steepness of the curve. If it is positive, the curve increases as X increases. If it is negative, the curve decreases as X increases. A standard competitive binding curve that follows the law of mass action has a slope of -1.0. If the slope factor is far from 1.0, then the binding does not follow the law of mass action with a single site.

In addition, column scatter graphs of absorbance at 350 nm against the concentration of the inhibitor in each reaction mixture were plotted and are hereby represented as insets in plots of percent polymerization against log concentration of the combretastatin analogs. It should be noted that in these column scatter graphs (insets), the horizontal position of each symbol has no quantitative meaning except that the symbols have been nudged to the column center to avoid overlap.

Results and Discussion

Tubulin Purification and Concentration

Tubulin was purified by a series of five cycles of cold and warm polymerization and centrifugation steps using a modified procedure described by Hamel and Lin *et al.,* 1984). Figure 2.20 shows a graph of tubulin protein estimation using the two-component UV- Spectrophotometric method.

Data analysis showed that both the 20- and 40-fold dilutions of the purified tubulin had the same concentration in the original stock solution. Whenever tubulin was purified using two batches of calf brain, between 48.0 - 98.3 mg (wet weight) of pure tubulin protein per purification were obtained. However, significant losses of tubulin through transfer from one apparatus to another can not be ruled out. Alternative methods of tubulin purification include ion-exchange chromatography. However, the tubulin obtained by the procedure we used is practically well suited for the tubulin polymerization assay.

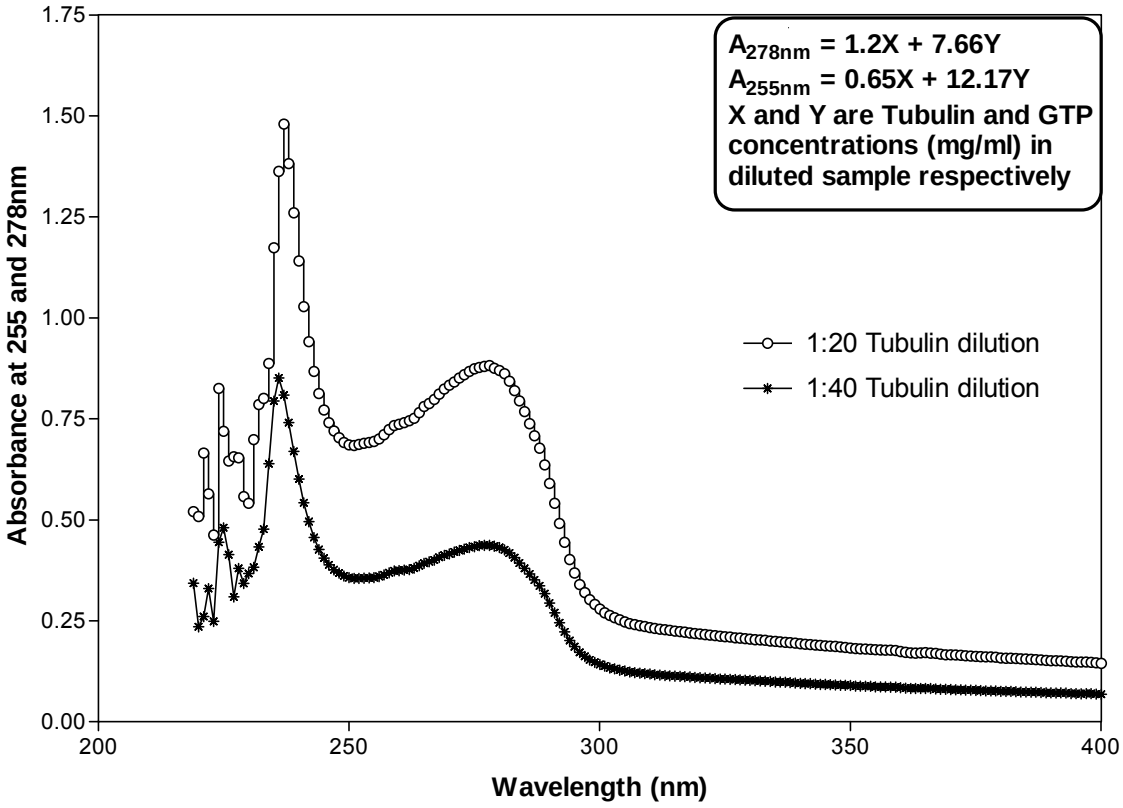

Figure 2.20. Determination of tubulin concentration at 255 and 278nm by UV spectrophotometry.

Tubulin Purity by SDS-PAGE

Electrophoresis is based on the migration of proteins in a charged field. The technique separates proteins by charge and size, with the largest protein moving least. Various proteins have discrete and defined charge properties based on the content of the different types of charged amino acid residues especially aspartic acid, glutamic acid, histidine, lysine and arginine within its structure.

The rate of particle migration is determined by the net charge density which is charge per unit mass, the voltage potential, the viscosity of the medium and the frictional coefficient of the particles which is also related to the shape of its structure. Sodium dodecyl sulfate (lauryl sulfate) which is amphiphillic in nature coats the protein chain and

gives it a uniform negative charge. The separation on polyacrylamide gels is based on the log molecular weight of the protein for most globular proteins.

The purity of tubulin from calf brain was determined using polyacrylamide gel electrophoresis which was performed using the analytical method described by Invitrogen life technologies. Figure 2.21 shows polyacrylamide gel electrophoresis results for a sample of purified tubulin. Tubulin purity was estimated to be greater than 99 % since no contaminating protein bands were visible, even at the highest loading as visualized by PAGE.

The tubulin samples exhibited same mobilities and the closely related α- and β-tubulin subunits are seen as a single band with an approximate molecular weight of 50 kDa. The high purity of the purified tubulin was also confirmed by its ability to polymerize into stable microtubules at 30°C in presence of glutamate and GTP and in absence of MAPs. These microtubules retained their inherent characteristic of depolymerizing into tubulin monomers upon switching the temperature of the reaction mixtures to 0°C. In addition, the ability of the purified tubulin to bind colchicine and other synthetic combretastatin analogs was further confirmation of the purity of the protein.

Stimulation of Endothelial Cell Signaling by CA-4P

In established tumor vasculature, endothelial cells undergo various tissue specific changes forming functionally differentiated blood vessels, processes that involve the endothelial cells responding to numerous extracellular signals. The key molecules

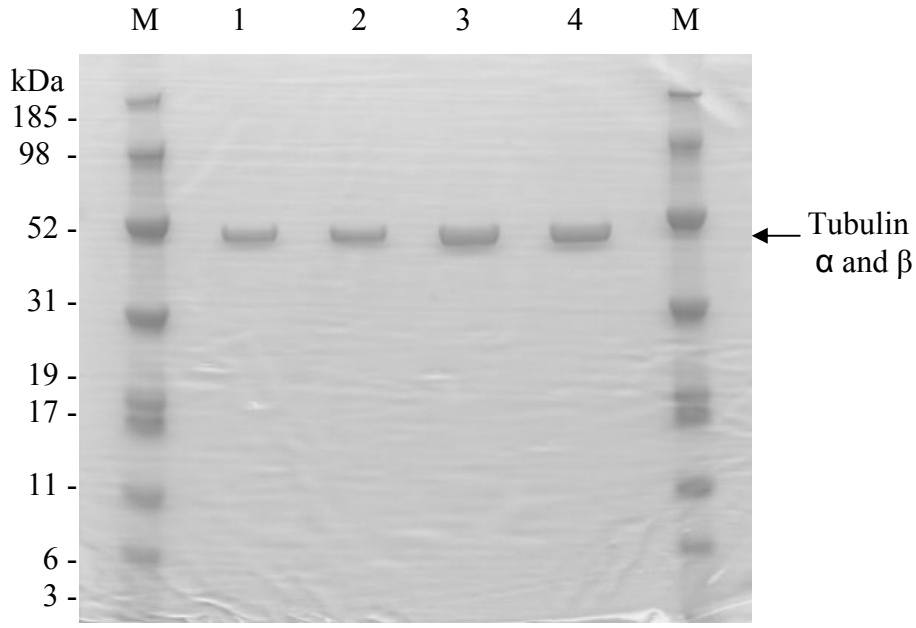

Figure 2.21. SDS-PAGE Analysis of Five Cycle Purified Tubulin. M, MultiMark® multi-colored standard, Lane 1,10 µL of purified tubulin (0.25mg/ml), Lane 2,10 µL of purified tubulin (0.25mg/ml), Lane 3,10 µL of purified tubulin (0.5mg/ml), Lane 4,10 µL of purified tubulin 0.5mg/ml). The MultiMark® multi-colored standard included proteins insulin, aprotinin, lysozyme, myoglobin blue, myoglobin red, carbonic anhydrase, glutamic dehydrogenase, phosphorylase B and myosin of sizes of 3, 6, 11,17, 19, 31, 52, 98 and 185 kDa respectively.

involved in this process are the vascular endothelial growth factor, angiopoietin and ephrin (Endo *et al*., 2002). VEGF is a very important growth factor for therapeutic angiogenesis. However the proliferation and permeability of endothelial cells coordinated by the VEGF may produce unwanted tumor angiogenesis (Chae *et al*., 2000). Signaling pathways associated with CA-4P and their effects on permeability involve the small GTPase Rho and Rho kinase, as well as stress-activated protein kinase 2 (SAPK2). The signaling processes that control vascular permeability in endothelial cells are highly complex and their modulation varies under different stimulatory conditions. Endothelial-cell signaling following exposure to CA-4P has been investigated (Kanthou *et al.,* 2002).

The small GTPase Rho and Rho kinase are key components of a CA-4P signaling pathway (Figure 2.22).

Myosin light chain (MLC) is phosphorylated within minutes of drug exposure, which accounts for the contractility of actinomyosin and the formation of focal adhesions within the endothelial cells. Within minutes of exposure to CA-4P, MLCK inhibitors increase the frequency of blebbing in endothelial cells without inhibiting the phosphorylation of MLC (Kanthou *et al.,* 2002). Microtubule disruption seems to be the triggering factor for these Rho-mediated signaling events, and similar conclusions have been made regarding other VTAs like nocodazole, vincristine and vinblastine (Verin *et al*., 2001). However, the mechanisms involved in the activation of Rho by microtubule-disruption are not clearly understood. Some guanine exchange factors seem to interact with microtubules, indicating a possible link between microtubule dynamics and Rho activation (Nakanashi *et al*., 2005). The colchicine induced depolymerization of microtubules activates the small GTPase RhoA which is believed to be the intracellular coordinator of the cytoskeleton rearrangement of microtubules and actin (Zheng, Y., 2004). RhoA-GDP is then activated by guanosine nucleotide exchange factors (GEFs) that generally promote the GTP nucleotide exchange. Microtubule depolymerization activates RhoA and binding to microtubules inhibits several proteins in the cytoskeleton. For example, GEF-H1 is inhibited by binding to microtubules but is reactivated by RhoA upon dissociation (Krendel *et al*., 2002). RhoA-GTP in turn activates a number of down

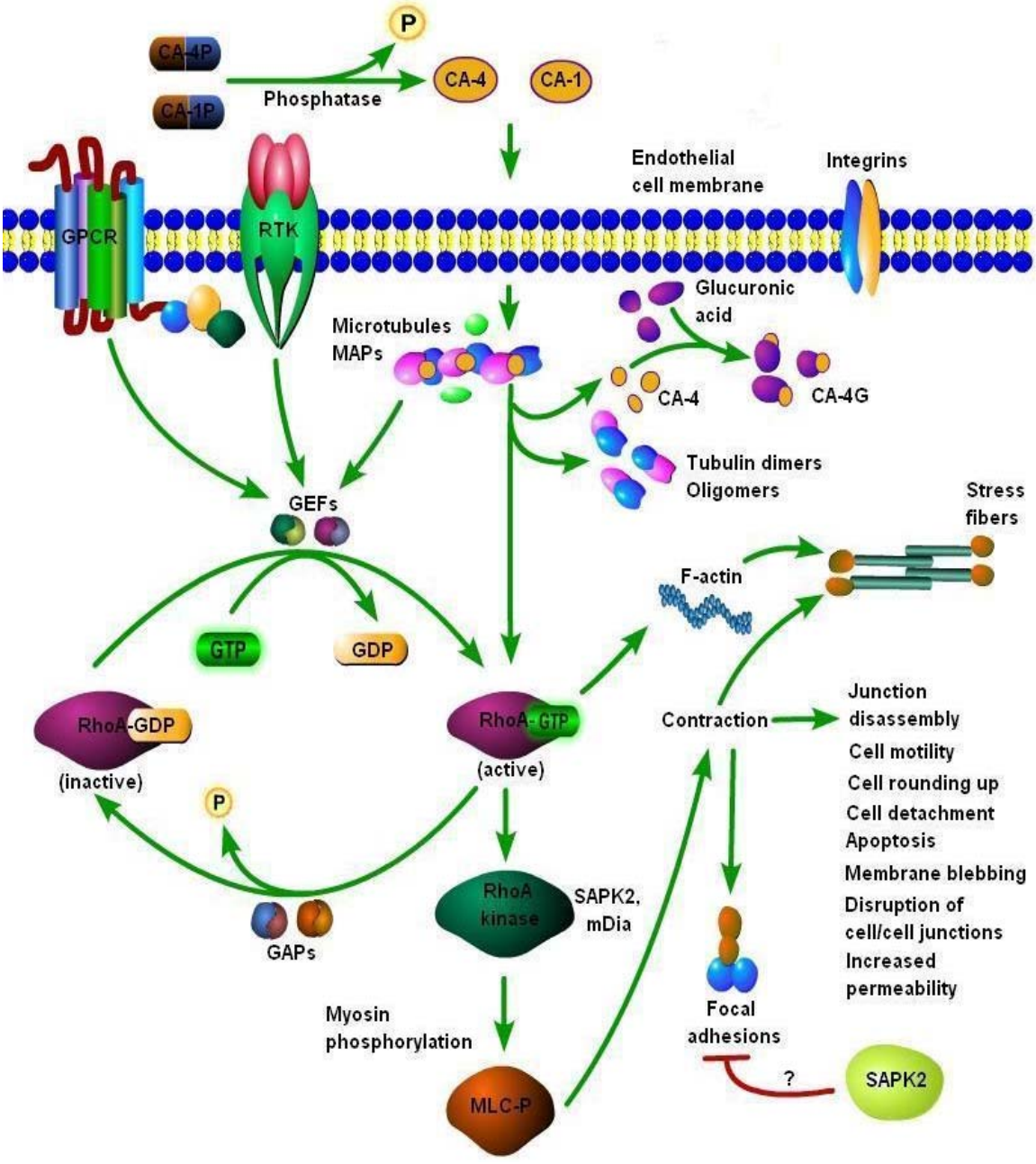

Figure 2.22. Proposed Molecular Mechanism of Endothelial-Cell Signaling Pathways by CA-4P. Produced and drawn by Benon E. Mugabe using Pathway Buider Tool 1.0.

stream effectors including RhoA kinase which is able to phosphorylate myosin resulting in increased actinomyosin contractility. Blebbing is considered as the extreme consequence of CA-4P-mediated disruption of interphase microtubules. Blebbing is also an early indication of rapid cell necrosis separate from the apoptotic pathway which is associated with the interference of mitotic-spindle formation (Tozer *et al.,* 2005). It is also another indication of continued breakdown of the endothelium.

Several anti-angiogenic anticancer agents currently in clinical trials target the activity of VEGF. Some small-molecule VEGF-receptor-tyrosine-kinase inhibitors that have different inhibitory profiles are now in clinical trials. VEGF acts as a survival factor for endothelial cells and its withdrawal can cause vascular damage (Abramovitch *et al.,* 1999; Tozer *et al.,* 2005). Inhibition of VEGF has become a possible target for drug development to block angiogenesis and definitely targeting VEGF signaling pathway will prove to be of vital importance in cancer chemotherapy in future.

*Effect of Colchicine (**1**) and CA-4 (**2**) on Tubulin Polymerization*

The effect of natural product *colchicine* **(1)** (Figure 2.23) on tubulin polymerization at 30ºC was investigated (Figure 2.24). Colchicine **(1)** inhibited tubulin polymerization with an IC_{50} value of 1.4 μM (Figure 2.25). The binding of colchicine to tubulin induces a conformational change in the structure of the protein upon binding and this association is characterized by inhibition of assembly into microtubules. Two mechanisms account for the substoichiometric inhibition of tubulin polymerization into microtubules. Firstly, it has been postulated that direct binding of colchicine is at the free ends of the microtubules, with tubulin molecules at the free end of the microtubule

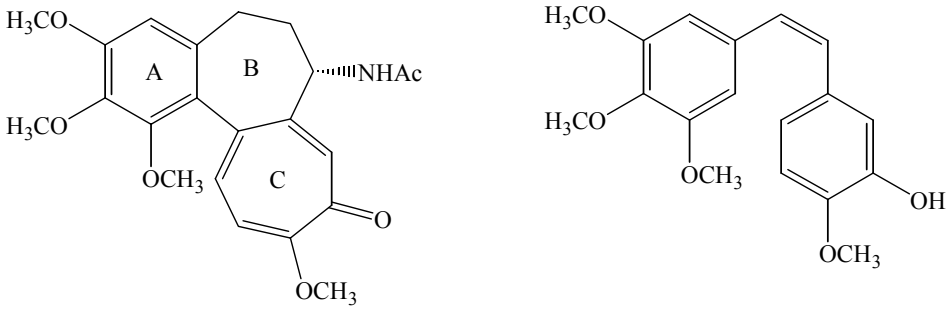

1 **2**

Figure 2.23. Structures of Colchicine (**1**) and Combretastatin A-4 (**2**).

having higher affinity for colchicine than soluble tubulin. This would subsequently lead to colchicine being liganded at the microtubule ends and the unassembled α,β-subunits could also remain unliganded. Secondly, the tubulin-colchicine complex could also bind at the free end of microtubules, thereby blocking the assembly of microtubules with the right orientation (Perez-Ramirez *et al.*, 1996).

(Z)-1-(3'-Hydroxy, 4'-methoxyphenyl)-2-(3",4",5"-trimethoxyphenyl)-ethene **(2)** CA-4 (Figure 2.23) is a well known tubulin–binding agent originally isolated from the South Africa shrub *Combretum caffrum*. A water soluble phosphate prodrug (CA-4P) has been synthesized in order to increase the bioavailability of CA-4. This water soluble phosphate prodrug is rapidly hydrolyzed by endogenous phosphatases *in vivo* producing the parent drug. CA-4 (**2**), a potent cytotoxic agent that is active against a range of multidrug resistant cancer cells, showed total inhibition of tubulin polymerization (Figure 2.26) with an IC_{50} value of 1.2 μM (Figure 2.27).

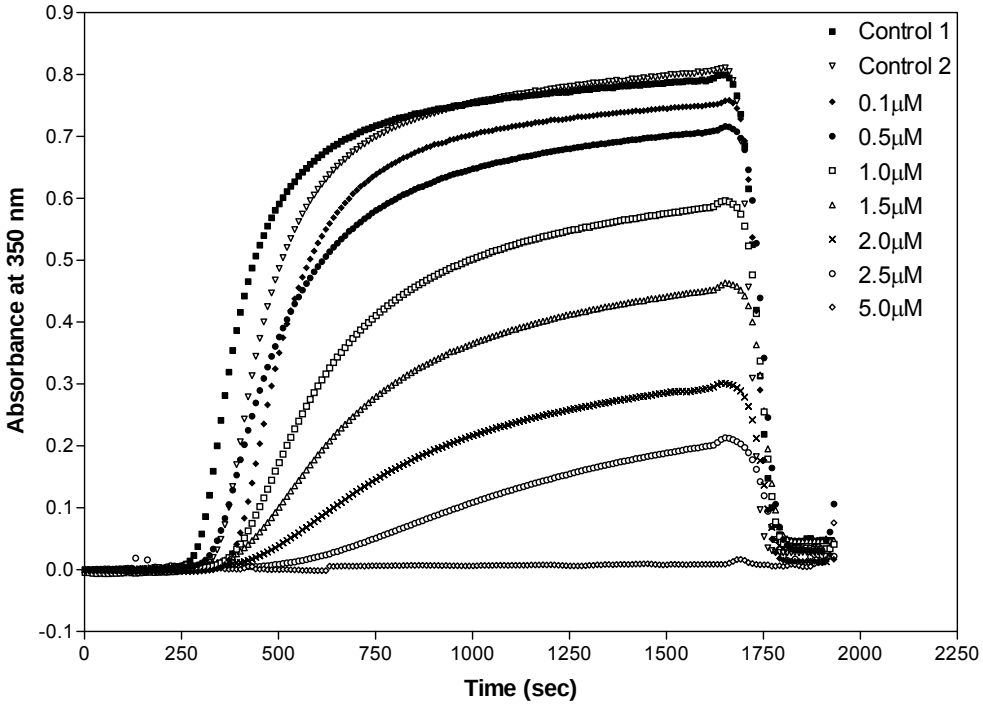

Figure 2.24. Inhibition of Tubulin Polymerization by Colchicine at 30ºC.

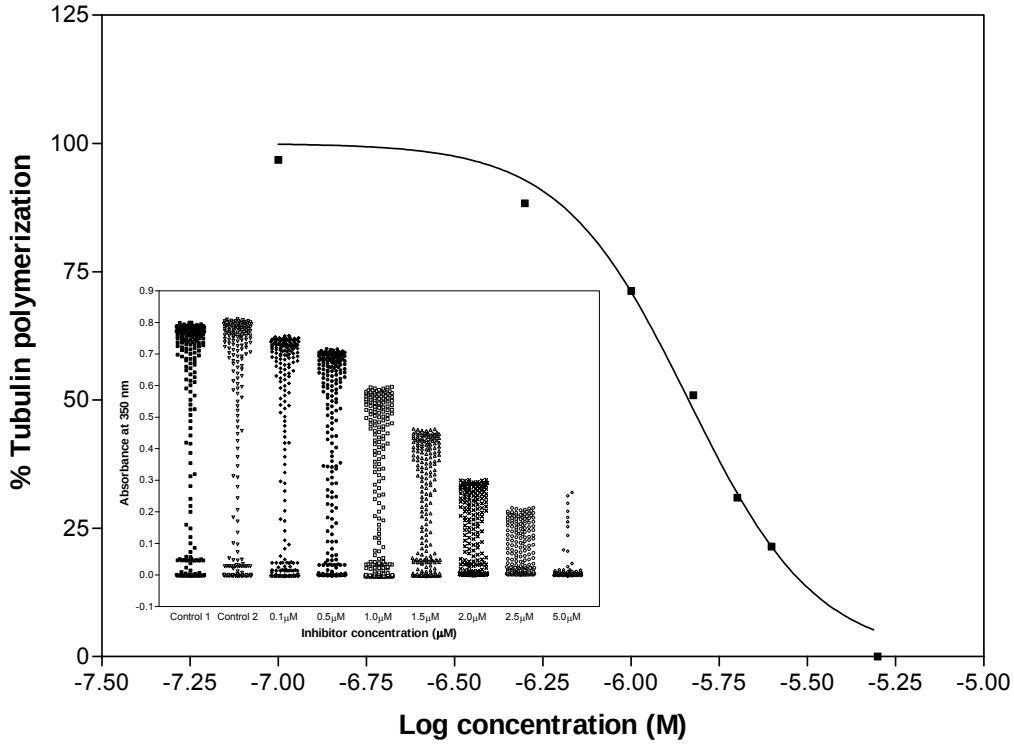

Figure 2.25. Percent Tubulin Polymerization against Log Concentration of Colchicine.

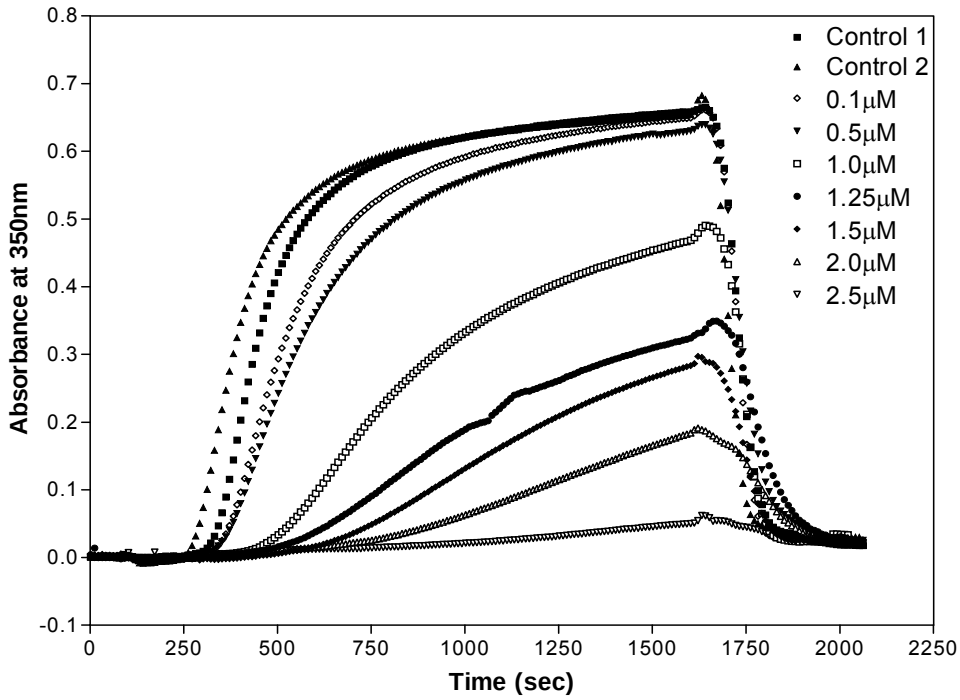

Figure 2.26. Inhibition of Tubulin Polymerization by CA-4 at 30ºC.

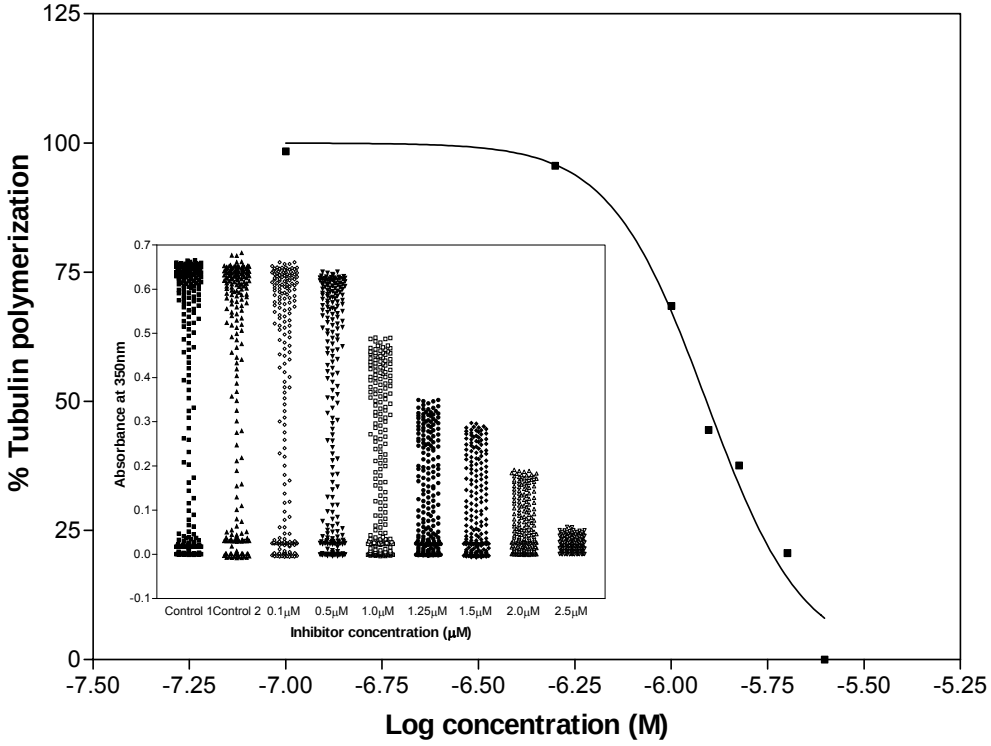

Figure 2.27. Percent Tubulin Polymerization against Log Concentration of CA-4.

*Effect of CA-1 (**3**) and CA-1 Dipotassium diphosphate on Tubulin Polymerization*

(Z)-1-(2',3'-Dihydroxy-4'-methoxyphenyl)-2-(3'',4'',5''-trimethoxyphenyl)-ethene **(3)** (Figure 2.28), was also evaluated for inhibition of tubulin polymerization at 30ºC (Figure 2.29). This stilbene proved to be a cytotoxic tubulin polymerization inhibitor (IC_{50} = 1.9 μM) with potency comparable to that of colchicine and CA-4 (Figure 2.30).

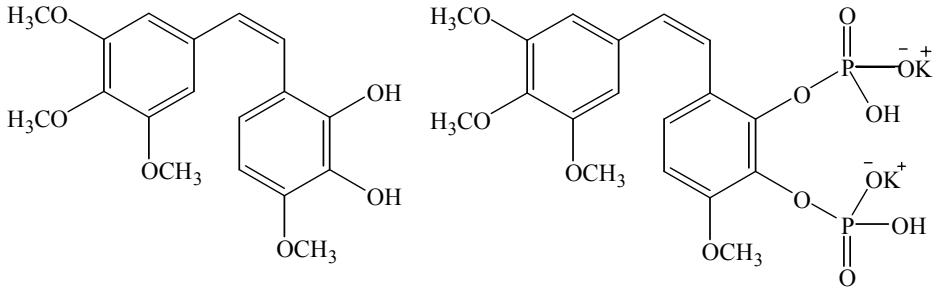

3 **4**

Figure 2.28. Structures of CA-1 (**3**) and CA-1 dipotassium phosphate (**4**).

(Z)-1-(4'-Methoxy-2',3'-dipotassiumphosphate)phenyl)-2-(3'',4'',5''-trimethoxyphenyl)-ethene **(4)** (Figure 2.28), a di-potassium water soluble derivative of CA-1, was analyzed for tubulin polymerization. This dipotassium phosphate salt of CA-1 did not inhibit tubulin polymerization but rather seemed to enhance formation of stable microtubules. CA-1P has been developed as a water-soluble derivative of CA-1. When a comparison was made with the clinically active CA-4 phosphate, CA-1P produced more tumor growth delays than the CA-4 analog at a dose of 50 mg/kg whereas the CA-4P produced no measurable growth delay until a dose of 150 mg/kg was administered in mice (Holwell *et al*., 2002).

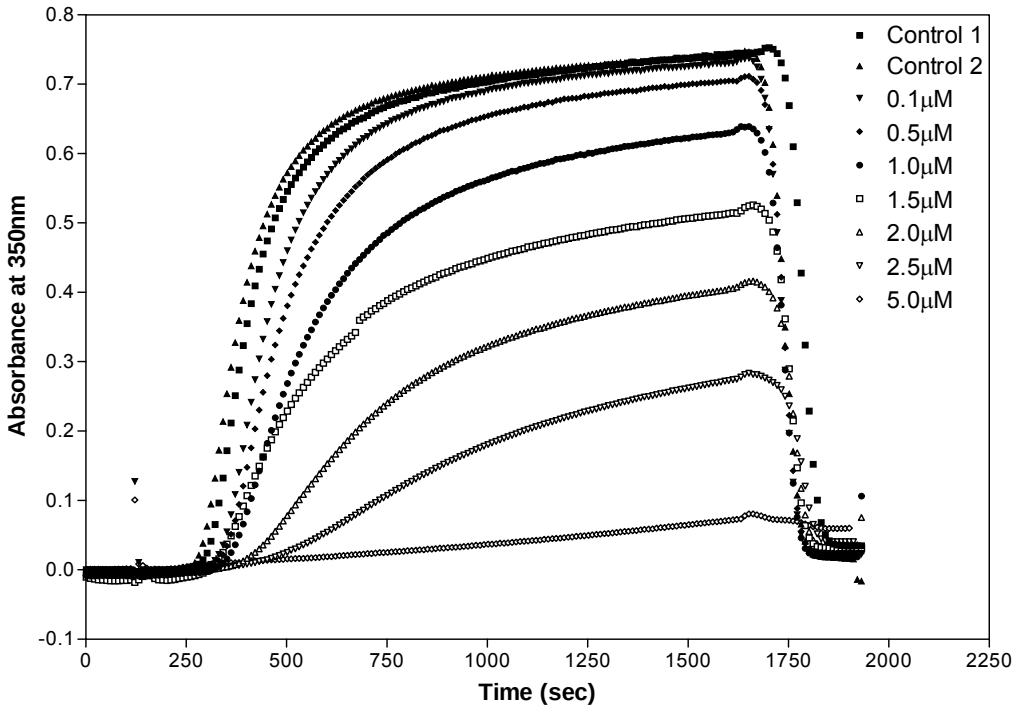

Figure 2.29. Inhibition of Tubulin Polymerization by CA-1 **(3)** at 30ºC.

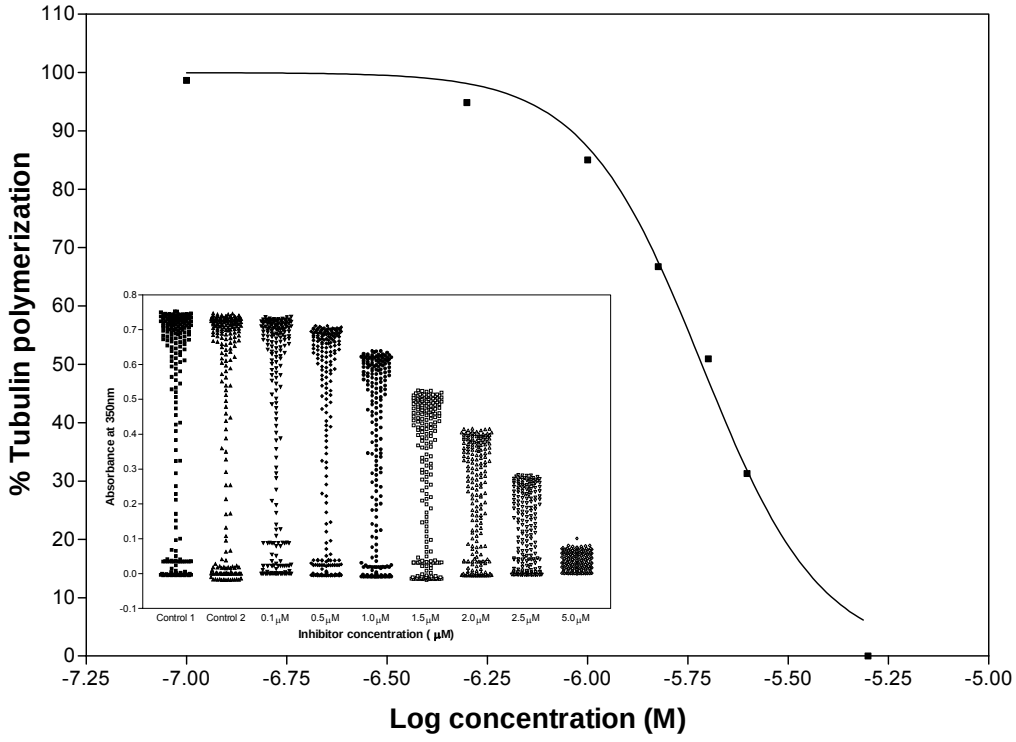

Figure 2.30. Percent Tubulin Polymerization against Log Concentration of CA-1.

Combretastatin A-1 phosphate causes very severe hemorrhagic necrosis in the tumor tissue and tumor death within 24 hours of treatment. The mechanism of action of CA-1 phosphate is almost similar to the CA-4 phosphate in that tumor vascular shutdown occurs within 4 hours of treatment. CA-1P developed as OXi4503 has been found to induce the shutdown of tumor blood vessels in a dose-dependent pattern with an ED_{50} at 3 mg/kg in contrast to 43 mg/kg of CA-4P (Hua *et al*., 2003). Thus, it has been proposed that CA-1 phosphate, the water-soluble analog of CA-1, is more potent against vascularised murine colon tumors than its predecessor CA-4 phosphate.

*Effect of Compounds **5** and **6** on Tubulin Polymerization*

In an effort to determine the importance of 3-hydroxyl and 4-methoxy groups in inhibition of tubulin polymerization, *(Z)-1-(4'-Hydroxy-3'-methoxyphenyl)-2-(3",4",5"-trimethoxyphenyl)-ethene* **(5)** and its di-sodium phosphate salt *(Z)-1-(3'-Methoxy- 4'-disodiumphosphate)phenyl)-2-(3",4",5"-trimethoxyphenyl)-ethene* **(6)** (Figure 2.31) in which the positions of the hydroxyl and methoxy groups had been reversed, were evaluated for inhibition of tubulin polymerization.

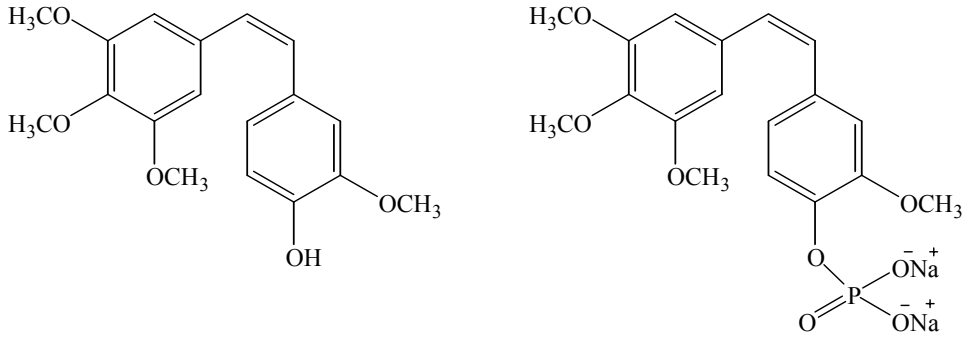

5 **6**

Figure 2.31. Structures of Compounds **5** and **6.**

Compound **5** showed 20.1 % inhibition of tubulin polymerization at 40 μM and Compound **6,** its disodium phosphate salt, showed no tubulin inhibitory activity at 40.0 μM. It has been reported that the 3-hydroxy group on the B-ring of CA-4 is crucial for potent antitubulin activity (Cushman, M *et al.,* 1991). These results show the importance of the presence of the 3-hydroxy-4-methoxy phenyl ring (ring B) in the combretastatin series.

*Effect of Compounds **7** and **8** on Tubulin Polymerization*

(Z)-1-(3',5'-Dihydroxy-4'-methoxyphenyl)-2-(3'',4'',5''-trimethoxyphenyl)-ethene **(7)** (Figure 2.32), a CA-4 derivative with a hydroxyl substitution on position 5 of ring B, was analyzed for antimitotic activity (Figure 2.33). Results showed a significant decrease in tubulin inhibition activity with an IC_{50} value of 6.1μM (Figure 2.34). This implied that an additional hydroxyl substitution on the 5-position of the B-ring of CA-4 is unacceptable if potent tubulin polymerization inhibition activity is to be observed.

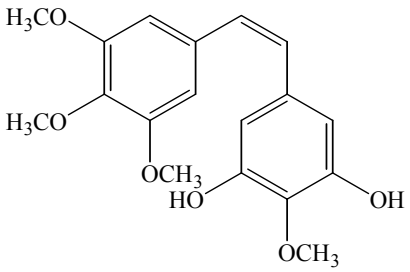

7

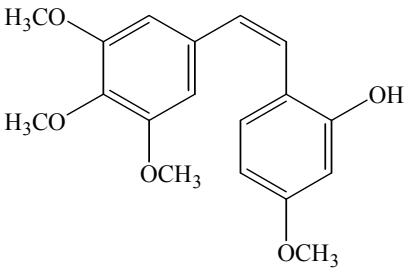

8

Figure 2.32. Structures of Compounds **7** and **8.**

Table 2.1. Biochemical Data for Compounds **1 - 10.**

Compound	IC_{50} (μM)	Log IC_{50} ± SE	Hillslope ± SE	R^2
1	1.4	-5.837 ± 0.01	-2.4 ± 0.2	0.99
2	1.2	-5.910 ± 0.01	-3.5 ± 0.5	0.98
3	1.9	-5.715 ± 0.02	-2.9 ± 0.2	0.99
4	> 40.0	-	-	-
5	> 40.0	-	-	-
6	> 40.0	-	-	-
7	6.1	-5.213 ± 0.02	-2.8 ± 0.3	0.99
8	1.6	-5.786 ± 0.04	-2.1 ± 0.4	0.97
9	6.2	-5.205 ± 0.01	-3.0 ± 0.2	0.99
10	29.5	-4.530 ± 0.06	-4.8 ± 2.0	0.91

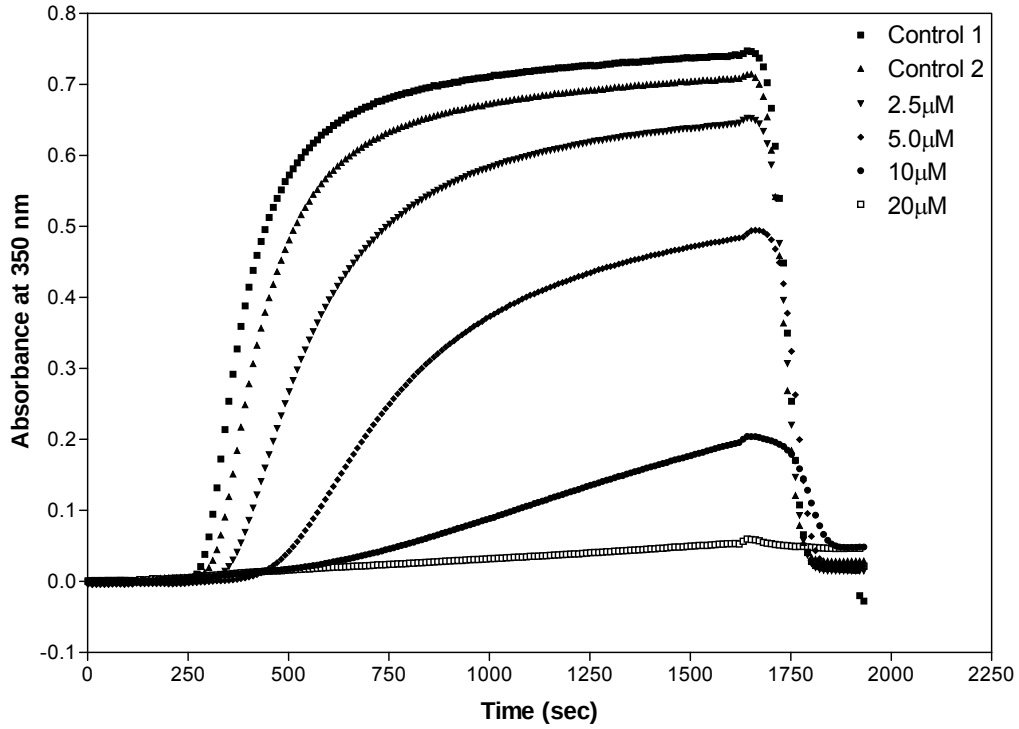

Figure 2.33. Inhibition of Tubulin Polymerization by Compound **7** at 30ºC.

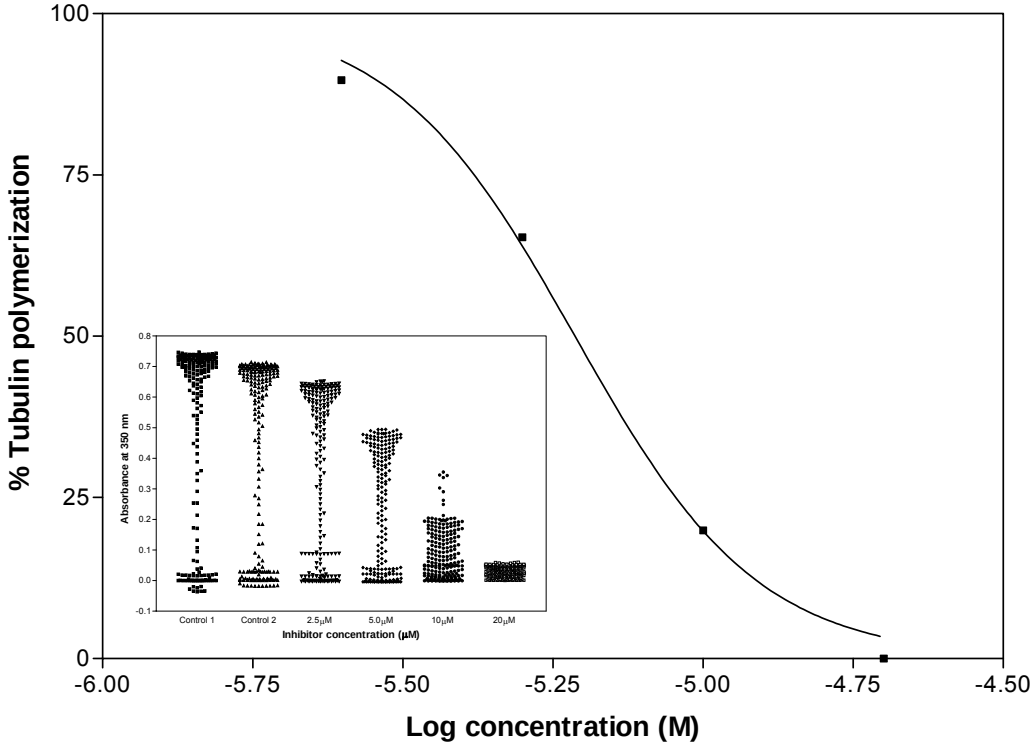

Figure 2.34. Percent Tubulin Polymerization against Log Concentration of Compound **7**.

(Z)-1-(2'-Hydroxy-4'-methoxyphenyl)-2-(3",4",5"-trimethoxyphenyl)-ethene **(8)** (Figure 2.32), a CA-1 derivative with no hydroxyl group on 3-position of the B-ring was also evaluated for inhibition of tubulin polymerization (Figure 2.35). The compound showed an IC_{50} value of 1.6 μM (Figure 2.36). These results revealed that removal of hydroxyl group from position 3 of ring B does not affect the potency of CA-1. This further suggested that the presence of at least one hydroxyl group on either the 2- or 3-positions in ring B is crucial for the inhibition of tubulin polymerization in both CA-1 and CA-4 natural products. This however is only true when a methoxy group is maintained in the 4-position of the stilbenes.

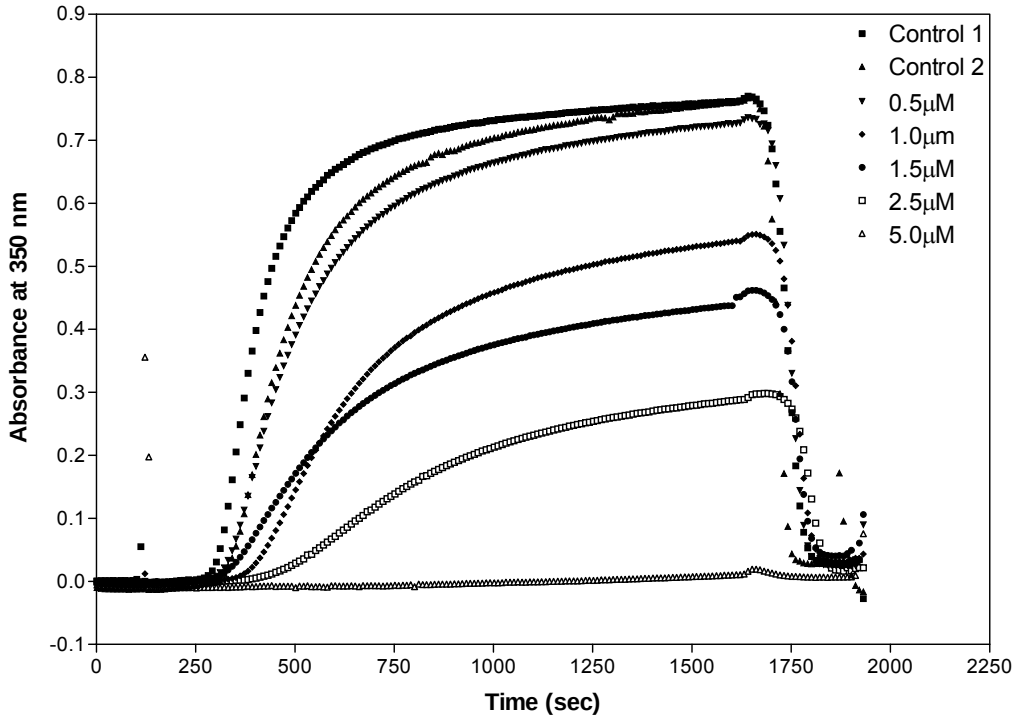

Figure 2.35. Inhibition of Tubulin Polymerization by Compound **8** at 30ºC.

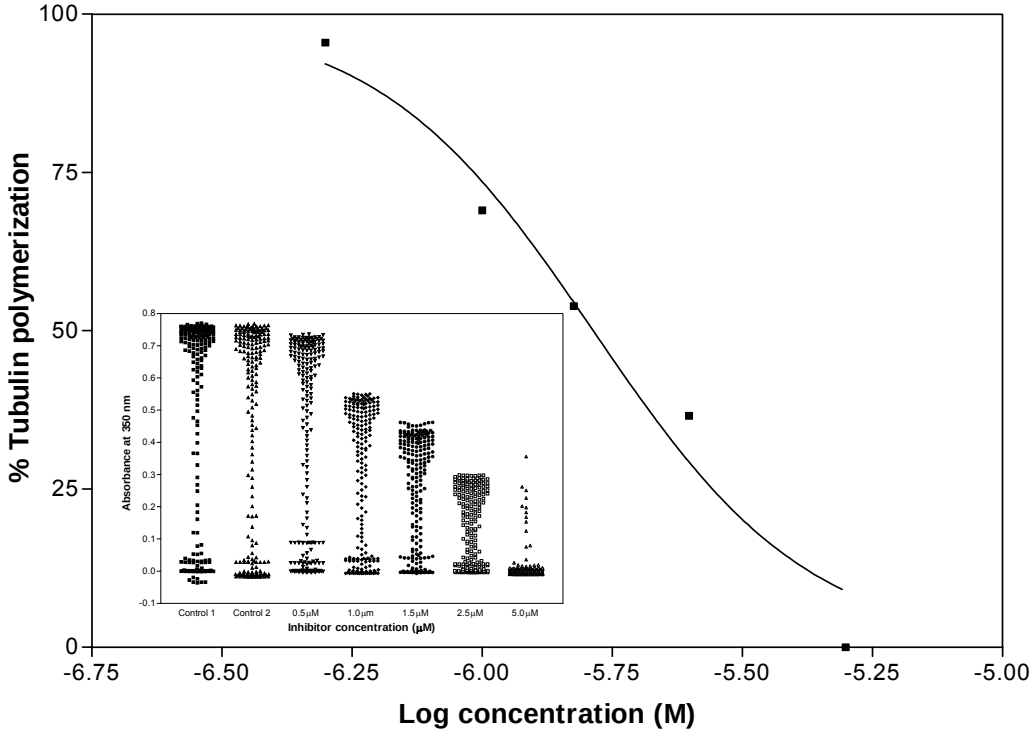

Figure 2.36. Percent Tubulin Polymerization against Log Concentration of Compound **8**.

*Effect of Compounds **9** and **10** on Tubulin Polymerization*

In an effort to explore the importance of a methoxy group in ring B of both CA-1 and CA-4, *(Z)-1-(2',3'-Dihydroxyphenyl)-2-(3",4",5"-trimethoxyphenyl)-ethene* **(9)** (Figure 2.37), a CA-1 derivative with no methoxy group in position 4 of ring B was analyzed for inhibition of tubulin polymerization (Figure 2.38). Removal of the 4-methoxy group from the B-ring significantly decreased the antitubulin activity with an IC_{50} of 6.2 μM (Figure 2.39), which was 3.3-fold less active than CA-1. This proved that a 4-methoxy is required in the B-ring for strong inhibition of tubulin polymerization. Whereas compound **8** with out a 3-hydroxy group retained its tubulin inhibitory activity comparable to that of CA-1, compound **9** lost its activity, further confirming the importance of the 4-methoxy group in antimitotic activity.

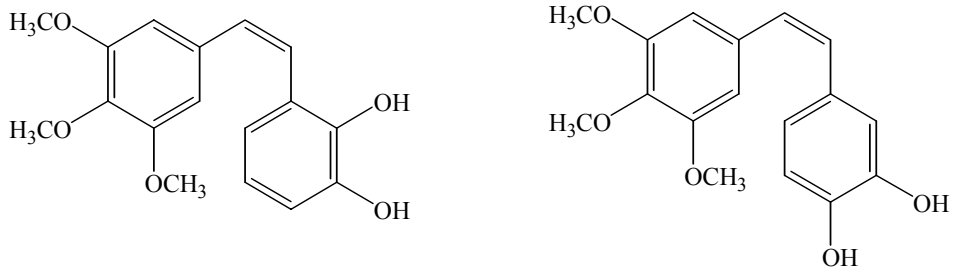

9 **10**

Figure 2.37. Structures of Compounds **9** and **10**.

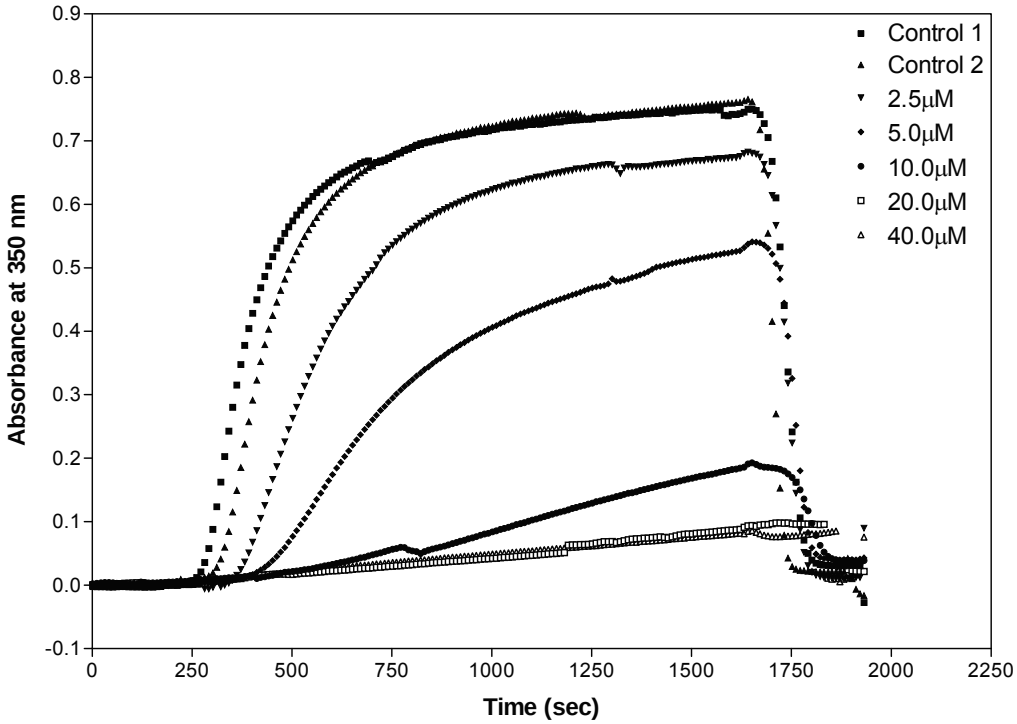

Figure 2.38. Inhibition of Tubulin Polymerization by Compound **9** at 30ºC.

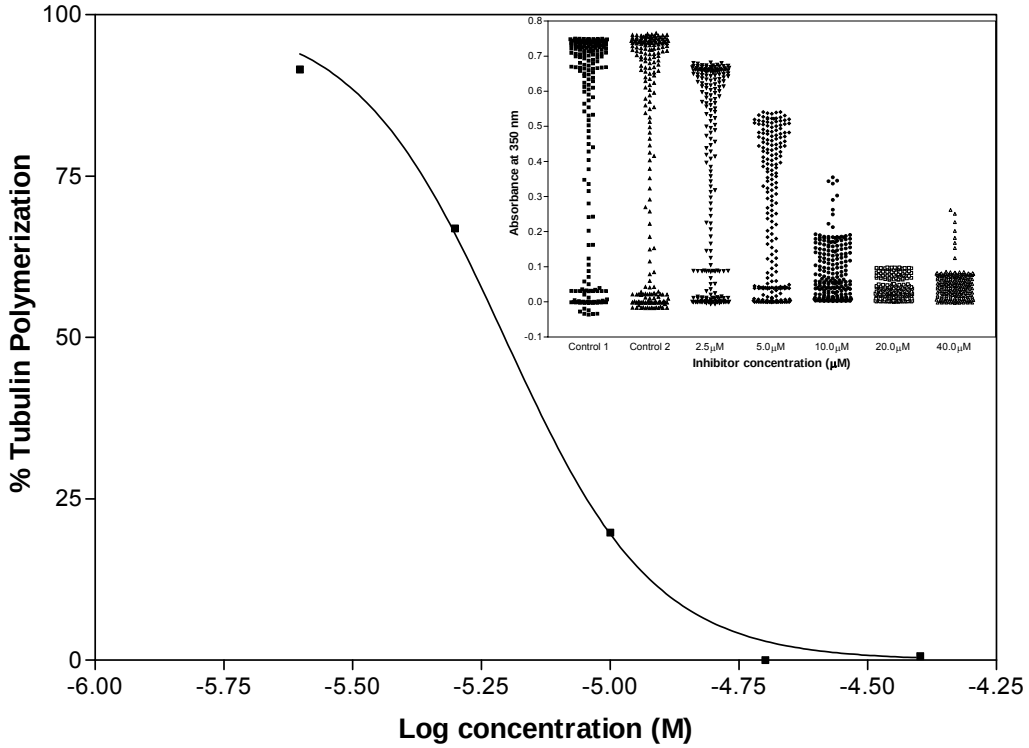

Figure 2.39. Percent Tubulin Polymerization against Log Concentration of Compound **9**.

The importance of the 4-methoxy group was further investigated by evaluating *(Z)-1-(3',4'-Dihydroxyphenyl)-2-(3",4",5"-trimethoxyphenyl)-ethene* **(10)** (Figure 2.37) for antimitotic activity (Figure 2.40). In this compound, the 4-methoxy group in the B-ring was substituted with a hydroxyl group. The kinetics of the experiment gave an IC_{50} value of 29.5 μM (Figure 2.41). This was a 25- fold loss of antitubulin activity compared to that of CA-4, further evidence that the 3-hydroxyl-4-methoxyphenyl ring arrangement in both CA-4 and CA-1 is crucial for maintenance of antitubulin activity in derivatives of both natural products.

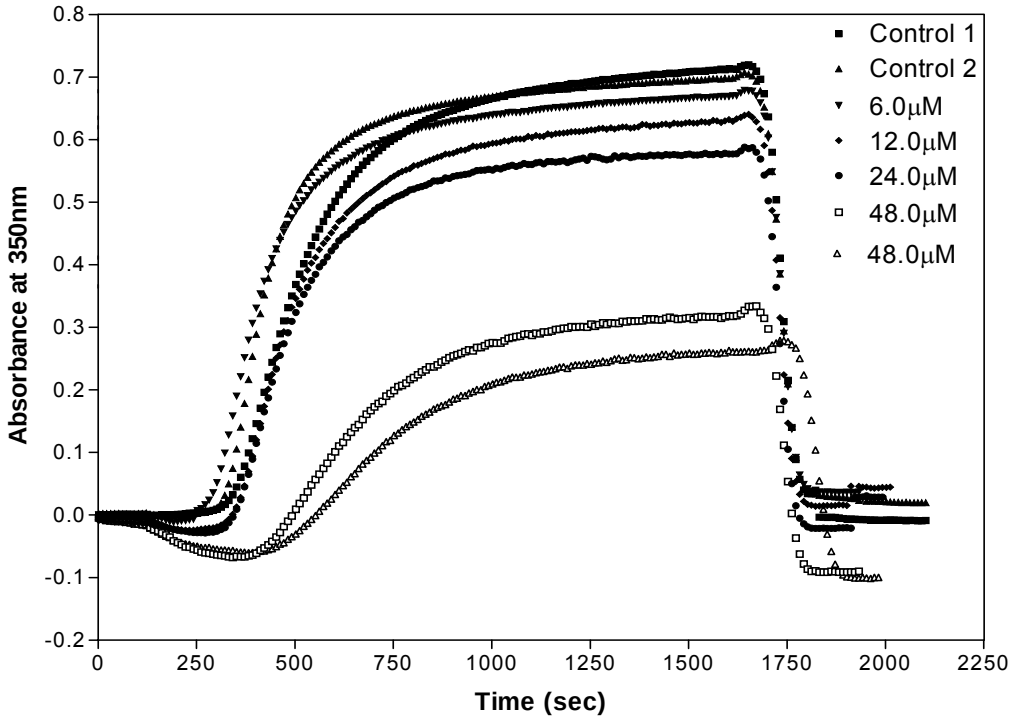

Figure 2.40. Inhibition of Tubulin Polymerization by Compound **10** at 30ºC.

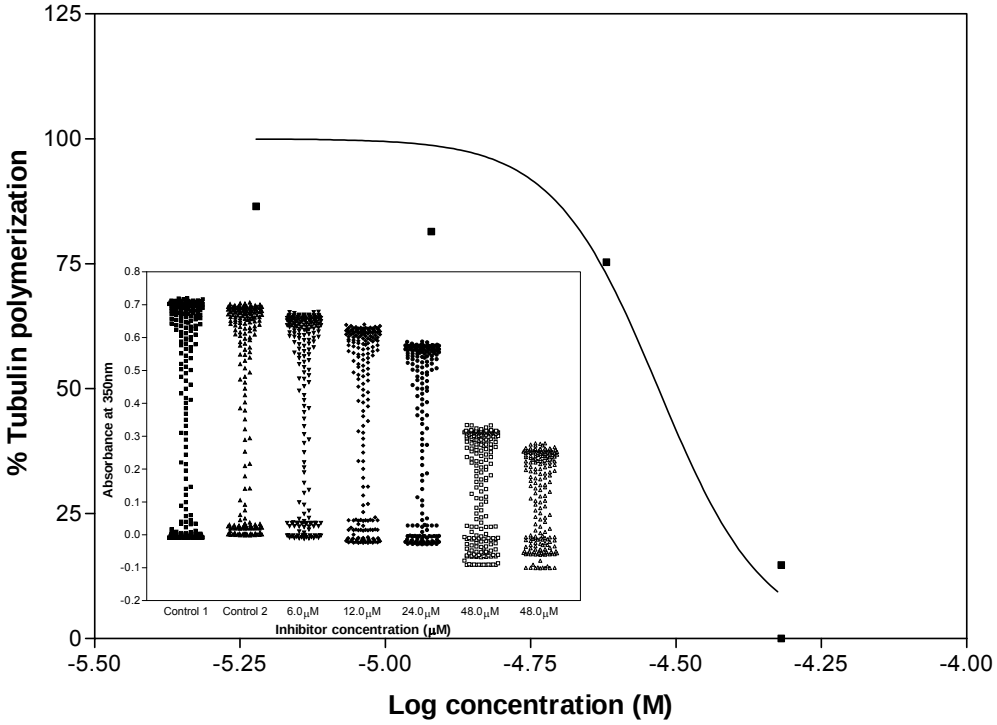

Figure 2.41. Percent Tubulin Polymerization against Log Concentration of Compound **10**.

*Effect of Compound **11** and **12** on Tubulin Polymerization*

(*Z)-1-(4'-Hydroxy)-2-(3",4",5"-trimethoxyphenyl)-ethene* **(11)**, with a universal phenolic hydroxyl group in ring B (Figure 2.42), was also evaluated. This compound did not prove to be a good inhibitor of tubulin polymerization ($IC_{50} \geq 20$ μM).

(Z)-1-(2',3'-Dihydroxy, 4'-methylphenyl)-2-(3",4",5"-trimethoxyphenyl)-ethene **(12)** (Figure 2.42), in which the 4-methoxy group in ring B of CA-1 was replaced by a methyl group showed very interesting results. This reduction in the size of the substituent on the 4-position of ring B resulted in a compound with more potency as an inhibitor of tubulin polymerization. Its antitubulin ability was determined (Figure 2.43) and results indicated an IC_{50} of 2.1 μM (Figure 2.44) which was almost equivalent to that of CA-1 (1.9 μM). From this finding, we can safely say that the importance of the presence of a methoxy group at position 4 in the B-ring is paramount. However, sterically smaller groups like the methyl group in compound **12** could as well lead to compounds with enhanced antitubulin activity.

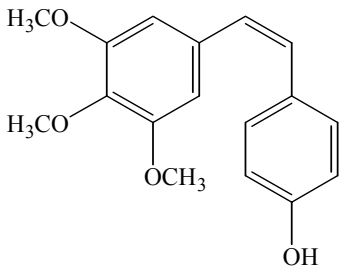

11

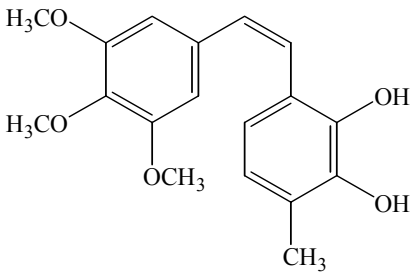

12

Figure 2.42. Structures of Compounds **11** and **12**.

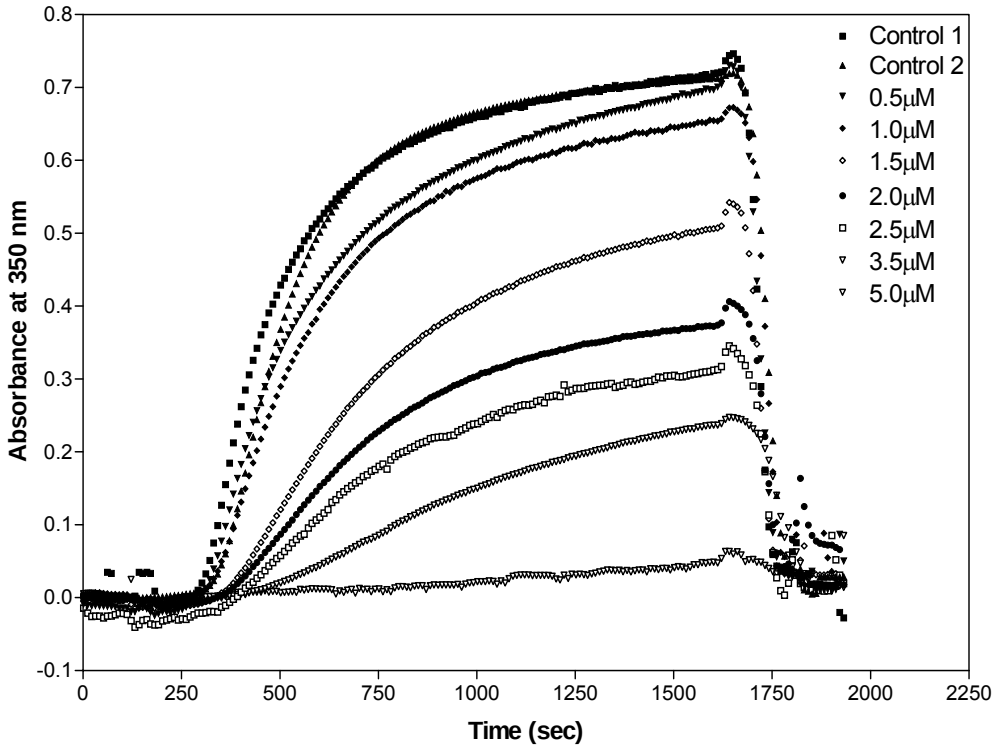

Figure 2.43. Inhibition of Tubulin Tolymerization by Compound **12** at 30ºC.

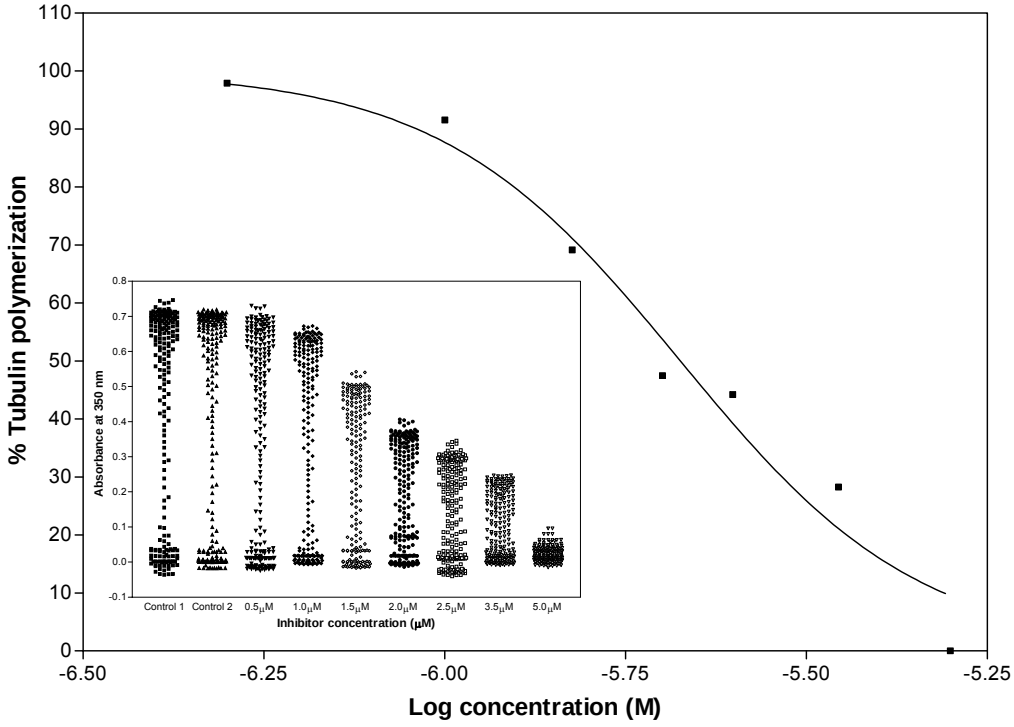

Figure 2.44. Percent Tubulin Polymerization against Log Concentration of Compound **12**.

*Effect of Compounds **13** and **14** on Tubulin Polymerization*

(Z)-1-(2'-Bromo-3'-hydroxy- 4'-methoxyphenyl)-2-(3",4",5"-trimethoxyphenyl)-ethene **(13)** (Figure 2.45), a CA-1 derivative resulting from replacement of the 2-hydroxyl group with a 2-bromo group on the B-ring, was evaluated in order to determine its activity on tubulin polymerization (Figure 2.46). Compound **13** showed strong inhibition of tubulin polymerization with an IC_{50} of 1.1 μM (Figure 2.47), which was comparable to that of the lead compound CA-4.

However replacement of 3-hydroxyl group with a 3-bromo group to give *(Z)-1-(3'-Bromo- 2'-hydroxy- 4'-methoxyphenyl)-2-(3",4",5"-trimethoxyphenyl)-ethene* **(14)** (Figure 2.45) resulted in diminished antitubulin activity. Figure 2.48 shows the kinetics of tubulin polymerization in the presence of Compound **14**. Analysis of the resultant data showed reduced inhibitory activity with an IC_{50} of 12.9 μM (Figure 2.49). This was a 7-fold decrease in antitubulin activity compared to that of CA-1.

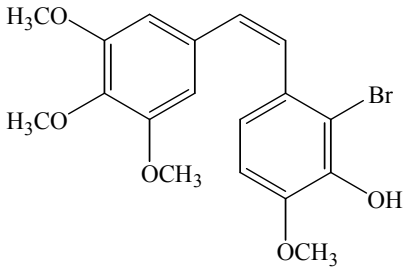

13

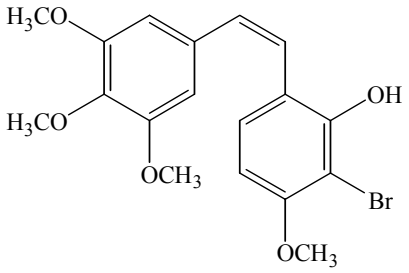

14

Figure 2.45. Structures of Compounds **13** and **14**.

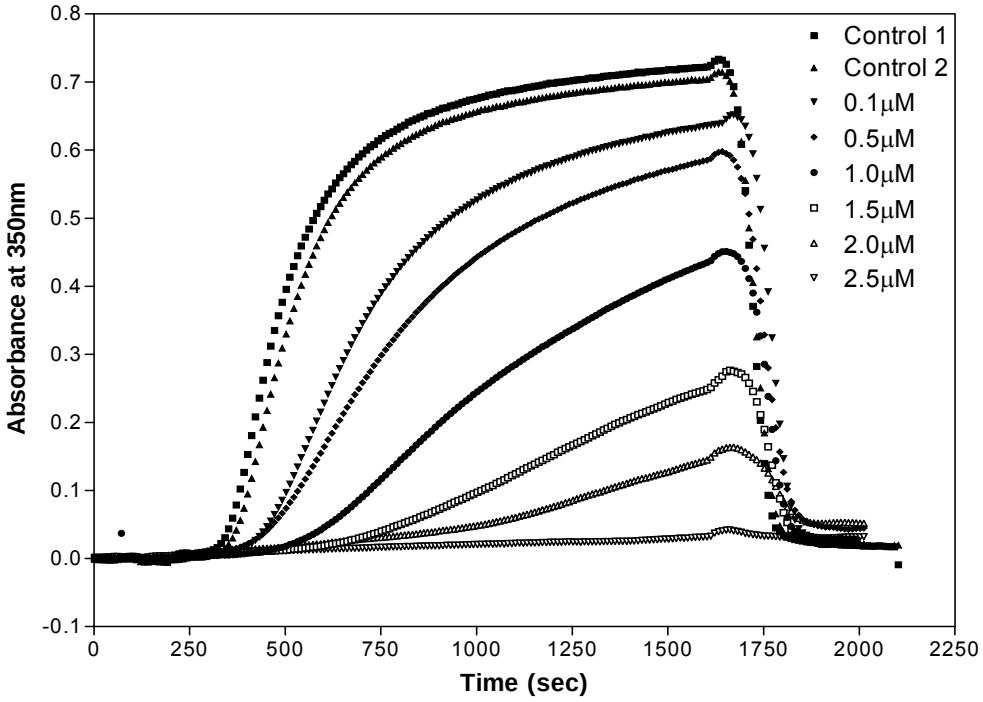

Figure 2.46. Inhibition of Tubulin Polymerization by Compound **13** at 30ºC.

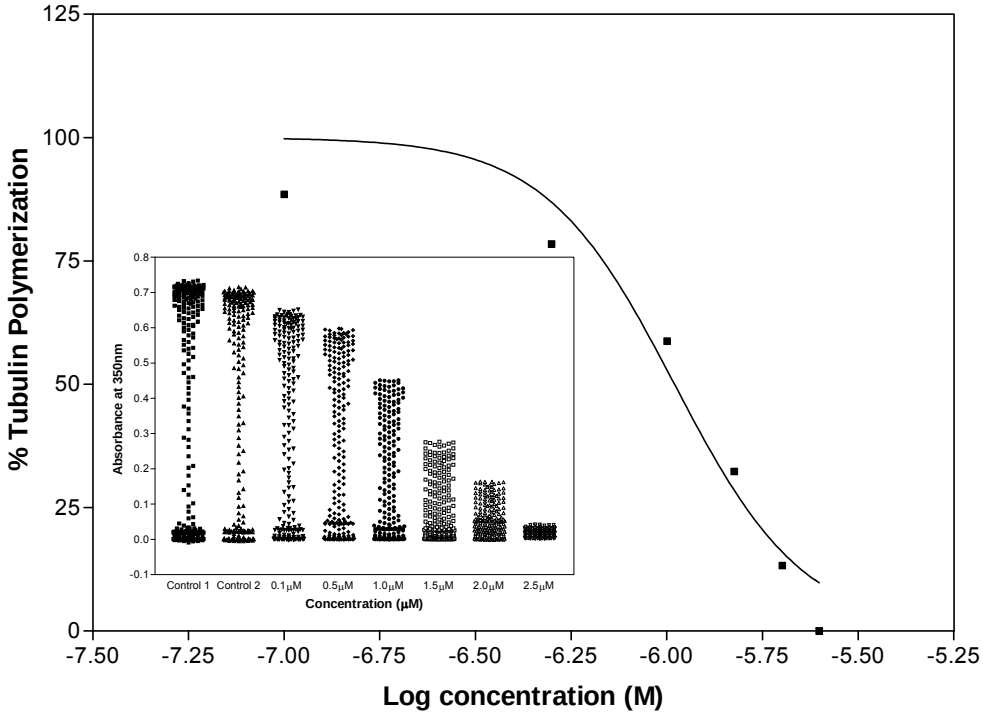

Figure 2.47. Percent Tubulin Polymerization against Log Concentration of Compound **13**.

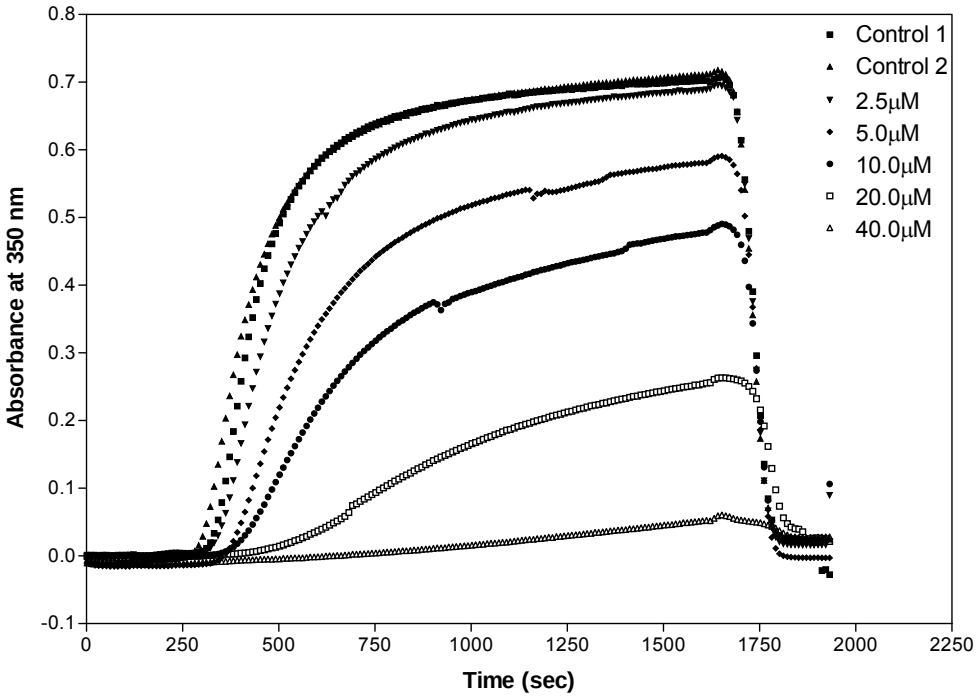

Figure 2.48. Inhibition of Tubulin Polymerization by Compound **14** at 30ºC.

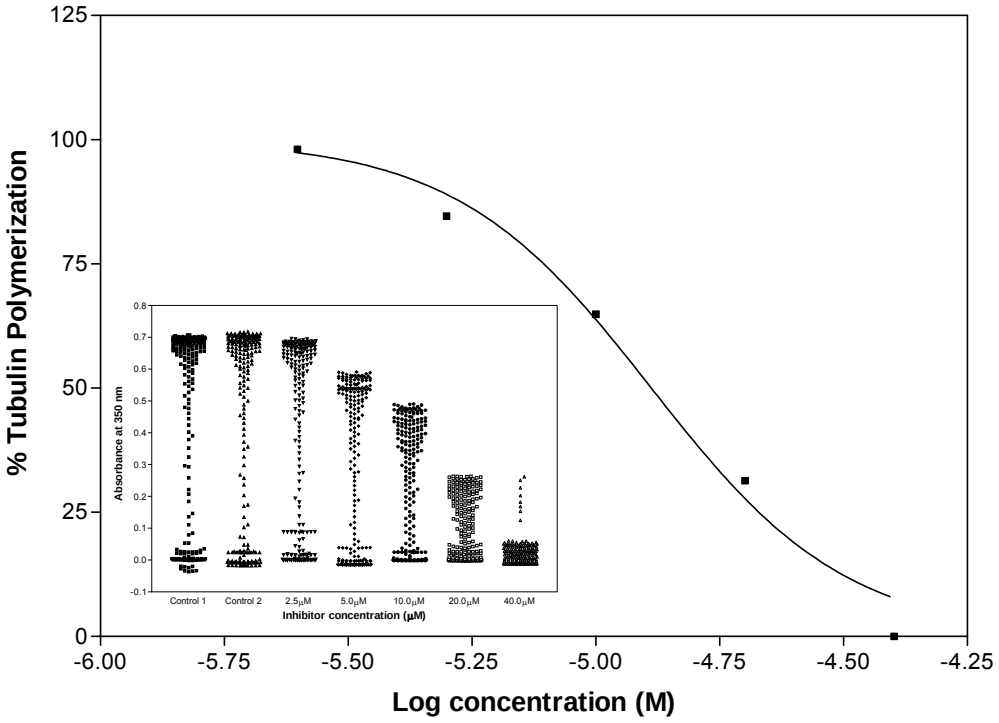

Figure 2.49. Percent Tubulin Polymerization against Log Concentration of Compound **14**.

*Effect of Compounds **15** and **16** on Tubulin Polymerization*

(Z)-1-(2'-Chloro, 3'-hydroxy, 4'-methoxyphenyl)-2-(3",4",5"-trimethoxyphenyl)-ethene **(15)** (Figure 2.50), a chloro-derivative of CA-1 was analyzed for its effect on tubulin polymerization (Figure 2.51). Replacement of 2-hydroxyl group with a chloro group on ring B, resulted in strong inhibitory activity with an IC_{50} of 1.9 μM (Figure 2.52), which was comparable to that of CA-1. In 1991, Cushman and co-workers (1991) reported an IC_{50} of 3.5 μM for a 2-chloro-4-methoxy phenyl trimethoxy stilbene with no hydroxyl group in the C-3 position.

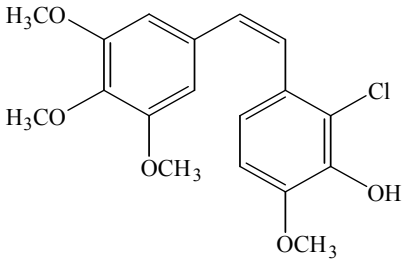

15

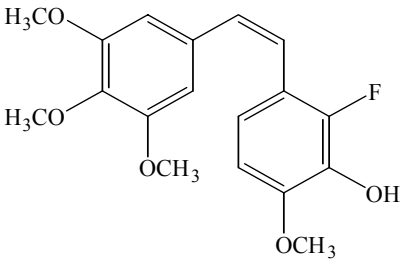

16

Figure 2.50. Structures of Compounds **15** and **16**.

(Z)-1-(2'-Fluoro-3'-hydroxy-4'-methoxyphenyl)-2-(3",4",5"-trimethoxyphenyl)-ethene **(16)**, a fluoro derivative of CA-1 (Figure 2.50), was also investigated for its antitubulin activity. Polymerization studies of compound **16** (Figure 2.53) showed an IC_{50} of 6.0 μM (Figure 2.54). This was 3.1- fold less potency than the natural compound CA-1. The presence of a fluoro group on the B-ring coupled with a hydroxyl group on the 3-position seemed to decrease antitubulin activity, compared to the other halogens (Compounds **13** and **15**) in the same position.

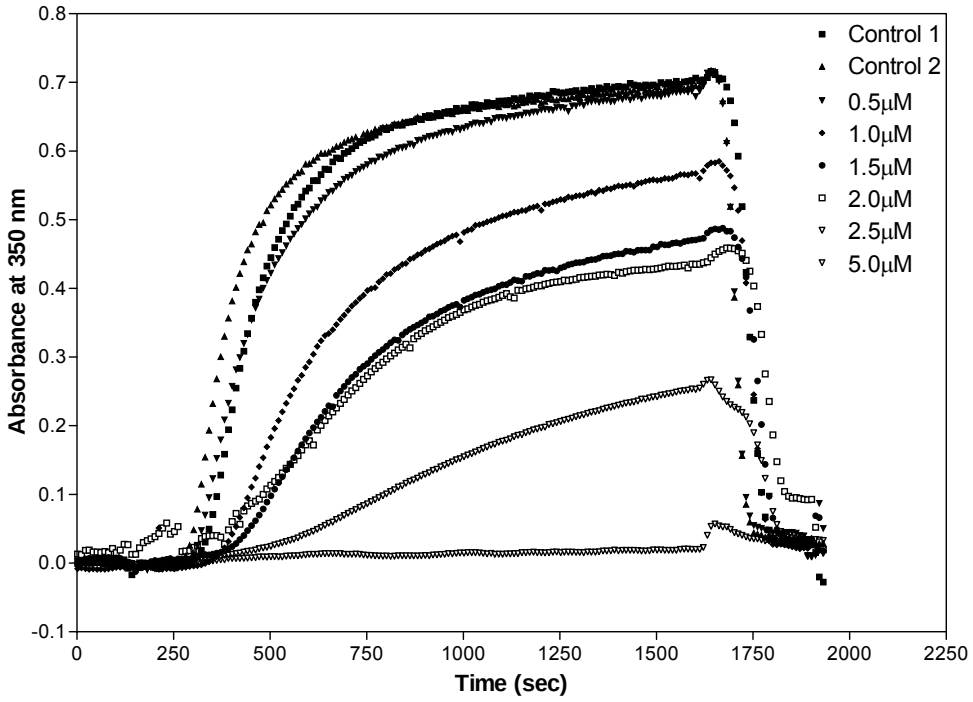

Figure 2.51. Inhibition of Tubulin Polymerization by Compound **15** at 30ºC.

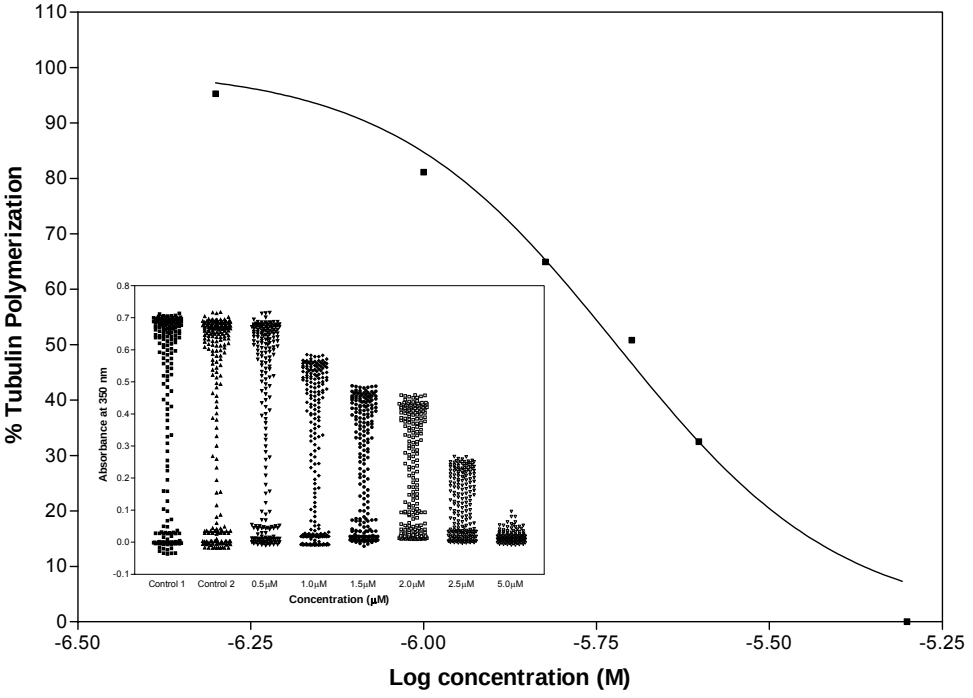

Figure 2.52. Percent Tubulin Polymerization against Log Concentration of Compound **15**.

Table 2.2. Biochemical Data for Compounds **11 - 20.**

Compound	IC_{50} (μM)	Log IC_{50} ± SE	Hillslope ± SE	R^2
11	> 20.0	-	-	-
12	2.1	-5.670 ± 0.02	-2.6 ± 0.4	0.97
13	1.1	-5.980 ± 0.04	-2.6 ± 0.6	0.94
14	12.9	-4.888 ± 0.03	-2.2 ± 0.3	0.98
15	1.9	-5.720 ± 0.02	-2.7 ± 0.3	0.99
16	6.0	-5.222 ± 0.03	-2.5 ± 0.3	0.98
17	> 40.0	-	-	-
18	2.4	-5.630 ± 0.02	-3.0 ± 0.4	0.97
19	13.1	-4.880 ± 0.02	-2.2 ± 2.0	0.98
20	> 40.0	-	-	-

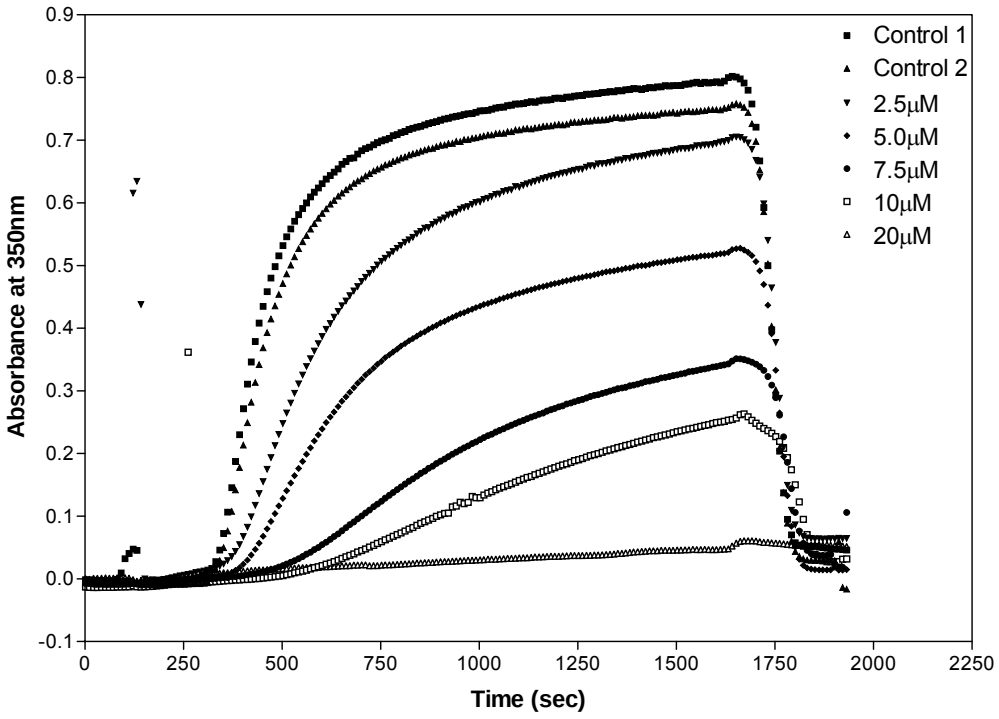

Figure 2.53. Inhibition of Tubulin Polymerization by Compound **16** at 30ºC.

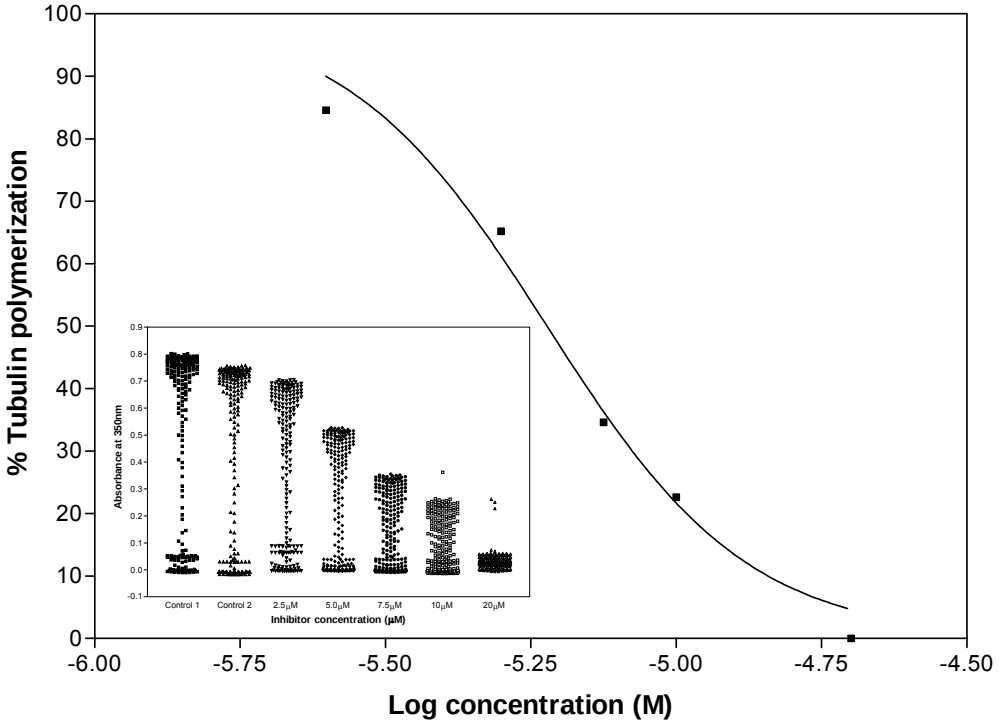

Figure 2.54. Percent Tubulin Polymerization against Log Concentration of Compound **16**.

*Effect of Compounds **17** and **18** on Tubulin Polymerization*

(Z)-1-(2'-Chloro, 3'- disodiumphosphate, 4'-methoxyphenyl)-2-(3",4",5"-trimethoxyphenyl)-ethene **(17)** (Figure 2.55), a disodium phosphate derivative of Compound **15**, was dissolved in distilled water and was analyzed for antitubulin activity. Compound **17** did not inhibit tubulin polymerization (IC_{50} > 40μM). The effect of chloro substitution at the C-3 position of the B-ring of CA-4 was also investigated. When *(Z)-1-(3'-Chloro,4'-methoxyphenyl)-2-(3",4",5"-trimethoxyphenyl)-ethene* **(18)** (Figure 2.55) which is a chloro-substituted CA-4 analog was analyzed for antitubulin activity, (Figure 2.56), it showed an IC_{50} value of 2.4 μM (Figure 2.57) which was 2.0-fold less active than CA-4. Gaukroger and co-workers (2003) have reported IC_{50} values of 0.4 μM and 0.085μM for trimethoxy-stilbenes with bromo and fluoro substituents in the C-3 position respectively. Thus halogenated stilbenes have an extremely high ability to interact with tubulin and inhibit its polymerization into microtubules.

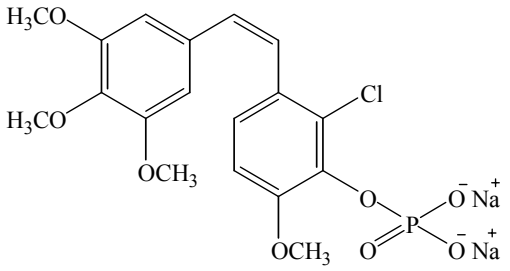

17

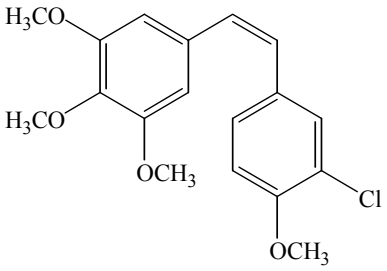

18

Figure 2.55. Structures of Compounds **17** and **18.**

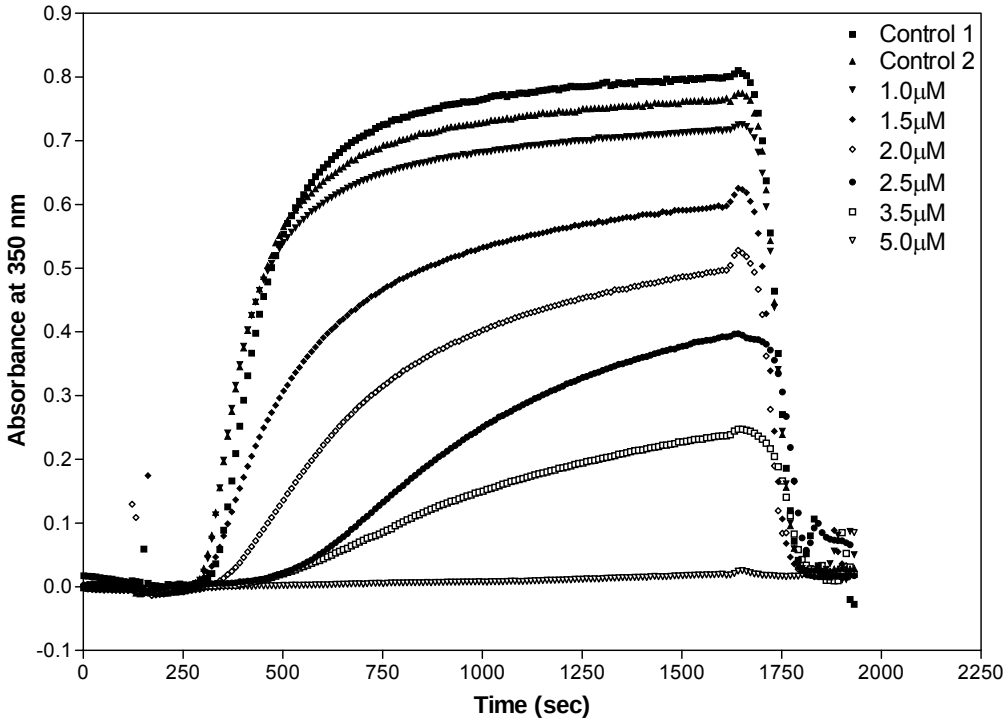

Figure 2.56. Inhibition of Tubulin Polymerization by Compound **18** at 30ºC.

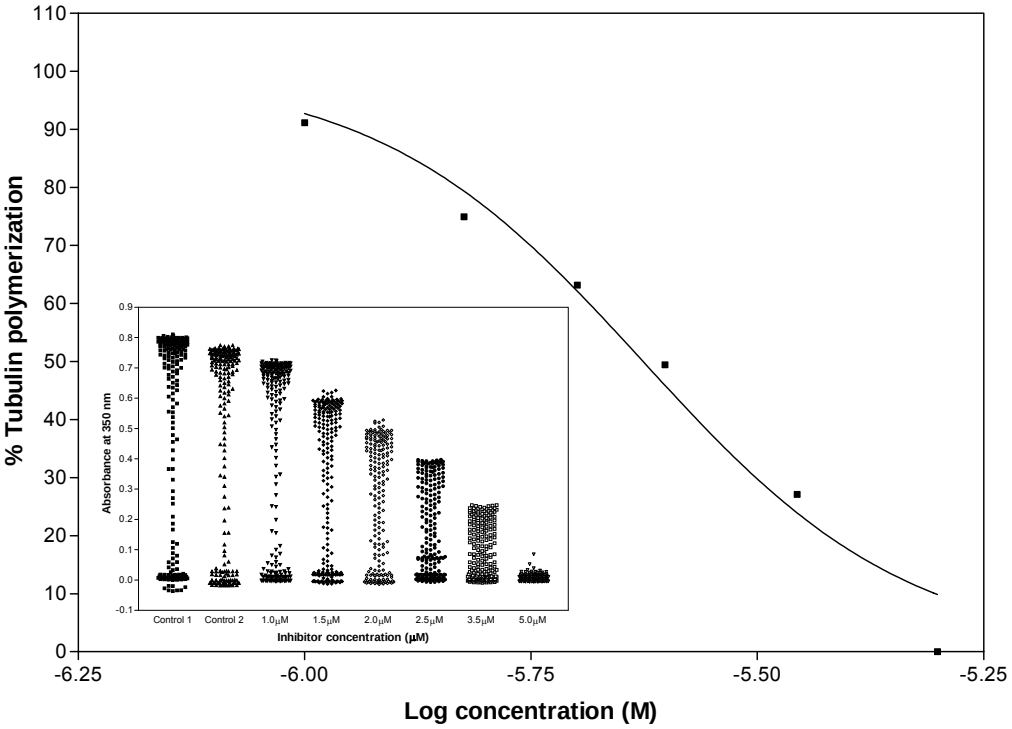

Figure 2.57. Percent Tubulin Polymerization against Log Concentration of Compound **18**.

*Effect of Compounds **19** and **20** on Tubulin Polymerization*

The effect of introduction of a chloro group in the C-2 position coupled by the removal of the 4-methoxy group in CA-4 was evaluated. *(Z)-1-(2'-Chloro-3'-hydroxyphenyl)-2-(3",4",5"-trimethoxyphenyl)-ethene* **(19)** (Figure 2.58) was analyzed for inhibition of tubulin polymerization (Figure. 2.59). The analysis revealed significant loss in antitubulin activity with an IC_{50} value of 13.1 μM (Figure 2.60). This was a 10.9-fold difference in antimitotic potency compared to CA-4. This loss in potency reaffirmed the importance of the presence of a 4-methoxy group in B-ring in the combretastatins. As expected, the di-sodium phosphate salt analog; *(Z)-1-(2'-chloro,(3'-disodiumphosphate) phenyl)-2-(3",4",5"-trimethoxyphenyl)-ethene* **(20)** (Figure 2.58) showed no inhibition of tubulin polymerization activity (IC_{50} > 40 μM).

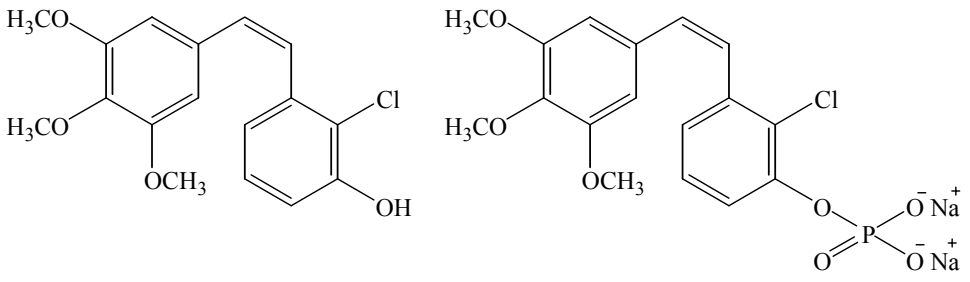

19 **20**

Figure 2.58. Structures of Compounds **19** and **20.**

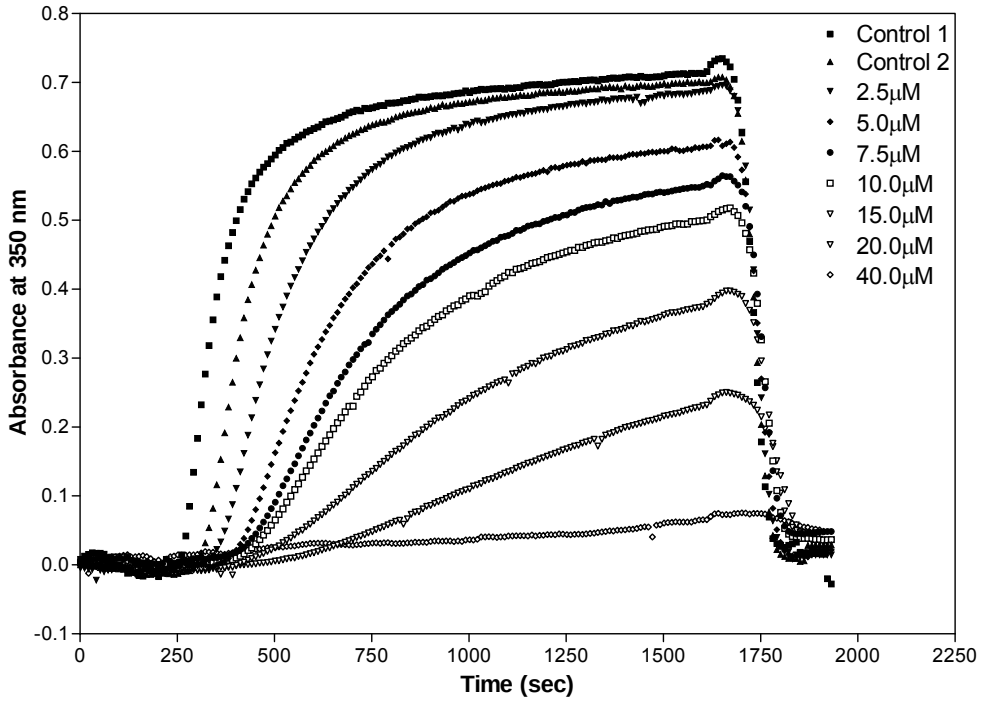

Figure 2.59. Inhibition of Tubulin Polymerization by Compound **19** at 30ºC.

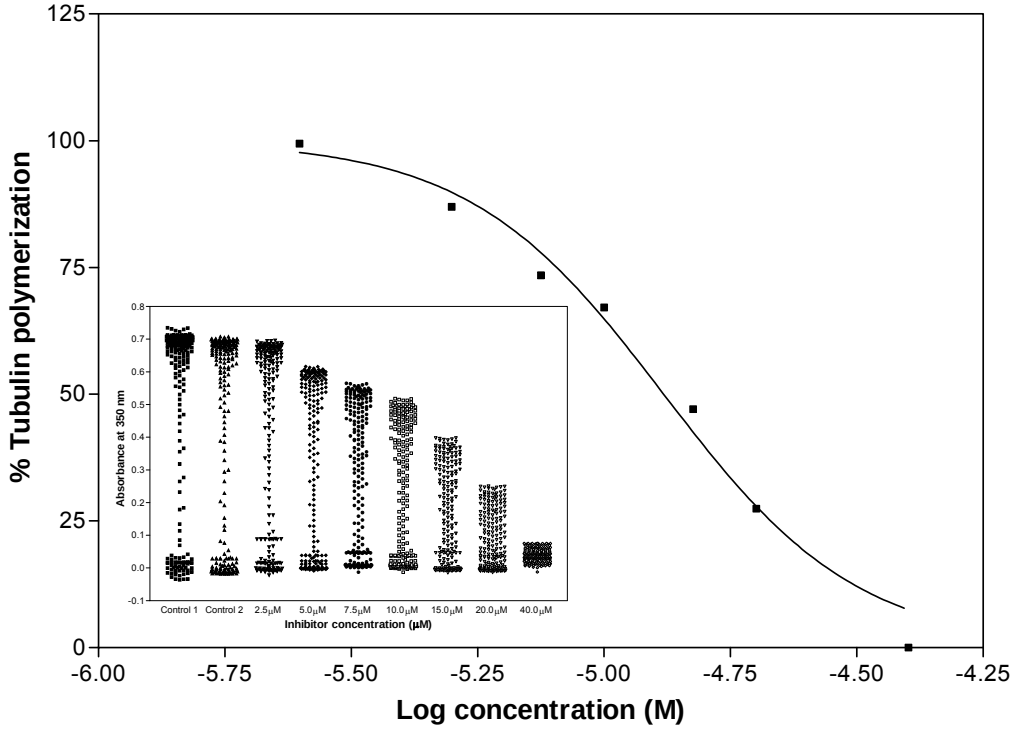

Figure 2.60. Percent Tubulin Polymerization against Log Concentration of Compound **19**.

*Effect of Compounds **21** and **22** on Tubulin Polymerization*

(Z)-1-(5'-Chloro, 4'-hydroxy, 3'-methoxyphenyl)-2-(3",4",5"-trimethoxyphenyl)-ethene **(21)** (Figure 2.61) was analyzed for inhibition of tubulin polymerization (Figure 2.62). Compound **21** showed a moderate IC_{50} value of 5.4 μM (Figure 2.63). Data from *(Z)-1-(5'-Iodo, 4'-hydroxy,3'-methoxyphenyl)-2-(3",4",5"-trimethoxyphenyl)-ethene* **(22)** is not yet available.

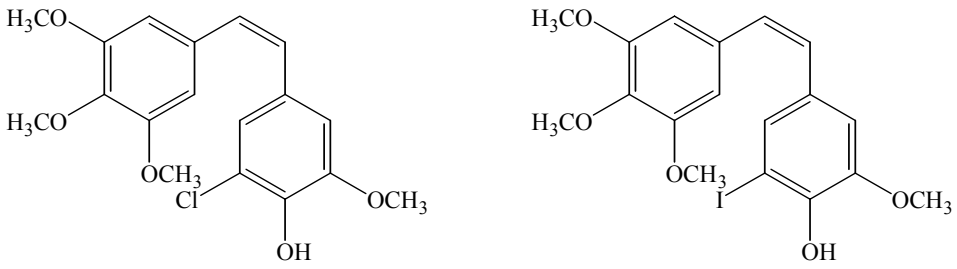

21 **22**

Figure 2.61. Structures of Compounds **21** and **22.**

*Effect of Compounds **23** and **24** on Tubulin Polymerization*

In an effort to determine the effect of dichloro substitution in the B-ring of trimethoxy-stilbenes, *(Z)-1-(2',4'-Dichloro-3'-hydroxyphenyl)-2-(3",4",5"-trimethoxyphenyl)-ethene* **(23)** (Figure 2.64) with 2,4-dichloro substitution was analyzed for its inhibition of tubulin polymerization activity (Figure 2.65). This compound showed a moderate IC_{50} value of 2.8 μM (Figure 2.66). This was 1.5-fold less active than CA-1.

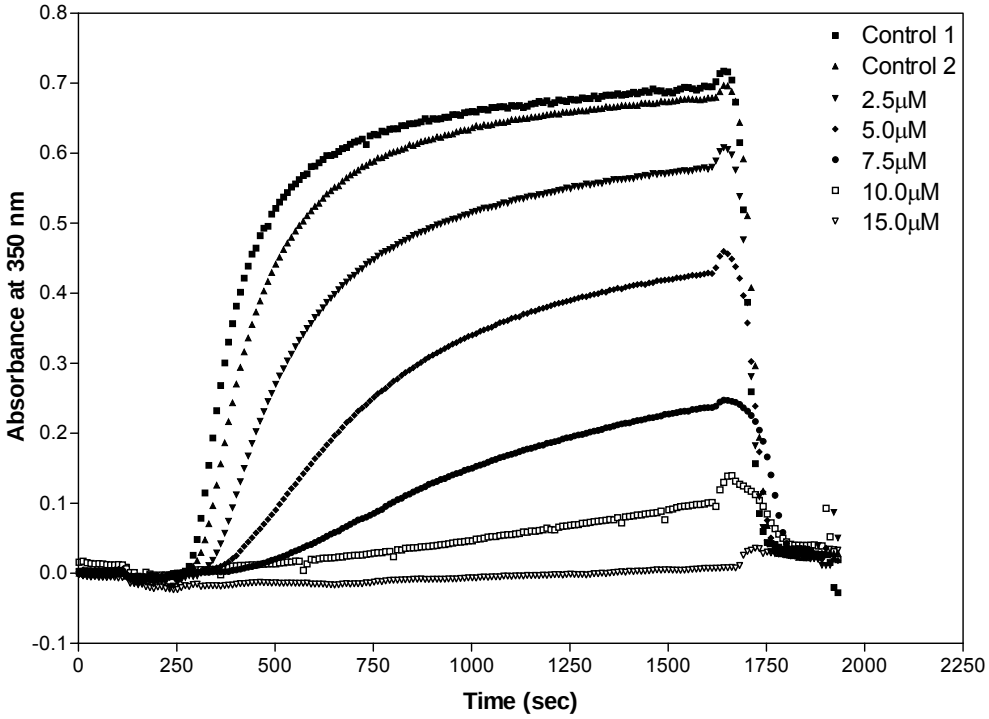

Figure 2.62. Inhibition of Tubulin Polymerization by Compound **21** at 30ºC.

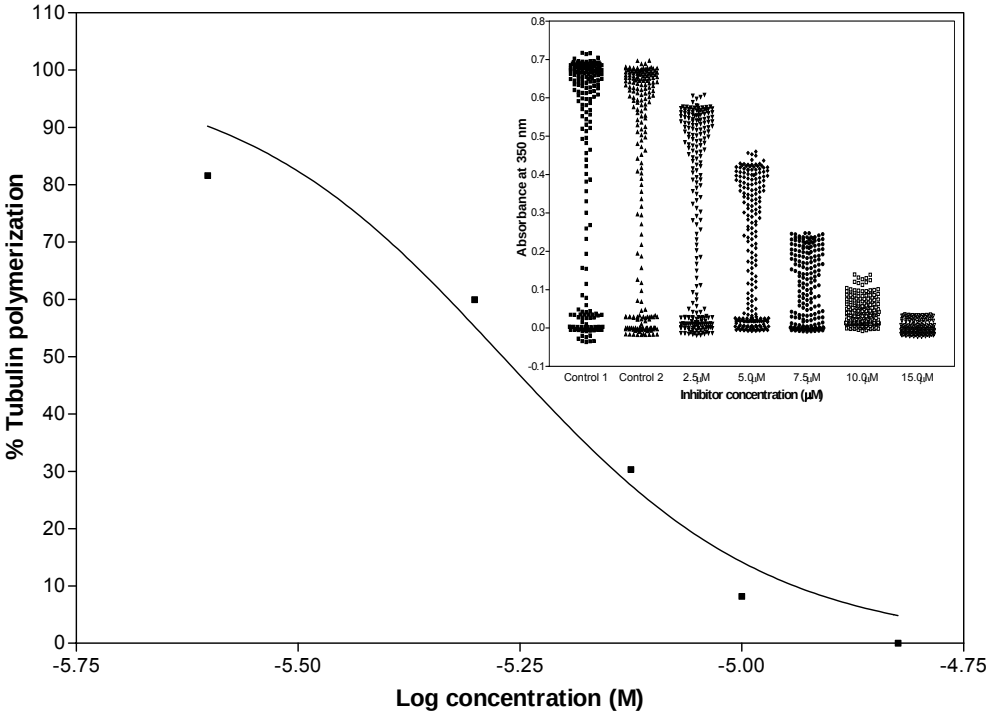

Figure 2.63. Percent Tubulin Polymerization against Log Concentration of Compound **21**.

Since compound **15** with a 4-methoxy group in ring B has the same activity as CA-1, it means that substitution of the 4-methoxy group in ring B with a chloride group decreases the antitubulin activity of the trimethoxy stilbene.

(Z)-1-(2',6'-Dichloro-3'-hydroxyphenyl)-2-(3'',4'',5''-trimethoxyphenyl)-ethene **(24)** (Figure 2.64) with 2,6-dichloro substitution in ring B showed 21.8% and 40.5% inhibition of tubulin polymerization at concentrations of 20 μM and 40 μM respectively. Gaukroger and coworker (2003) showed that molecules having functionalities other than trimethoxy could also interact with tubulin and inhibit tubulin polymerization. Several molecules resembling these combretastatin analogs have been synthesized by Garner and coworkers and they include a series of mono and di-chloro combretastatin derivatives.

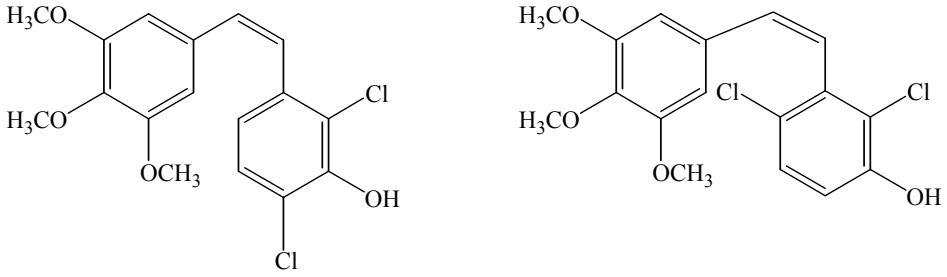

23 **24**

Figure 2.64. Structures of Compounds **23** and **24.**

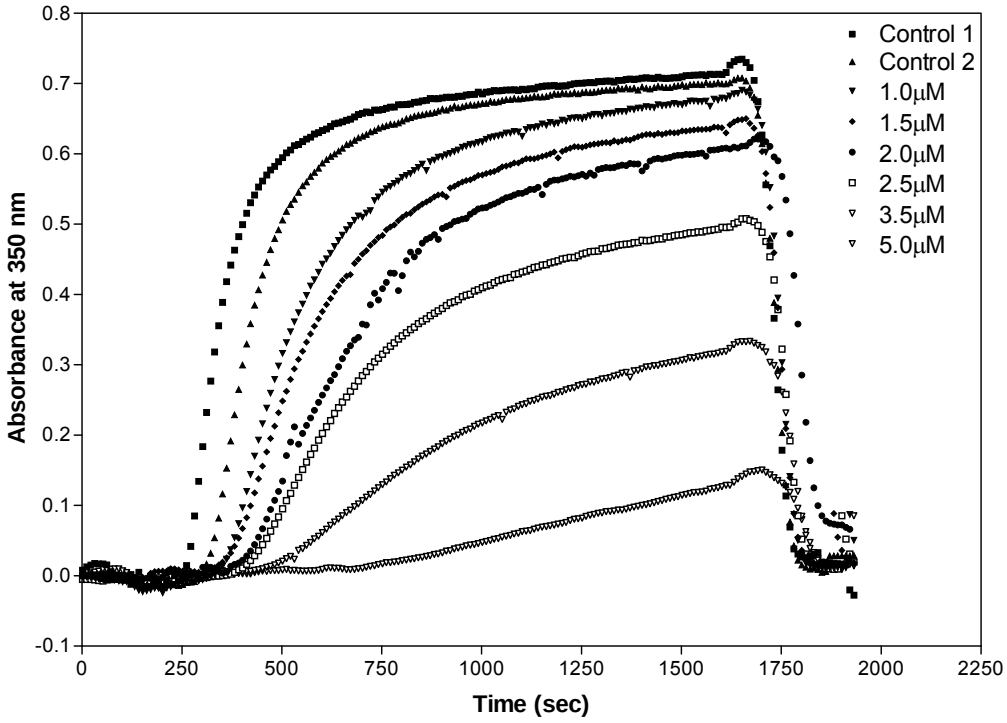

Figure 2.65. Inhibition of Tubulin Polymerization by Compound **23** at 30ºC.

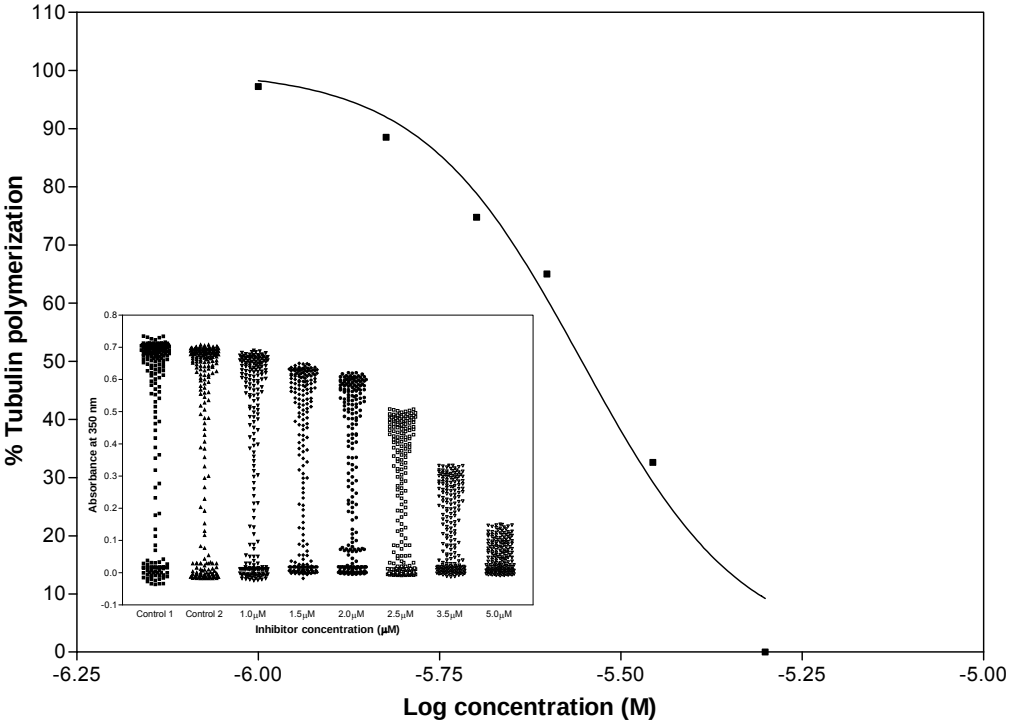

Figure 2.66. Percent Tubulin Polymerization against Log Concentration of Compound **23**.

*Effect of Compounds **25** and **26** on Tubulin Polymerization*

(Z)-1-(3'-Hydroxy,4'-methoxyphenyl)-2-(3"-chloro,4",5"-dimethoxyphenyl)-ethene **(25)** (Figure 2.67) with a chloride group in the C-3 position of ring A of CA-4 was analyzed for its activity on tubulin polymerization (Figure 2.68). Results showed that compound **25** inhibited tubulin polymerization with an IC_{50} value of 1.8 μM (Figure 2.69) which was comparable to that of CA-4 and CA-1.

(Z)-1-(2',3'-Dihydroxy,4'-methoxyphenyl)-2-(5"-chloro-3",4"-dimethoxyphenyl)-ethene **(26)** (Figure 2.67) with a chloride substitution on C-5 position of ring A of CA-1 was analyzed for its inhibitory activity on tubulin polymerization (Figure 2.70). Compound **26** like its counterpart, also inhibited polymerization of tubulin into microtubules with an IC_{50} value of 2.2 μM (Figure 2.71) which was slightly weaker than CA-1.

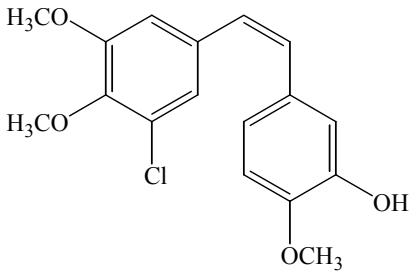

25

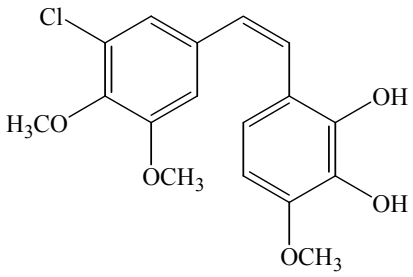

26

Figure 2.67. Structures of Compounds **25** and **26.**

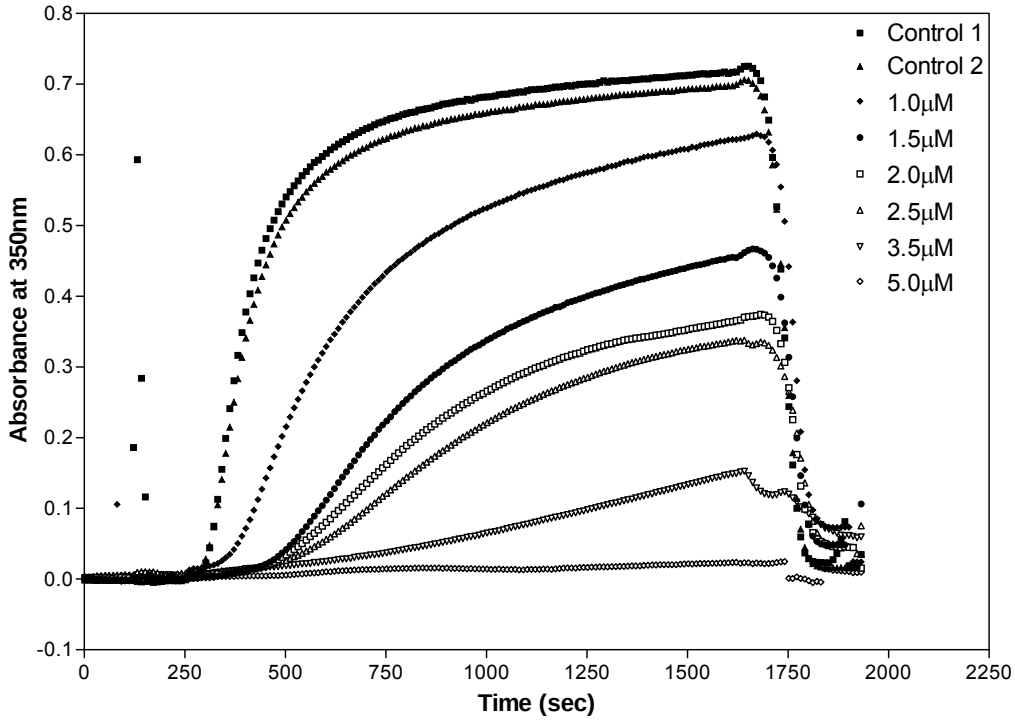

Figure 2.68. Inhibition of Tubulin Polymerization by Compound **25** at 30ºC.

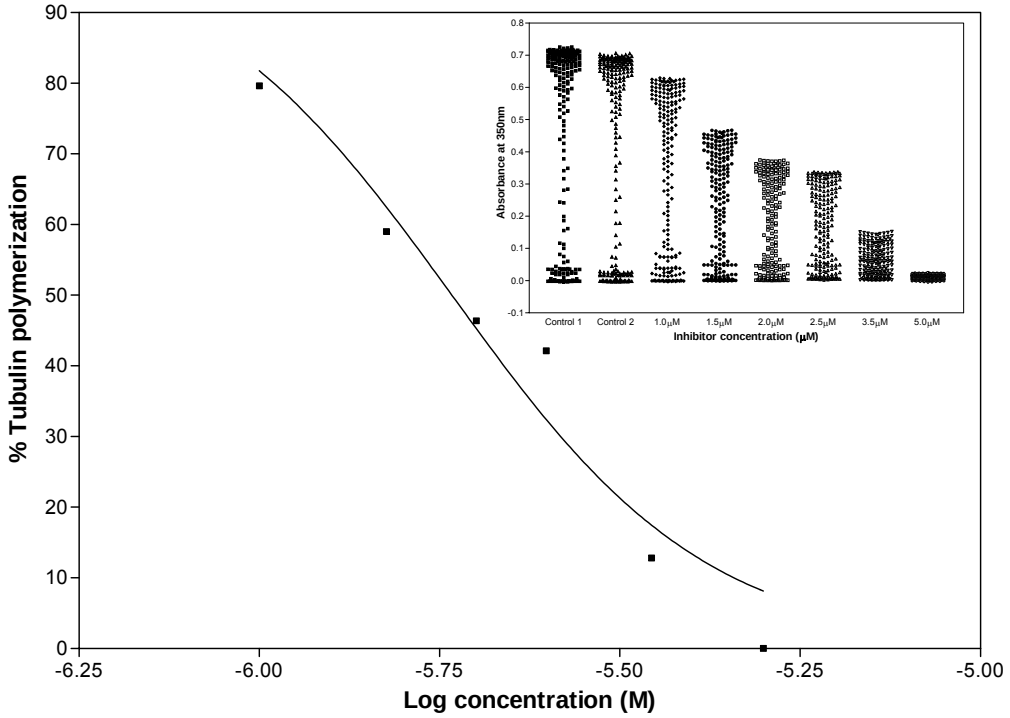

Figure 2.69. Percent Tubulin Polymerization against Log Concentration of Compound **25**.

Table 2.3. Biochemical Data for Compounds **21 - 30.**

Compound	IC_{50} (μM)	Log IC_{50} ± SE	Hillslope ± SE	R^2
21	5.4	-5.270 ± 0.03	-2.9 ± 0.6	0.97
22	-	-	-	-
23	2.8	-5.550 ± 0.02	-3.9 ± 0.6	0.98
24	> 40.0	-	-	-
25	1.8	-5.730 ± 0.03	-2.4 ± 0.4	0.95
26	2.2	-5.650 ± 0.01	-4.4 ± 0.6	0.98
27	1.7	-5.770 ± 0.02	-3.4 ± 0.4	0.98
28	3.0	-5.520 ± 0.03	-3.9 ± 1.0	0.93
29	1.4	-5.861 ± 0.02	-2.0 ± 0.3	0.98
30	1.5	-5.832 ± 0.06	-1.8 ± 0.5	0.89

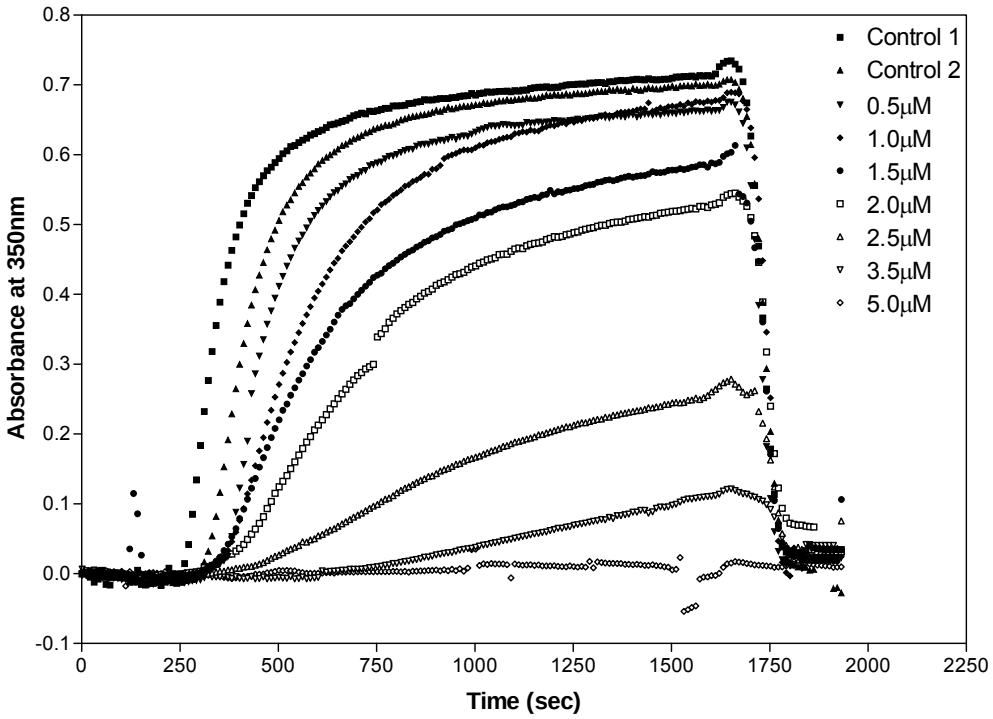

Figure 2.70. Inhibition of Tubulin Polymerization by Compound **26** at 30ºC.

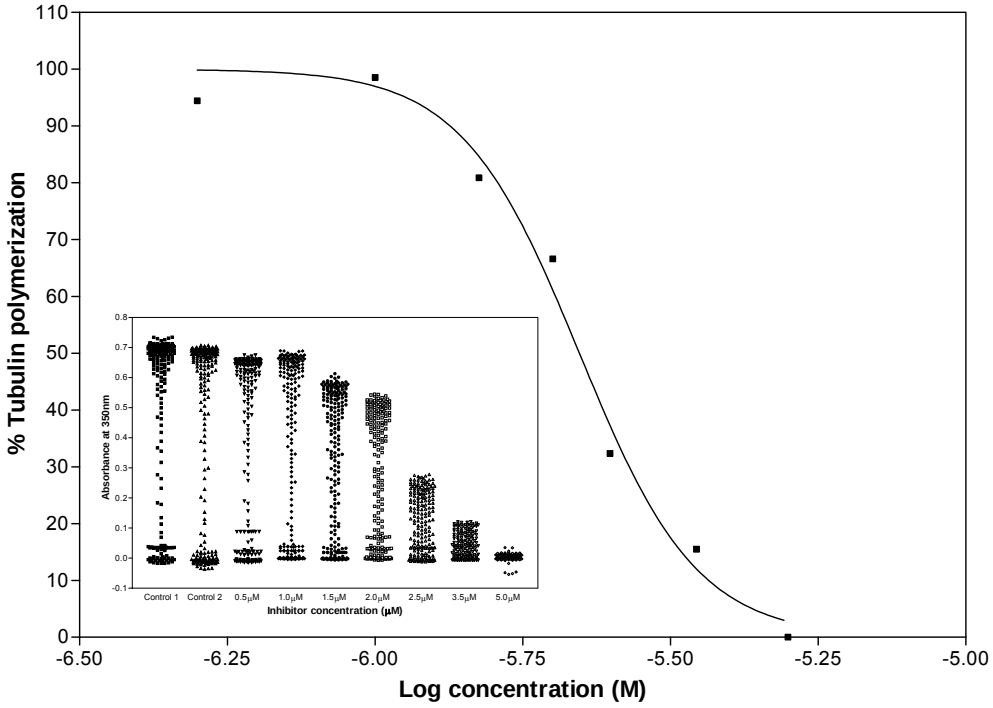

Figure 2.71. Percent Tubulin Polymerization against Log Concentration of Compound **26**.

*Effect of Compounds **27** and **28** on Tubulin Polymerization*

(Z)-1-(3'-Hydroxy,4'-methoxyphenyl)-2-(3",5"-dichloro-4"-methoxyphenyl)-ethene **(27)** (Figure 2.72) with a 3, 5-dichloro substitution in ring A was analyzed for antimitotic activity by determining its effect on tubulin polymerization (Figure 2.73). This analog showed excellent inhibition of tubulin polymerization with an IC_{50} value of 1.7 μM (Figure 2.74). Thus a 3,5-dichloro substitution on ring A leads to combretastatin analogs with significant activity. It would be interesting to find the effect of trichloro substitution in ring A on tubulin polymerization.

(*Z)-1-(2',3'-Dihydroxy,4'-methoxyphenyl)-2-(3",4",5"-trifluorophenyl)-ethene* **(28)**, (Figure 2.72) was analyzed in order to evaluate the effect of trifluoro substitution in ring A on tubulin polymerization. Analysis of compound **28** for inhibition of tubulin polymerization (Figure 2.75) gave a moderate IC_{50} value of 3.0 μM (Figure 2.76). This was 1.6-fold lower than the CA-1 activity. Gaukroger and coworkers synthesized a trifluoro CA-4 derivative which showed an IC_{50} value of 4.5 μM. Thus it is clear that replacement of the trimethoxy moiety with the smaller trifluoro halogen functionality led to a reduction in the potency for an analog to inhibit tubulin polymerization.

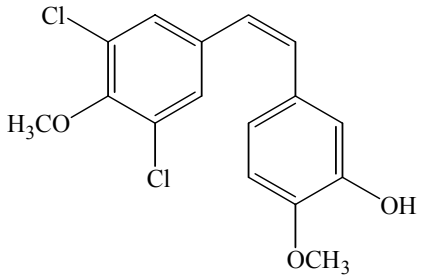

27

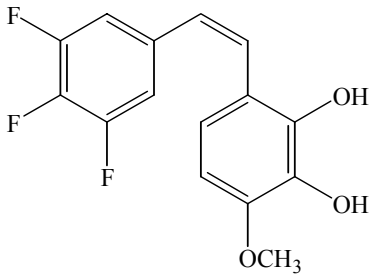

28

Figure 2.72. Structures of Compounds **27** and **28.**

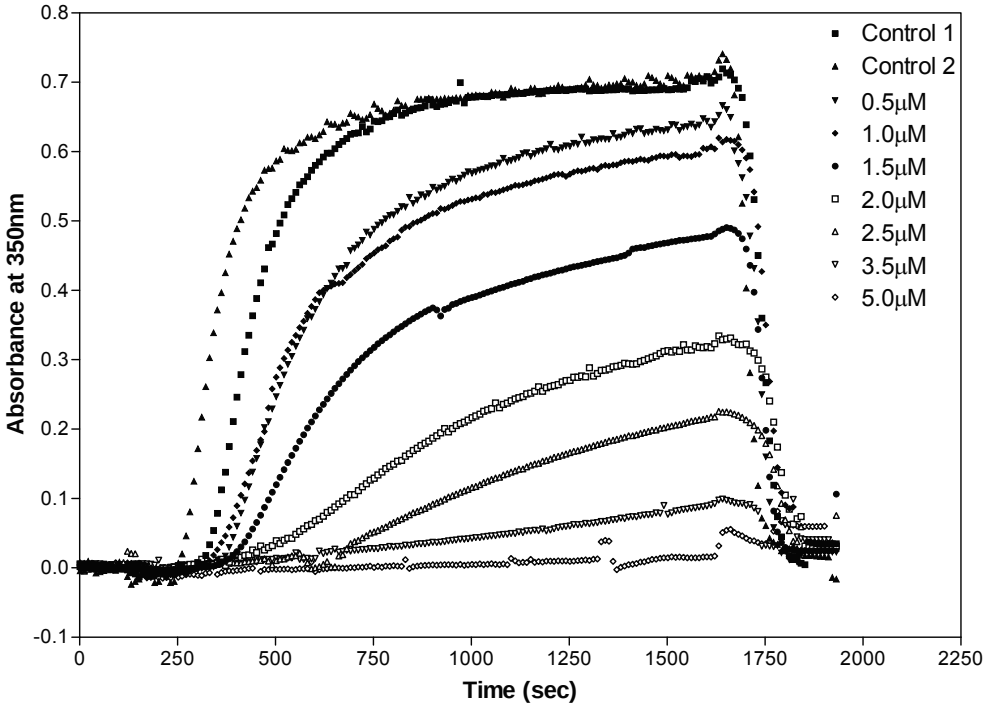

Figure 2.73. Inhibition of Tubulin Polymerization by Compound **27** at 30ºC.

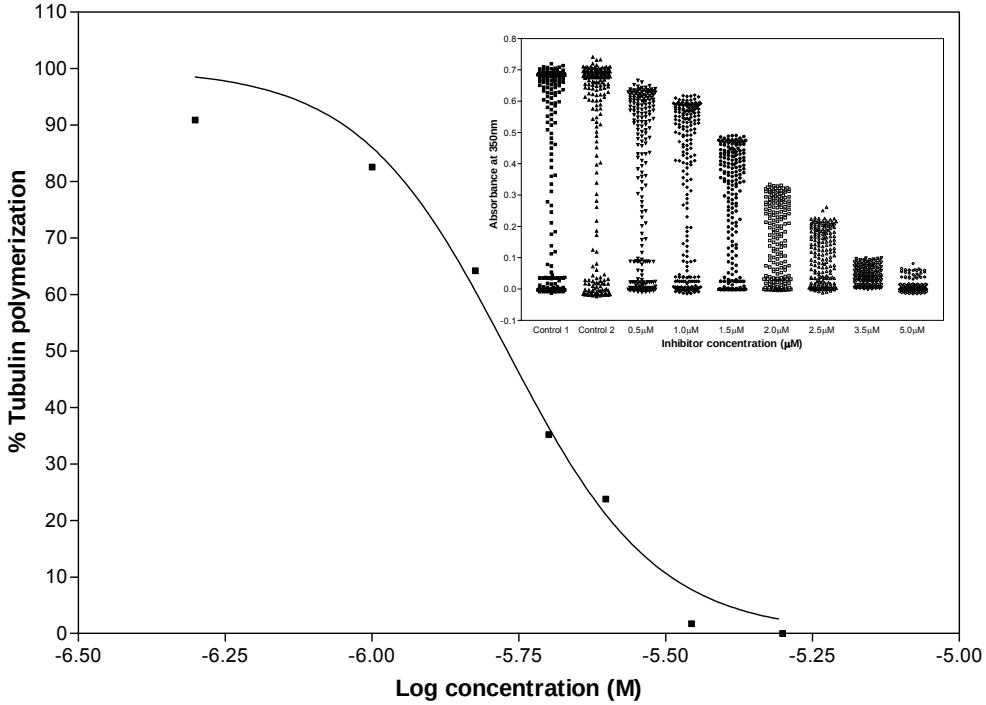

Figure 2.74. Percent Tubulin Polymerization against Log Concentration of Compound **27**.

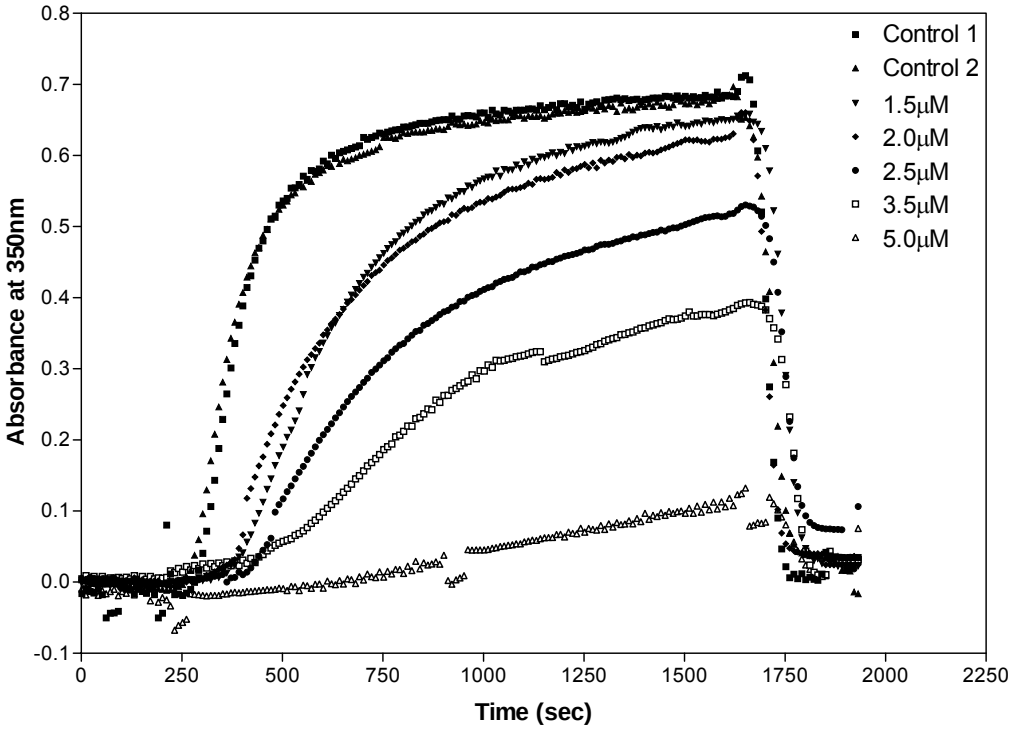

Figure 2.75. Inhibition of Tubulin Polymerization by Compound **28** at 30ºC.

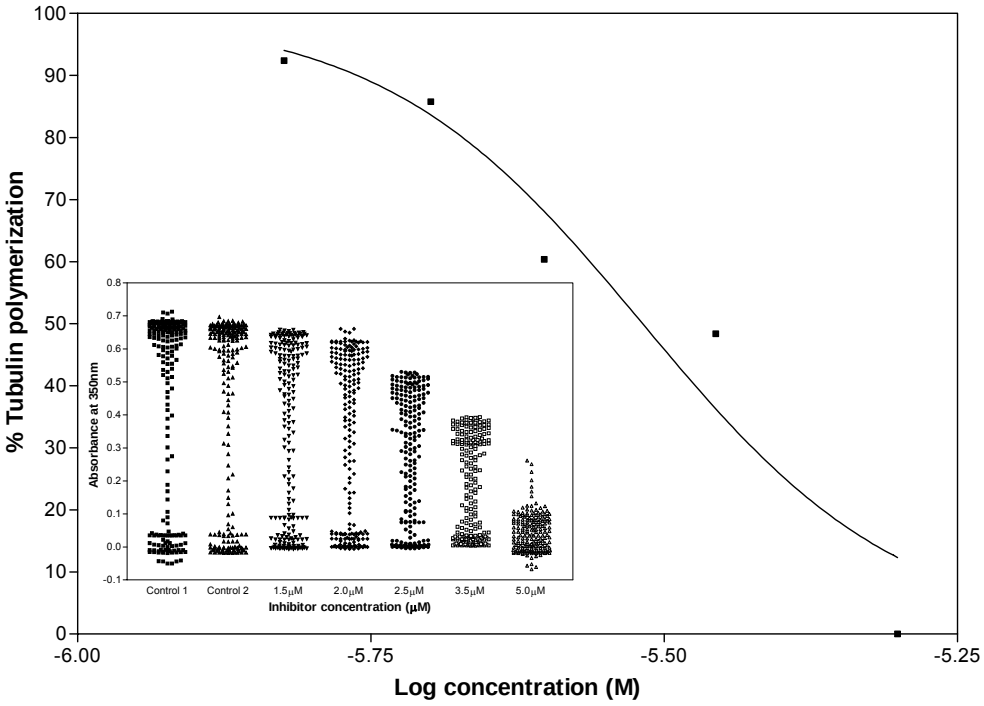

Figure 2.76. Percent Tubulin Polymerization against Log Concentration of Compound **28**.

*Effect of Compounds **29** and **30** on Tubulin Polymerization*

(Z)-1-(3'-Hydroxy-4'-methoxy-2'-nitrosophenyl)-2-(3",4",5"-trimethoxyphenyl)-ethene **(29)** (Figure 2.77), a 2-nitroso CA-1 derivative was analyzed for inhibitory activity on tubulin polymerization (Figure 2.78). Replacement of the hydroxyl group in CA-1 with a nitroso group resulted in a compound with excellent activity with an IC_{50} value of 1.4 μM (Figure 2.79). Introduction of a nitro group in the C-2 position of ring B results in *(Z)-1-(3'-Hydroxy- 4'-methoxy-2'-nitrophenyl)-2-(3",4",5"-trimethoxyphenyl)-ethene* **(30)** (Figure 2.77). When compound **30** was analyzed for antitubulin activity (Figure 2.80), the 2-nitro CA-1 derivative showed strong antitubulin activity with an IC_{50} value of 1.5 μM (Figure 2.81), which was almost equal to that of the 2-nitroso CA-1 derivative.

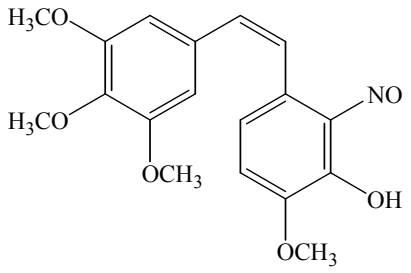

29

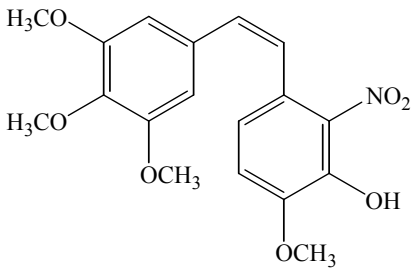

30

Figure 2.77. Structures of Compounds **29** and **30.**

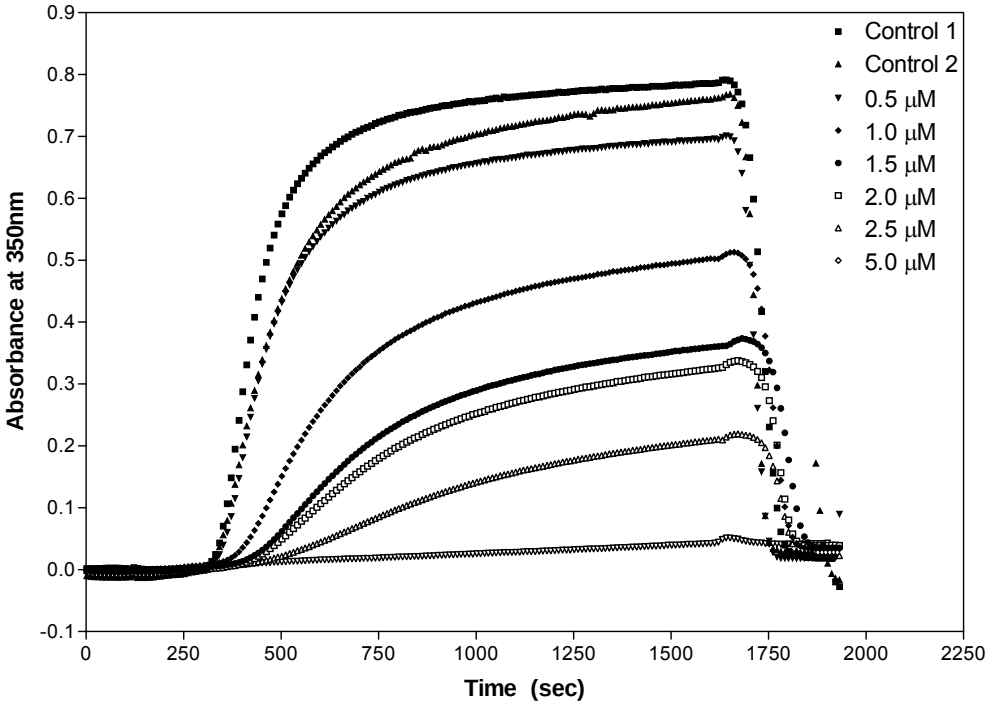

Figure 2.78. Inhibition of Tubulin Polymerization by Compound **29** at 30ºC.

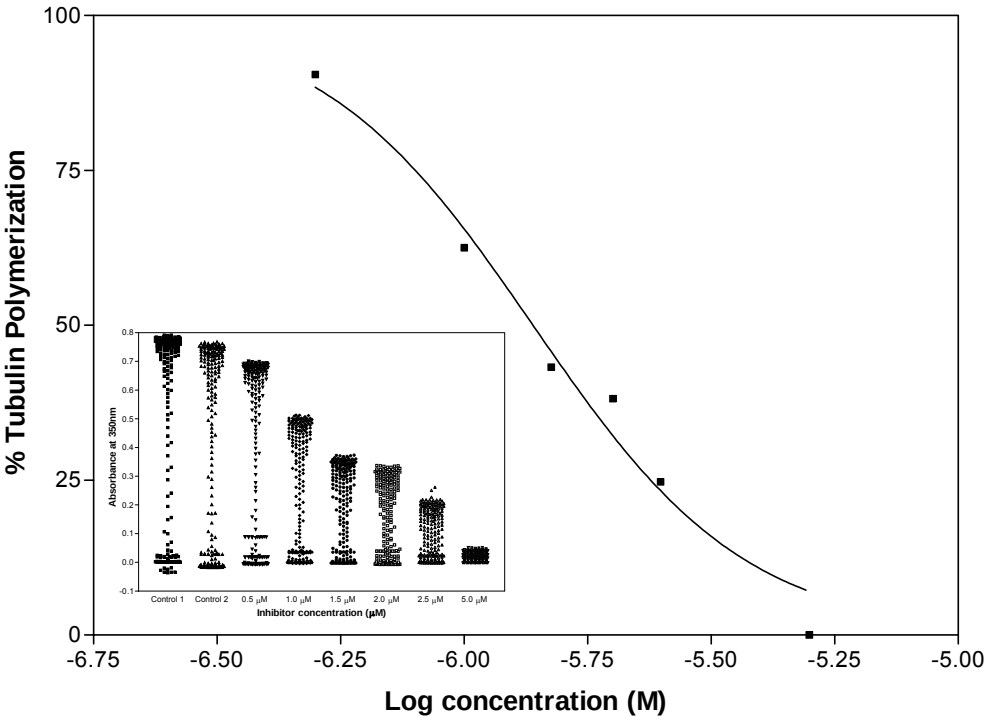

Figure 2.79. Percent Tubulin Polymerization against Log Concentration of Compound **29**.

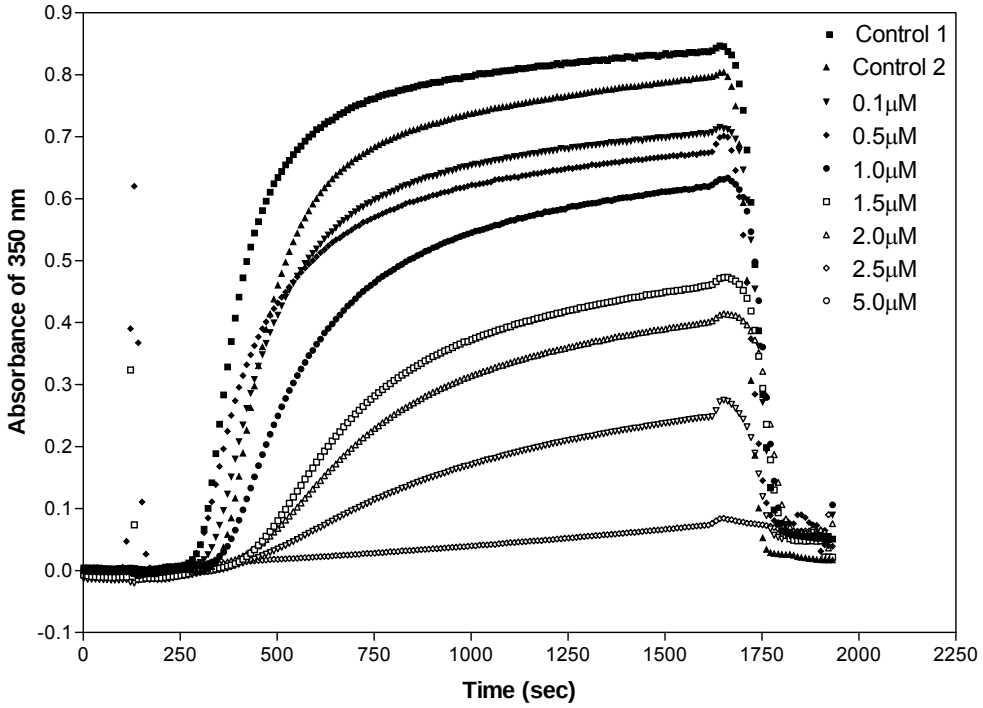

Figure 2.80. Inhibition of Tubulin Polymerization by Compound **30** at 30ºC.

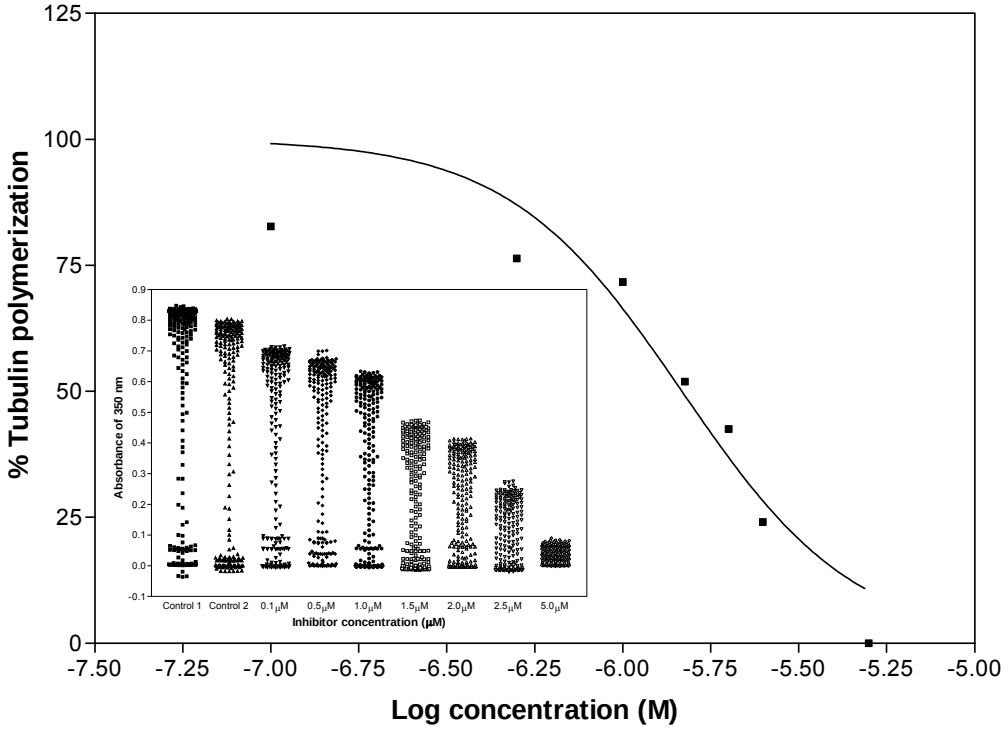

Figure 2.81. Percent Tubulin Polymerization against Log Concentration of Compound **30**.

*Effect of Compounds **31** and **32** on Tubulin Polymerization*

(Z)-1-(3'-Hydroxy-4'-methoxy-5'-nitrophenyl)-2-(3",4",5"-trimethoxyphenyl)-ethene **(31)** (Figure 2.82), was analyzed for antitubulin activity (Figure 2.83). This compound showed excellent antimitotic activity with an IC_{50} value of 2.0 μM (Figure 2.84), which was equivalent to that of CA-1. This meant that the presence of a nitro group in the C-5 position of the B-ring does not significantly affect the potency of the CA-4 derivative so long as the 3-hydroxy, 4-methoxy arrangement is maintained in the B-ring.

However, when *(Z)-1-(4'-Hydroxy-3'-methoxy-5'-nitrophenyl)-2-(3",4",5"-trimethoxyphenyl)-ethene* **(32)** (Figure 2.82), a 5-nitro-stilbene derivative with 3-methoxy and 4-hydroxyl groups was analyzed, the compound showed 5.0% and 34.0% inhibition of tubulin polymerization at 5.0 μM and 40.0 μM. This meant that the positions of the two groups in relation to the nitro-group on the B-ring are fundamental in influencing antitubulin activity.

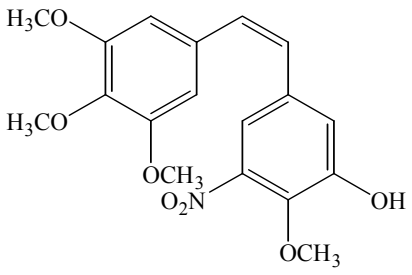

31

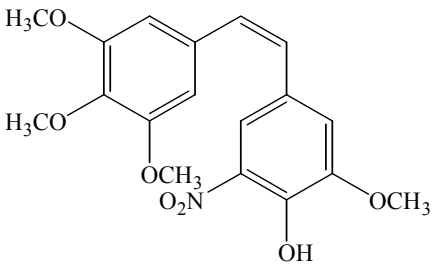

32

Figure 2.82. Structures of Compounds **31** and **32.**

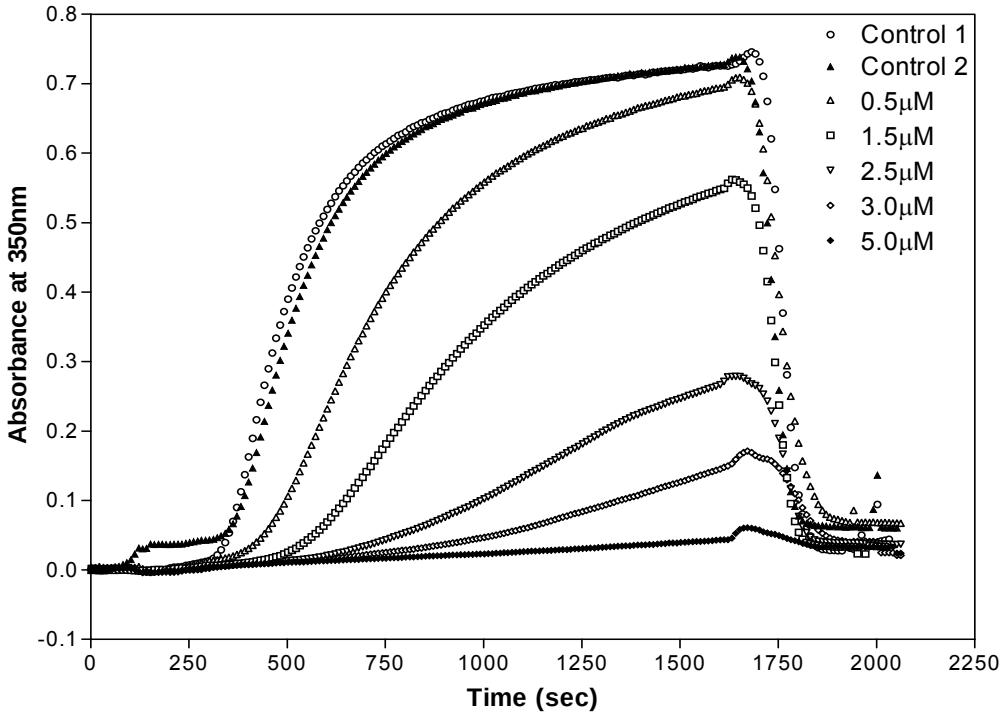

Figure 2.83. Inhibition of Tubulin Polymerization by Compound **31** at 30ºC.

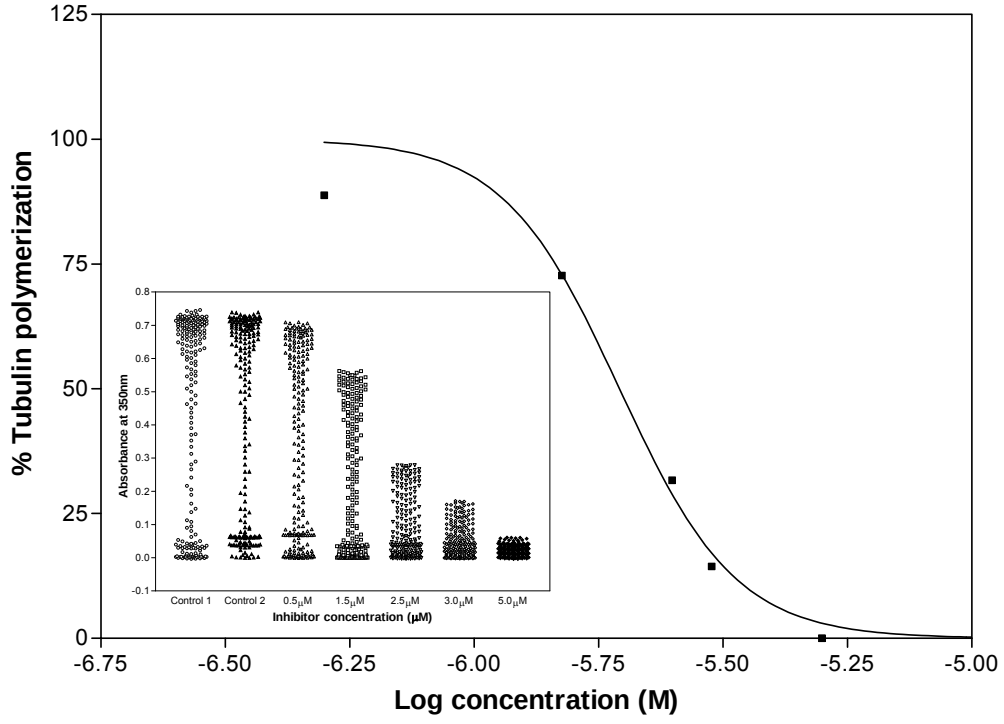

Figure 2.84. Percent Tubulin Polymerization against Log Concentration of Compound **31**.

*Effect of Compounds **33** and **34** on Tubulin Polymerization*

(Z)-1-(5'-Hydroxy-4'-methoxy-2'-nitrophenyl)-2-(3",4",5"-trimethoxyphenyl)-ethene **(33)** (Figure 2.85), a 2-nitro-stilbene derivative with 5-hydroxy and 4-methoxy substitutions was also analyzed for antimitotic activity. This compound showed 13.7% and 34.4% inhibition of tubulin polymerization at 5.0 and 40.0μM respectively.

(Z)-1-(4'-Hydroxy,5'-methoxy,2'-nitrophenyl)-2-(3",4",5"-trimethoxyphenyl)-ethene **(34)** (Figure 2.85), a 2-nitro-stilbene derivative with 4-hydroxy and 5-methoxy substitutions, was also analyzed for antimitotic activity. This compound showed 23.7% inhibition of tubulin polymerization at 40.0 μM .

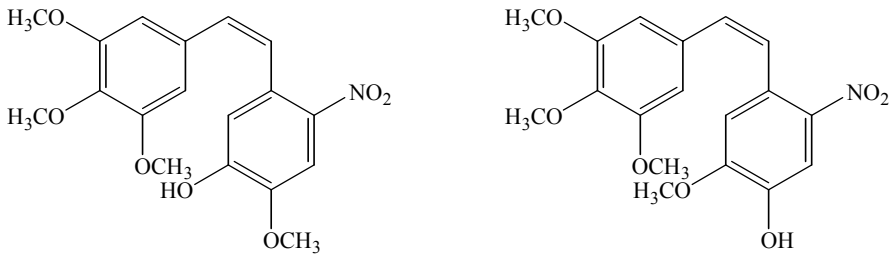

33 **34**

Figure 2.85. Structures of Compounds **33** and **34.**

*Effect of Compounds **35** and **36** on Tubulin Polymerization*

A series of modifications in the position of the nitro, hydroxyl and methoxy groups on the B-ring failed to yield a derivative superior to 2-nitro-CA-1 as inhibitors of tubulin polymerization. When the positions of hydroxyl and methoxy groups in compound **30** were switched giving *(Z)-1-(4'-Hydroxy-3'-methoxy-2'-nitrophenyl)-2-(3",4",5"-trimethoxyphenyl)-ethene* (**35**)(Figure 2.86) with a 3-methoxy and 4-hydroxyl substitution on the B-ring, the resultant 2-nitro- stilbene derivative lost antitubulin

activity and only showed 9.2% inhibition of tubulin polymerization at 40.0 μM upon analysis.

Similarly, when *(Z)-1-(2',3'–Dinitro,4-methoxyphenyl)-2-(3'',4'',5''-trimethoxyphenyl)-ethene* **(36)** (Figure 2.86) was analyzed for antitubulin activity, the compound showed minimal activity with 4.0 % and 40.1 % inhibition of tubulin polymerization at 5.0 and 40.0 μM respectively.

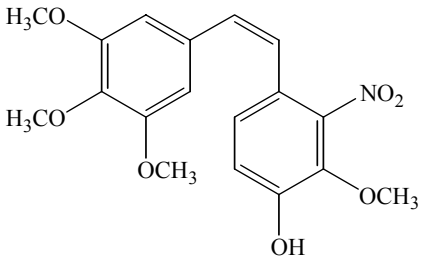

35

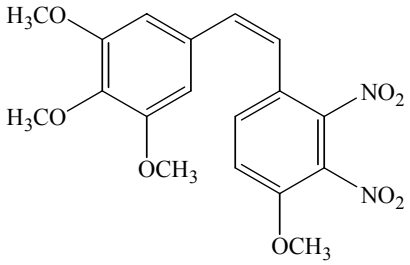

36

Figure 2.86. Structures of Compounds **35** and **36.**

*Effect of Compounds **37** and **38** on Tubulin Polymerization*

(Z)-1-(3',5'–Dinitro,4-methoxyphenyl)-2-(3'',4'',5''-trimethoxyphenyl)-ethene **(37)** (Figure 2.87), a 3,5-dinitrosubstituted combretastatin analog, when analyzed for inhibition of tubulin polymerization (Figure 2.88), showed moderate antimitotic activity with an IC_{50} value of 7.4 μM (Figure 2.89), which was 3.7-fold less effective than

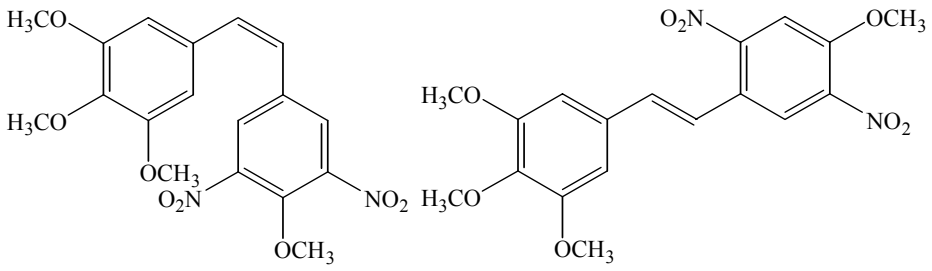

37 **38**

Figure 2.87. Structures of Compounds **37** and **38.**

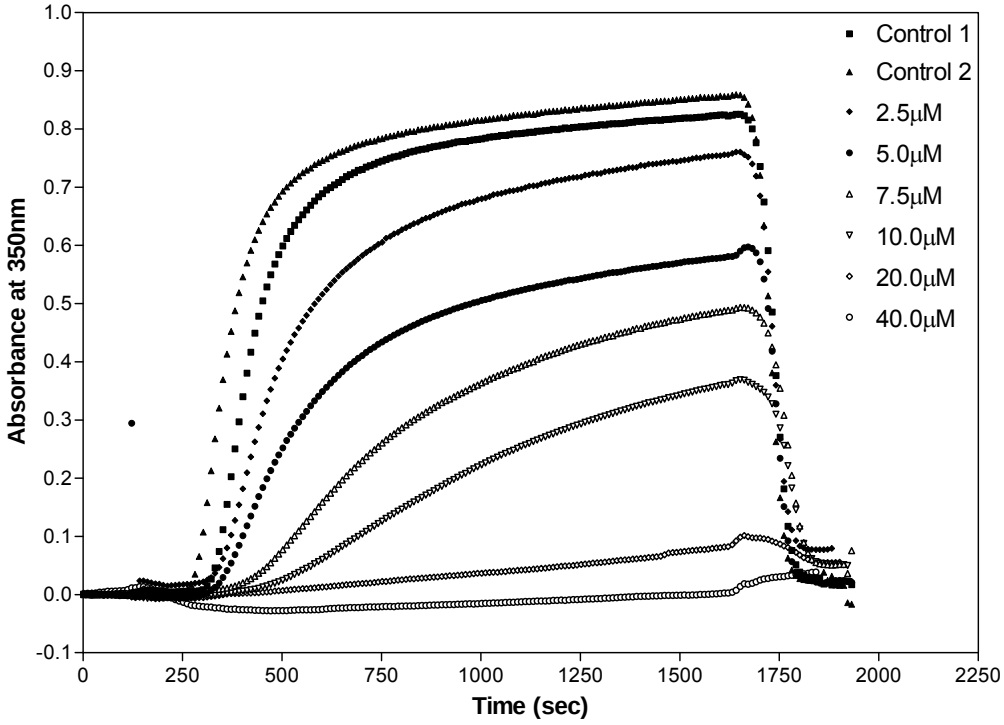

Figure 2.88. Inhibition of Tubulin Polymerization by Compound **37** at 30ºC.

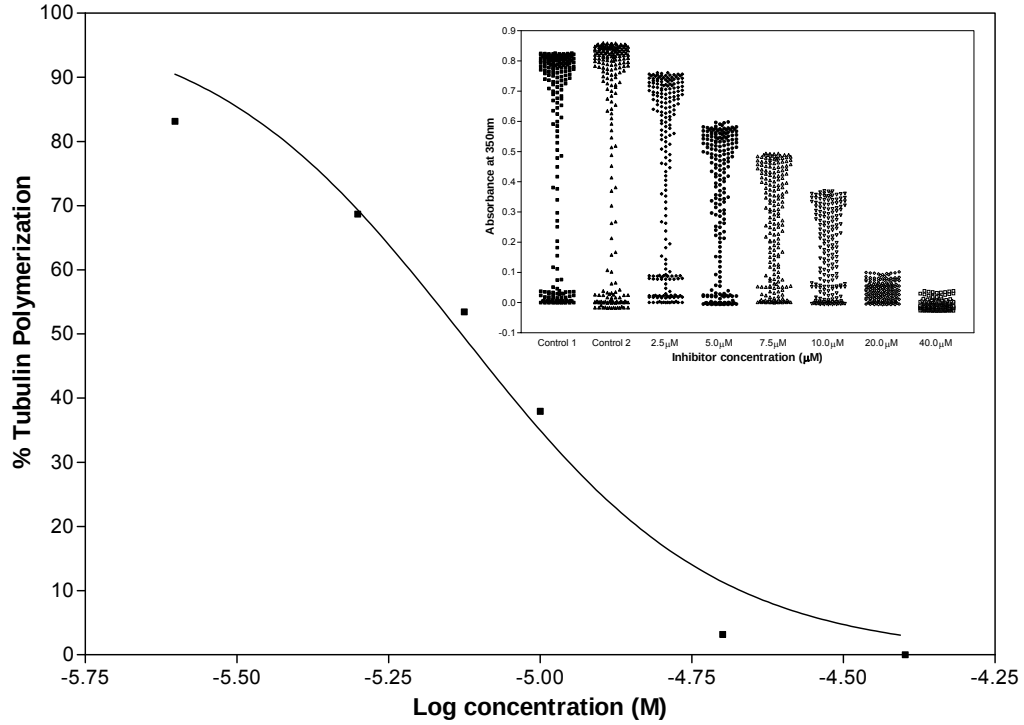

Figure 2.89. Percent Tubulin Polymerization against Log Concentration of Compound **37**.

(*Z)-1-(3'-Hydroxy-4'-methoxy-5'-nitrophenyl)-2-(3",4",5"-trimethoxyphenyl)-ethene* **(31)** and CA-1. Compound *(E)-1-(2',5'–Dinitro,4-methoxyphenyl)-2-(3",4",5"-trimethoxyphenyl)-ethene* **(38)** (Figure 2.87), a *trans* 2, 5-dinitrosubstituted combretastatin derivative, was essentially inactive. When this compound was analyzed for inhibition of tubulin polymerization, it showed less than 2.0% inhibitory effect on microtubule assembly at 40.0 μM. This result underlined and confirmed earlier reports on the loss of potency by *trans* stilbene isomers documented by various investigators in most combretastatin analogs (Cushman *et al*., 1991).

Table 2.4. Biochemical Data for Compounds **31 - 40.**

Compound	IC_{50} (μM)	Log IC_{50} ± SE	Hillslope ± SE	R^2
31	2.0	-5.704 ± 0.02	-3.6 ± 0.6	0.98
32	-	-	-	-
33	> 40.0	-	-	-
34	> 40.0	-	-	-
35	> 40.0	-	-	-
36	> 40.0	-	-	-
37	7.4	-5.130 ± 0.03	-2.1 ± 0.3	0.97
38	> 40.0	-	-	-
39	2.5	-5.596 ± 0.03	-2.5 ± 0.3	0.96
40	2.0	-5.704 ± 0.02	-3.9 ± 1.0	0.98

*Effect of Compounds **39** and **40** on Tubulin Polymerization*

In order to determine the inhibitory effect of amino substitution in CA-1 on tubulin polymerization, *(Z)-1-(2'-Amino-3'-hydroxy-4'-methoxyphenyl)-2-(3",4",5"-trimethoxyphenyl)-ethene* **(39)** (Figure 2.90), a 2-amino CA-1 analog was analyzed for antitubulin activity (Figure 2.91). Results showed that compound **39** inhibits tubulin polymerization with an IC_{50} value of 2.5 μM (Figure 2.92). This was a 1.3-fold decrease in activity than CA-1(Monk *et al*., 2005).

In order to improve the aqueous solubility of this 2-amino CA-1 derivative, *(Z)-1-(2'-Amino-3'-hydroxy-4'-methoxyphenyl)-2-(3",4",5"-trimethoxyphenyl)-ethene hydrochloride* **(40)** (Figure 2.90), a water-soluble hydrochloride salt of compound **39**, was formulated and analyzed for its antitubulin activity (Figure 2.93). Compound **40** showed excellent inhibition of tubulin polymerization with an IC_{50} value of 2.0 μM (Figure 2.94) which was similar and comparable to that of CA-1. Although different pharmacokinetics were expected for both compound **39** and its hydrochloride salt compound **40**, there seemed to be no significant differences in their individual interactions with tubulin at the colchicine binding site.

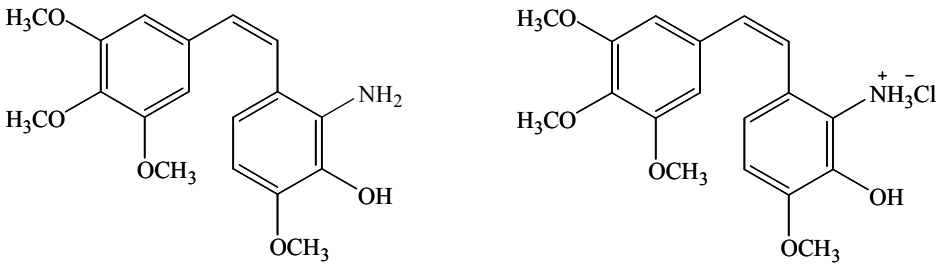

39 **40**

Figure 2.90. Structures of Compounds **39** and **40**.

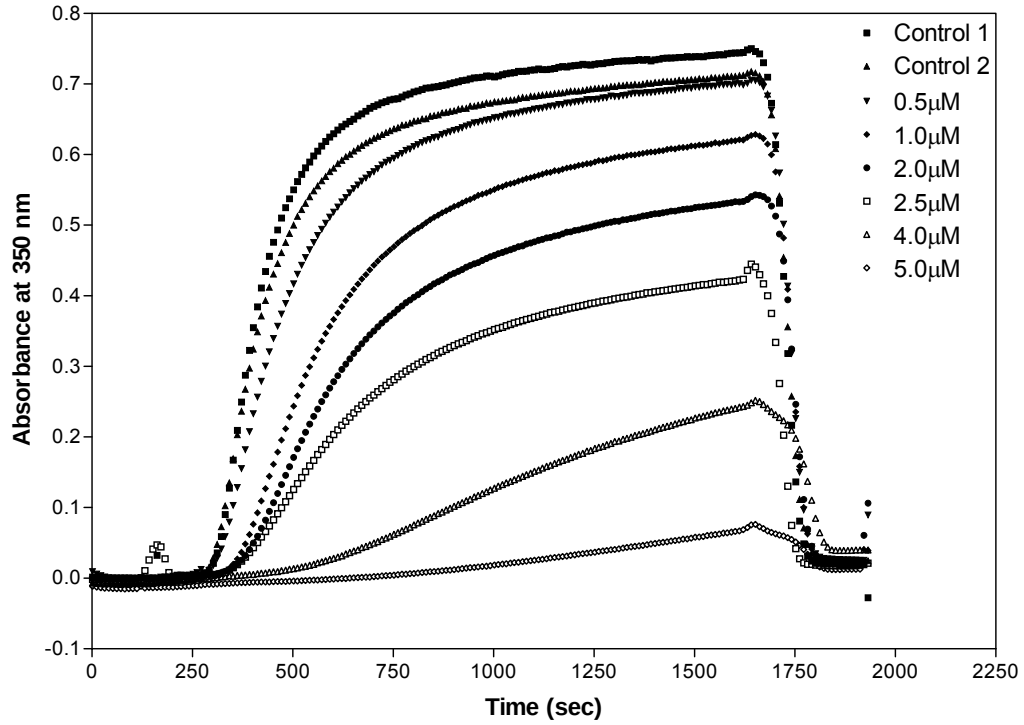

Figure 2.91. Inhibition of Tubulin Polymerization by Compound **39** at 30ºC.

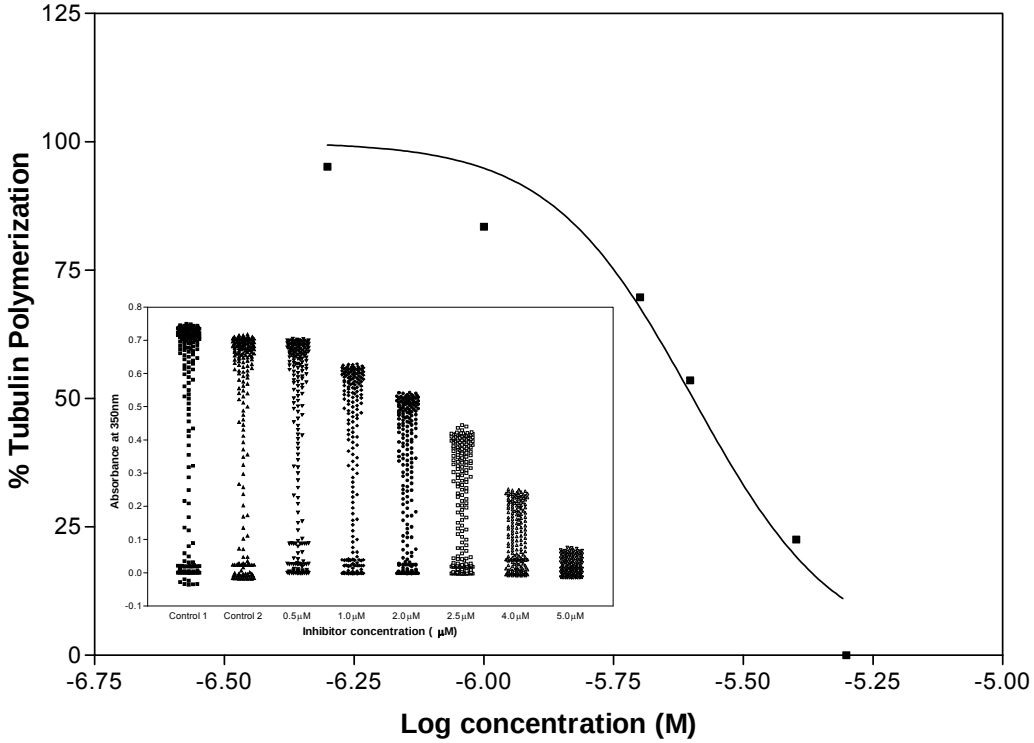

Figure 2.92. Percent Tubulin Polymerization against Log Concentration of Compound **39**.

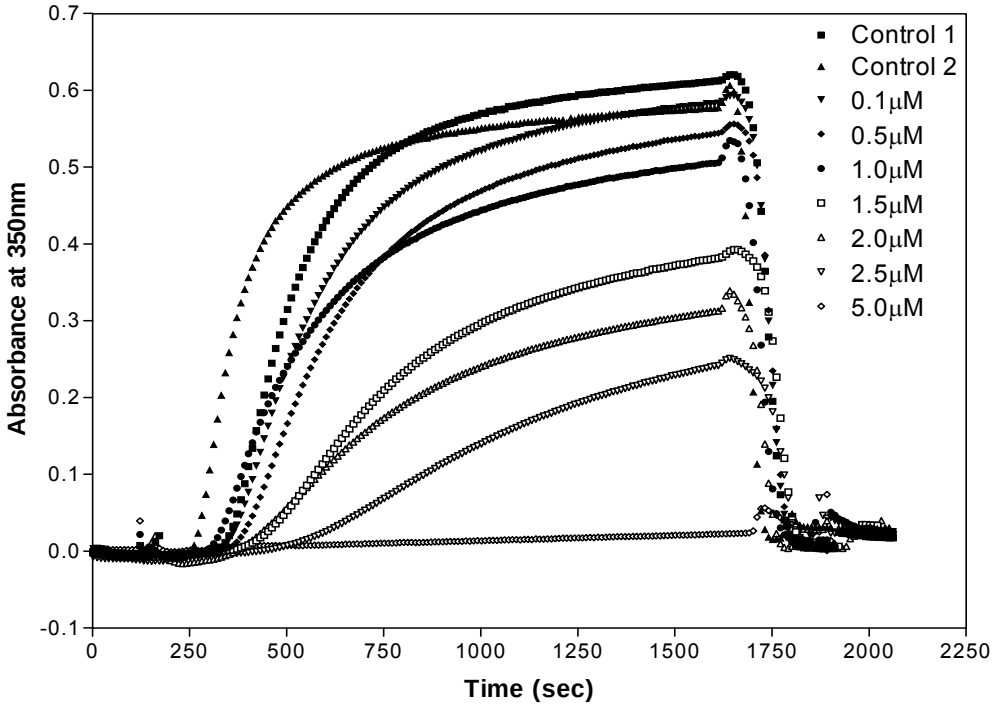

Figure 2.93. Inhibition of Tubulin Polymerization by Compound **40** at 30ºC.

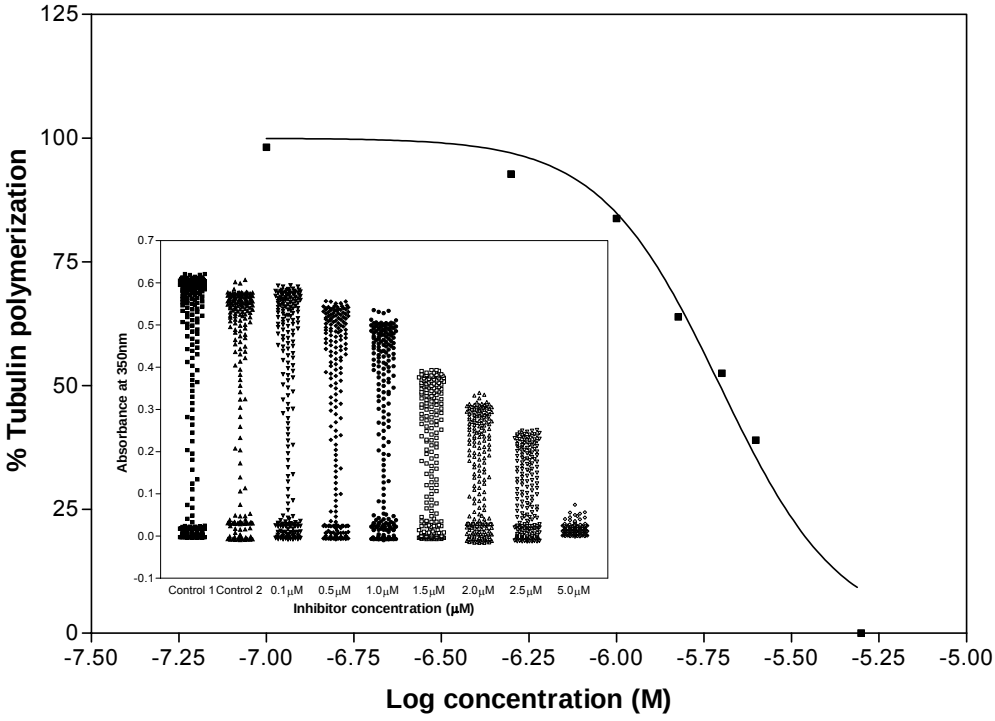

Figure 2.94. Percent Tubulin Polymerization against Log Concentration of Compound **40**.

*Effect of Compound **41** on tubulin polymerization*

(Z)-1-(2'-Amino,4'-hydroxy,3'-methoxyphenyl)-2-(3",4",5"-trimethoxyphenyl)-ethene (**41**) (Figure 2.95), a CA-1 derivative with a 3-methoxy -4-hydroxy substitution in the B-ring did not inhibit tubulin polymerization.

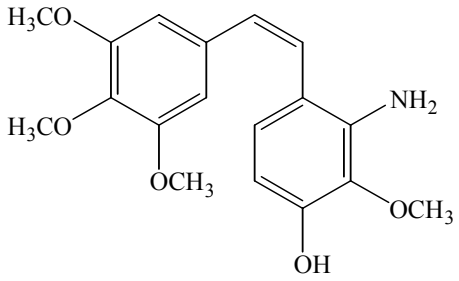

41

Figure 2.95. Structure of Compound **41.**

*Effect of Compounds **42** and **43** on Tubulin Polymerization*

(Z)-1-(2'-Amino, 4'-methoxyphenyl)-2-(3",4",5"-trimethoxyphenyl)-ethene (**42**) (Figure 2.96), was also analyzed for antitubulin activity (Figure 2.97). This compound exhibited excellent inhibition of tubulin polymerization with an IC_{50} value of 1.4 μM (Figure 2.98) which was comparable to that of the lead compound CA-4. *(Z)-1-(2'-Amino,4'-methoxyphenyl)-2-(3",4",5"-trimethoxyphenyl)-ethene hydrochloride* (**43**) (Figure 2.96), a water soluble derivative of compound **42** was equally effective in inhibiting polymerization of tubulin into microtubules. Total inhibitory activity was observed at both concentrations of 5.0 and 40.0 μM.

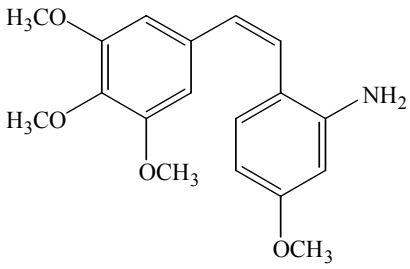

42

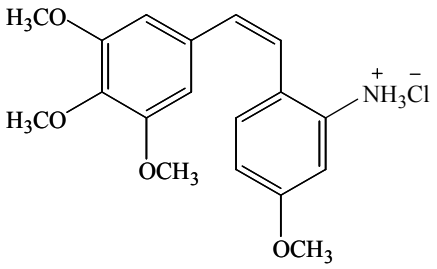

43

Figure 2.96. Structures of Compounds **42** and **43.**

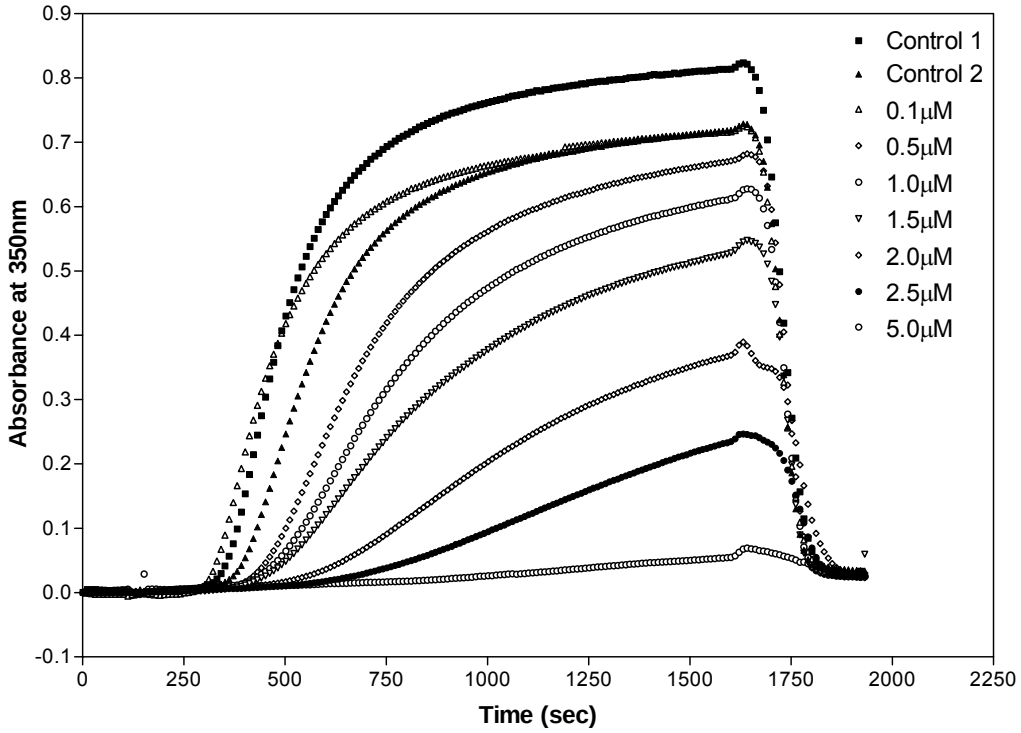

Figure 2.97. Inhibition of Tubulin Polymerization by Compound **42** at 30ºC.

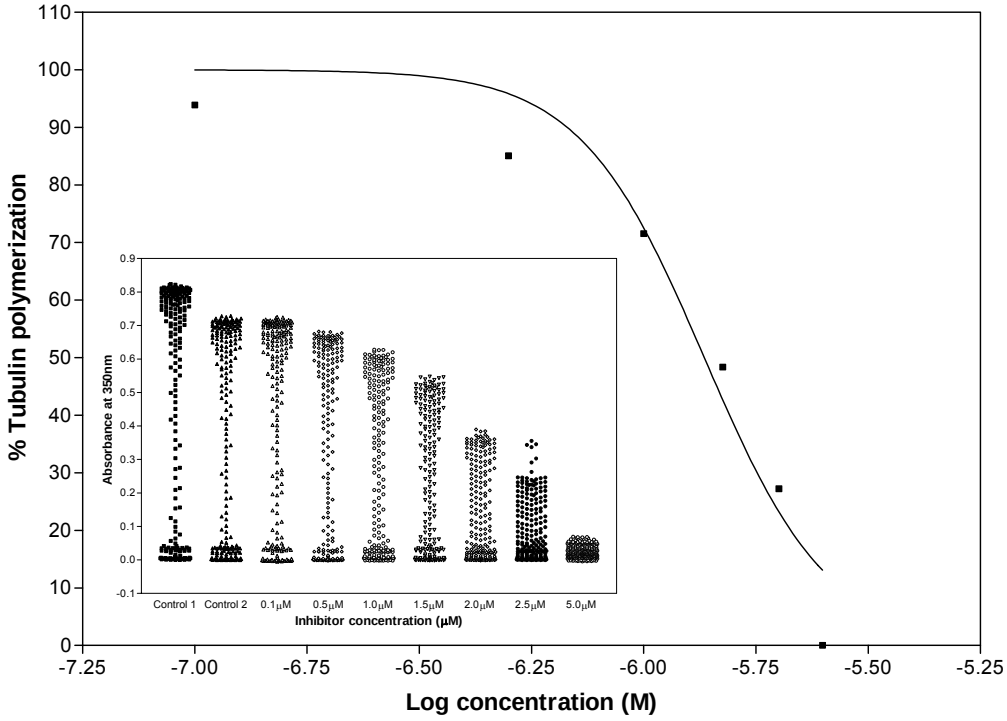

Figure 2.98. Percent Tubulin Polymerization against Log Concentration of Compound **42**.

These results pointed to the importance of maintaining a more nucleophilic substitute in the C-2 position if significant antitubulin activity is to be envisaged in the combretastatin analogs. In presence of a 4-methoxy group in the B-ring, amino or hydroxyl substitution on any of the C-2 or C-3 positions leads to potent derivatives.

*Effect of Compounds **44** and **45** on Tubulin Polymerization*

When the phenolic hydroxyl group in combretastatin A-4 was replaced with an amino group, the resultant *(Z)-1-(3'-Amino-4'-methoxyphenyl)-2-(3",4",5"-trimethoxyphenyl)-ethene* **(44)** (Figure 2.99) was tested for antitubulin activity (Figure 2.100). This compound revealed potent antitubulin activity with an IC_{50} value of

2.6 μM (Figure 2.101). However this was a 2.2-fold decrease in inhibition of tubulin polymerization activity when compared to the lead compound combretastatin A-4. Ohsumi and coworkers (1998) have reported an antitubulin activity for this compound with an IC_{50} value of 4.0 μM and Pinney and coworkers (2000) reported an IC_{50} value of 1.2 μM.

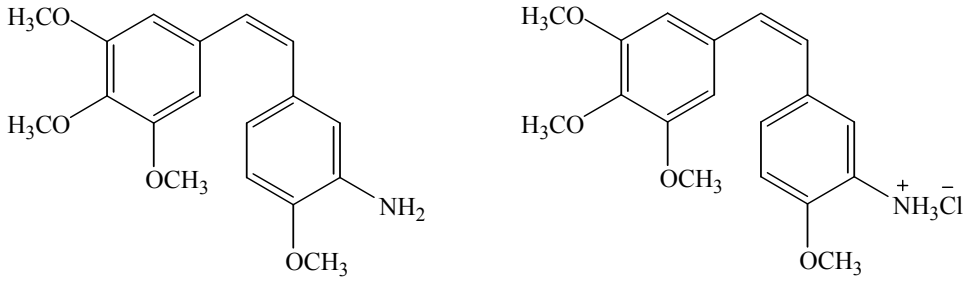

44 **45**

Figure 2.99. Structures of Compounds **44** and **45**.

(Z)-1-(3'-Amino-4'-methoxyphenyl)-2-(3",4",5"-trimethoxyphenyl)-ethene hydrochloride **(45)** (Figure 2.99), a water soluble derivative of compound **44** upon testing (Figure 2.102), showed excellent antitubulin characteristics with an IC_{50} value of 1.3 μM (Figure 2.103).

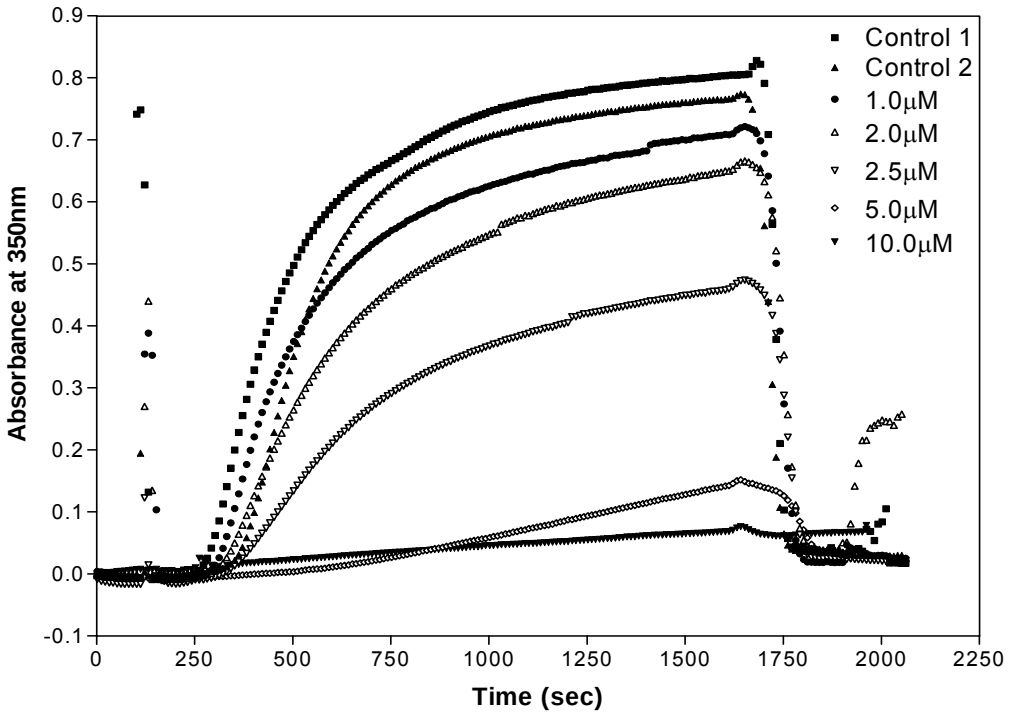

Figure 2.100. Inhibition of Tubulin Polymerization by Compound **44** at 30ºC.

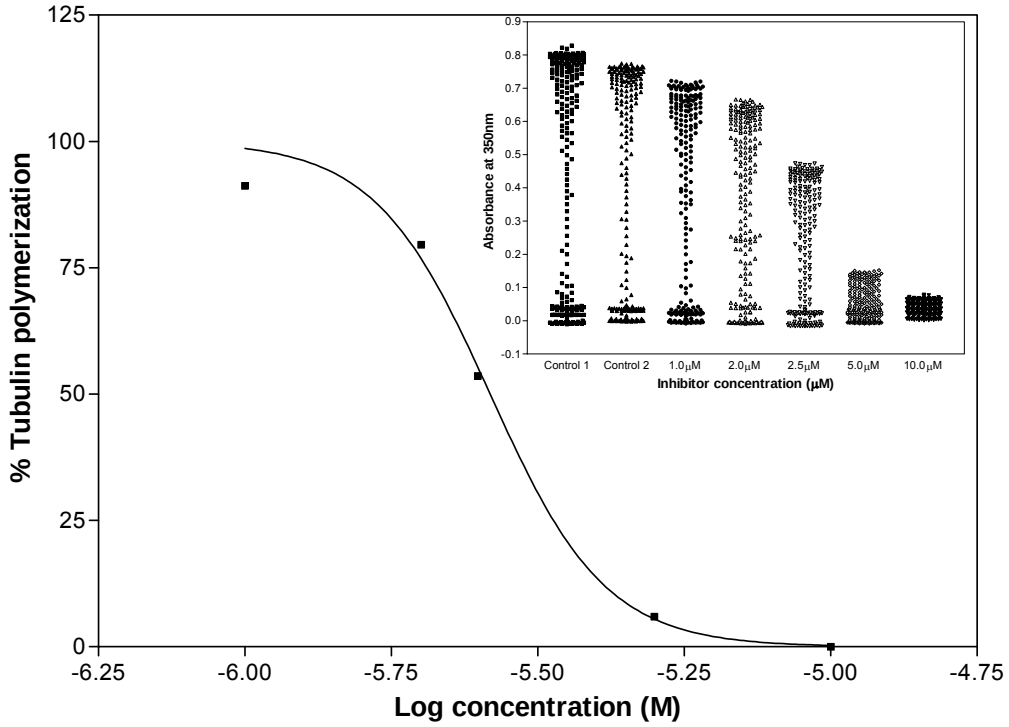

Figure 2.101. Percent Tubulin Polymerization against Log Concentration of Compound **44**.

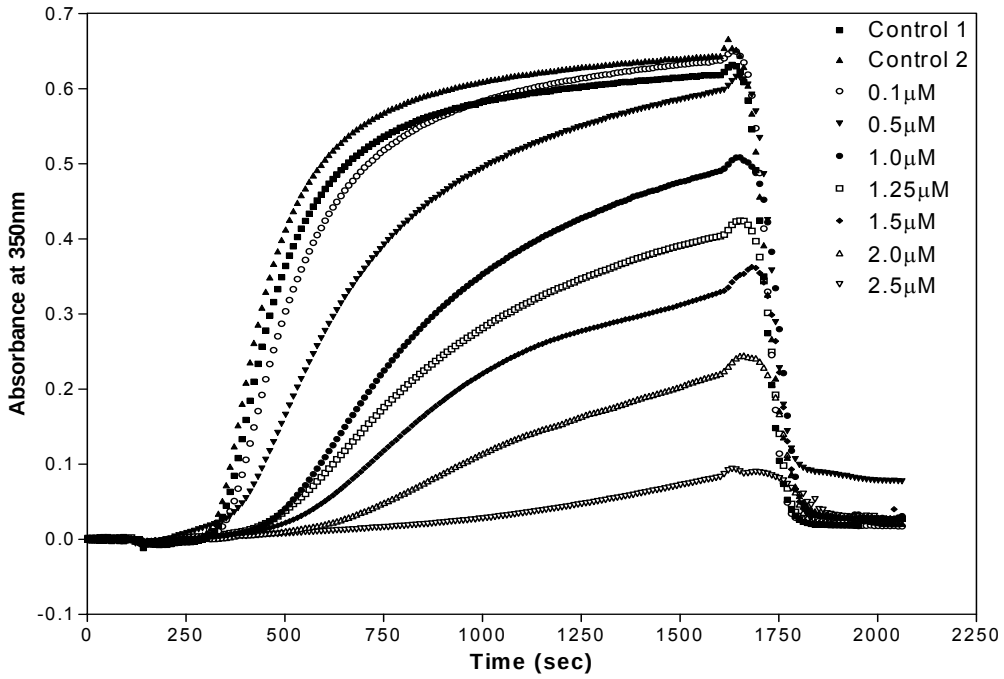

Figure 2.102. Inhibition of Tubulin Polymerization by Compound **45** at 30ºC.

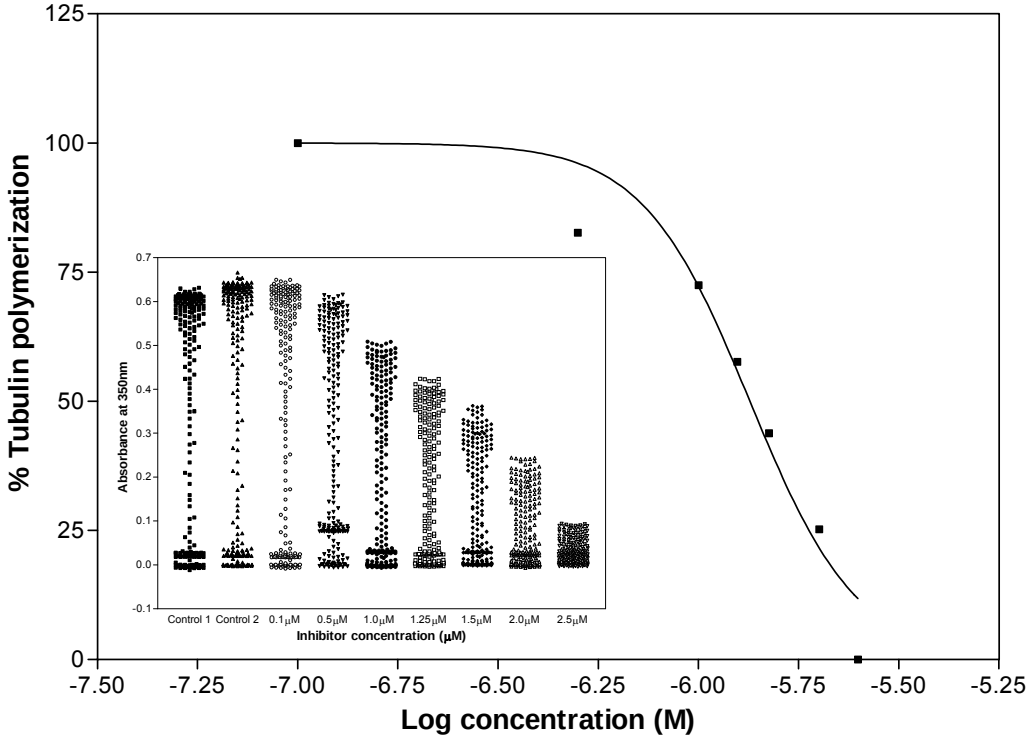

Figure 2.103. Percent Tubulin Polymerization against Log concentration of Compound **45**.

Effect of Compounds ***46*** *and* ***47*** *on Tubulin Polymerization*

(Z)-1-(2'-Amino-4'-methoxyphenyl)-2-(3",4",5"-trimethoxyphenyl)-ethene-L-serinamide **(46)** (Figure 2.104), a serinamide derivative of CA-4 with no hydroxyl group at position 3, was analyzed for antitubulin activity. This compound showed 20.0 % inhibition of tubulin polymerization at 40.0 μM.

(*Z)-1-(2'-Amino-4'-methoxyphenyl)-2-(3",4",5"-trimethoxyphenyl)-ethene-L-serinamide hydrochloride* **(47)** (Figure 2.104), a C-2 position CA-1 serinamide hydrochloride salt derivative with no hydroxyl group on position 3 of ring B, was also evaluated for antitubulin activity. This compound showed 35.8 % and 49.0 % inhibition of tubulin polymerization at 40.0 μM and 50.0 μM respectively. The absence of the hydroxyl group in the C-3 position of the B-ring may have led to the diminished antitubulin nature of this CA-1 analog.

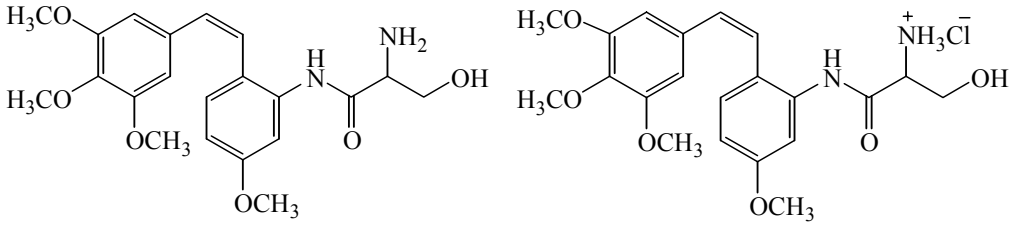

46 **47**

Figure 2.104. Structure of Compound **46** and **47**.

*Effect of Compounds **48** and **49** on Tubulin Polymerization*

(Z)-1-(3'-Amino-4'-methoxyphenyl)-2-(3",4",5"-trimethoxyphenyl)-ethene-L-serinamide **(48)** (Figure 2.105), a serinamide derivative of CA-4, was analyzed for antitubulin activity (Figure 2.106). This compound showed decreased antitubulin activity with an IC_{50} value of 9.6 μM (Figure 2.107). Ohsumi and coworkers (1999) have reported that this serine derivative of amine **48** is the most active among several other amino acid derivatives of CA-4.

(Z)-1-(3'-Amino-4'-methoxyphenyl)-2-(3",4",5"-trimethoxyphenyl)-ethene-L-serinamide hydrochloride **(49)** (Figure 2.105), a water soluble serinamide hydrochloride salt derivative of CA-4 was analyzed for antitubulin activity (Figure 2.108), the compound showed reduced inhibition of tubulin polymerization activity with an IC_{50} value of 11.3 μM (Figure 2.109). This was a 1.2- and 9.4-fold decrease in antitubulin activity compared to the CA-4 serinamide (compound **48**) and CA-4 respectively.

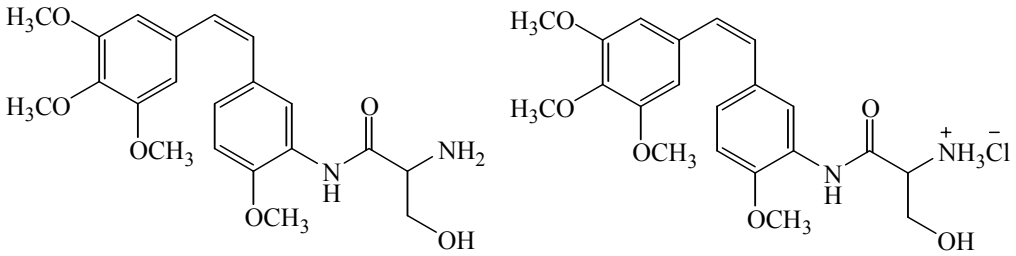

48 **49**

Figure 2.105. Structures of Compounds **48** and **49**.

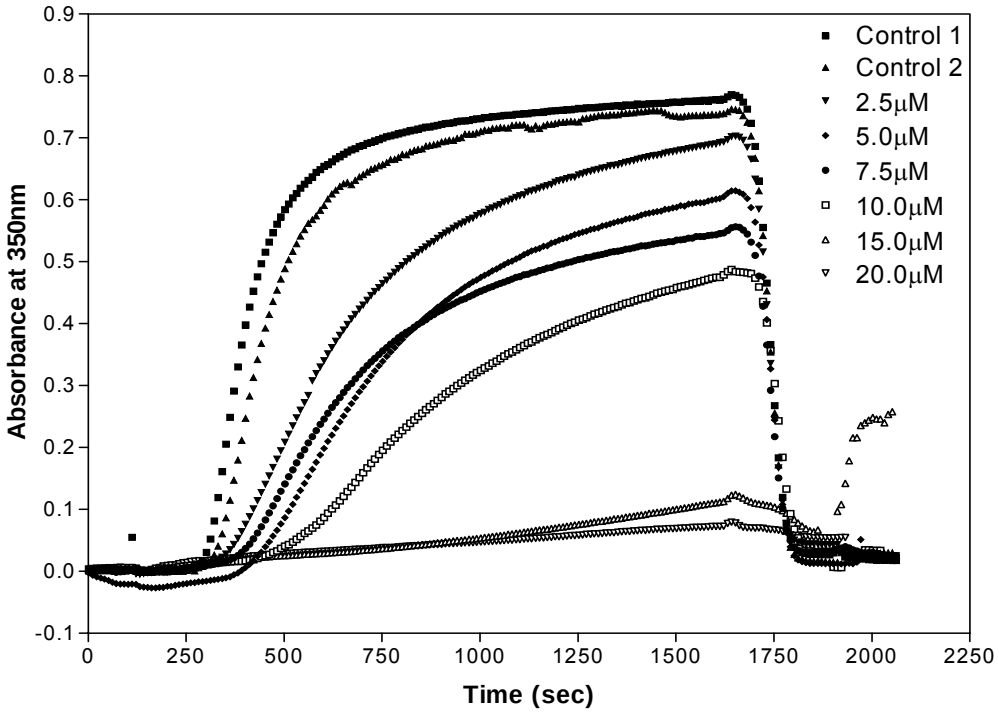

Figure 2.106. Inhibition of Tubulin Polymerization by Compound **48** at 30ºC.

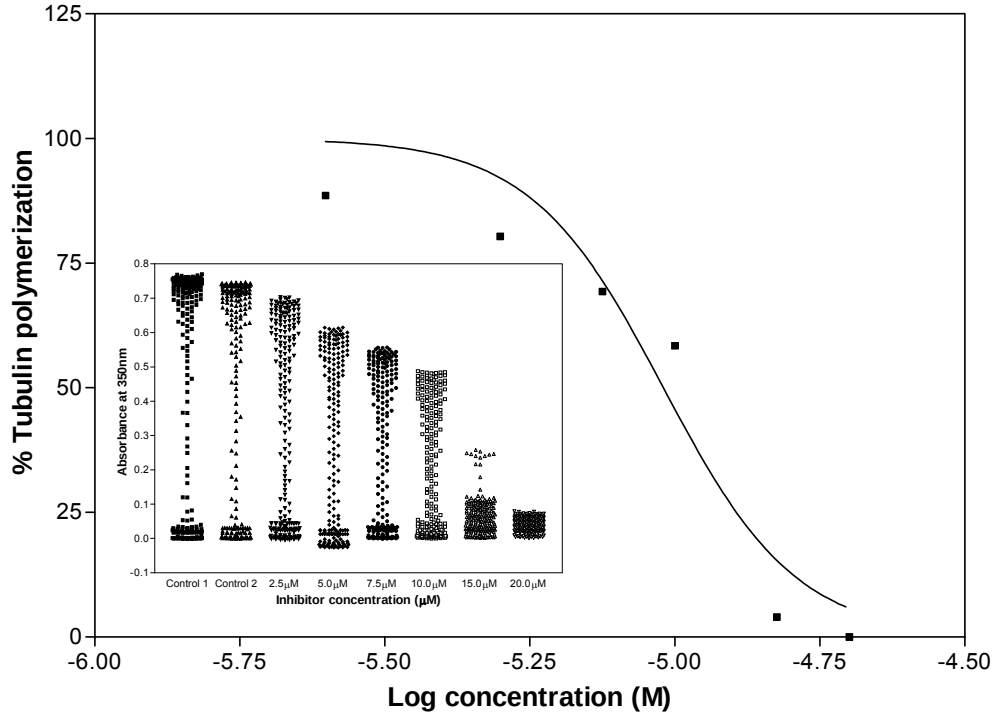

Figure 2.107. Percent Tubulin Polymerization against Log Concentration of Compound **48**.

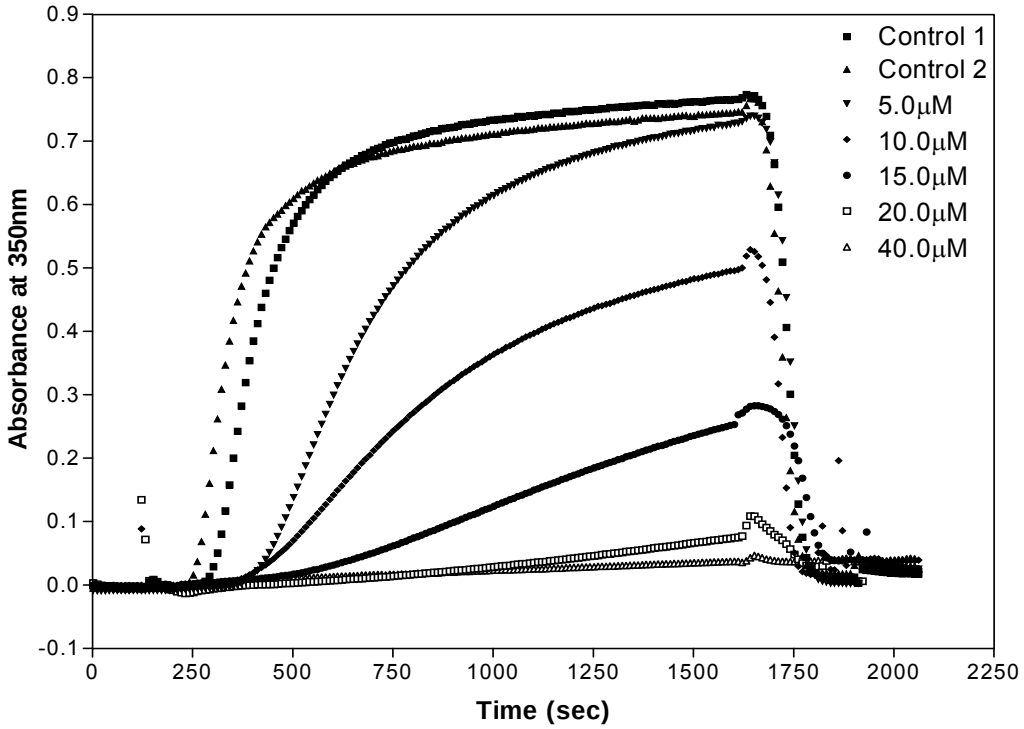

Figure 2.108. Inhibition of Tubulin Polymerization by Compound **49** at 30ºC.

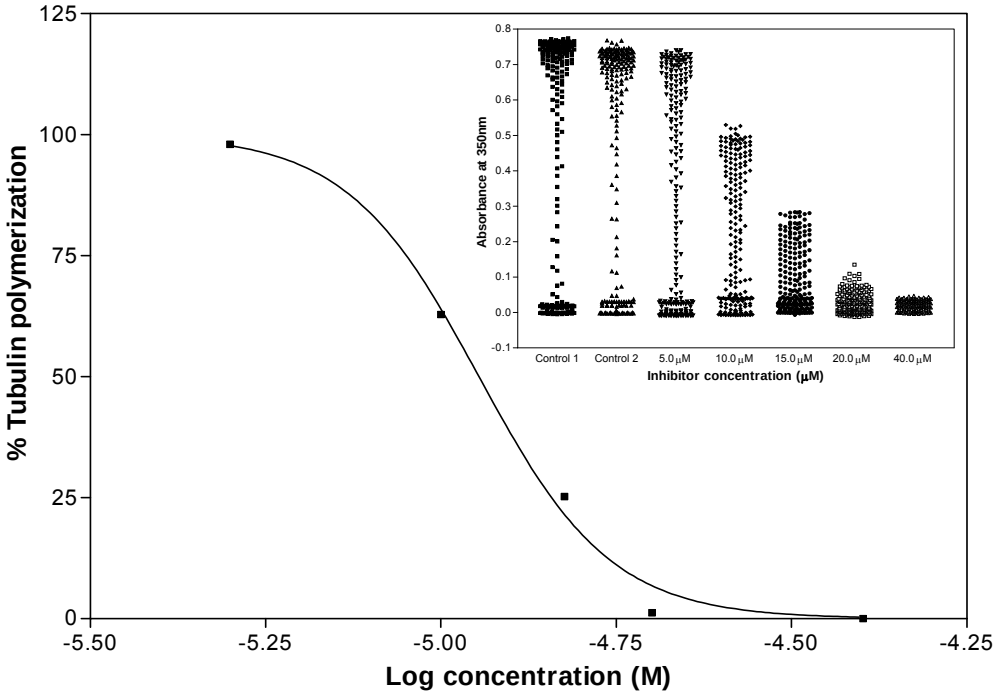

Figure 2.109. Percent Tubulin Polymerization against Log Concentration of Compound **49**.

Effect of Compounds ***50*** *and* ***51*** *on Tubulin Polymerization*

(Z)-1-(3',5'-Diamino-4'-methoxyphenyl)-2-(3",4",5"-trimethoxyphenyl)-ethene-L-di-serinamide **(50)** (Figure 2.110), was analyzed for inhibitory effect on tubulin polymerization. Incorporation of another serinamide moiety on position 5 of ring B of *(Z)-1-(3'-Amino-4'-methoxyphenyl)-2-(3",4",5"-trimethoxyphenyl)-ethene-L-serinamide* giving the finger-like analog resulted in total loss of inhibition of tubulin polymerization potency (Rogelio *et al*., 2005).

(Z)-1-(2'-Amino-4'-methoxy-5'-nitrophenyl)-2-(3",4",5"-trimethoxyphenyl)-ethene **(51)** (Figure 2.110), a 2-amino, 4-methoxy and 5-nitrophenyl CA-1 derivative was analyzed for antitubulin activity (Figure 2.111). This compound showed diminished inhibition of tubulin polymerization with an IC_{50} value of 17.4 μM (Figure 2.112). This decreased activity observed in these compounds (**46 - 51**) underlined the importance of the 2,3-dihydroxy-4-methoxyphenyl arrangement in natural CA-1 and the tremendous effect it plays on its antitubulin characteristics.

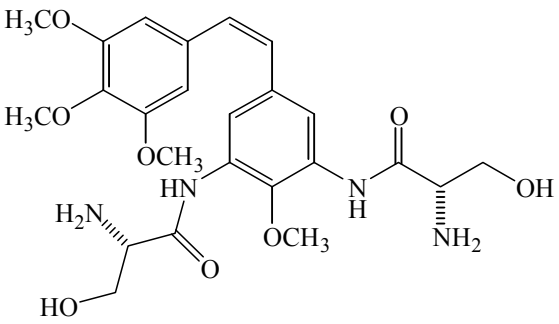

50

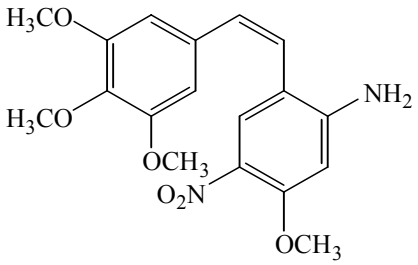

51

Figure 2.110. Structures of Compounds **50** and **51**.

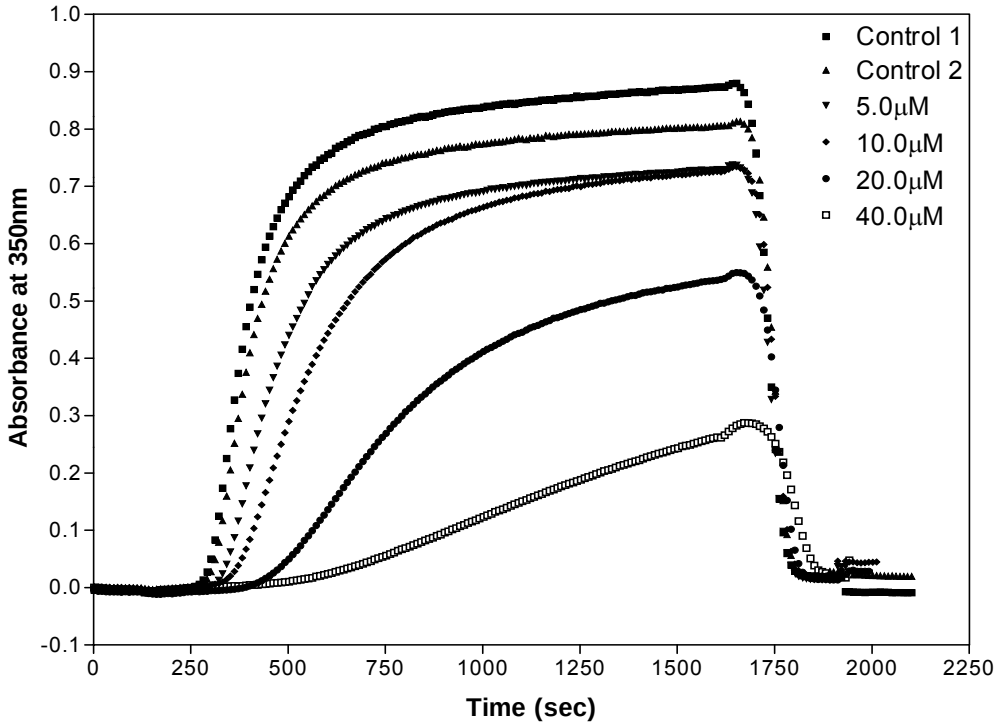

Figure 2.111. Inhibition of Tubulin Polymerization by Compound **51** at 30ºC.

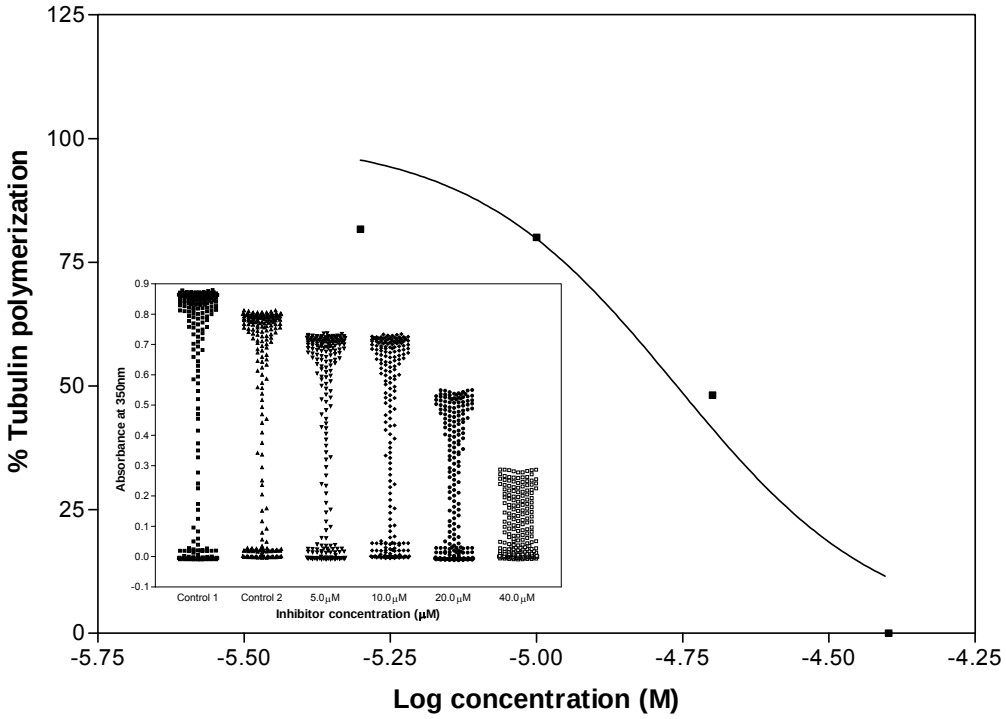

Figure 2.112. Percent Tubulin Polymerization against Log Concentration of Compound **51**.

Table 2.5. Biochemical Data for Compounds **41 - 50.**

Compound	IC_{50} (μM)	Log IC_{50} ± SE	Hillslope ± SE	R^2
41	> 40.0	-	-	-
42	1.4	-5.865 ± 0.04	-3.1 ± 0.8	0.94
43	< 5.0	-	-	-
44	2.6	-5.580 ± 0.02	-4.4 ± 0.3	0.99
45	1.3	-5.872 ± 0.02	-3.2 ± 0.3	0.95
46	> 40.0	-	-	-
47	> 40.0	-	-	-
48	9.6	-5.020 ± 0.04	-3.8 ± 1.2	0.92
49	11.3	-5.872 ± 0.02	-3.2 ± 0.3	0.95
50	> 40.0	-	-	-

Effect of Compounds ***52*** *and* ***53*** *on Tubulin Polymerization*

(Z)-1-(2'-Amino-5'-hydroxy-4'-methoxyphenyl)-2-(3",4",5"-trimethoxyphenyl)-ethene **(52)** (Figure 2.113), a 2-amino CA-1 derivative with 4-methoxy and 5-hydroxy functionalities in ring B was analyzed for antitubulin activity (Figure 2.114). This compound showed moderate inhibition of tubulin activity with an IC_{50} value of 6.2 μM (Figure 2.115).

Analysis of *(Z)-1-(2'-Amino,4'-hydroxy,5'-methoxyphenyl)-2-(3",4",5"-trimethoxyphenyl)-ethene* **(53)** (Figure 2.113), a 2-amino CA-1 derivative with hydroxyl and methoxy groups at the C-4 and C-5 positions of ring B respectively showed no antitubulin activity at 40.0 μM.

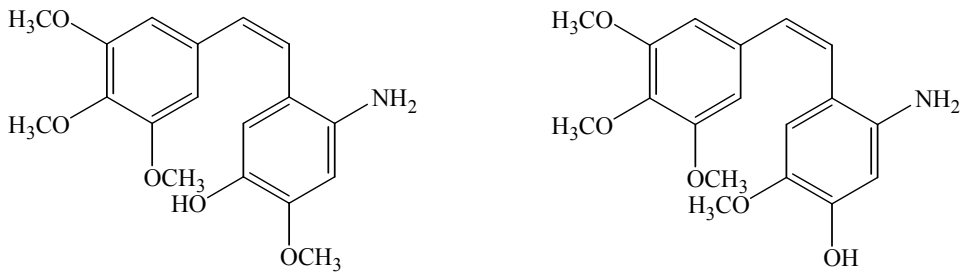

52 **53**

Figure 2.113. Structures of Compounds **52** and **53**.

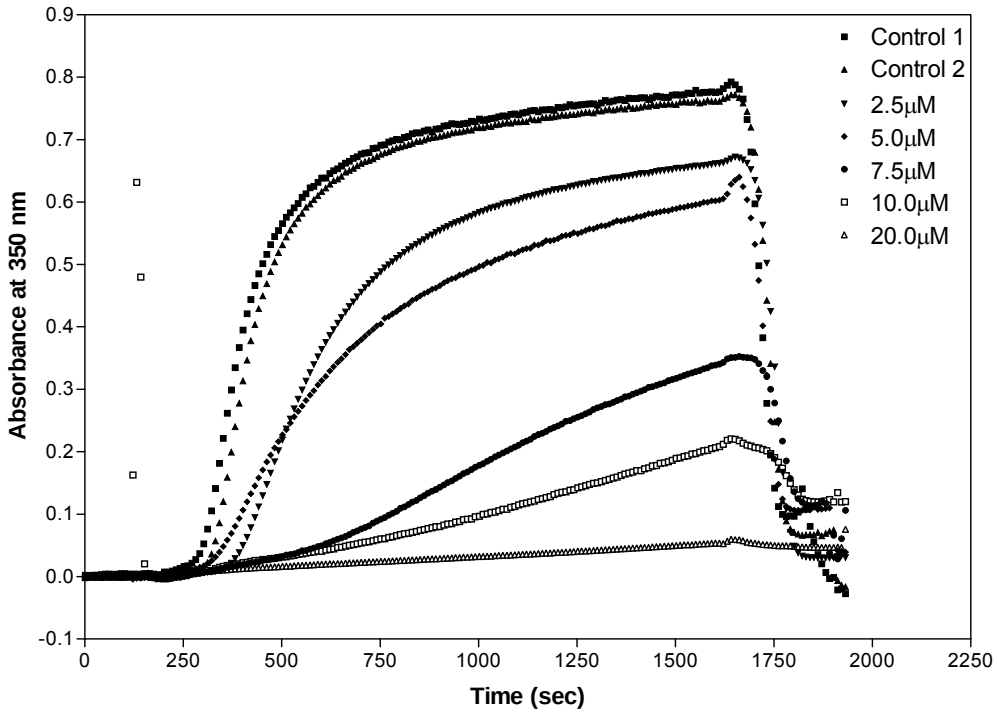

Figure 2.114. Inhibition of Tubulin Polymerization by Compound **52** at 30ºC.

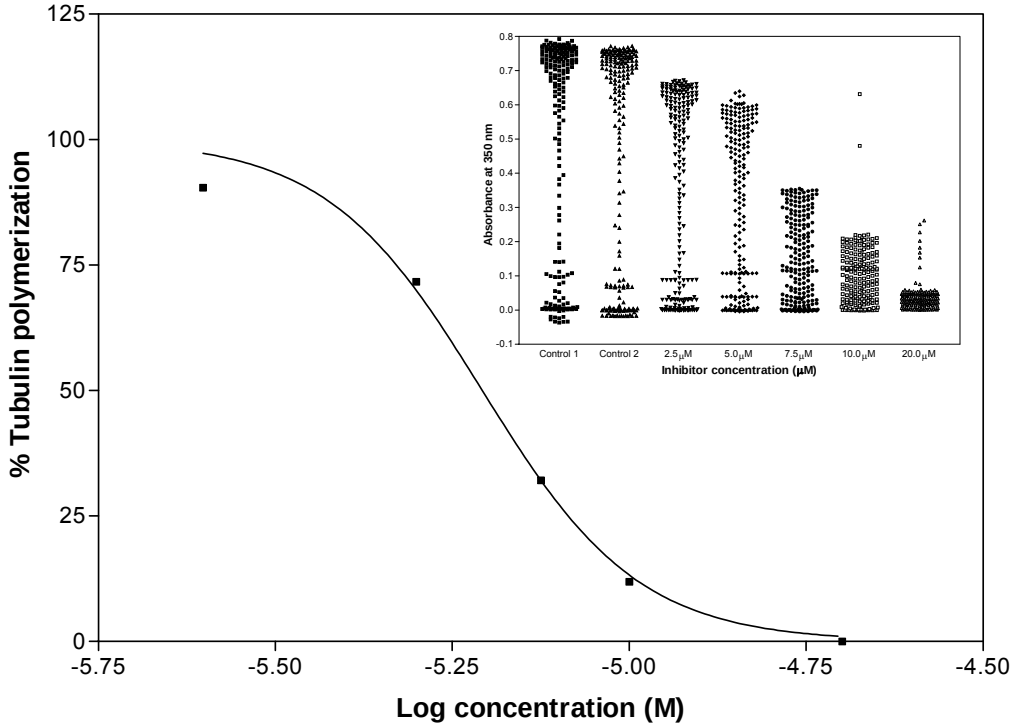

Figure 2.115. Percent Tubulin Polymerization against Log Concentration of Compound **52**.

Effect of Compounds ***54*** *and* ***55*** *on Tubulin Polymerization*

(Z)-1-(5'-Amino- 4'-hydroxy- 3'-methoxyphenyl)-2-(3",4",5"-trimethoxyphenyl)-ethene **(54)** (Figure 2.116) with an amino group at the C-5 position together with methoxy and hydroxyl groups at the C-3 and C-4 positions respectively did not inhibit tubulin polymerization at 40.0 μM.

(Z)-1-(5'-Amino, 3'-hydroxy, 4'-methoxyphenyl)-2-(3",4",5"-trimethoxyphenyl)-ethene **(55)** (Figure 2.116) with an amino substitution in the C-5 position together with hydroxyl and methoxy groups in the C-3 and C-4 positions respectively showed about 41.9 % inhibition of tubulin polymerization at 40.0 μM.

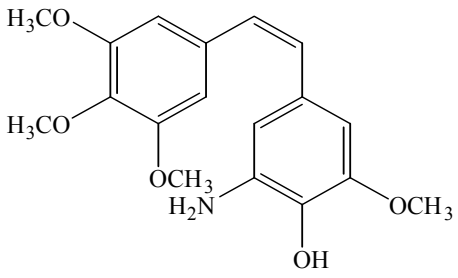

54

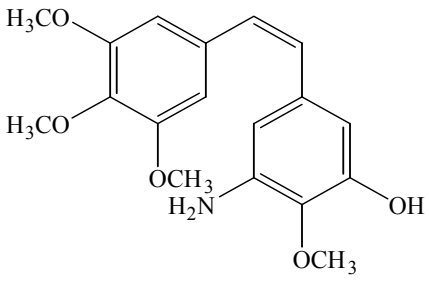

55

Figure 2.116. Structures of Compounds **54** and **55**.

Effect of Compounds ***56*** *and* ***57*** *on Tubulin Polymerization*

Improvement of potency of combretastatin derivatives by exploring di-amino substitutions in the B ring was also investigated.

(Z)-1-(2',3',-Diamino,4'-methoxyphenyl)-2-(3",4",5"-trimethoxyphenyl)-ethene ***(56)*** (Figure 2.117), a 2,3-diamino CA-1 derivative was analyzed for antitubulin activity (Figure 2.118). Compound **56** exhibited good antitubulin activity with an IC_{50} value of

2.9 μM (Figure 2.119). However this was 1.5-fold decrease in potency compared to CA-1. *(Z)-1-(2',3',-Diamino,4'-methoxyphenyl)-2-(3",4",5"-trimethoxyphenyl)-ethene hydrochloride* **(57)** (Figure 2.117), a water soluble 2,3-diamino hydrochloride CA-1 analog of compound **56** was analyzed (Figure 2.120), its polymerization kinetics showed stronger antitubulin activity with an IC_{50} value of 1.8 μM (Figure 2.121), which was comparable to that for CA-1. Amino substitution on either the C-2 or C-3 position of the B ring enhances potency of the combretastatin analogs.

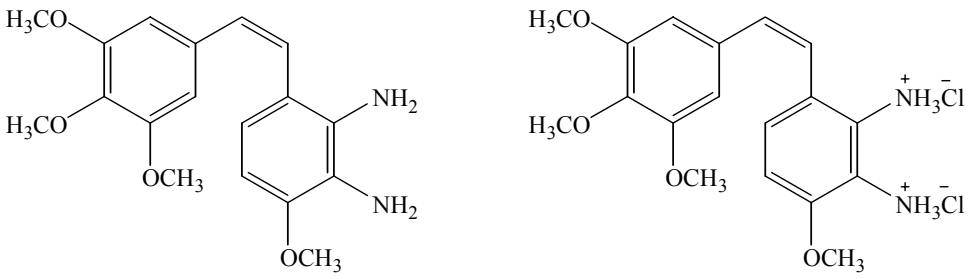

56 **57**

Figure 2.117. Structures of Compounds **56** and **57**.

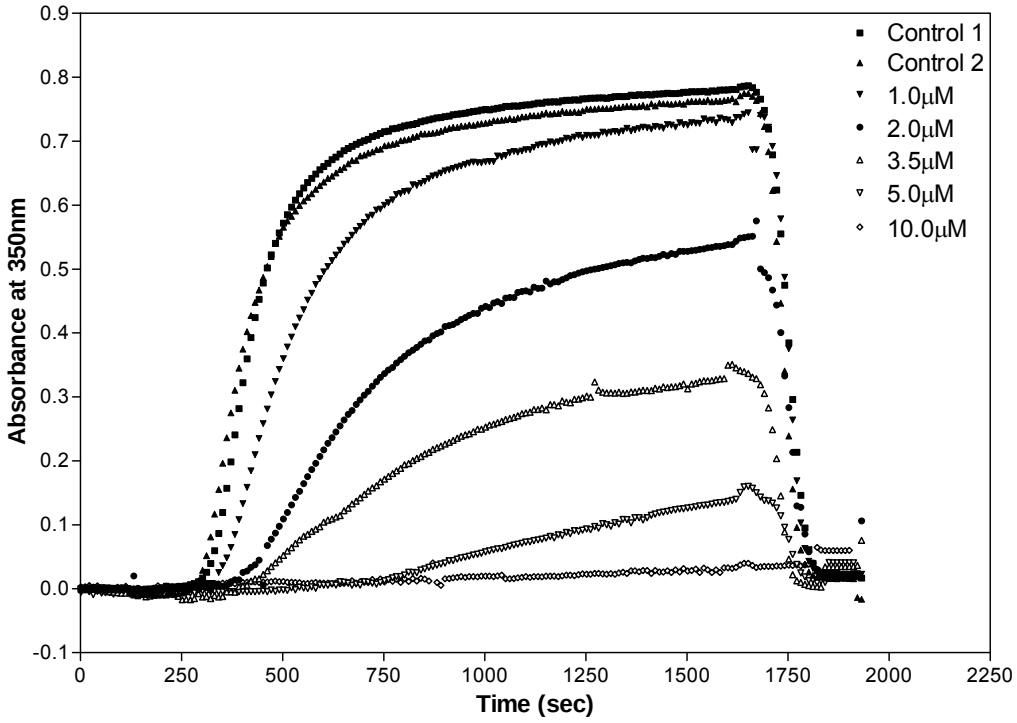

Figure 2.118. Inhibition of Tubulin Polymerization by Compound **56** at 30ºC.

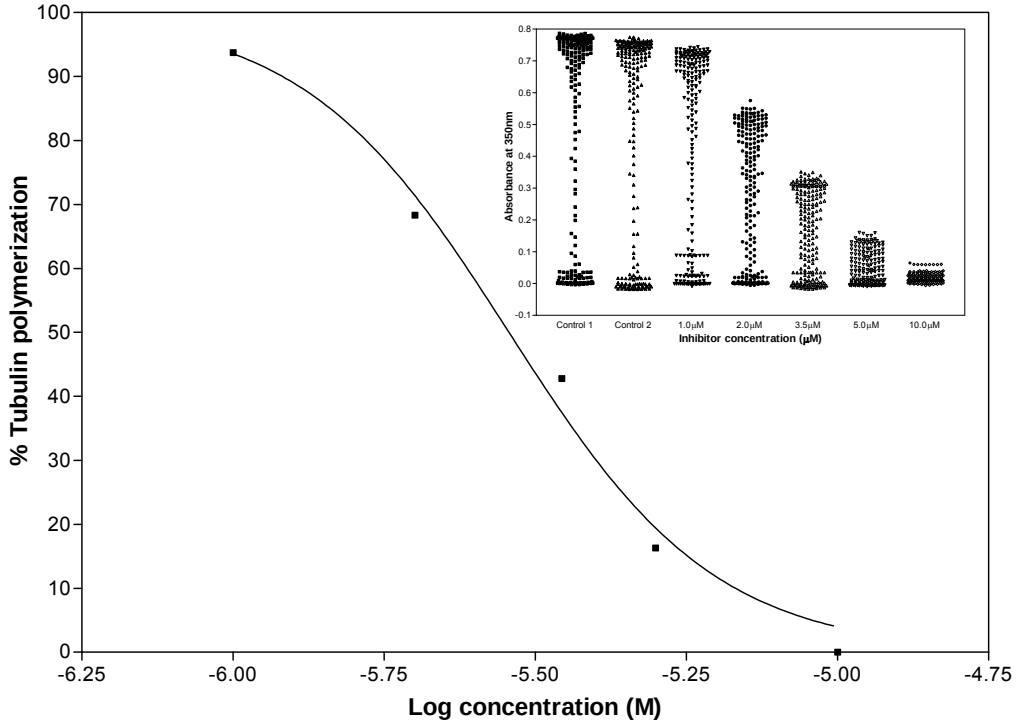

Figure 2.119. Percent Tubulin Polymerization against Log Concentration of Compound **56**.

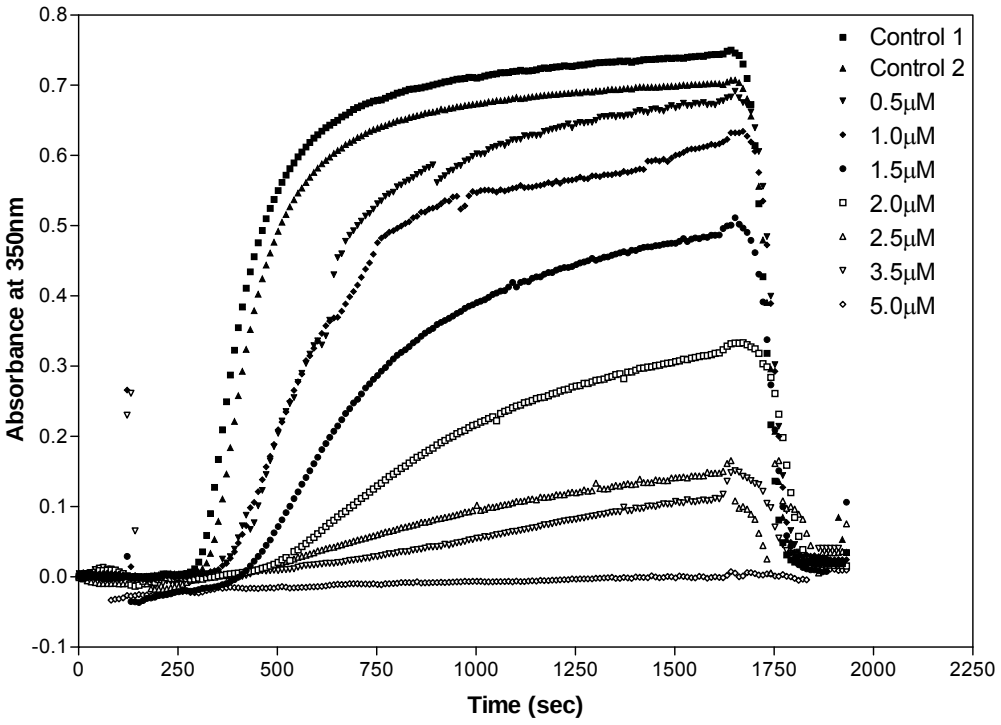

Figure 2.120. Inhibition of Tubulin Polymerization by Compound **57** at 30ºC.

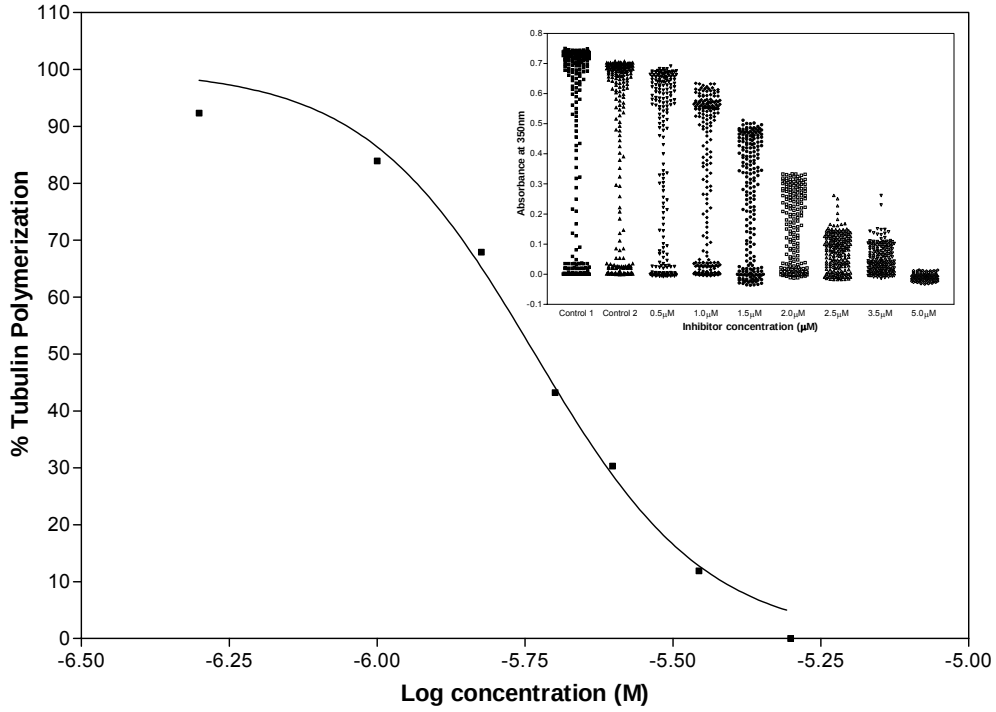

Figure 2.121. Percent Tubulin Polymerization against Log Concentration of Compound **57**.

*Effect of Compounds **58** and **59** on Tubulin Polymerization*

(Z)-1-(2',5'-Diamino, 4'-methoxyphenyl)-2-(3",4",5"-trimethoxyphenyl)-ethene **(58)** (Figure 2.122), a 2,5-diamino CA-1 analog was also analyzed for antimitotic activity and it showed 44.5 % inhibition of tubulin polymerization at 40.0 μM. 5-amino substitution on the B-ring without a hydroxyl group on the C-3 position does not promote inhibition of tubulin polymerization.

(Z)-1-(2',5'-Diamino,4'-methoxyphenyl)-2-(3",4",5"-trimethoxyphenyl)-ethene hydrochloride **(59)** (Figure 2.122), a 2,5-diamino hydrochloride CA-1 salt derivative of compound **54** was also analyzed for antitubulin activity (Figure 2.123). This 2,5 – diamino CA-1 derivative showed reduced antitubulin activity with an IC_{50} value of 14.1 μM (Figure 2.124). This was a 7.4-fold decrease in potency compared to combretastatin A-1.

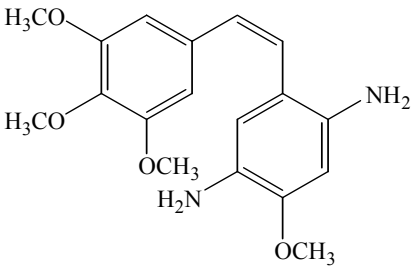

58

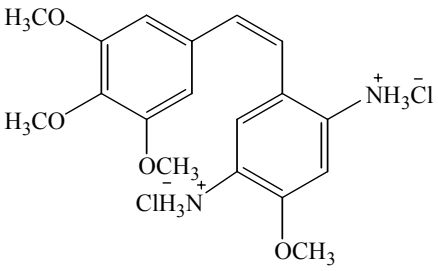

59

Figure 2.122. Structures of Compounds **58** and **59**.

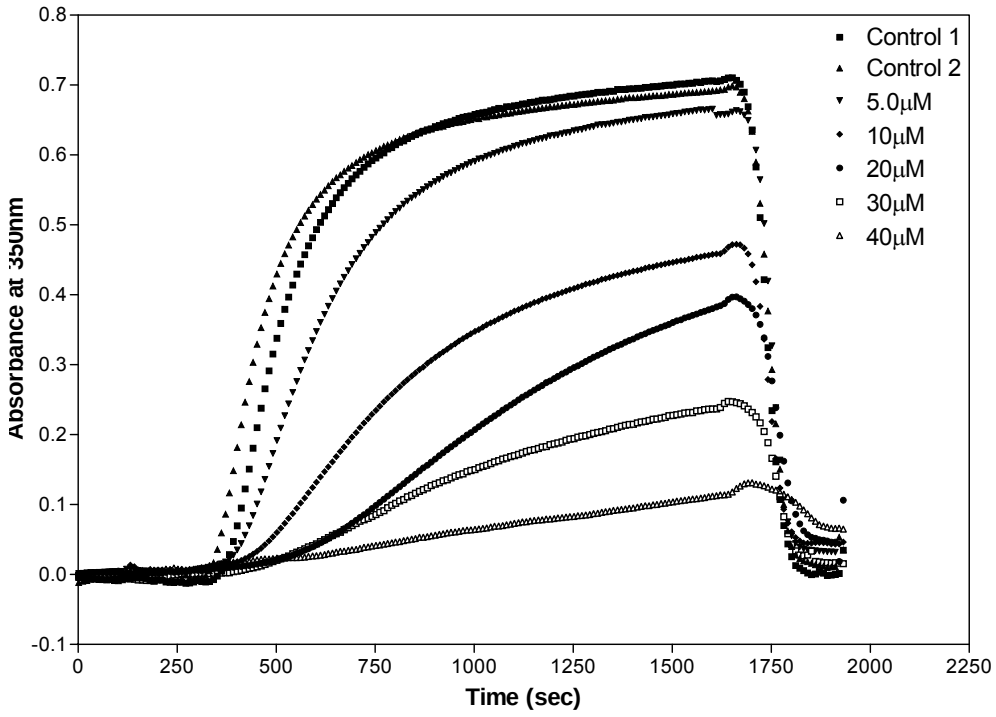

Figure 2.123. Inhibition of Tubulin Polymerization by Compound **59** at 30ºC.

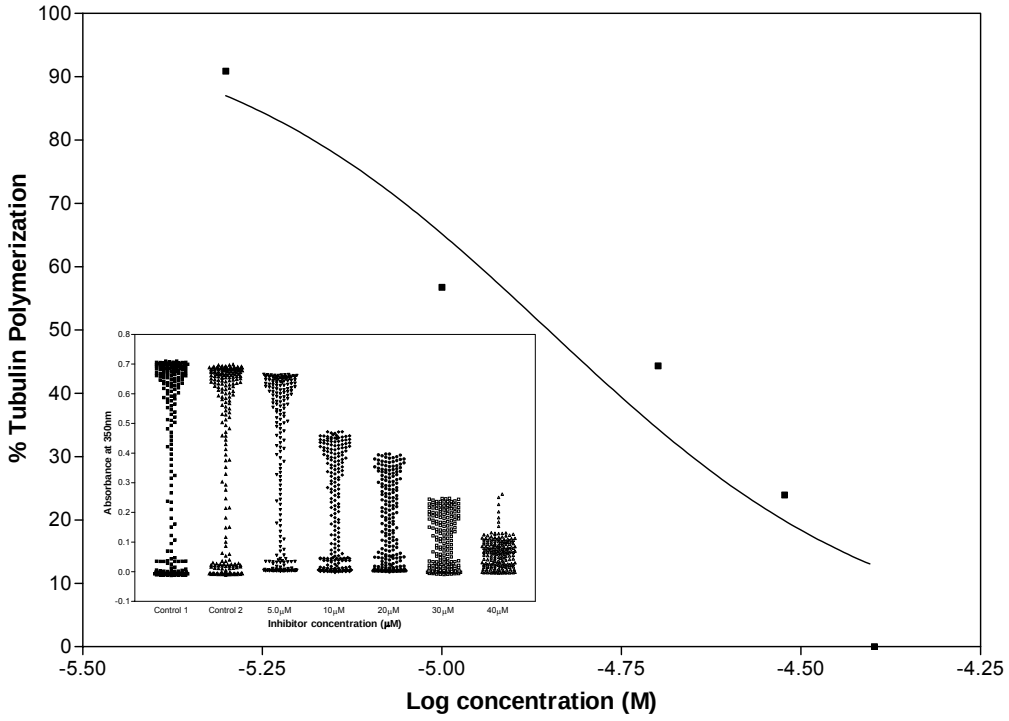

Figure 2.124. Percent Tubulin Polymerization against Log Concentration of Compound **59**.

Table 2.6. Biochemical Data for Compounds **51 - 60.**

Compound	IC_{50} (μM)	Log $IC_{50} \pm$ SE	Hillslope $\pm$ SE	R^2
51	17.4	-4.760 $\pm$ 0.08	-2.5 $\pm$ 1.0	0.92
52	6.2	-5.208 $\pm$ 0.01	-3.9 $\pm$ 0.5	0.99
53	> 40.0	-	-	- .
54	> 40.0	-	-	-
55	> 40.0	-	-	-
56	2.9	-5.540 $\pm$ 0.02	-2.5 $\pm$ 0.3	0.99
57	1.8	-5.730 $\pm$ 0.01	-3.0 $\pm$ 0.3	0.99
58	> 40.0	-	-	-
59	14.1	-4.850 $\pm$ 0.07	-1.8 $\pm$ 0.5	0.92
60	> 40.0	-	-	-

*Effect of Compounds **60** and **61** on Tubulin Polymerization*

The effect of *(Z)-1-(3',5'-Diamino,4'-methoxyphenyl)-2-(3'',4'',5''-trimethoxyphenyl)-ethene* **(60)** (Figure 2.125), a 3,5-diamino CA-4 derivative, on tubulin polymerization was also investigated. Upon analysis, this analog showed decreased potency with 33.0 % and 40.1 % total inhibition of tubulin polymerization at 20.0 μM and 40.0 μM respectively.

(Z)-1-(3',5'-Diamino,4'-methoxyphenyl)-2-(3'',4'',5''-trimethoxyphenyl)-ethene hydrochloride **(61)** (Figure 2.125), a 3,5-diamino hydrochloride derivative of compound **60** showed limited activity with 43.1 % total inhibition of tubulin polymerization at 40.0 μM.

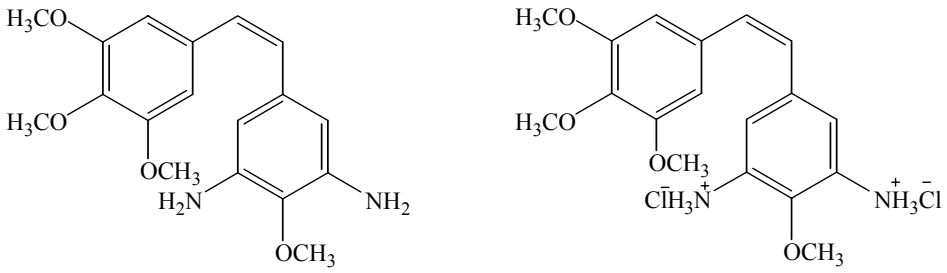

60 **61**

Figure 2.125. Structures of Compounds **60** and **61**.

*Effect of Compounds **62** and **63** on Tubulin Polymerization*

(Z)-1-(3',4'-Dimethoxy, 2'-hydroxyphenyl)-2-(3'',4'',5''-trimethoxyphenyl)-ethene **(62)**, (Figure 2.126) was also analyzed for antitubulin activity. Introduction of a second methoxy group in the C-3 position on the B-ring of CA-1 resulted in total loss of tubulin polymerization inhibitory activity.

Similarly, *(Z)-1-(3'-Hydroxy,4',5'-dimethoxyphenyl)-2-(3'',4'',5''-trimethoxyphenyl)-ethene* **(63)** (Figure 2.126) with two methoxy groups in the C-4 and C-5 positions of the B-ring did not show any antitubulin activity at 40.0 μM. These results demonstrated that one extra larger substituent like a methoxy group can not be accommodated in the colchicine binding site on the tubulin dimer and this results in reduced antitubulin activity of the analog.

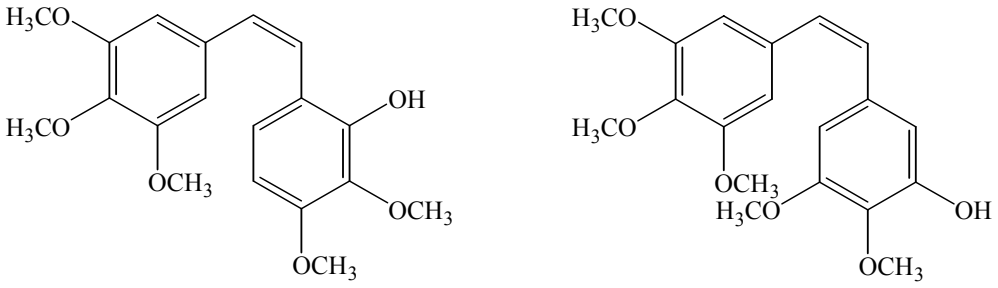

62 **63**

Figure 2.126. Structures of Compounds **62** and **63**.

*Effect of Compounds **64** and **65** on Tubulin Polymerization*

Sulfonates have been reported to show excellent proliferative antitubulin activity and the sulfonate group is considered an effective replacement of the *cis* olefin of CA-4 (Gwaltney *et al.*, 2001). *(Z)-1-(3'-Propan-1-ol-sulfonyloxy, 4'-methoxyphenyl)-2-(3'',4'',5''-trimethoxyphenyl)-ethene sodium* salt **(64)** (Figure 2.127), a water soluble analog of CA-4, was analyzed for antitubulin activity. This compound showed diminished antitubulin activity of 4.6 %, 18.1 % and 48.5 % at 5.0, 20.0 and 40.0 μM respectively.

(Z)-1-(3'5'-Disodiumphosphate,4'-methoxyphenyl)-2-(3'',4'',5''-trimethoxyphenyl)-ethene **(65)** (Figure 2.127) upon analysis showed less than 5.0% inhibition of tubulin polymerization at both 20.0 and 40.0 μM.

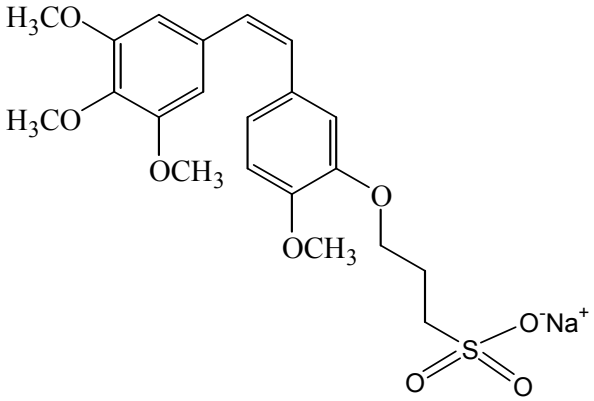

64

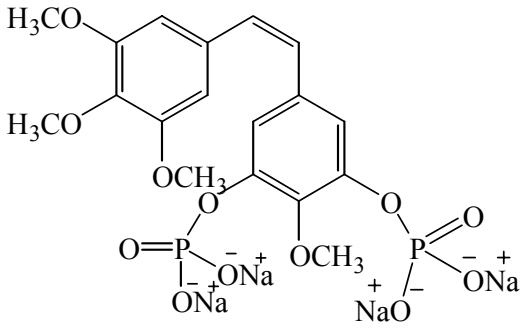

65

Figure 2.127. Structures of Compounds **64** and **65**.

*Effect of Compounds **66** and **67** on Tubulin Polymerization*

Pinney and coworkers have previously prepared benzo[*b*]thiophene derivatives which they described as possible tubulin binding agents although they were less potent than CA-4 (Pinney *et al.*, 1999). In order to increase the antitubulin and antimitotic activities of these compounds, they have synthesized a series of indole based phenol ligands. Among them, *2-[(3'-Hydroxy,4'-methoxy)-phenyl]-3-[(3'',4'',5''-trimethoxy)-benzoyl]-6-methoxyindole* **(66)** (Figure 2.128) was tested for its effect on tubulin polymerization (Figure 2.129). This compound revealed excellent antitubulin activity with an IC_{50} value of 0.8 μM (Figure 2.130).

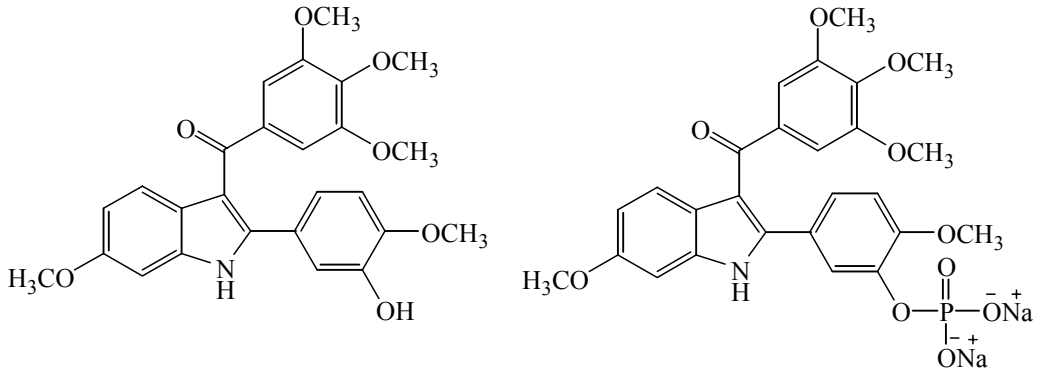

66 **67**

Figure 2.128. Structures of Compounds **66** and **67**.

2-[(3'-Disodiumphosphate-4'-methoxy)-phenyl]-3-[(3",4",5"-trimethoxy)-benzoyl]-6-methoxyindole **(67)** (Figure 2.128), also an indole based phosphate prodrug **66**, was analyzed for antitubulin activity (Figure 2.131). To our surprise, this phosphate salt inhibited tubulin polymerization with an IC_{50} value of 3.6 μM (Figure 2.132). This high potency was unexpected of a phosphate salt. However this was 4.5-fold less potent than the indole based phenol ligand which had showed an IC_{50} value of 0.8 μM. These potent antitubulin characteristics indicated that indole based phenol ligands could lead to powerful antitumor agents with similar or better activities than those of CA-4 and CA-1 phosphate prodrugs.

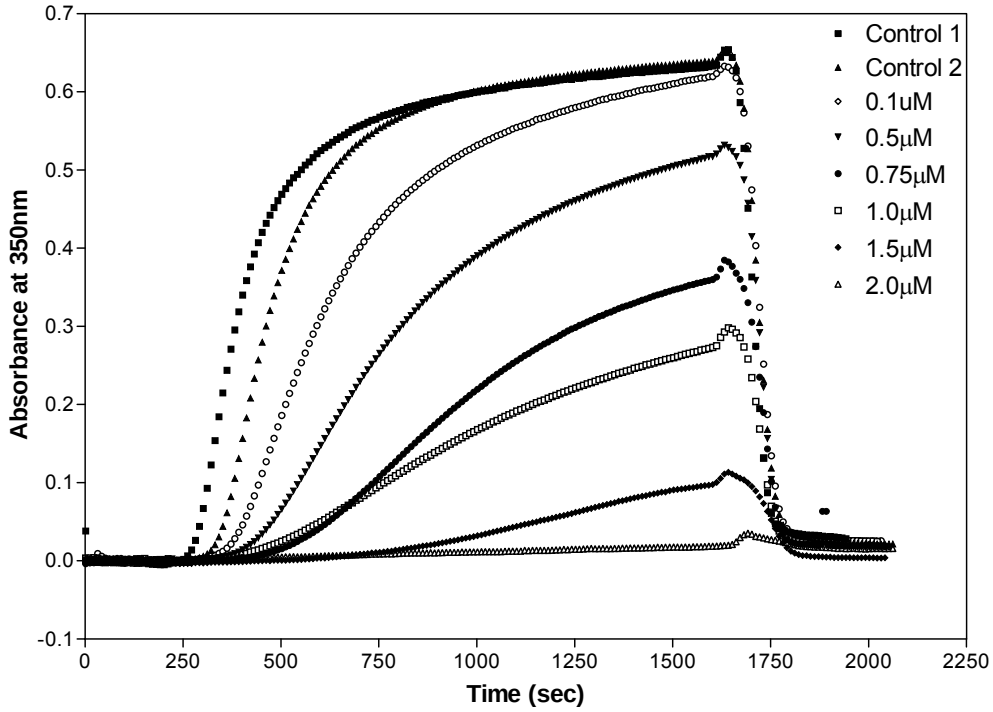

Figure 2.129. Inhibition of Tubulin Polymerization by Compound **66** at 30ºC.

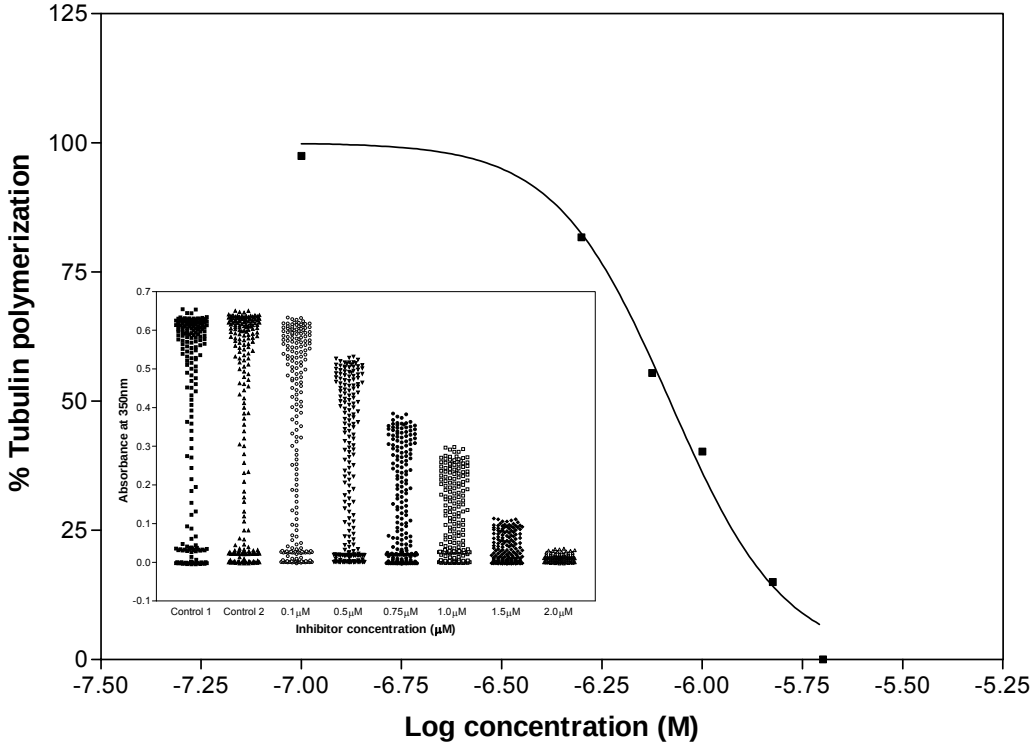

Figure 2.130. Percent Tubulin Polymerization against Log Concentration of Compound **66**.

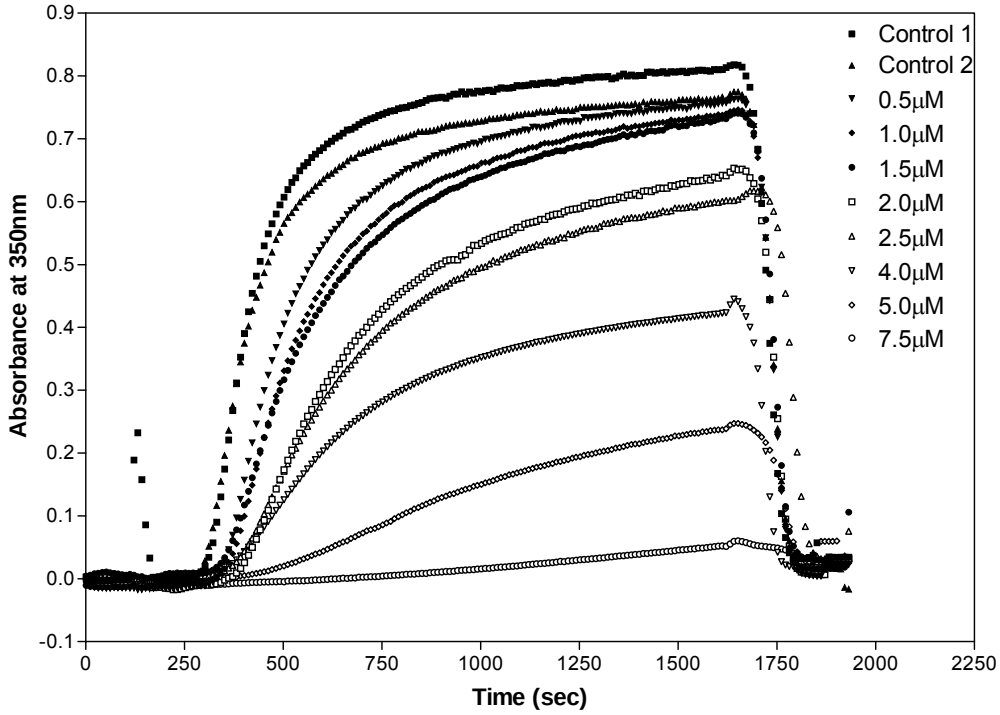

Figure 2.131. Inhibition of Tubulin Polymerization by Compound **67** at 30ºC.

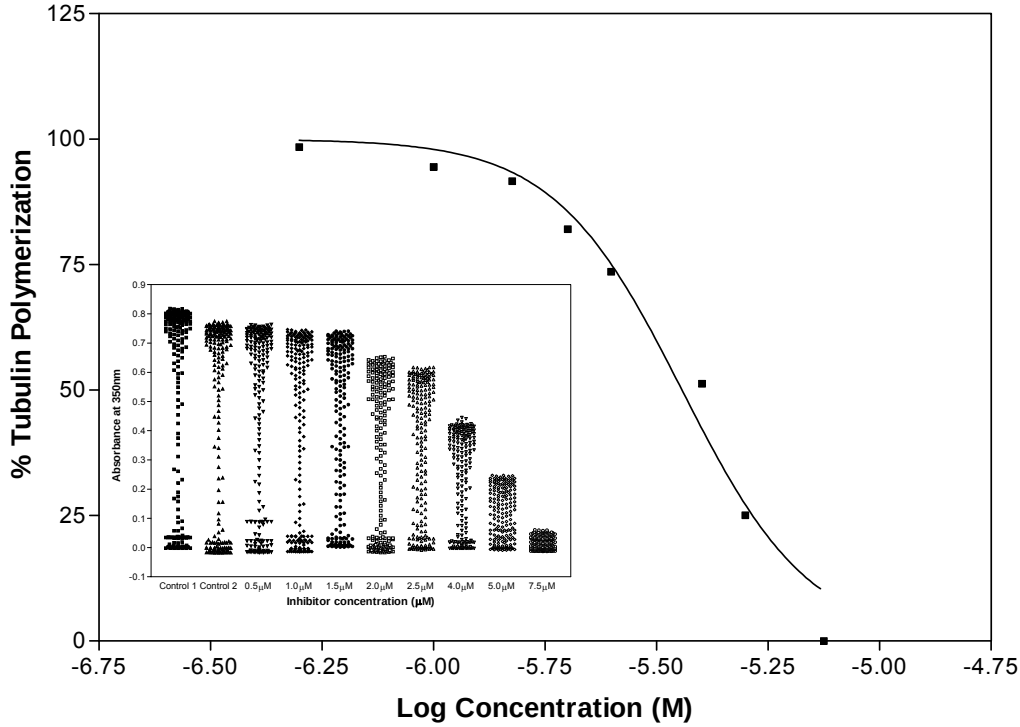

Figure 2.132. Percent Tubulin Polymerization against Log Concentration of Compound **67**.

*Effect of Compounds **68** and **69** on Tubulin Polymerization*

In order to determine if there was any correlation between ring separation in diaryl compounds and inhibition of tubulin polymerization, a series of compounds with and with out an ethene bridge were analyzed.

2'-Methoxy-5-(3",4",5"-trimethoxyphenyl)-phenol **(68)** (Figure 2.133) was analyzed for antitubulin activity. Compound **68** did not significantly inhibit polymerization of tubulin but showed 10 % inhibition at 40.0 μM.

2'-Methoxy-5-(3",4",5"-trimethoxyphenyl)-phenol-disodiumphosphate (**69)** (Figure 2.133), a water soluble di-sodium phosphate salt of compound **68**, did not have any significant inhibitory effect on tubulin polymerization but showed only 8.8 % inhibition at 40.0 μM.

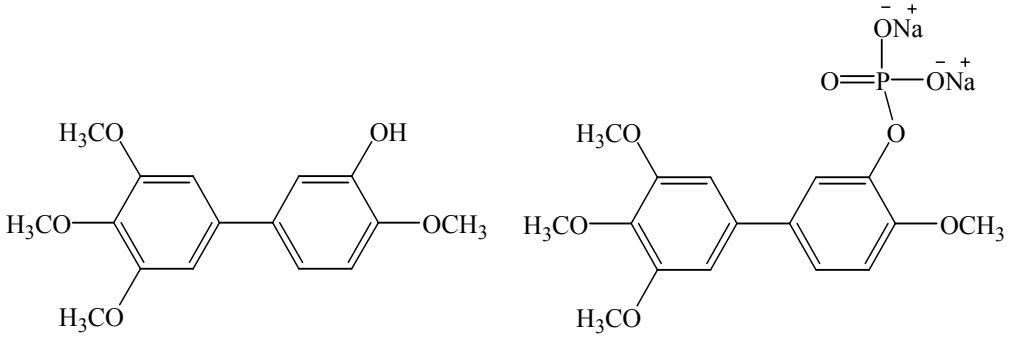

68 **69**

Figure 2.133. Structures of Compounds **68** and **69.**

Table 2.7. Biochemical Data for Compounds **61 - 70.**

Compound	IC_{50} (μM)	Log IC_{50} ± SE	Hillslope ± SE	R^2
61	> 40.0	-	-	-
62	> 40.0	-	-	-
62	> 40.0	-	-	-
64	> 40.0	-	-	-
65	> 40.0	-	-	-
66	0.8	-6.081 ± 0.01	-3.0 ± 0.3	0.99
67	3.6	-5.443 ± 0.02	-3.0 ± 0.4	0.98
68	> 40.0	-	-	-
69	> 40.0	-	-	-
70	3.3	-5.480 ± 0.02	-2.8 ± 0.4	0.98

*Effect of Compounds **70** and **71** on Tubulin Polymerization*

When *2'-Methoxy-5-[(3",4",5"-trimethoxyphenyl)methyl]-phenol* **(70)** (Figure 2.134) with one methylene unit separating the aryl moieties, was analyzed for antitubulin activity (Figure 2.135), it showed good antitubulin activity with a moderate IC_{50} value of 3.3 μM (Figure 2.136). This IC_{50} value was consistent with the results of Pettit and coworkers (1998) on the same compound. However it differed with the results published by Getahun and coworkers (1992) who reported an IC_{50} value of 2.3 μM at 30 ºC.

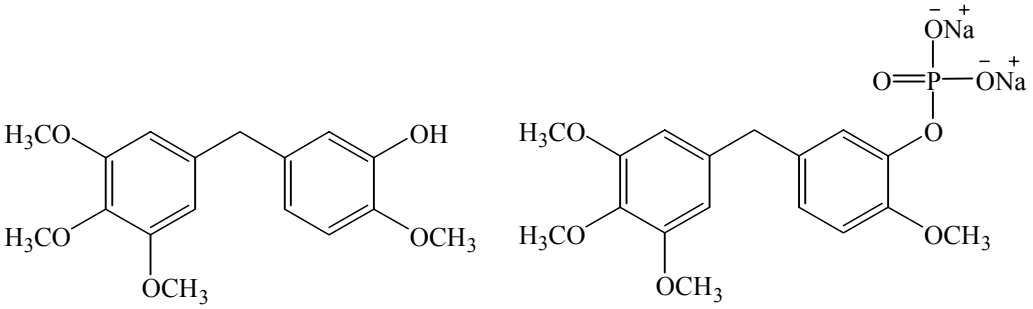

70 **71**

Figure 2.134. Structure of Compounds **70** and **71**.

2'-Methoxy-5-[(3",4",5"-trimethoxyphenyl)methyl]-phenol disodium phosphate **(71)** (Figure 2.134), a water soluble disodium phosphate derivative of compound **70**, did not inhibit the polymerization of tubulin monomers into microtubules.

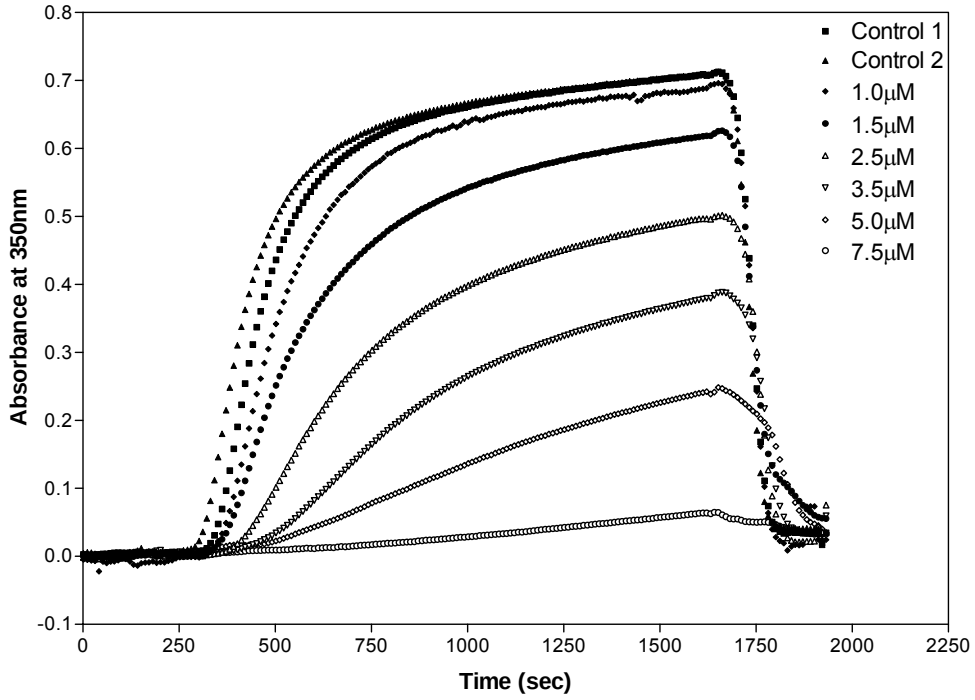

Figure 2.135. Inhibition of Tubulin Polymerization by Compound **70** at 30ºC.

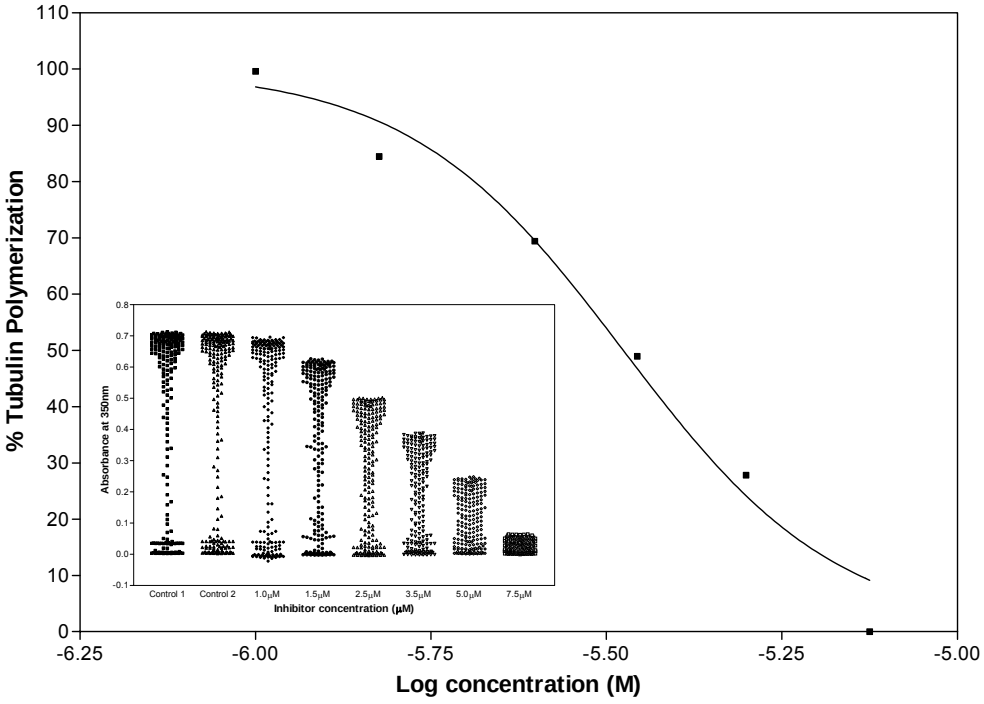

Figure 2.136. Percent Tubulin Polymerization against Log Concentration of Compound **70**.

*Effect of Compounds **72** and **73** on Tubulin Polymerization*

(E)-1-(4',6',-Dimethoxy, 2'-hydroxy, phenyl)-2-(3",4",5"-trimethoxyphenyl)-ethene **(72)** (Figure 2.137), a *trans* analog of CA-1 was analyzed for antitubulin activity. This compound showed 50.5 % inhibition of tubulin polymerization at 40.0 μM. *(E)-1-(4',6',-Dimethoxy, (2'- disodium phosphate) phenyl)-2-(3",4",5"-trimethoxyphenyl)-ethene* **(73)** (Figure 2.137), a disodium phosphate salt derivative of compound **72**, was equally not a good inhibitor of tubulin polymerization but showed 9.9 % and 15.9 % inhibitory activity at 20.0 and 40.0 μM respectively.

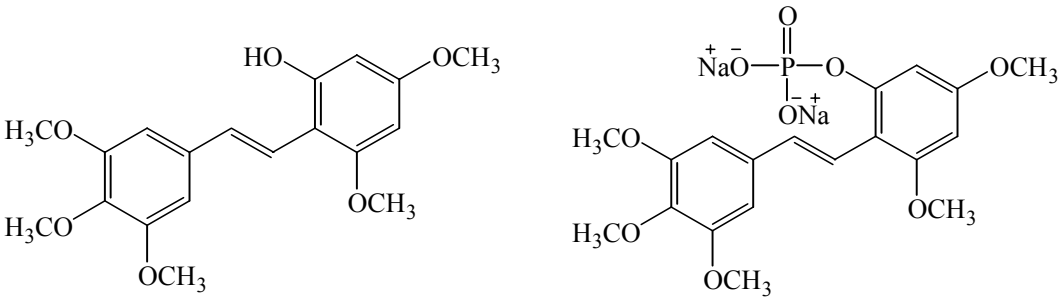

72 **73**

Figure 2.137. Structure of Compounds **72** and **73.**

*Effect of Compound **74** on Tubulin Polymerization*

(Z)-1-(3'-Hydroxy,4'-methoxyphenyl)-3-(3",4",5"-trimethoxyphenyl)-propane-1,3-dione **(74)** (Figure 2.138), which had been modeled against phenstatin, a relatively new compound that is an effective inhibitor of tubulin polymerization, was analyzed for antitubulin activity (Figure 2.139). This compound showed moderate antitubulin activity with an IC_{50} value of 4.7 μM (Figure 2.140).

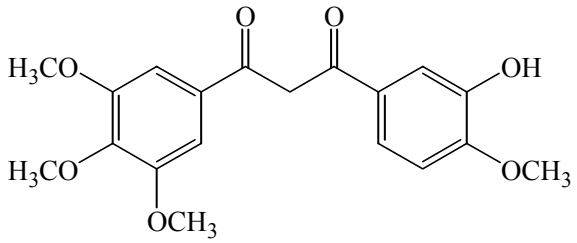

74

Figure 2.138. Structure of Compound **74.**

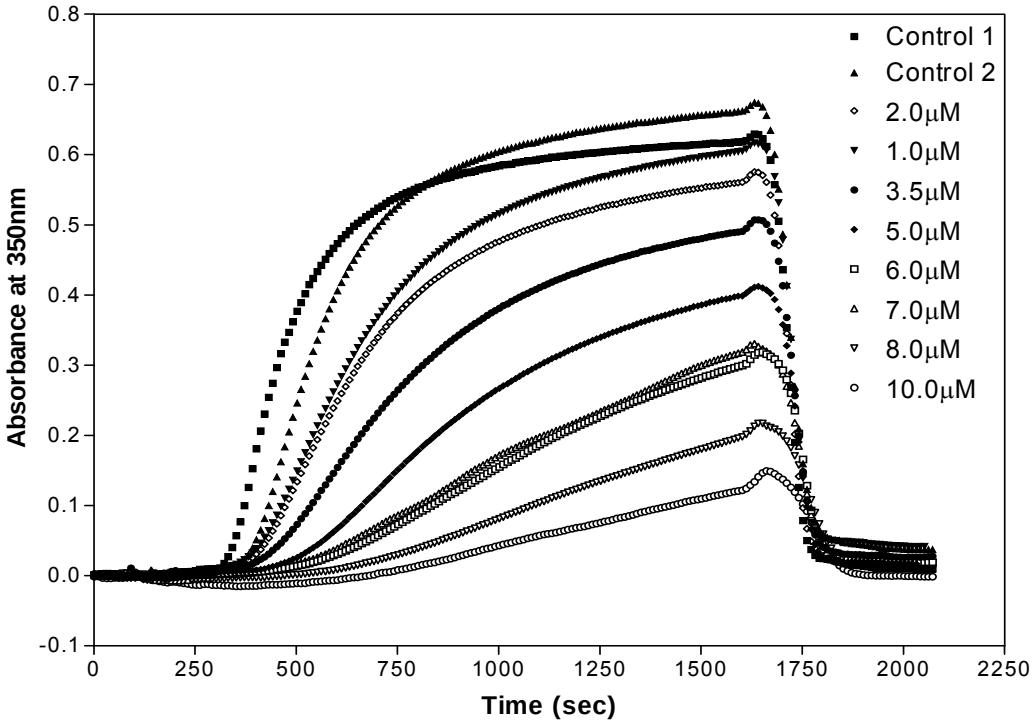

Figure 2.139. Inhibition of Tubulin Polymerization by Compound **74** at 30ºC.

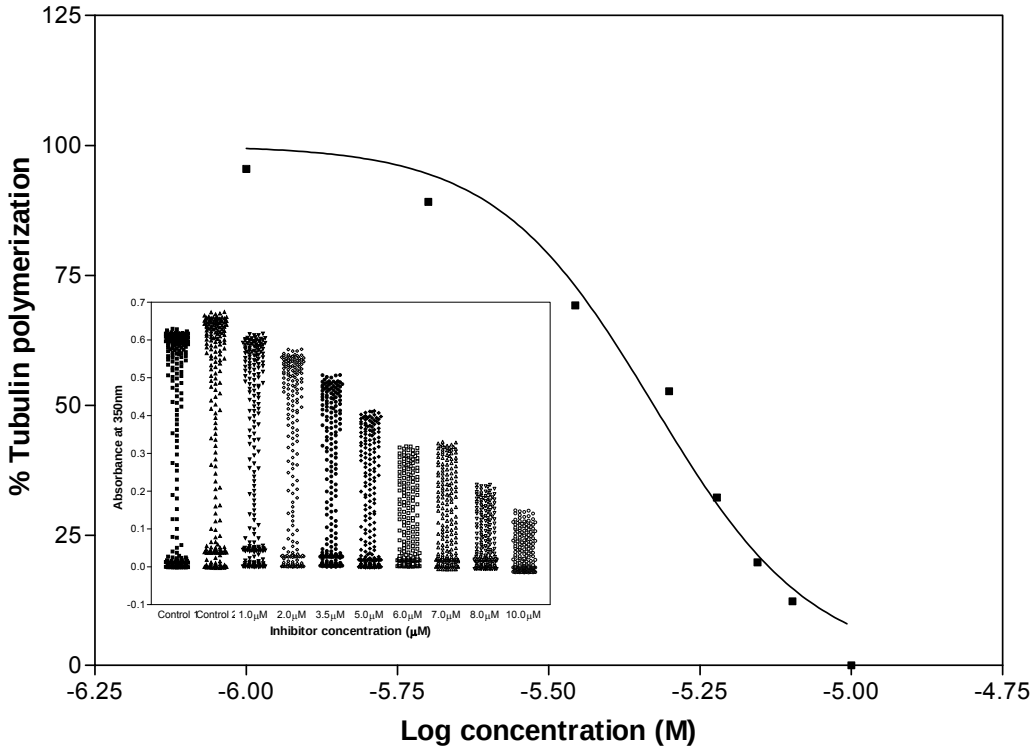

Figure 2.140. Percent Tubulin Polymerization against Log Concentration of Compound **74**.

Effect of Compound **75** *on Tubulin Polymerization*

3-(3', 4', 5'-Trimethoxybenzoyl)-6-hydroxy-7-methoxy-2H-chromene (**75**)

(Figure 2.141), a flavonoid derivative of DMXAA, was analyzed for antitubulin polymerization. Flavonoids, a series of polycyclic compounds consisting of two benzene rings with a linear spacer of 3 carbon atoms have been found to be strong VTAs. Among these series, 5,6-dimethylxanthenone-4 acetic acid (DMXAA) is currently being used as a variation of flavonoids in vascular targeting chemotherapy. Compound **75** did not inhibit tubulin polymerization at 40.0 μM, an indication that probably it induces antimitotic properties through a unique mechanism different from that followed by CA-4 analogs which are known to act by binding at the colchicine binding site.

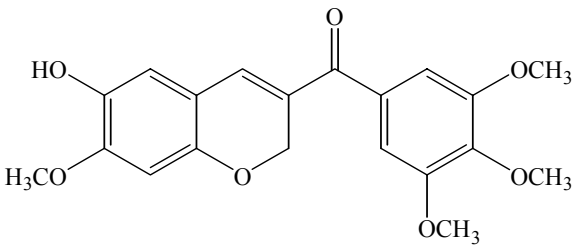

75

Figure 2.141. Structure of Compound **75**.

*Effect of Compounds **76** and **77** on Tubulin Polymerization*

The effects of colchicine-like analogs on *in vitro* microtubule assembly were analyzed. *3-Methoxy-9-(3,4,5-trimethylphenyl)-6,7-dihydro-5H-benzocycloheptene* (**76**) (Figure 2.142), a compound that mimics the structure of colchicine, in which rings A and B have been separated by a bridge, was analyzed for inhibition of tubulin polymerization (Figure 2.143). This compound demonstrated potent inhibition of tubulin polymerization with an IC_{50} value of 1.4 μM (Figure 2.144) which is comparable to that of natural alkaloid colchicine.

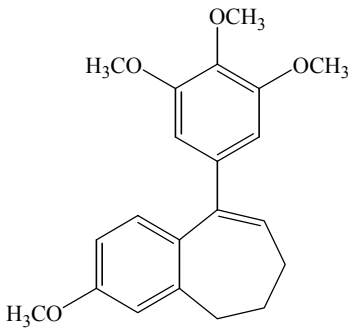

76

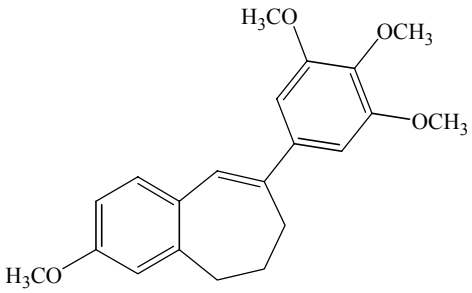

77

Figure 2.142. Structures of Compounds **76** and **77.**

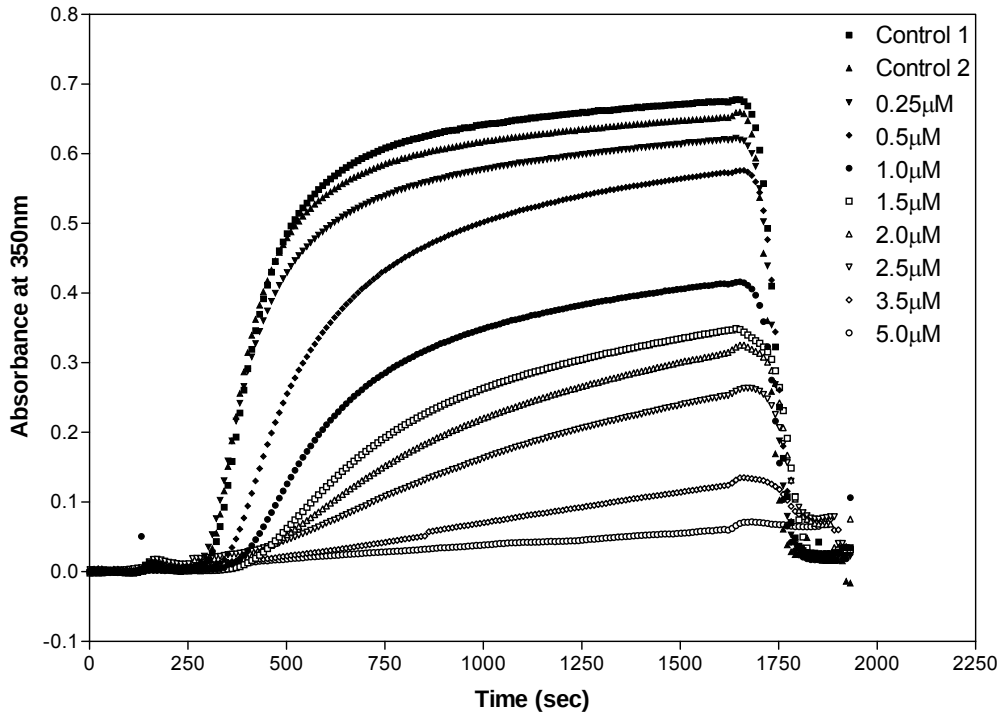

Figure 2.143. Inhibition of Tubulin Polymerization by Compound **76** at 30ºC.

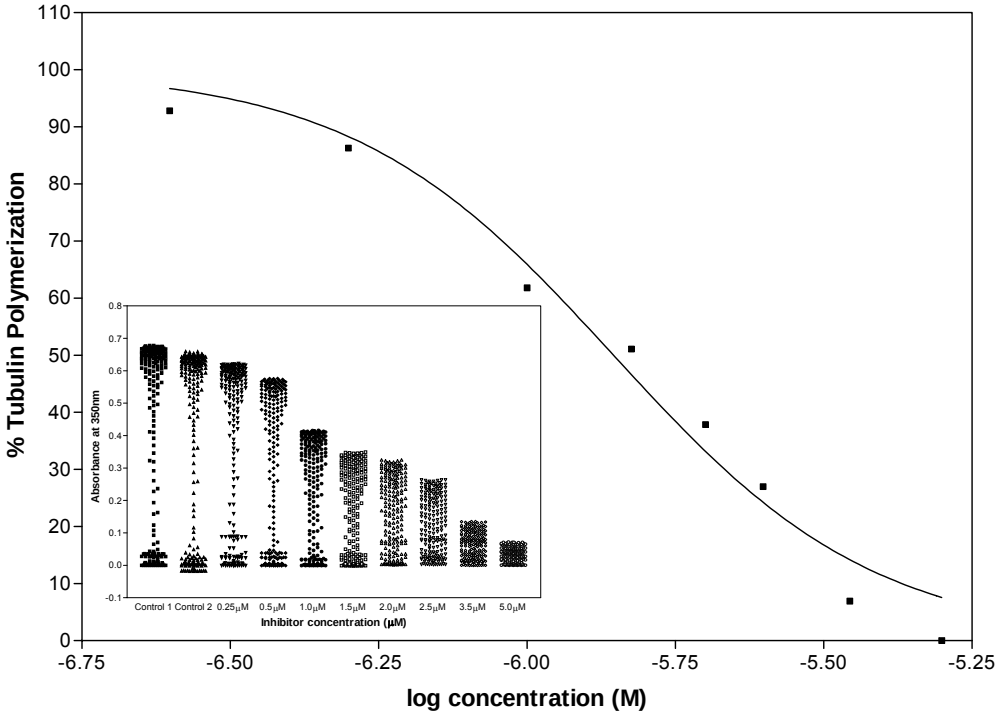

Figure 2.144. Percent Tubulin Polymerization against Log Concentration of Compound **76**.

3-Methoxy-8-(3,4,5-trimethylphenyl)-6,7-dihydro-5H-benzocycloheptene (**77**) (Figure 2.142), another compound with colchicine structural characteristics, was also evaluated for its antimitotic activity. Surprisingly, this compound was not a potent inhibitor of tubulin polymerization but showed only 30.2 % inhibitory activity at 40.0 μM respectively.

*Effect of Compound **78** on Tubulin Polymerization*

CA-4P is rapidly dephosphorylated *in vivo* to the active CA-4 molecule by a phosphatase enzyme within a few minutes after uptake. CA-4 is further metabolized at a slower rate to the CA-4 glucuronide, which is then excreted.

Combretastatin A-4 Glucuronide **(78)** (Figure 2.145), a metabolite of CA-4, did not inhibit tubulin polymerization at 40 μM.

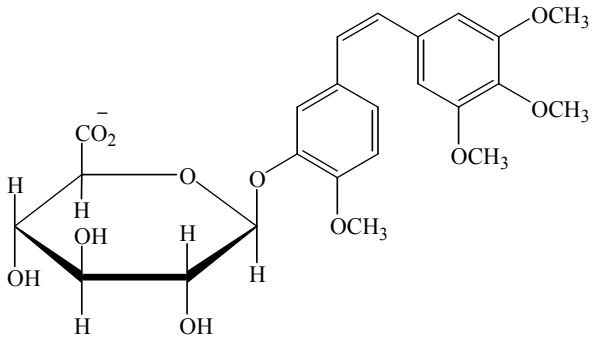

78

Figure 2.145. Structure of Compound **78.**

Table 2.8. Biochemical Data for Compounds **71 - 78.**

Compound	IC_{50} (μM)	Log $IC_{50} \pm$ SE	Hillslope $\pm$ SE	R^2
71	> 40.0	-	-	-
72	> 40.0	-	-	-
73	> 40.0	-	-	-
74	4.7	-5.324 $\pm$ 0.02	-3.3 $\pm$ 0.5	0.97
75	> 40.0	-	-	-
76	1.4	-5.854 $\pm$ 0.02	-2.0 $\pm$ 0.5	0.98
77	> 40.0	-	-	-
78	> 40.0	-	-	-

Effect of CA-1 Diphosphate Dipotassium (100 μM) Prodrug on Tubulin Polymerization

Combretastatin A-1 diphosphate dipotassium (OX16C) (100 μM) did not inhibit tubulin polymerization (Figure 2.146). This compound showed a shift in the normal kinetics of the reaction during the first 100 seconds which continued until 350 seconds. Whereas there is not supposed to be any polymerization during this phase when the mixture is being held at 0°C, the CA-1 diphosphate dipotassium (OX16C) prodrug – tubulin mixture showed a steady increase in polymerization just before the temperature jump from 38° to 30°C. Upon inducing depolymerization, there was an immediate collapse of the microtubules. However, although complete depolymerization was achieved upon a temperature jump to 0°C, the depolymerized mixture maintained a turbidity of approximately 0.2 even though normally it is supposed to be approximately zero.

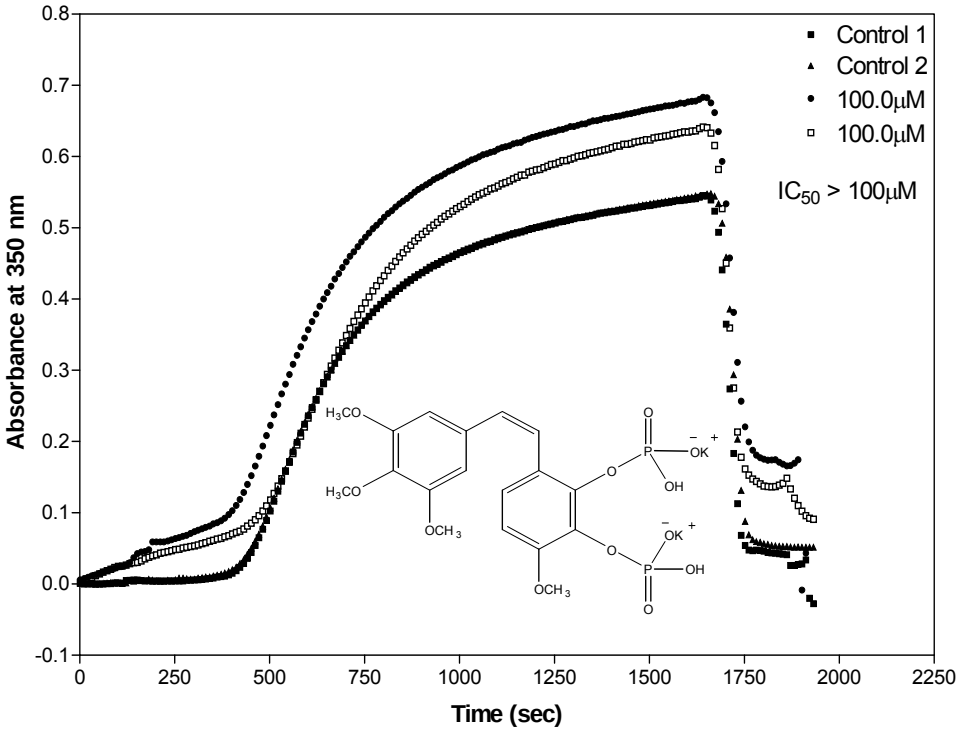

Figure 2.146. Effect of CA-1 Diphosphate Dipotassium (100 μM) on Tubulin Polymerization.

Effect of a Mixture of CA-1 Diphosphate Dipotassium (100 μM) and CA-1 on Tubulin Polymerization

In order to determine the effect of CA-1 presence in CA-1 diphosphate dipotassium prodrug samples on tubulin polymerization, a standard experiment was designed in which various concentrations of CA-1 were prepared and spiked into CA-1 diphosphate dipotasssium solutions as described in the methodology section. The reaction mixture consisted of 8 μl of each CA-1 solution, 8 μl of CA-1 diphosphate dipotassium (2.5 mM) solution, 8 μl of GTP (10 mM) and 176 μl of tubulin (1.0 mg/ml) in sodium glutamate (1.0M) solution giving a total final volume of 200 μl. CA-1 diphosphate spiked with (8.0 μl) of CA-1 (25, 50, 62.5 and 125.0 μM in DMSO), giving a final concentration of 100.0 μM OX16C containing CA-1 (1.0, 2.0, 2.5 and 5.0 μM) showed 65.3, 88.6, 98.6, and, 90.65 % inhibition of tubulin polymerization respectively (Figure 2.147).

Figure 2.148 shows the Box and Whisker plots indicating the range and quartiles of the extent of inhibition of tubulin polymerization by CA-1 diphosphate. The boxes extend from the 25^{th} percentile to the 75^{th} percentile. The 50^{th} percentile is indicated with a line at the median. The whiskers extending above and below the box are showing the highest and lowest absorbance values during the course of the reaction. From the plot, it is evident that the presence of even 1.0 % CA-1 in a CA-1P sample can be detected by studying the kinetics of the interaction of the sample with tubulin.

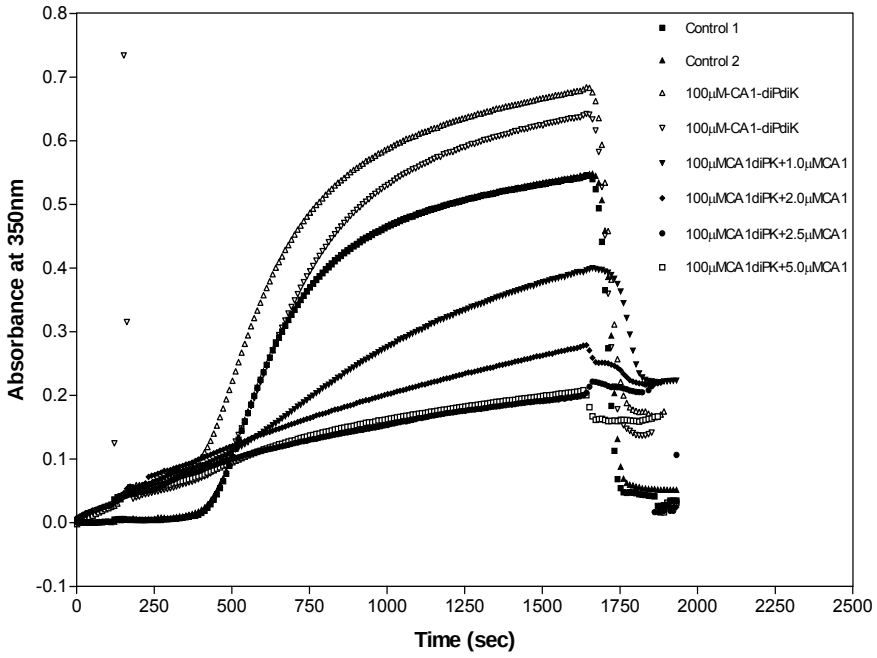

Figure 2.147. Effect of CA-1 Diphosphate Dipotassium (100 μM) containing CA-1 on Tubulin Polymerization.

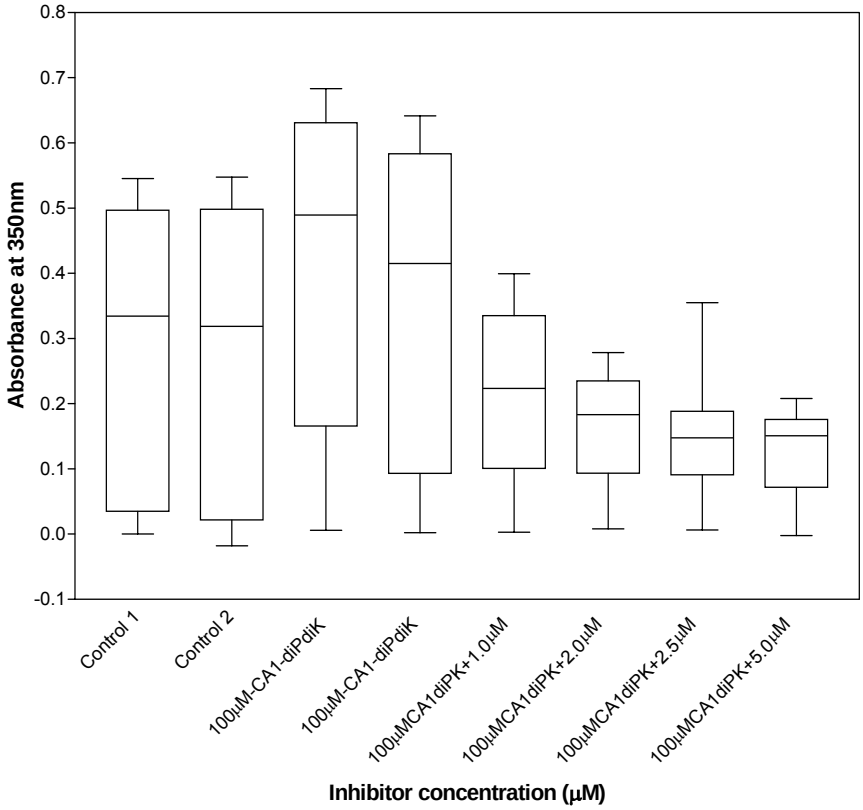

Figure 2.148. Effect of Combretastatin A-1 Diphosphate Dipotassium (100 μM) Prodrug containing 1.0, 2.0, 2.5 and 5.0 μM of CA-1 on Tubulin Polymerization.

Effect of Combretastatin A-1 Diphosphate Dipotassium (25°C/60%RH)(100 µM) and (40°C/75%RH)(100 µM) on Tubulin Polymerization.

CA-1 diphosphate dipotassium sample (25°C/60%RH) (duplicate analysis of three samples) did not inhibit tubulin polymerization (Figure 2.149). This sample showed an average of 0.6 % (2.18, 0.1 and 0.1 %) inhibition of tubulin polymerization. This meant that CA-1P does not undergo any decomposition when kept at 25°C in an environment of 60 % relative humidity.

CA-1 diphosphate dipotassium sample (40°C/75%RH) (duplicate analysis of three samples) showed on average 31.8 % (34.8, 28.5 and 32.1 %) inhibition of tubulin polymerization upon analysis (Figure 2.150). This meant CA-1P is unstable and undergoes decomposition releasing CA-1 when kept at 40°C in an environment of 75 % relative humidity. Most probably, at elevated temperatures, CA-1P can decompose completely into its natural CA-1 state.

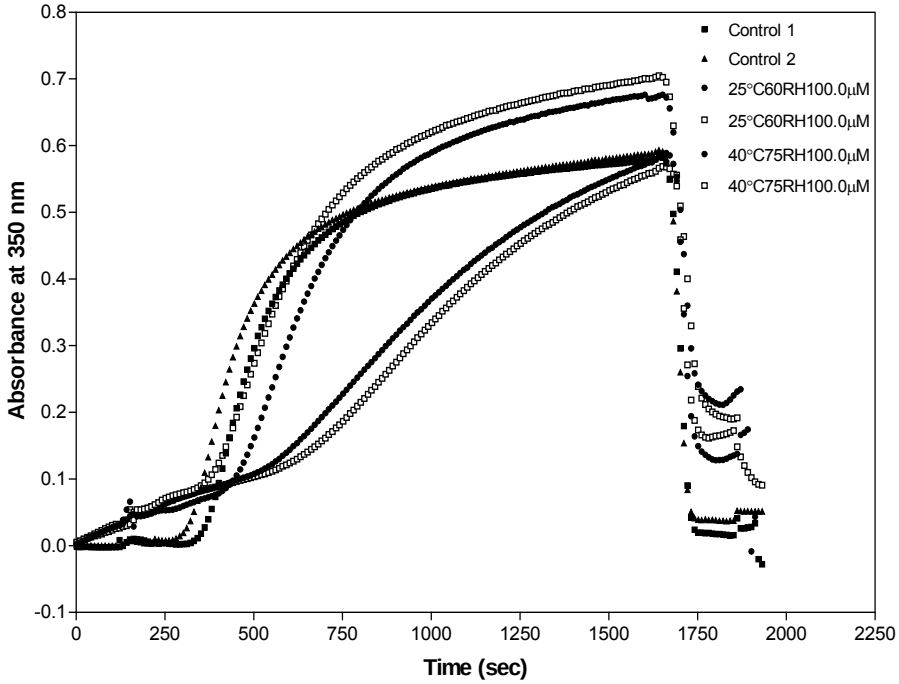

Figure 2.149. Effect of 25°C60%RH and 40°C75%RH Combretastatin A-1 Diphosphate Dipotassium (100 µM) Prodrug on Tubulin Polymerization.

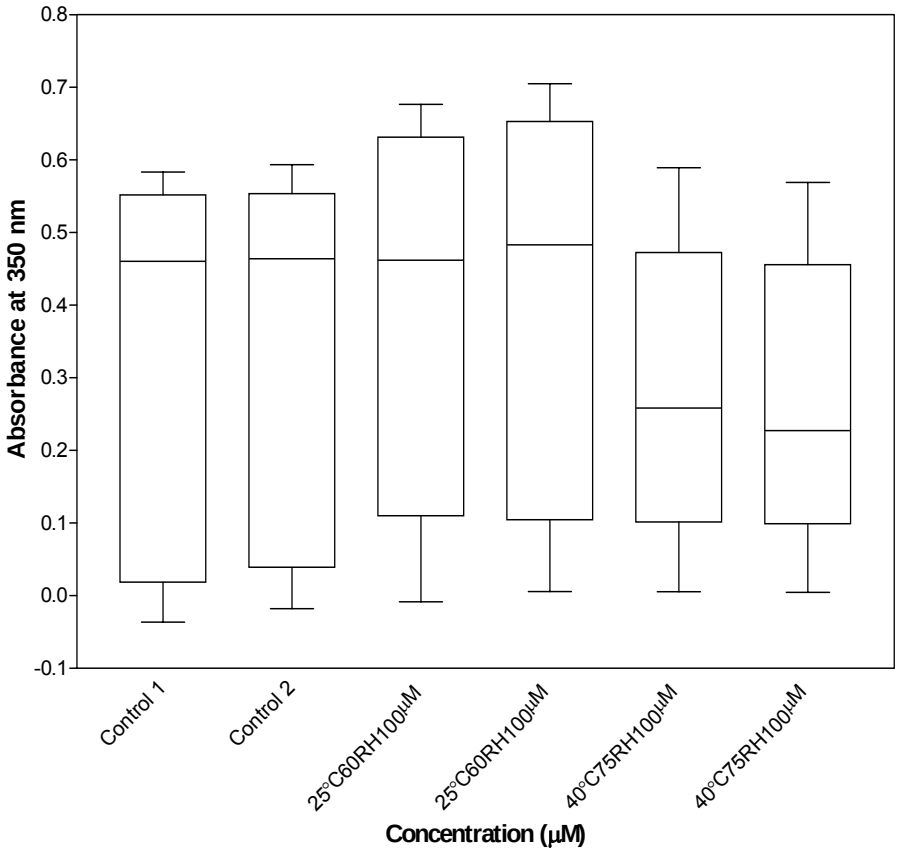

Figure 2.150. Column Boxes showing Effect of CA-1 Diphosphate Dipotassium 25°C60%RH (100 μM) and 40°C75%RH (100 μM) Prodrug containing CA-1 on Tubulin Polymerization.

Conclusions

In order for binding and consequently inhibition to occur, the combretastatin analog has to fit in the colchicine binding site on the tubulin molecule. The overall size, position and electronegativity of the functional group on the phenolic ring seem to play a big role in the potency of the analogs. Replacement of the 2-position hydroxy group on the phenolic ring of CA-1 with bromo, chloro, nitro, nitroso drastically increased its inhibitory activity. TheseCompounds were among the best analogs tested with IC_{50} values ranging from 1.1 – 2.0μM. 2,4-Dichloro- substitution in ring B of CA-1 resulted in a compound of good tubulin inhibitory characteristics. 2-Fluoro substitution in the

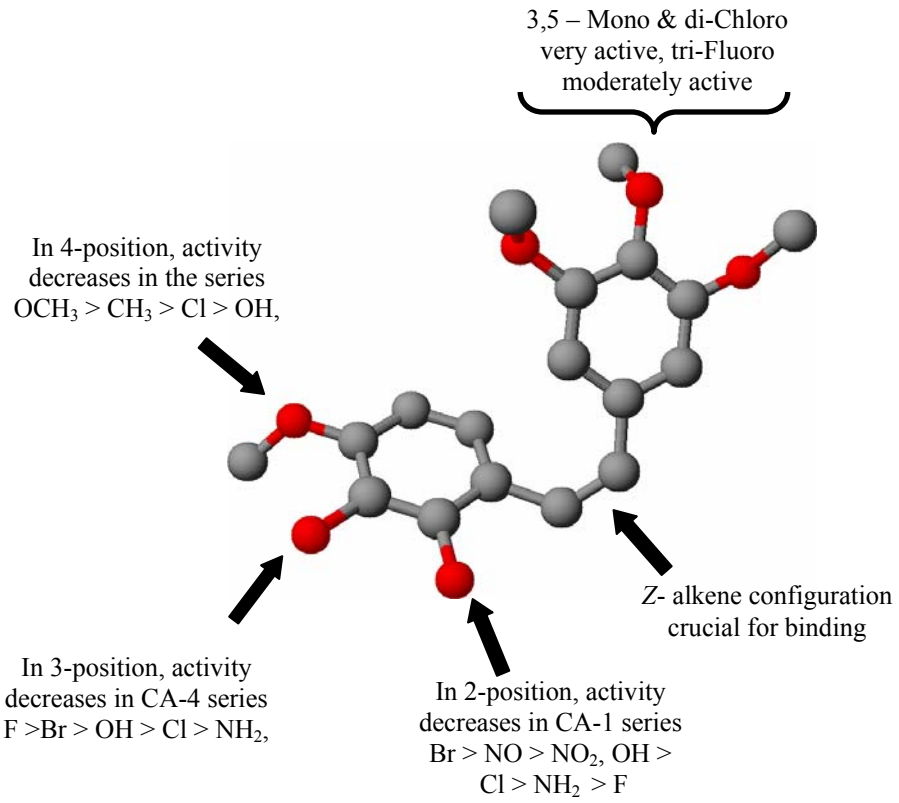

Figure 2.151. Summary of Structure Activity Relationships.

B-ring produced the least active compound among the 2-position halogen substituted analogs. The hydrochloride salt of 3-amino substituted CA-4 had potency almost equal to that of CA-4. The loss of the 4-position methoxy group among the combretastatin analogs does not favor activity which pointed to its importance in the tubulin binding interaction. Removal of the 4-methoxy group from CA-1 led to a compound of moderate potency. However replacement of this same methoxy group with a methyl group produces a compound of almost similar antitubulin activity as CA-1. Thus less bulky groups in the 4-position of ring-B seem not to affect the binding of these analogs to tubulin. 2,3-dinitrosubstitution in the B-ring renders the CA-1 totally in active. However reduction of the nitro groups to a 2,3-diamino-CA-1 in the B-ring results in an analog of moderate potency (IC_{50} value = 3.0 μM). Its 2,3-diaminohydrochloride salt was 1.6-fold

more active than the di-amino substituted CA-1 analog. 3,5-diamino-CA-1 substitution does not favor inhibition of tubulin polymerization. Similarly, the 3,5- diamino hydrochloride salts of CA-1 are not effective inhibitors of tubulin polymerization. Reversal of the 3-hydroxy, 4-methoxy arrangement on the B-ring to 3-methoxy, 4-hydroxy arrangement renders every compound with that conformation non-effective. Replacement of the ethene bridge in CA-4 with a methylene group produces a compound of moderate activity. Complete removal of the bridge renders the compound totally ineffective. All mono-phosphate sodium salts which are the soluble forms of the many combretastatin analogs bearing a hydroxyl group on their B-ring did not inhibit tubulin polymerization. The Aventis CA-4 serinamide derivative (AVE8062A) showed low activity with an IC_{50} value of 9.6 μM which was the best amongst a series of amino and aminohydrochloride serinamide derivatives.

Mono or dichloro-substitution in the trimethoxyphenyl ring leads to analogs with excellent antitubulin activity equal to that of CA-1. Monochloro substitution in the 3 or 5-position of ring A showed excellent anti-tubulin activity (IC_{50} ranging between 1.8 - 2.2 μM). 3,5-dichloro-substitution in the A-ring resulted in a highly potent compound with an IC_{50} value of 1.7 μM. 3,4,5 trifluorophenyl substitution in the A-ring of CA-1 led to a compound of moderate activity with an IC_{50} value of 3.0 μM. These results validated the findings of Gaukroger *et al*., (2003) which showed that whereas the trimethoxy phenyl functionality is important for combretastatin binding to tubulin, it may not totally be crucial for inhibition of tubulin polymerization activity. Other small groups like chloro and fluoro in ring-A can also lead to effective inhibitors of tubulin polymerization.

CHAPTER THREE

Application of Isothermal Titration Calorimetry in Thermodynamic Studies on the Binding of Combretastatin A-1 and A-4 Analogs to Tubulin

Introduction

Despite the enormous biological importance of combretastatins as vascular targeting agents through inhibition of tubulin polymerization, the ligand binding thermodynamics of most molecular interactions of VTAs with tubulin are still lacking. During drug development and design, fast decisions have to be made as to which compounds need to be pursued as leads from a pool of potent VTAs. During drug design, optimization of binding affinity is crucial and therefore information on the binding thermodynamics is very important especially if several lead compounds are exhibiting similar potency and structure activity relationships. For compounds with almost similar inhibitory properties, determination of which compounds have the highest binding affinity and the most favorable ΔH terms would be of utmost importance in order to identify which lead compounds need further chemical modification for maximum potency (Cliff *et al*., 2004). The need for optimization of binding affinity, binding acceptability and improvement of binding selectivity to specific targets has to be counterbalanced by minimizing the affinity of the drug to unwanted targets (Schön *et al*., 2003). Isothermal titration calorimetric procedures are the only means of direct measurement of observed molar enthalpy (ΔH_{obs}) of binding and molecular interactions. As a result the investigators are relieved from the necessity of determining equilibrium binding constants at different temperatures in order to determine ΔH from the van't Hoff

equation which is a long and time consuming methodology. The van't Hoff equation is an expression for the slope of a plot of the equilibrium constant (specifically, ln *K*) as a function of temperature. It can be expressed in either of the two ways:

$$\text{(a)} \quad \frac{\mathrm{d} \ln K}{\mathrm{d}T} = \frac{\Delta_r H^o}{RT^2} \qquad \text{(b)} \quad \frac{\mathrm{d} \ln K}{\mathrm{d}(1/T)} = -\frac{\Delta_r H^o}{R}$$

Equation (a) shows that $d \ln K / d\mathrm{T} < 0$ for an exothermic reaction under standard conditions ($\Delta_r H^o < 0$). A negative slope means that ln *K*, and therefore *K* itself, decreases as the temperature increases. It also follows from equation (b) that provided the reaction molar enthalpy can be assumed to be independent of temperature, a plot of – ln *K* against $1/T$ would be a straight line with a slope of $\Delta_r H^o / R$. This is a non-calorimetric method for the measurement of reaction enthalpies. One of the problems of this method is that reaction enthalpies are actually temperature dependent and so the plot is expected to be perfectly linear. However, in biophysical – chemical studies, practically the method is not very accurate although it is often the only method available for use (Atkins, 2000). The other commonly used methods for determining binding constants are equilibrium dialysis, ultracentrifugation, gel exclusion chromatography (Connors, 1987). Although these methods also allow partitioning of macromolecule and the ligand and can therefore allow the measurement of both the free and bound ligands, the methods are not efficient considering both time and the reactants as they necessitate sample loading and lengthy equilibration for each point needed in constructing the binding isothermal (Wiseman *et al*., 1989).

In contrast, ITC has been developed as a commercially available tool directed at understanding and elucidating molecular interactions in numerous reactions. ITC offers

many potential advantages over other techniques since it takes advantage of the heat signal produced during the binding process, a universal property of binding reactions and thus a valuable tool in the characterization of the biological interactions. By changing the composition of the sample by titration of a required reactant, ITC is capable of measuring the bioenergetics of biochemical reactions or molecular interactions such as protein-ligand binding, protein-protein binding phenomena and enzyme-substrate interactions at constant temperature (Freire *et al*., 1990, Cliff *et al*., 2004). This is achieved by sensing changes in power required to keep a constant temperature in the reaction sample cell as one component (usually the ligand) is titrated into the other (protein).

The heat associated with the reaction is the direct thermodynamic observable and is directly related to the enthalpy and the extent of the reaction. For an ITC experiment in which all the ligand injected binds to the protein in the reaction cell, the observed ΔH (ΔH_{obs}) is directly generated by integrating the power with respect to the time required to reach equilibrium. The independent variable under experimental control is the total concentration of the reactants. However when characterizing interactions between a biological macromolecule *M* and a small ligand *X,* for example, $M + X = MX;\ MX + X = MX_2;\ MX_{n-1} + X = MX_n$, the single site binding constant, *K*, the binding enthalpy; ΔH, and the number of binding sites *n* in the set are the independent variables of thermodynamic interest (Wiseman *et al*., 1989). The heat per injection produced as the protein in the sample cell goes from the unbound to the bound state serves as an indicator of the extent of the reaction. Hence, the concentration of both the bound and free ligand at any particular point in the titration process and therefore the equilibrium binding affinity

(K_b) can be determined (Cliff *et al*., 2004). With ΔH and K_b, obtained, the free energy ΔG and entropy ΔS of binding which are required for complete thermodynamic characterization at a given constant temperature can be calculated from the following relationships:

$$\Delta G = -RT \ln K_b, \text{ and } \Delta S = (\Delta H - \Delta G)/T$$

where R is the gas constant and T is the experimental temperature.

The main purpose of this study was to explore the application of isothermal titration calorimetry in determining the thermodynamics of interactions of combretastatin analogs with tubulin and to ascertain whether there is a correlation between the binding affinity and the antitubulin activity of the ligands. Using ITC as our method of choice, a survey was carried out in order to investigate the thermodynamic parameters of the molecular interactions between tubulin and combretastatin A-1 and A-4 analogs that bind at the colchicine binding site. The interaction process of tubulin with these novel combretastatin analogs has not been characterized and thus it was important to investigate the thermodynamic properties for the tubulin-combretastatin analog complex formation. The survey attempted to investigate thermodynamically, the influence of small group substitutions on the CA-1 and CA-4 phenolic rings and dichloro-substitutions in the trimethoxyphenyl ring of CA-4 on their binding properties. Insights into the binding affinities K_b, the enthalpies (ΔH), the free energies (ΔG) and the entropies (ΔS) of their interaction with tubulin were obtained. We report the thermodynamics of the interactions of several good combretastatin A-1 and A-4 analogs with tubulin and the thermodynamic signatures that are exhibited by these interactions.

Background

Purpose of the Isothermal Titration Calorimetry Research Experiments

Taking into account the limited availability of tubulin from the calf brain and the low IC_{50} values of some of the combretastatin A-1 and A-4 analogs tested for tubulin polymerization, the ITC experiments were restricted to analogs with more potent antitubulin activity. This survey was aimed at establishing thermodynamic scientific data which for these newly synthesized combretastatin analogs is currently lacking. Optimization of Binding Affinity in drug design is of utmost importance in order to make drugs which bind to their target with the highest binding affinity (Holdgate, G.A., 2001). Higher affinity results in lower dosage requirement, greater specificity, better drug efficacy, reduced side effects, and less drug resistance. Research by Ernesto Freire and coworkers at Johns Hopkins University has shown that thermodynamics from ITC data can be used to characterize HIV-1 protease inhibitors, and binding affinity is optimized by overcoming enthalpy-entropy compensation (Velazquez-Campoy *et al*., 2000, 2001, 2002; Ohtaka *et al*., 2002, 2003).

ITC is the method of choice for providing comprehensive thermodynamic characterization of interactions between proteins and small molecule ligands, since it gives direct access to all thermodynamic parameters of the interaction. These include K_b (binding affinity or association constant), ΔG (free energy), ΔH (enthalpy), ΔS (entropy) or $T\Delta S$ and n (number of binding sites). For spontaneous and exothermic reactions, ΔG is negative, and is directly related to the binding affinity of the compound to the protein target. The tighter the binding, the more negative the ΔG. Enthalpy and entropy both contribute to ΔG. Usually a negative ΔH value points to polar and Van der Waals interactions (Laurine *et al*., 2003). ΔH (enthalpy) is indicative of the strength of the

interaction between the protein and the ligand as compared to the strength between them and the solvent, which are usually due to formation of hydrogen bonds and Van der Waals contacts (MicroCal, 2003). Hydrogen bonds form whenever a strongly electronegative atom approaches a hydrogen atom which is covalently attached to a second strongly electronegative atom. The more negative the value of ΔH is, the more enthalpically driven is the reaction.

Positive ΔS values are indicative of hydrophobic contacts and entropy driven processes. High negative enthalpy values are usually a reflection of binding via polar or Van der Waals interaction and ionization of the buffer in which the exothermic reaction process is occurring. Thus positive $T\Delta S$ results in entropically favored binding reactions. The favorable entropy changes are solely due to hydrophobic interactions, due to an increase in solvent entropy from burial of hydrophobic groups and release of water upon binding, as well as minimal loss of conformational degrees of freedom (MicroCal, 2003).

In structure-based drug design (SBDD), although molecular modeling can be used in predicting quantitative structure-activity relationships (QSAR), it is nevertheless limited by a lack of experimental bioenergetics data to verify the models generated. In such instances, ITC is the method of choice that provides complete thermodynamic characterization of the binding of a drug to its intended therapeutic target.

Some of the expected different thermodynamic signatures that can be observed for compounds binding to the same binding site of the protein are illustrated in Figure (3.1) according to MicroCal^{TM} (2003).

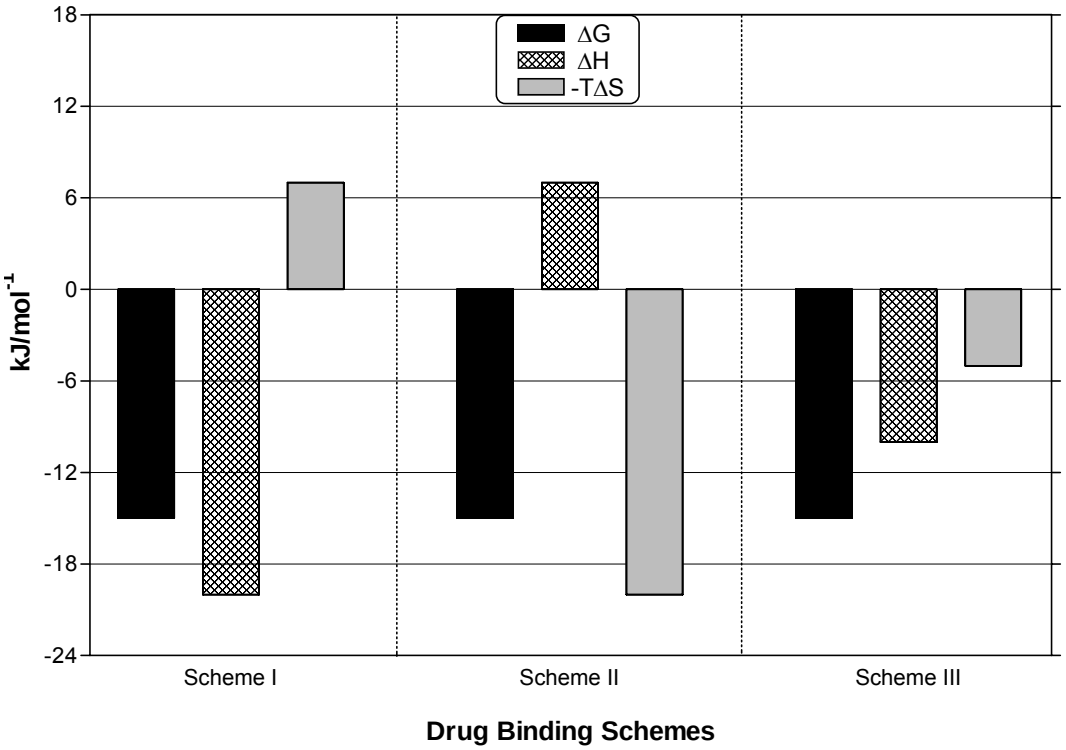

Figure 3.1. Thermodynamic Signatures for Three Different Drugs Binding to the Same Site.

Scheme I is indicative of good hydrogen bonding and a conformational change. It has favorable ΔH, characteristic of hydrogen bond formation, and an unfavorable TΔS. Hydrogen bonds (D—H---A) are predominantly electrostatic interactions between a weakly acidic donor group (D—H) and an acceptor atom (A) that bares a lone pair of electrons. In biological systems, D and A can both be the highly electronegative N and O atoms and occasionally S atoms. The D---A distance is normally in the range of 2.7 to 3.1 Å. Drugs showing this binding profile typically have large degree of flexibility, as well as high polarity, which could cause problems with membrane permeability *in vivo*.

Scheme II shows prodrug-protein binding characterized by hydrophobic interactions. The hydrophobic effect is the name given to those influences that cause nonpolar substances to minimize their contacts with water. The scheme has a favorable TΔS, indicating that binding is driven by hydrophobic interactions, and an unfavorable

ΔH. Drugs showing this binding profile are very hydrophobic and are poorly soluble, and there are also conformational restraints leading to lack of adaptability and consequently a high susceptibility to mutations that can cause drug resistance (MicroCal^{TM} (2003).

Scheme III shows favorable hydrogen bonding and hydrophobic interactions between the protein and the ligand. Such a scheme is characterized by favorable ΔH and ΔS. Most favorable tight binding reactions are characterized by this thermodynamic profile. Usually, effective drugs are expected to have high binding affinity and selectivity for their specific targets. The incorporation of enthalpically favorable interactions is sometimes difficult in molecular design and consequently, enthalpically favorable lead compounds provide a better starting point for subsequent optimization since manipulation of entropy contributions either by change in hydrophobicity or by the introduction of conformational constraints is easier to implement (Velzquez-Campoy *et al.,* 2001).

Thermodynamics of Colchicine Binding to Tubulin

Several compounds are known to interfere with microtubule formation in tumor cells through inhibition of the tubulin polymerization process. Colchicine (Col), which is a potent inhibitor of mitosis, has been known to bind to tubulin with an apparently high binding affinity (at 37 ºC, K_b = 1.6 x 10^7 M^{-1}; ΔH = - 20.9 kJmol^{-1} and ΔS = + 64.8 J K^{-1}mol^{-1} as observed from equilibrium measurements (Perez-Ramirez et *al*., 1996). However Diaz and Andreu (1991) reported thermodynamic data of ΔG = - 42.0 kJmol^{-1}; ΔH = - 26.4 kJmol^{-1} and ΔS = + 68.3 J K^{-1}mol^{-1}. Tubulin is also known to have one high-affinity binding site for colchicine (Andreu and Timasheff, 1982; Diaz and Andreu, 1991). The kinetic pathway of the binding of colchicine to tubulin follows a complex

two step mechanism characterized by an initial fast and reversible bimolecular binding reaction followed by a slow monomolecular binding reaction as shown in the following equation:

$$\text{Tubulin + Col} \overset{K_1}{\rightleftharpoons} \text{Tubulin . Col} \underset{k_{-2}}{\overset{k_2}{\rightleftharpoons}} \text{(Tubulin . Col)'}$$

(Menendez *et al*., 1989; Garland, 1978; Lambeir & Engelborghs, 1981). The reaction involved a weak first binding step and a backward rate constant is very small. However a lot of problems were encountered during the equilibrium characterization of the tubulin-colchicine interaction which led Menendez and coworkers to characterize simpler ligands (Menendez *et al*., 1989). They observed that single ring analogs of the trimethoxy phenyl and tropolone methyl ether groups of the colchicine molecule bind to tubulin reversibly, specifically and noncooperatively, with small free energy changes of -12.6 to -16.7 kJ mol^{-1} that account for the affinity of colchicine for tubulin (Andreu and Timasheff, 1982; Andreu *et al*., Timasheff *et al*., 1991).

Andreu and Timasheff (1982) have described the high binding affinity of colchicine to tubulin in terms of a simple thermodynamic model that incorporates the non-cooperative binding of a bifunctional ligand to two independent subsites on the tubulin-colchicine binding site. They postulated that the colchicine tropolone methyl ether ring binds to the tubulin heterodimer by means of ring stacking and possibly hydrogen bonding while the trimethoxyphenyl moiety binds to another subsite through hydrophobic interactions. They concluded that colchicine-tubulin complex existed in a conformational state very different from the unbound tubulin (Andreu and Timasheff, 1982; Andrea et al., 1984). The role of the elimination of ring B and /or the modification

of ring C of colchicine in tubulin binding kinetics and thermodynamics has been characterized using four different molecules with results showing that modifications of both rings are cumulative with respect to overall binding (Dumortier *et al.*, 1996). Podophyllotoxin, another well known inhibitor of tubulin polymerization, binds faster and reversibly to tubulin at the colchicine binding site. Ravelli and coworkers (2004) have determined the 4.2 Å structure of a ternary tubulin – podophyllotoxin: RB3-SLD complex and found that podophyllotoxin binds at the colchicine binding site (Figure 3.2). This was consistent with its ability to compete with colchicine for the same

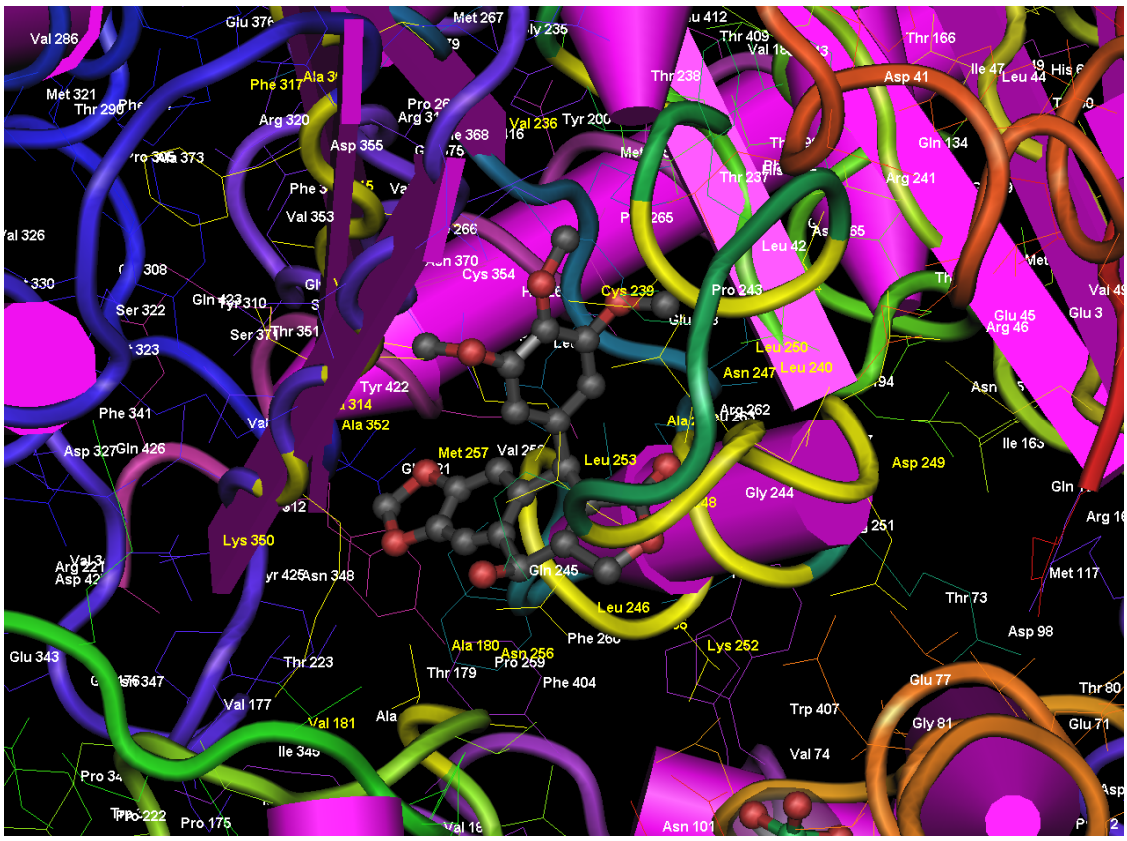

Figure 3.2. Structure of a Ternary tubulin – podophyllotoxin: RB3-SLD complex (Ravelli *et al.*, 2004). Amino acids residues within 3.5 Å distance from podophyllotoxin are shown in yellow. From *http:www.ncbi.nlm.nih.gov*; drawn and labeled using Cn3D - 4.1 by Benon Mugabe.

site (Wilson *et al*., 1974), although there had been no evidence to suggest any conformational changes in tubulin induced by podophyllotoxin binding (Wilson and Bryan, 1974) and no thermodynamic data has been reported.

Thermodynamic Interactions of Chloro-substituted Sulfonamides with Tubulin

Recently, Banerjee and coworkers (2005) reported thermodynamic profiles of tubulin binding to antimitotic sulfonamides with an indole scaffold. They urged that these compounds resemble the combretastatins and colchicine which possess a 3,4,5-trimethoxyphenyl moiety by possessing a 4-methoxyphenyl group (Figure 3.3). The rest of the structure is very different from that of colchicine, CA-1 or CA-4. These sulfonamides which possess an indole scaffold are known to inhibit tubulin polymerization (2 - 4μM) by binding at the colchicine binding site (Owa *et al*., 1999, 2000, 2002). They also competitively inhibit colchicine binding to tubulin. The thermodynamics of binding of these sulfonamide drugs to tubulin were studied using ITC in order to determine the influence of the position of chloro substitution on the binding thermodynamics of the non-chlorosubstituted lead compound. The free energies of sulfonamides with chloro substitutions in the 2-position (B) (T = 25°C, K_a = 2.84 x 10^5, ΔH = -20.3 kJ mol^{-1}, ΔG = -31.0 kJ mol^{-1}, ΔS = +36.4 J $mol^{-1}K^{-1}$) and at the 5-position (E) (T = 25°C, K_a = 4.36 x 10^5, ΔH = -8.2 kJ mol^{-1}, ΔG = -32.0 kJ mol^{-1}, ΔS = +80.3 J $mol^{-1}K^{-1}$) varied greatly with temperature whereas ΔS varied with ΔH in a compensatory manner. The thermodynamics of tubulin interaction of chlorosubstitution in the 4-position (D) showed favorable changes in enthalpy (T = 25°C, K_a = 0.79 x 10^5, ΔH = -65.4 kJ mol^{-1}, ΔG = -27.8 kJ mol^{-1}, ΔS = -125.6 J $mol^{-1}K^{-1}$) whereas the binding of

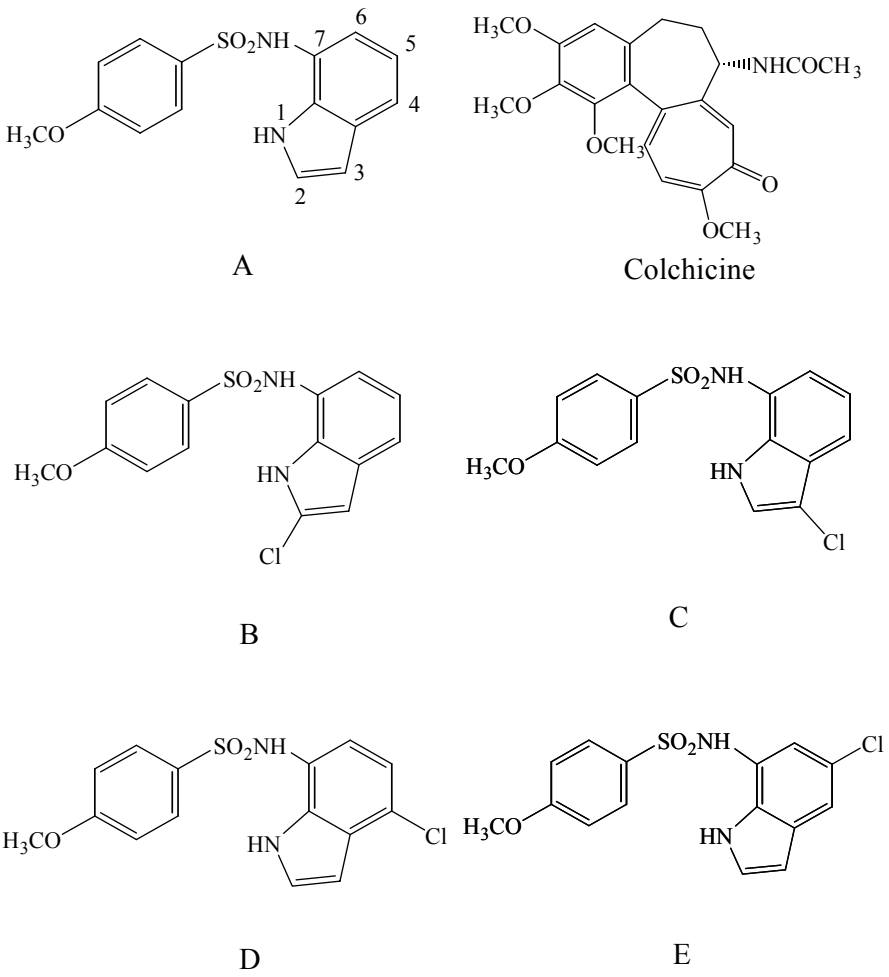

Figure 3.3. Chlorinated Sulfonamides with the Indole Scaffold (Banerjee et al., 2005).

the 3-chloro substituted analog (C) was entropically driven (T = 25°C, K_a = 0.18 x 10^5, ΔH = -3.6 kJ mol^{-1}, ΔG = -23.7 kJ mol^{-1}, ΔS = +69.4 J $mol^{-1}K^{-1}$). All these observations were attributed to conformational changes in the tubulin structure following ligand binding (Banerjee *et al*., 2005).

Thermodynamic Interactions of HTI-286 with Tubulin

Interactions of HTI-286, a synthetic analog of hemiasterlin and a known inhibitor of tubulin polymerization, with tubulin and microtubules are associated with release of heat (Krishnamurthy *et al.*, 2003). The difference between HTI-286 and hemiasterlin lies

in the presence of a phenyl ring at the N-terminus in HTI-286 instead of an indole (Figure 3.4). HTI-286 is known to inhibit cell proliferation and polymerization of tubulin in cell free assay mixtures. Krishnamurthy and coworkers have characterized the binding of HTI-286 with tubulin and the effect of this interaction on the stability of the tubulin and the microtubules formed upon polymerization.

Using ITC and a combination of other biophysical methods, Krishnamurthy and coworkers (2003) characterized the thermodynamics of HTI-286-tubulin interaction and were able to demonstrate that the initial binding of HTI-286 to tubulin is enthalpically driven and that although HTI-286 oligomerizes tubulin to discrete 18.5 S species, the

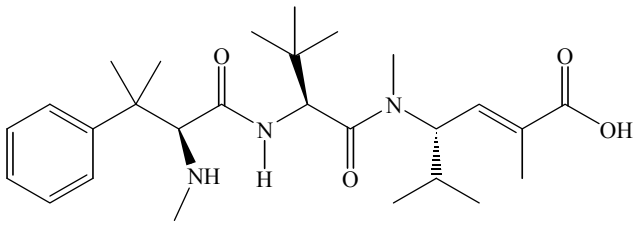

HTI-286

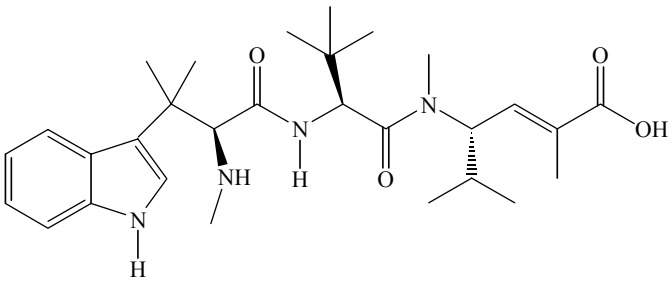

Hemiasterlin A

Figure 3.4. Structures of HTI-286 and Hemiasterlin A.

formation of this 18.5 S tubulin oligomer did not significantly contribute to the observed enthalpy. The heat evolved during the duration of injection, is consistent with rapid binding of HTI-286 to tubulin. The heat evolved increased with increase in the bound density of HTI-286. HTI-286 reportedly binds tubulin rapidly and the initial association is enthalpically driven with a ΔG value of -44.8 $kJmol^{-1}$ and ΔH = -57.6 $kJmol^{-1}$ and a dissociation constant of 100nM. Thus ITC results suggested that the heat evolved is primarily associated with the binding of HTI-286 to tubulin monomer. The stoichiometry of binding was one molecule of HTI-286 per tubulin monomer.

Interactions of BisANS and ANS to Tubulin

Interactions of 4,4'-Bis (1-anilinonaphthalene 8-sulfonate) (bis-ANS) and anilinonaphthalene 8-sulfonate (ANS) (Figure 3.5) to tubulin in the presence and absence of GTP, have been studied by Gupta and Coworkers and the binding thermodynamic parameters determined by ITC (Gupta *et al.*, 2003). It has been established that the addition of GTP to tubulin makes it compact and rigid thus accounting for the GTP-induced stabilization of the tubulin structure. However destabilization of the tubulin structure has never been noticed with ANS although just like bisANS, it possesses many lower affinity binding sites. Tubulin has two classes of binding sites for bisANS; a high-affinity site, which is responsible for the inhibition of tubulin self assembly and some low-affinity sites whose exact numbers vary by different reports. It has been suggested that bisANS binds to nucleotide binding site on proteins (Takashi *et al.,* 1977), and that the preincubation of tubulin with GTP prevents multiple binding to lower affinity sites (Chakraborty *et al.,* 1999).

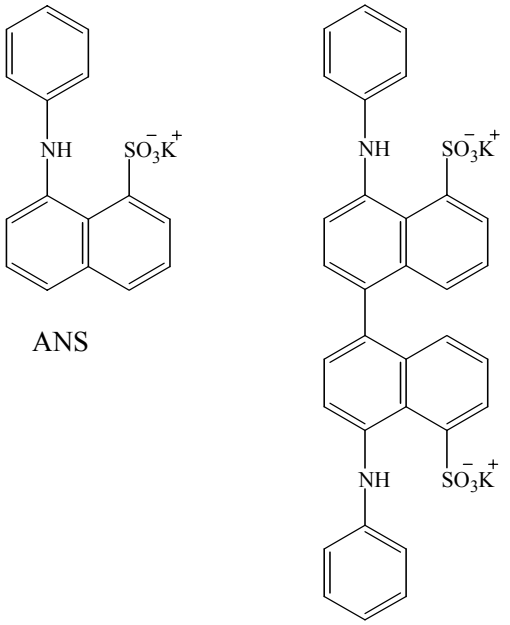

Figure 3.5. Structures of 4,4'-Bis(1-anilinonaphthalene 8-sulfonate) (bis-ANS) and anilinonaphthalene 8-sulfonate (ANS).

Like bisANS binding to tubulin, a large number of lower affinity ANS binding sites in addition to 1-2 higher affinity sites were observed (Gupta *et al.*, 2003). Gupta and coworkers (2003) proposed that the unique structure of biANS which binds tubulin as a bifunctional ligand in the absence of GTP is responsible for the changes in the structure of tubulin. When the binding interactions of ANS and bisANS with tubulin were studied in presence and absence of GTP using ITC, the results indicated a monotonic decrease in the exothermic heat of binding upon successive small injections of the ligand until saturation. ITC data analysis was carried out using a nonlinear least square fit of the data by means of two sets of binding site model. From the results, it was evident that the addition of GTP decreases the number of bisANS binding to both higher and lower binding affinity sites of tubulin and the affinities for higher and lower sites are two times less than those observed when GTP has been added. Binding of bisANS and

tubulin revealed a process that is both enthalpically and entropically driven. However, the low – affinity binding of biANS to tubulin is predominantly entropy driven. Thermodynamics data from the binding of ANS to tubulin which was carried out under similar conditions using ITC revealed a large number of lower affinity ANS binding sites and 1-2 higher affinity sites. Compared to bisANS, the binding affinities of ANS to tubulin seem to be higher in presence of GTP. The binding of ANS to tubulin was entropy driven at the lower affinity sites where as in absence of GTP, the high affinity binding for ANS is enthalpically and entropically driven. For high-affinity ANS binding to tubulin in presence of GTP, enthalpy was the dominant term (Gupta *et al.*, 2003).

Thermodynamics of the Interaction of Stathmin with Tubulin

The biophysical and structural characteristics of the interaction of stathmin with tubulin have also been investigated (Honnappa *et al.*, 2003). Stathmin is an intrinsically disordered protein involved in the regulation of the microtubule filament system. One function of stathmin is to sequester tubulin dimers into assembly incompetent complexes with two tubulin dimmer binding sites per stathmin molecule. Human Op18/stathmin is a 17-kDa monomeric cytoplasmic phosphoprotein which has been conserved through evolution. Stathmin is known to bind to tubulin dimers thus increasing the catastrophe frequency of microtubules especially in vitro (Belmont and Mitchson, 1996). Using high sensitivity ITC, Honnappa *et al.,* (2003) investigated the biophysical and structural characteristics of stathmin-tubulin interaction. They reported that at $10^{o}C$ and under conditions of 80mM PIPES buffer, pH 6.8, 1mM $MgCl_2$, 1mM EGTA, 1mM GTP, stathmin binds two tubulin subunits with equal affinity and the major driving force in this

reaction is the hydrophobic effect (Honnappa *et al.,* 2003). When the thermodynamic binding isotherms were analyzed, the data revealed a simple two-site binding mechanism. This interaction involves two binding sites both of which are characterized by equal binding affinity with an equilibrium constant of $K_b = 6.0 \times 10^6\ M^{-1}$.

Thermodynamic Modeling

The thermodynamics of ligand binding to macromolecules have been thoroughly investigated (Freire *et al.*, 1990 and Wiseman *et al.*, 1989). The most common model for a binding experiment is the independent set of multiple binding sites model. This model was adopted in the combretastatin ligand-tubulin binding experiments, in which the heat determined for a given titration was equal to the difference in the enthalpy of the system after and before the injection. The system was defined as the contents of the sample cell after the injection, and as the contents of the sample cell plus the material to be injected before the injection. The enthalpy of the system was given as the product of average excess enthalpy, ΔH, and moles of protein tubulin. Therefore, the heat observed for the i^{th} injection was given as:

$$q_i = (\Delta H)_i C_i V_i + (\Delta H)_{i+1} C_{i+1} V_{i+1} + (\Delta H)_{inj} C_{inj} V_{inj} \qquad [3.1]$$

where C = concentration of the protein tubulin, and V = volume of the sample cell.

Since there was no tubulin in the injection syringe, and assuming ideal solutions, (meaning that there was no dilution heat), then the last term was zero. The cumulative heat at the i^{th} injection was given as:

$$Q_i = A_i q_i = \Delta H_i C_i V_i \qquad [3.2]$$

To determine binding constants and enthalpy changes from the ITC data collected, we established a model for the mean excess enthalpy terms. The binding model used was for one combretastatin ligand binding to tubulin with a binding constant of K and an enthalpy of binding of ΔH. In this state, tubulin existed in two states, either bound or free. The sum of the accessible states of the tubulin expressed as concentrations was given as:

$$[M]_{tot} = [M] + [MX] = [M](1 + K[X]) \qquad [3.3]$$

where M is tubulin, and X is a combretastatin analog and $[M]_{tot}$ is the same as C in [3.1]. The amount of bound tubulin, P_b was given by:

$$P_b = \frac{[MX]}{[M] + [MX]} = \frac{K[X]}{1 + K[X]} \qquad [3.4]$$

Therefore, the average excess enthalpy of binding was given as the sum of the population of each state, j, multiplied by the change in enthalpy of binding to get to that state, ΔH_j. In this case,

$$\Delta H = \Sigma_j P_j \Delta H_j = \Delta H \frac{K[X]}{1 + K[X]} \qquad [3.5]$$

This value was then substituted into equation [3.1] or [3.2]. However, [3.4] was given in terms of concentration of free ligand, [X], whereas the quantity we controlled in the experiments was total concentration of the ligand, $[X]_{tot}$. Thus it was necessary to express [3.4] in terms of total ligand concentration. The total concentration of the ligand was then given by:

$$[X]_{tot} = [X] + [MX] = [X](1 + K[M] \quad [3.6]$$

Combining [3.6] with [3.3], the concentration of free ligand in terms of total concentrations of combretastatin ligand and tubulin became:

$$[X] = \frac{-1-K([M]_{tot} - [X]_{tot}) + \sqrt{\{(1+K([M]_{tot} - [X]_{tot}))^2 + 4K[X]_{tot}\}}}{2K} \quad [3.7]$$

which was then substituted into [3.5] giving a general analytical expression for q_i for each injection. Assuming multiple sites which are identical and independent, we multiplied by $[M]_{tot}$ (equation 3.3] by N, the number of sites. For ITC binding experiments with this model of binding, the analytical solution for the total heat was determined using the formula:

$$Q = V.\ \Delta H\ .\left([L] + \frac{1 + [M].n.K - \sqrt{\{(1+[M].n.K - [L].K)^2 + 4.K.[L]\}}}{2.K} \right) \quad [3.8]$$

The different variable parameters for the model were: ΔH = enthalpy of binding, K = binding constant, n = number of binding sites, V = volume of the cell, [L] = total Ligand concentration and [M] = protein concentration. Generally, it was assumed that the stoichiometry of combretastatin ligand-tubulin binding would be one binding site per tubulin. However, the experimental value of (n) still varied, most probably due to errors in protein estimation or tubulin transfer or degradation of tubulin. Since these binding experiments were performed under conditions in which presumably K could be determined, the value of (n) did not affect the fitted values of K or ΔH obtained.

Materials and Methods

Preparation of 50mM PEM, pH 7.0 Buffer Containing 0.1mM GDP.

PIPES, free acid (1.058 g, 3.5 mmol), PIPES, sodium salt (2.079 g, 6.4 mmol), EGTA (76 mg, 1.0 mmol), $MgCl_26H_2O$ (20.2 mg, 0.5 mmol), were dissolved in 200 ml of double purified water and heated gently on a heating block with stirring until all acid and base components had dissolved. The pH of the buffer was adjusted to 7.0 by addition of 10 - 20 drops of HCl (1.0M). The resultant PEM buffer (50mM PIPES, 1.0mM EGTA, 0.5mM $MgCl_2$, pH 7.0) was cooled and GDP (8.86 mg, 0.1 mmol) was dissolved in 200 mL of PEM buffer. The buffer was kept in the refrigerator at 4°C until use.

Preparation of Tubulin Samples for ITC Experiments

Purified tubulin (16 vials each containing 250 µl, 12.069 mg/ml) were removed from liquid nitrogen and thawed in cold water for 20 minutes. The tubulin, which had been purified according to the method of Hamel and Lin (1984), was pooled into a 10 mL ultracentrifuge tube and tubulin was clarified with a 40 minute 2°C centrifugation at 39,000 rpm. 0.1M GTP (40 µl) was added to the supernatant to bring it to 1.0mM GTP. Tubulin polymerization was performed by incubating the tubulin solution for 1 hour at 37°C, and then recovering the tubulin with a 40 minute 37°C 39,000 rpm centrifugation. The pellet was then homogenized in PEM buffer (50mM PIPES, 1.0mM EGTA, 0.5mM $MgCl_2$, pH 7.0) containing GDP (0.1mM). The concentration of the tubulin solution was determined by the UV spectrophotometric method described in Chapter 2. The solution was left on ice for 1 hour, clarified as before with a 40-minute 2°C 39,000 rpm

centrifugation. The purified tubulin supernatant with a final concentration of 6.2 mg/mL was then aliquoted into screw capped vials, flash frozen and stored in liquid nitrogen at -70°C.

Preparation of Combretastatin Ligand Solutions

Combretastatin A-1 and A-4 ligands were weighted using a Mettler Toledo AX microbalance with a readability of 0.01 mg. The PEM buffer (15.0 ml) containing GDP (0.1mM) was degassed for 10 – 15 minutes until all dissolved gas had been removed from the solution. The ligands were dissolved in DMSO (99.9%) giving 0.1M stock solutions. Each combretastatin ligand (10.0µl, 0.1M) was then made to 1000 µl using degassed PEM buffer (50mM PIPES, 1.0mM EGTA, 0.5mM $MgCl_2$, pH 7.0) containing GDP (0.1mM), giving 1.0 mmol ligand solutions. To the ligand solutions (500 µl, 1.0 mmol) was added 500 µl of degassed PEM buffer containing GDP (0.1mM), giving 0.5 mmol ligand solutions.

Direct Measurement of Independent Tubulin Binding Thermodynamics by ITC

All ITC experiments were performed using the CSC 4200, Provo, Utah Isothermal Titration Calorimeter according to the procedure described in the user's manual. The Model 4200 measures the heat produced when two solutions are mixed in a reaction cell. The heat change caused by any reaction occurring as the solutions are mixed, is detected by the thermoelectric device sensor, amplified and is converted by the electronic output circuit to a signal corresponding to the heat change. The signal produced is computerized in a data-collection system. The reaction cell and the titrant

cell are contained in an ultra-stable constant temperature bath. The temperature of the titrant and the titrate are kept equal through thermal shunts.

In the experimental design to measure K_b, there is a curvature in a plot of heat versus the number of injections. It is the fitting of this curvature that permits the determination of K_b. To achieve a curvature in the titration experiment, the product of K_b and the protein concentration, C_{prot}, must be between 10 and 1000 (Wiseman *et al.,* 1989). When this product is too high, there is no curvature in the plot. When this constant is low, the curvature is too gradual to allow a good determination of K_b. Thus very low concentrations of the protein are required to measure very tight affinity constants. However, the need to keep the product of K_b and C_{prot} as low as possible had to be counter balanced by the need for a detectable heat.

Degassed PEM buffer (1075 µl) containing GDP (0.1mM) was added to tubulin (325 µl, 9.558 mg/ml) in the screw cap vial giving 1.4 ml (2.2 mg/ml, or 22.0 µmol) of tubulin. Tubulin (1.4 ml, 22.0 µmol) was then loaded into the ITC sample cell using a 250 µl Burette Syringe equipped with an 11.25" 22 Gauge needle. Degassed PEM buffer containing GDP (0.1mM) was loaded into the ITC reference cell using a 2.5 ml Syringe equipped with a 15 gauge, 12" needle until the buffer was observed coming out of the Hastelloy-C Cell Assembly. For every experiment, each combretastatin analog (250 µl, 0.5 mmol) was loaded into another 250 µl Burette Syringe also equipped with an 11.25" 22 Gauge needle. After the ITC system had equilibrated, the ligand was titrated into the tubulin with a stirring speed of 300 rpm, standard equilibration time of 200 seconds and an interval of 200 seconds between injections. In all titration experiments, 25 injections (10.0 µl per injection) of the combretastatin analogs were made. The serial ITC

experiments measured the total heat of the reaction due to the 25 successive titrations of the combretastatin analogs into the tubulin at a constant spacing of 200 seconds between injections. All binding experiments were carried out at 25 ^{o}C.

Blank ITC Titrations

The heat effect measured in a titration experiment includes the heat of dilution of the titrant, in addition to the heat generated from the binding reaction. Following each binding titration experiment, a blank titration identical to the binding experiment was performed in order to determine the heat of dilution of the combretastatin analogs but with the PEM buffer only present in the cells. Both the ITC sample and reference cells were cleaned and dried using nitrogen gas and then placed back on their respective Hastelloy-C Cell Assemblies. Degassed PEM buffer containing GDP (0.1mM) was then loaded into both ITC cells using a 2.5 ml syringe equipped with a 15 gauge, 12" needle until the buffer was observed coming out of the hastelloy-cell assemblies. For every blank experiment, each combretastatin analog (250 µl, 0.5 mmol) was loaded into a 250 µl Burette Syringe also equipped with an 11.25" 22 Gauge needle. After the ITC system had equilibrated, the ligand was titrated into the PEM buffer only, with no tubulin present, at a stirring speed of 300 rpm, standard equilibration time of 200sec and an interval of 200 seconds between injections. 25 injections (10.0 µl per injection) of the combretastatin analogs were made. The serial ITC experiments measured the total heat of the reaction due to the 25 successive titrations of the combretastatin analogs into the PEM buffer at a constant spacing of 200 seconds between injections. All blank experiments were carried out at 25 ^{o}C using the same conditions as the tubulin-ligand titration.

Data Analysis

Titration curves and data were analyzed using Titration BindWorks 1.1 software supplied with the ITC equipment. There are several ways in which a calorimeter may be designed. The heat measured may be based on a temperature rise measured in a system of known heat capacity (ΔT); the measured change in power (which is typically resistance heating) required to maintain a system at constant temperature, power compensation; and a direct measure of the heat flowing between the system and large sink maintained at a constant temperature (heat flow). The CSC ITC uses a twin heat flow design for maximum sensitivity. ITC incorporates semiconducting thermopiles for its heat flow detectors, passive shields between the isothermal calorimeter block and the thermostat.

In the ITC titration experiments performed, the data generated took the form of power (μW) as a function of time (seconds). In order to analyze the data, heat as a function of the number of injections (or moles of added ligand) was obtained by integrating the peaks from the experiment using the BindWorks program. Nonlinear regression analysis was done by fitting a single binding model using the independent set of multiple binding sites model. At each injection, tubulin was bound to the combretastatin analog, leading to a characteristic signal. The area under each injection peak was proportional to the heat produced. The enthalpy of binding (ΔH), the binding affinity constant (K_b) and the molar binding stoichiometry (N) were obtained using the independent model. Thermodynamic parameters such as changes in free energy (ΔG) and entropy (ΔS) and (-TΔS) were calculated from the following relationship:

$$\Delta G = -RT\ln K_b = \Delta H - T\Delta S$$

Results and Discussion

Thermodynamic Interaction of Combretastatin A-1 with Tubulin

ITC was also used to determine the bioenergetics of CA-1 (figure 3.6) and tubulin binding. Figure 3.7 shows the raw data from microcalorimetric titrations of tubulin with combretastatin A-1 in power (μW) versus time (seconds). The area under each peak was directly proportional to the heat produced. Typically, the titration consisted of addition of 10.0μl aliquots of CA-1 (0.5mM) per injection at 200 seconds intervals to tubulin (0.022mM) in PEM (50mM, pH 7.0) buffer with GDP (0.1mM) at 298°K.

Results from the experiment exhibited a monatomic decrease in exothermic heat produced per every successive injection until saturation was reached. Figure 3.8 shows the binding isotherm produced by plotting heat injected (μJ) from integrated peaks against the molar ratio of CA-1 to tubulin in the cell. Data analysis was carried out using BindWorks software supplied by CSC with the ITC machine. Using the independent set of multiple binding sites, CA-1 was found to bind tubulin with a high binding affinity ($8.1 \times 10^5\ M^{-1}$) and a favorable free energy of binding ($-33.7\ kJ\ mol^{-1}$) at 298°K. Table 3.1 shows the thermodynamic parameters of binding of CA-1 to tubulin. The binding of CA-1 to tubulin was also associated with high enthalpy change ($-33.2\ kJ\ mol^{-1}$) and a low entropy change ($+1.81\ Jmol^{-1}K^{-1}$). Although both colchicine and CA-1 are very good inhibitors of tubulin polymerization, colchicine binding to tubulin is almost entirely entropy driven where as CA-1 binding to tubulin is enthalpy driven. The combretastatin A-1-tubulin binding stoichiometry was 1.4 which pointed to a single CA-1 binding site.

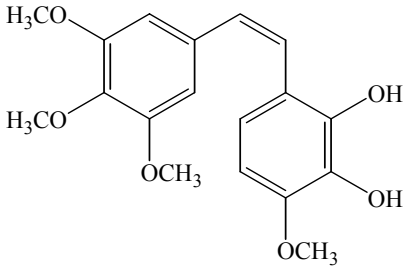

3

$K_b = 8.1 \times 10^5\ M^{-1}$

$IC_{50} = 1.9\ \mu M$

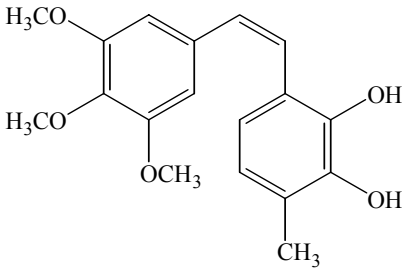

12

$K_b = 2.1 \times 10^5\ M^{-1}$

$IC_{50} = 2.1\ \mu M$

Figure 3.6. Structures of Compounds **3** and **12** Analyzed by ITC.

Table 3.1. Thermodynamics Data for Binding of CA-1 **(3)** and **12** to Tubulin.

Parameters	Independent Set of Multiple Binding Sites	
Compound	**(3)**	**(12)**
N	1.4	1.3
K (M^{-1})	8.1×10^5	2.1×10^5
$\Delta G°$ (kJ mol^{-1})	-33.7	-30.4
$\Delta H°$ (kJ mol^{-1})	-33.2	-23.8
$\Delta S°$ (J $mol^{-1}K^{-1}$)	+1.8	+22.3
$-T\Delta S°$ (kJ mol^{-1})	-0.5	-6.6

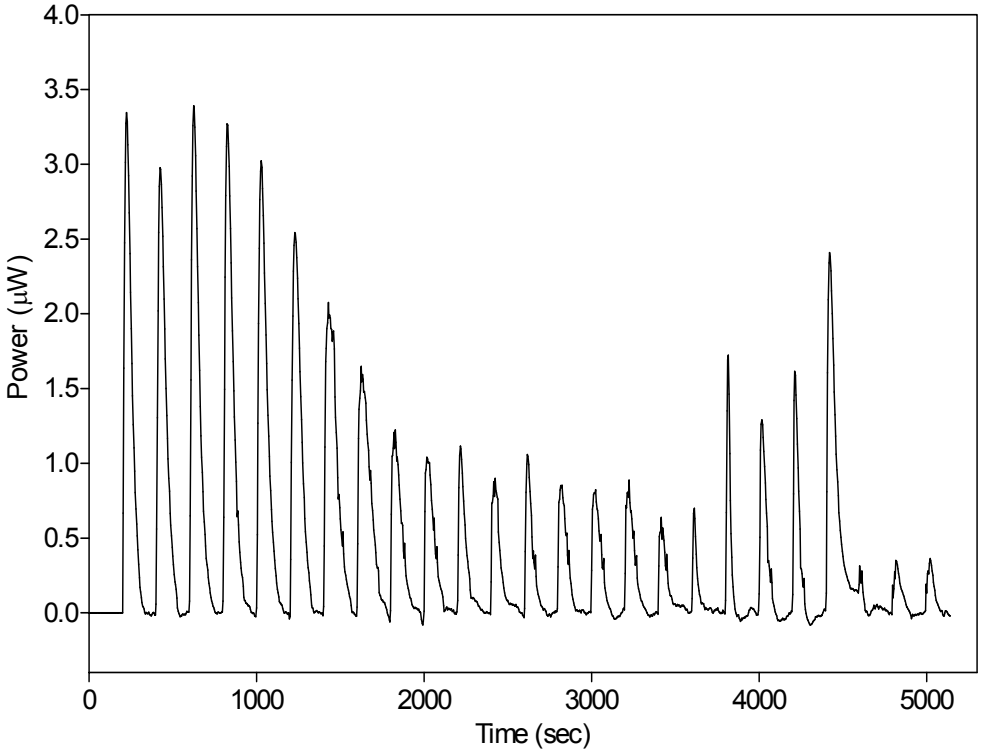

Figure 3.7. ITC Raw Data for Titration of Tubulin with Compound **3**.

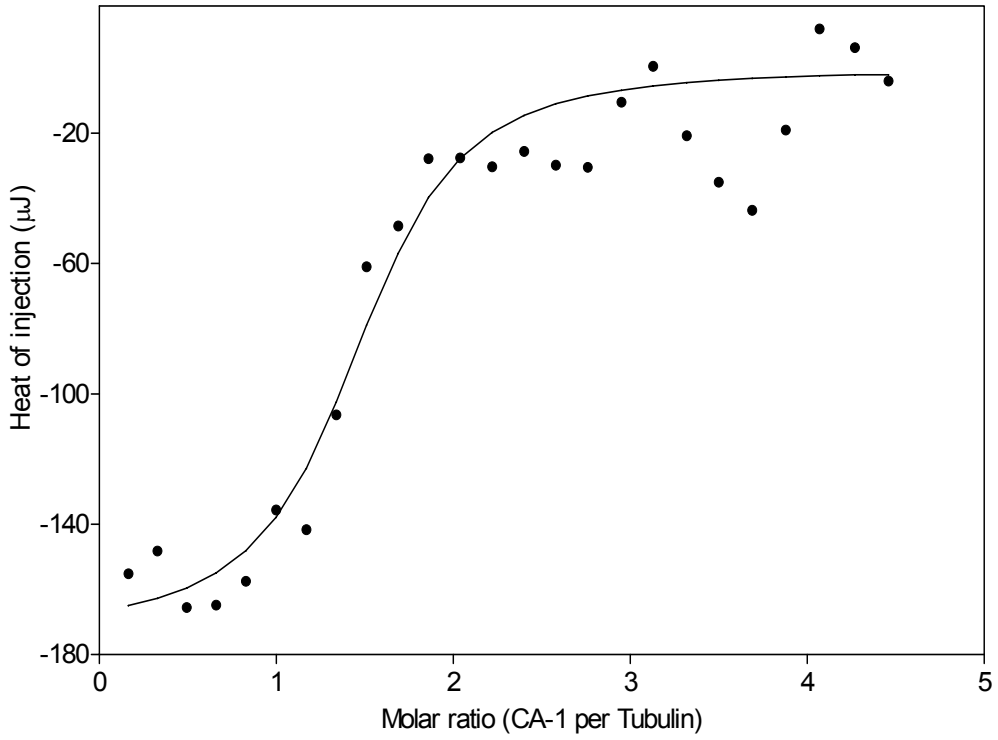

Figure 3.8. Heat Measured at each Injection versus Molar Ratio of Cumulative Compound **3** added per Tubulin.

*Thermodynamic Interaction of Compound **12** with Tubulin*

The binding of compound **12** (figure 3.6) to tubulin was studied using ITC. The structure of Compound **12** resembles that of CA-1 except that the 4-methoxy group in ring B of CA-1 had been substituted with a methyl group. Figure 3.9 shows the raw data from successive ITC microcalorimetric titrations of tubulin with compound **12** in power (μW) versus time (seconds). The area under each peak is directly proportional to the heat produced after injection. Typically, the titration experiment consisted of addition of 10.0μl aliquots of compound **12** (0.5mM) per injection at 200 seconds intervals to tubulin (0.022mM) in PEM (50mM, pH 7.0) buffer with GDP (0.1mM) at 298°K. Figure 3.10 shows the binding isotherm produced by plotting heat of injection (μJ) of integrated peaks against the molar ratio of Compound **12** added to tubulin in the cell. Data analysis was carried out using BindWorks software supplied by CSC with the machine. Using the independent set of multiple binding sites, the analog was found to bind tubulin with a binding affinity ($2.1 \times 10^5\ M^{-1}$) and a favorable free energy of binding ($-30.4\ kJ\ mol^{-1}$) at 298°K. Table 3.1 shows a summary of the thermodynamic parameters of binding of this Compound **12** to tubulin. When measured at 298°K, the binding of compound **12** to tubulin was equally associated with moderate enthalpy change ($-23.8\ kJ\ mol^{-1}$) and entropy change ($+22.3\ J\ mol^{-1}K^{-1}$). This observed enthalpy – entropy balance is usually a unique and desirable property when searching for lead compounds and greatly enhances subsequent optimization. It is worthy noting that this analog has almost the same antitubulin potency as CA-1 which are both characterized by IC_{50} values of 2.1 μM and 1.9 μM respectively. However CA-1 showed a 4-fold higher binding affinity to tubulin

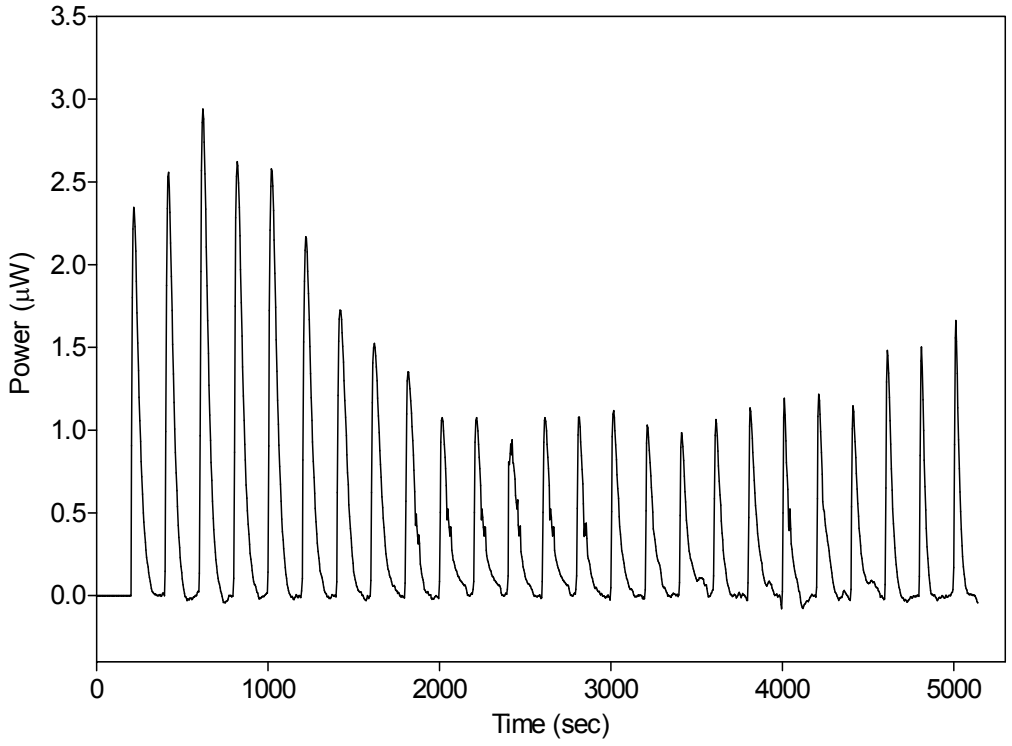

Figure 3.9. ITC Raw Data for Titration of Tubulin with Compound **12**.

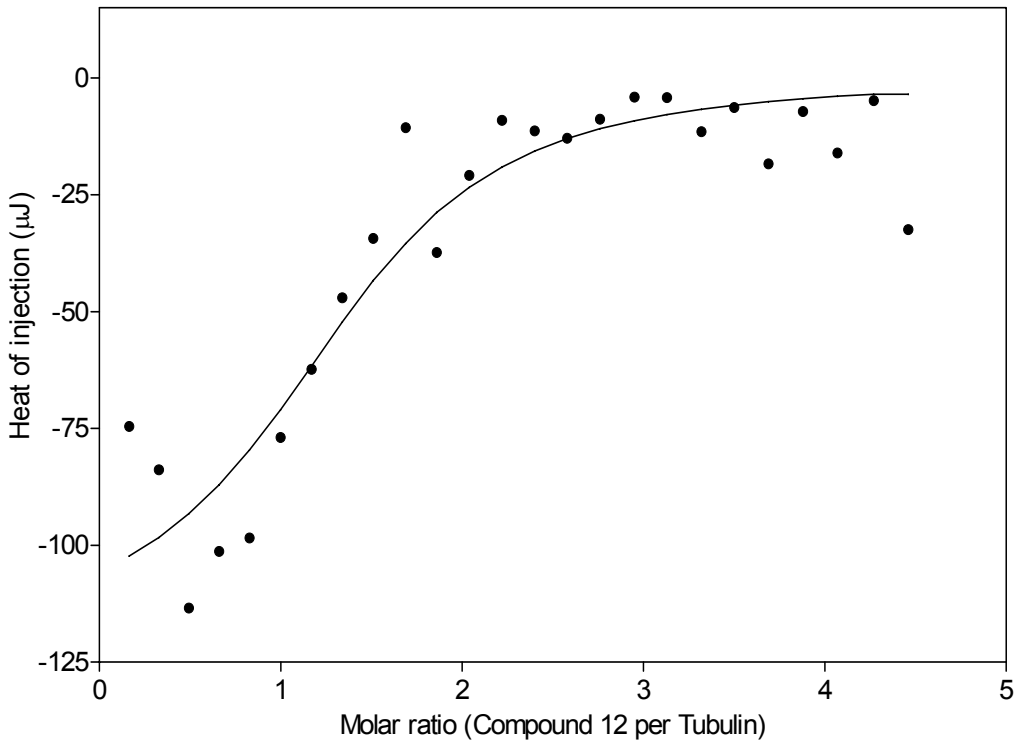

Figure 3.10. Heat Measured at each Injection versus Molar Ratio of Cumulative Compound **12** added per Tubulin.

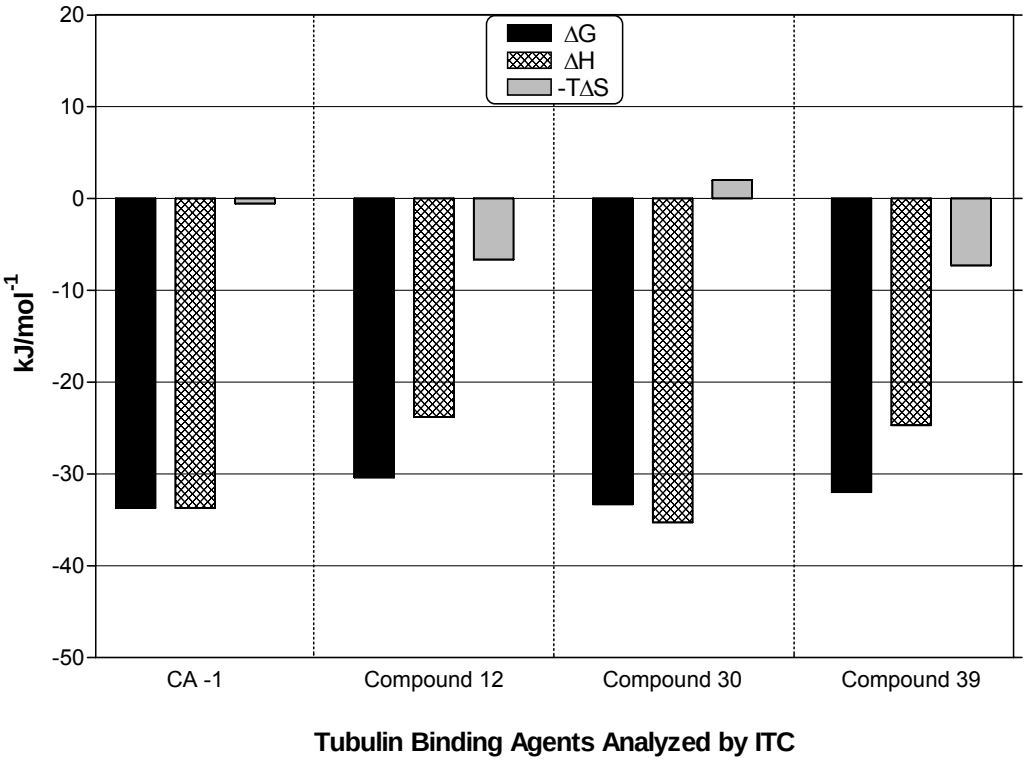

Figure 3.11. Thermodynamic Signatures of Binding of CA-1 Analogs to Tubulin.

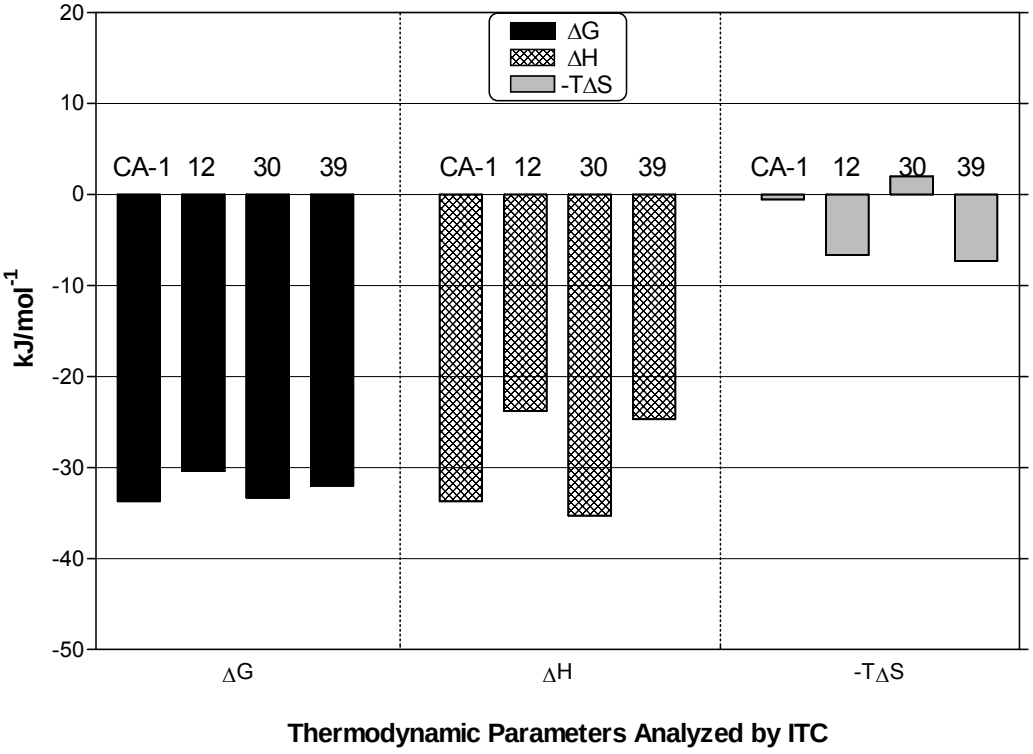

Figure 3.12. Thermodynamic Variations in Binding of CA-1 Analogs to Tubulin.

than compound **12**, which may be attributed to the ability of the methoxy group on ring B forming more hydrogen bond interactions with the polar amino acid side chains of tubulin with in the colchicine binding site more easily than the methyl moiety. The stoichiometry of this compound binding with tubulin was 1.3 which is almost similar to that observed in the case of CA-1 binding to tubulin (Mugabe, B.E. *et al*, 2005).

*Binding Energetics of a 2-Nitro-Substituted CA-1 Analog (**30**) to Tubulin*

Isothermal titration calorimetry was also used to study the binding affinity of compound **30** (figure 3.13) and the associated bioenergetics. Figure 3.14 represents raw calorimetric data for successive titrations of tubulin with compound **30** in power (μW) versus time (seconds). The area under each peak is directly proportional to the heat produced. Typically, the titration consisted of addition of 10.0μl aliquots of Compound **30** (0.5mM) per injection at 200 seconds intervals to tubulin (0.022mM) in PEM (50mM, pH 7.0) buffer with GDP (0.1mM) at 298°K. Results from the experiment exhibited almost constant exothermic heat for the compound **30** molar ratio of 0 to 3 and then gradually showed a monatomic decrease in exothermic heat produced upon additional ligand injection until saturation was reached. Figure 3.15 shows the binding isotherm produced by plotting heat of injection (μJ) of integrated peaks against the molar ratio of compound **30** added to tubulin in the cell. Data analysis was carried out using BindWorks software supplied by CSC with the ITC machine. A negative ΔH value reflects polar interaction and Van der Waals contacts whereas a positive ΔS reflects hydrophobic contacts (Laurine *et al*., 2003). Using the independent set of multiple binding sites, compound **30** was found to bind tubulin with a high binding affinity ($6.7 \times 10^5\ M^{-1}$) and a favorable Gibbs energy of binding of -33.3 kJ mol^{-1} at 298°K.

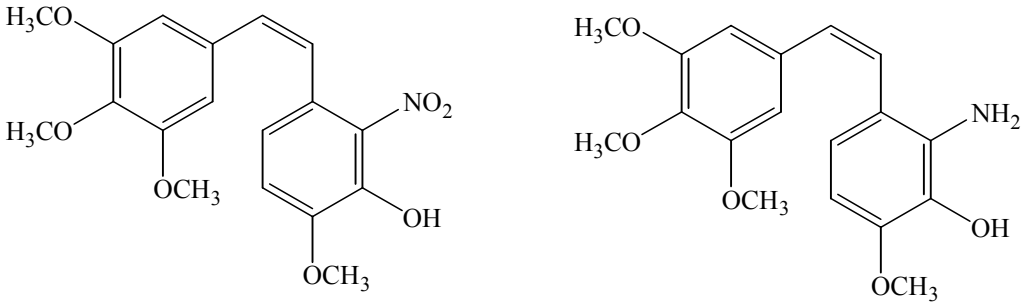

30
$K_b = 6.7 \times 10^5\ M^{-1}$
$IC_{50} = 1.5\ \mu M$

39
$K_b = 4.0 \times 10^5\ M^{-1}$
$IC_{50} = 2.5\ \mu M$

Figure 3.13. Structures of Compounds **30** and **39** Analyzed by ITC.

Table 3.2. Thermodynamics Data for Binding of Compounds **30** and **39** to Tubulin.

Parameters	Independent Set of Multiple Binding Sites	
Compound	**30**	**39**
N	1.6	1.3
K (M^{-1})	6.7×10^5	4.0×10^5
$\Delta G°$ (kJ mol^{-1})	-33.3	-32.0
$\Delta H°$ (kJ mol^{-1})	-35.3	-24.7
$\Delta S°$ (J $mol^{-1}K^{-1}$)	-6.7	+24.5
$-T\Delta S°$ (kJ mol^{-1})	+2.0	-7.3

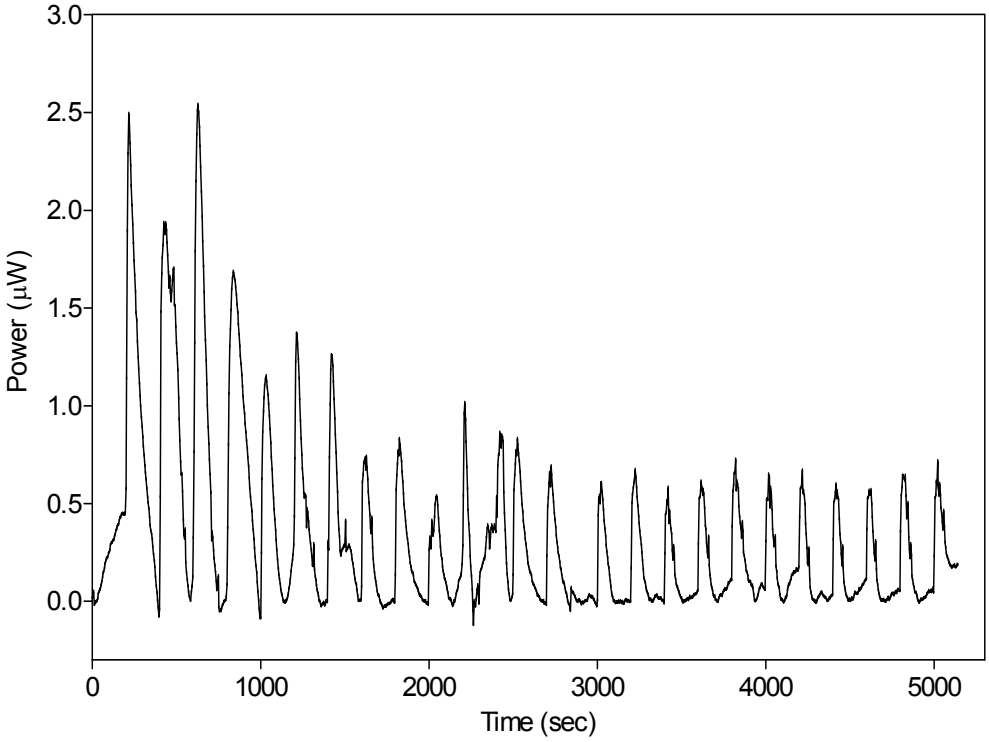

Figure 3.14. ITC Raw Data for Titration of Tubulin with Compound **30**.

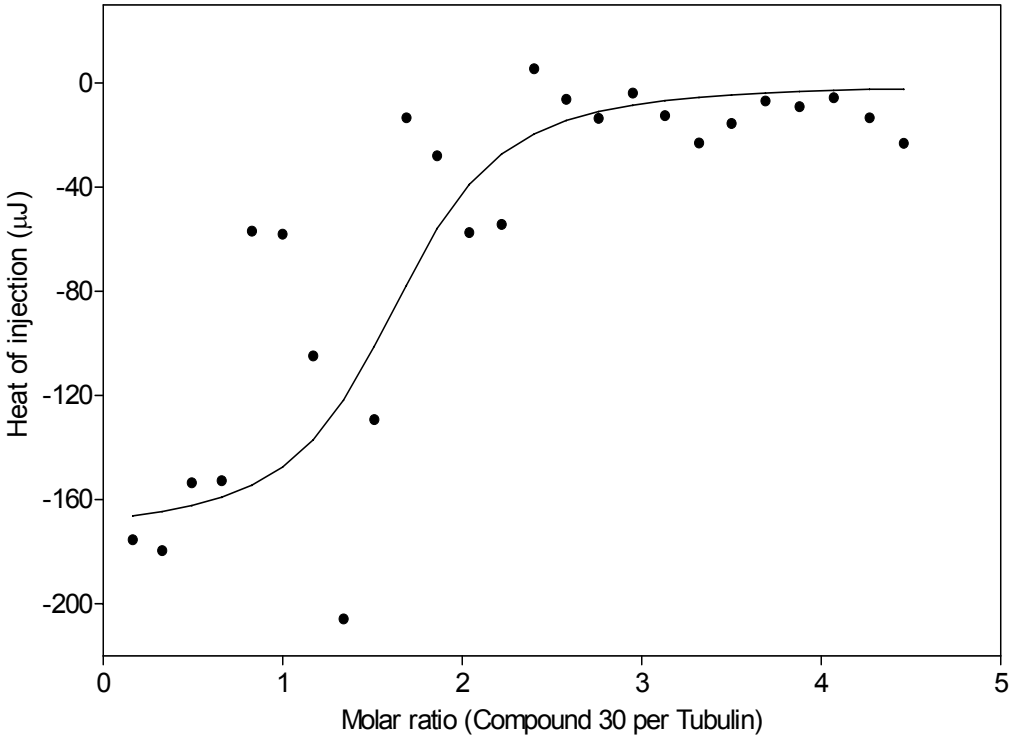

Figure 3.15. Heat Measured at each Injection versus Molar Ratio of Cumulative Compound **30** added per Tubulin.

Table 3.2 shows the thermodynamic parameters associated with the binding of compound **30** to tubulin. The binding of compound **30** to tubulin was also associated with high enthalpy change (-35.3 kJ mol^{-1}) and a low negative entropy change (-6.7 $Jmol^{-1}K^{-1}$) thus an unfavorable TΔS. Compound **30** is a very good inhibitor of tubulin polymerization with an IC_{50} value of 1.5 μM. The binding of compound **30** to tubulin is enthalpy driven compared to colchicine binding to tubulin which is almost entirely entropy driven. The process of CA-1 binding to tubulin was also found to be enthalpy driven together with a small entropy contribution. From these results, it seems that compound **30** induces favorable hydrogen bonding and a conformational change upon binding to tubulin, which leads to tight binding. The number of binding sites associated with the binding of compound **30** to tubulin was 1.6.

*Binding Thermodynamics of a 2-Amino-Substituted CA-1 Analog (**39**) to Tubulin*

Compound **39** (figure 3.13) is known to inhibit polymerization of tubulin with an IC_{50} value of 2.5 μM. This is a 66.7 % decrease in antitubulin potency compared to compound **30** which has an IC_{50} value of 1.5 μM. Figure 3.16 shows ITC raw data for titration of tubulin (0.022mM) with 10.0μL injections of compound **39** (0.5mM) in PEM buffer (50mM, pH 7.0), containing GDP (0.1mM). The heat obtained by integrating the peaks was plotted against molar ratio of cumulative amounts of compound **39** added per tubulin in the sample cell which was represented by a saturation curve with a sigmoid characteristic (Figure 3.17).

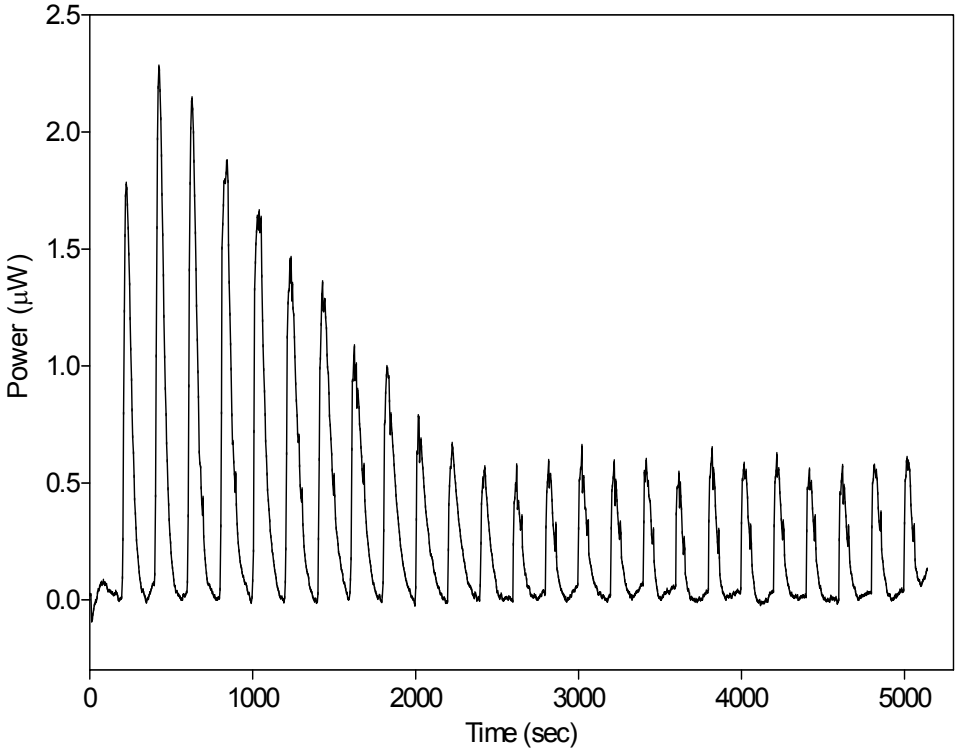

Figure 3.16. ITC Raw Data for Titration of Tubulin with Compound **39**.

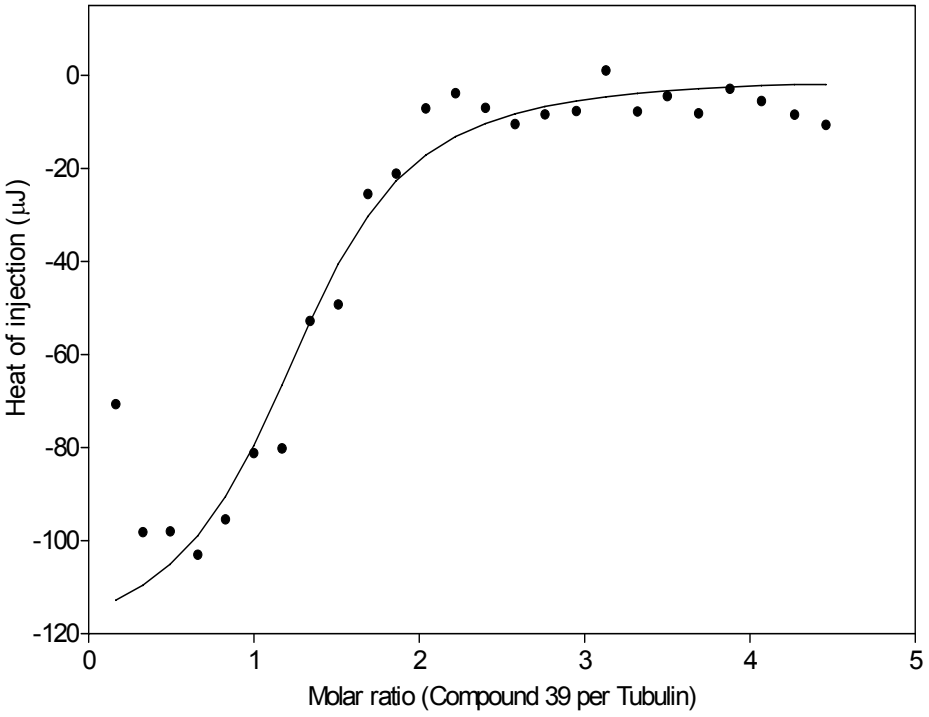

Figure 3.17. Heat Measured at each Injection versus Molar Ratio of Cumulative Compound **39** added per Tubulin.

ITC thermodynamic analysis indicated that compound **39** binds to tubulin with a binding constant, K_b, of 4.0 x 10^5 M^{-1}, which corresponds to a Gibbs free energy of binding ($\Delta G = \Delta H - T\Delta S$) of -32.0 kJ mol^{-1} (Table 3.2). In addition, the binding of this analog to tubulin was highly favored by enthalpy (-24.7 kJ mol^{-1}). This kind of binding is usually characterized by favorable hydrogen bonding and hydrophobic interactions. The process of the binding of compound **39** is entropically driven. The calculated entropy of the interaction was +24.5 $Jmol^{-1}K^{-1}$. This favorable TΔS observed pointed to a thermodynamic profile of tight binding by the ligand on the tubulin binding site. The number of binding sites observed in this interaction was 1.3.

*Binding Thermodynamics of a 2-Chloro-Substituted CA-1 Analog (**15**) to Tubulin*

Chlorosubstituted sulfonamide drugs are known to bind to tubulin on the colchicine binding site (Banerjee *et al*., 2005). Banerjee and coworkers have found that a mere alteration in the position of a single chlorine atom on the indole scafford leads to significant changes in the binding thermodynamics of these sulfonamides. The binding energetics of compound **15** (figure 3.18) to tubulin was also measured by ITC (Figure 3.19). From the ITC binding experiment, a binding affinity (2.3 x 10^5 M^{-1}) was observed which corresponded to Gibbs energy of binding of -30.6 kJ mol^{-1} at 298°K. Table 3.3 shows a summary of the thermodynamic parameters of binding of compound **15** to tubulin. The enthalpy change associated with heat obtained by integrating the peaks from the experiment when plotted against the molar ratio of compound **15** to tubulin was -10.0 $kJmol^{-1}$ and a favorable entropy change of +69.21 $Jmol^{-1}K^{-1}$ was also observed (Figure 3.20).

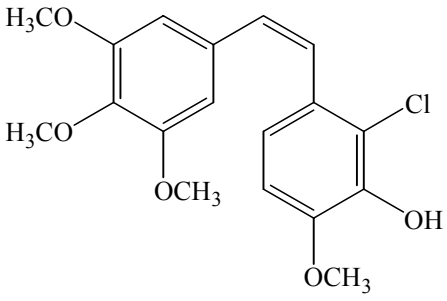

15

$K_b = 2.3 \times 10^5 M^{-1}$

$IC_{50} = 1.5\ \mu M$

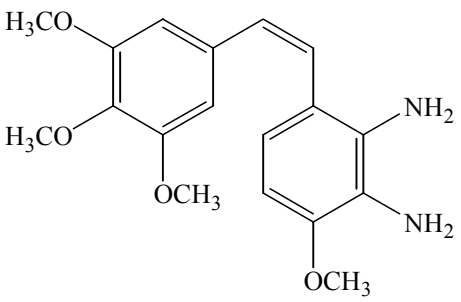

56

$K_b = 3.3 \times 10^4 M^{-1}$

$IC_{50} = 2.9\ \mu M$

Figure 3.18. Structures of Compounds **15** and **56** Analyzed by ITC.

Table 3.3. Thermodynamic Parameters of Binding of Compounds **15** and **56** to Tubulin.

Parameters	Independent Set of Multiple Binding Sites	
Compound	**15**	**56**
N	3.0	1.3
K (M^{-1})	2.3×10^5	3.3×10^4
$\Delta G°$ (kJ mol^{-1})	-30.6	-25.8
$\Delta H°$ (kJ mol^{-1})	-10.0	-41.2
$\Delta S°$ (J $mol^{-1}K^{-1}$)	+69.2	-51.7
$-T\Delta S°$ (kJ mol^{-1})	-20.6	+15.4

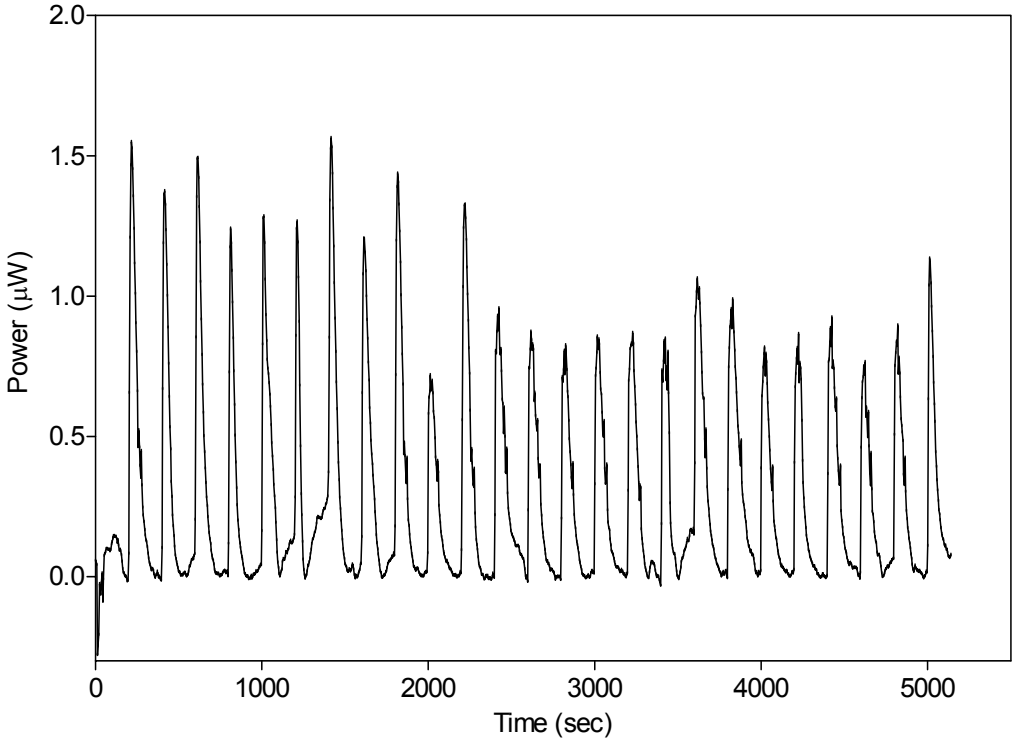

Figure 3.19. ITC Raw Data for Titration of Tubulin with Compound **15**.

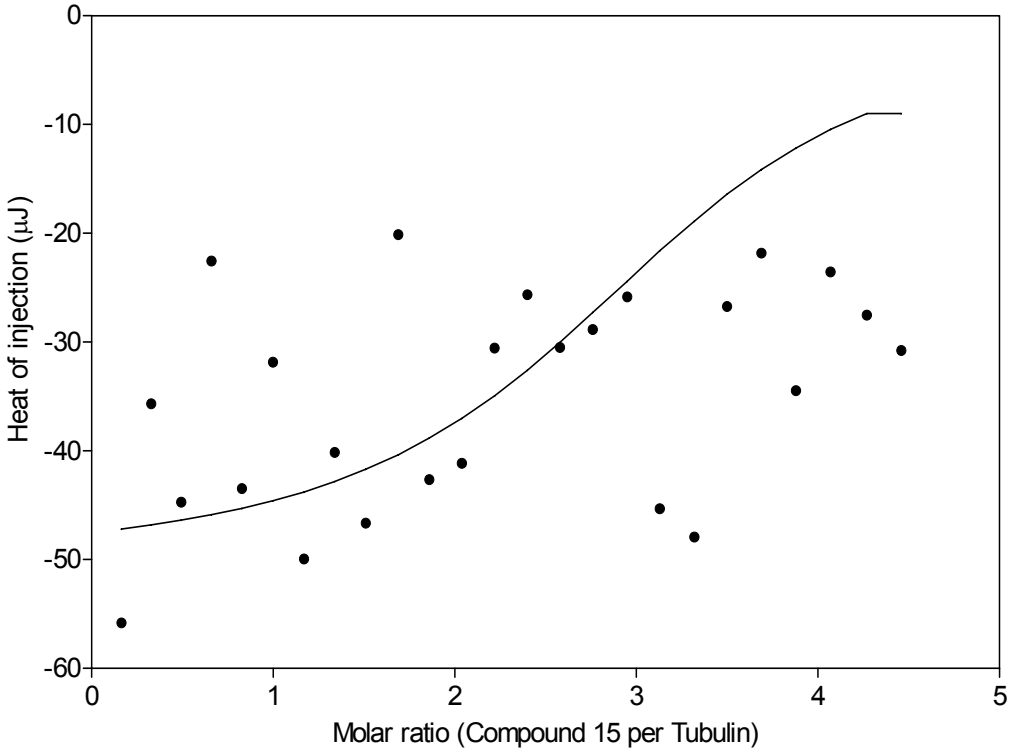

Figure 3.20. Heat Measured at each Injection versus Molar Ratio of Cumulative Compound **15** added per Tubulin.

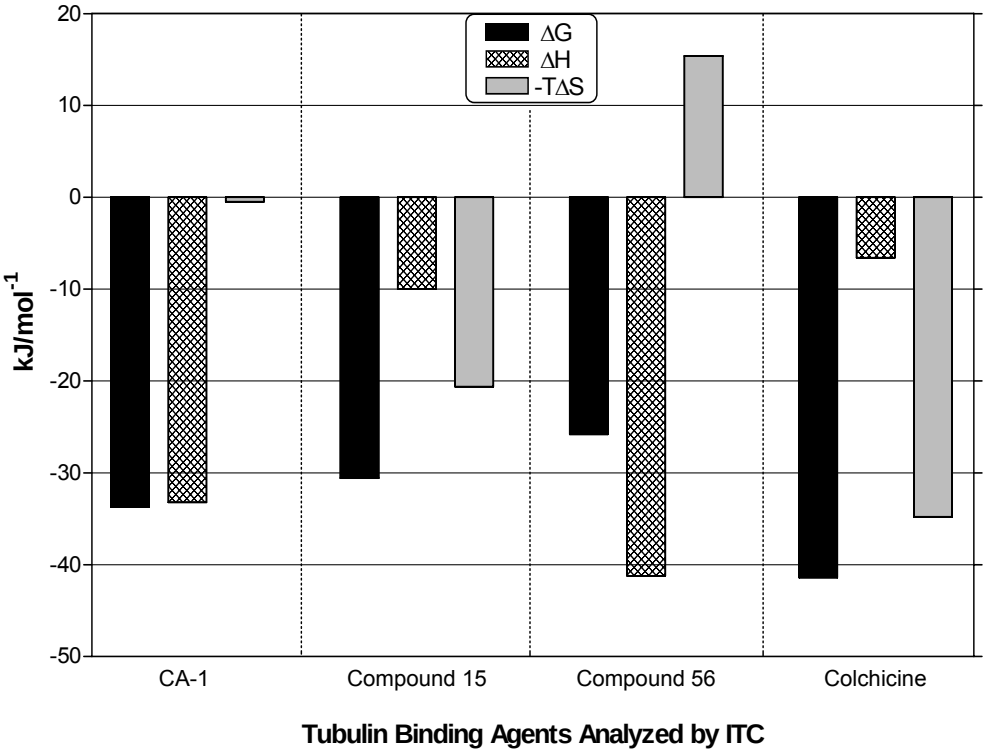

Figure 3.21. Thermodynamic Signatures of Binding of CA-1 Analogs to Tubulin.

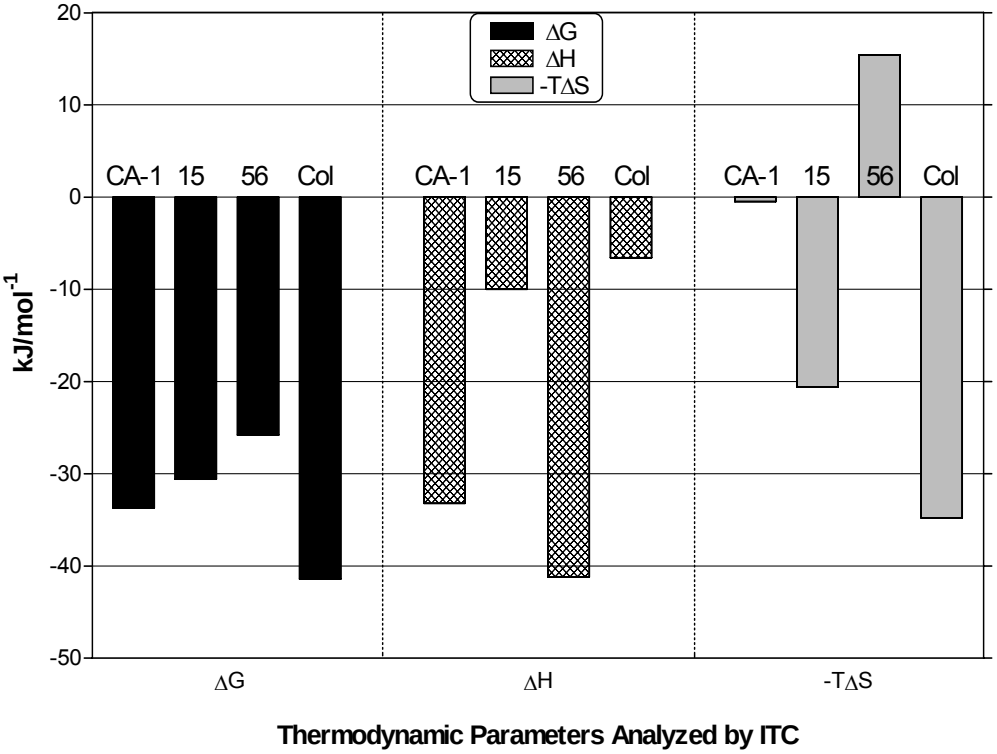

Figure 3.22. Thermodynamic Variations in Binding of CA-1 Analogs to Tubulin.

The number of binding sites involved in this interaction was 3.1. These results did not indicate tight binding of compound **15** to tubulin, but pointed to a possible involvement of solvent mediated effects due to changes in the structure of water induced by favorable hydrogen bonding interactions.

*Binding Energetics of 2,3 Di-Amino-Substituted CA-1 Analog (**56**) to Tubulin*

Ligand binding to the colchicine binding site of tubulin by compound **56** (figure 3.18) was also studied by isothermal titration calorimetry. Titration experiments were performed in order to determine the binding constant (K_b) of the interaction between compound **56** and tubulin, the number of binding sites of compound **56** per mole of tubulin, and the bioenergetics ($\Delta G = \Delta H - T\Delta S$) associated with the reaction. Figure 3.23 shows ITC raw data for titration of tubulin (0.022mM) with 10.0μL injections of compound **56** (0.5mM) in PEM buffer (50mM, pH 7.0), containing GDP (0.1mM). Each peak corresponds to the shift of heat, arising from the change in the concentration of compound **56** before and after each injection.

The exothermic heat measured at each injection from integrated peaks was plotted against molar ratio of cumulative compound **56** added per tubulin in the sample cell (Figure 3.24). The net heat effect observed at each injection was obtained by subtracting the heat of dilution of the ligand in the buffer. ITC thermodynamic analysis revealed decreased affinity of compound **56** to tubulin since it binds to tubulin with a low binding constant, $K_{b,}$ of 3.3 x 10^4 M^{-1}. This corresponds to a Gibbs free energy of binding ($\Delta G = \Delta H - T\Delta S$) of -25.8 kJ mol^{-1} (Table 3.3). In addition, the binding of this 2,3-diamino- CA-1 analog to tubulin was highly favored by enthalpy (-41.2 kJ mol^{-1}) which may have risen from the formation of the ligand – tubulin complex.

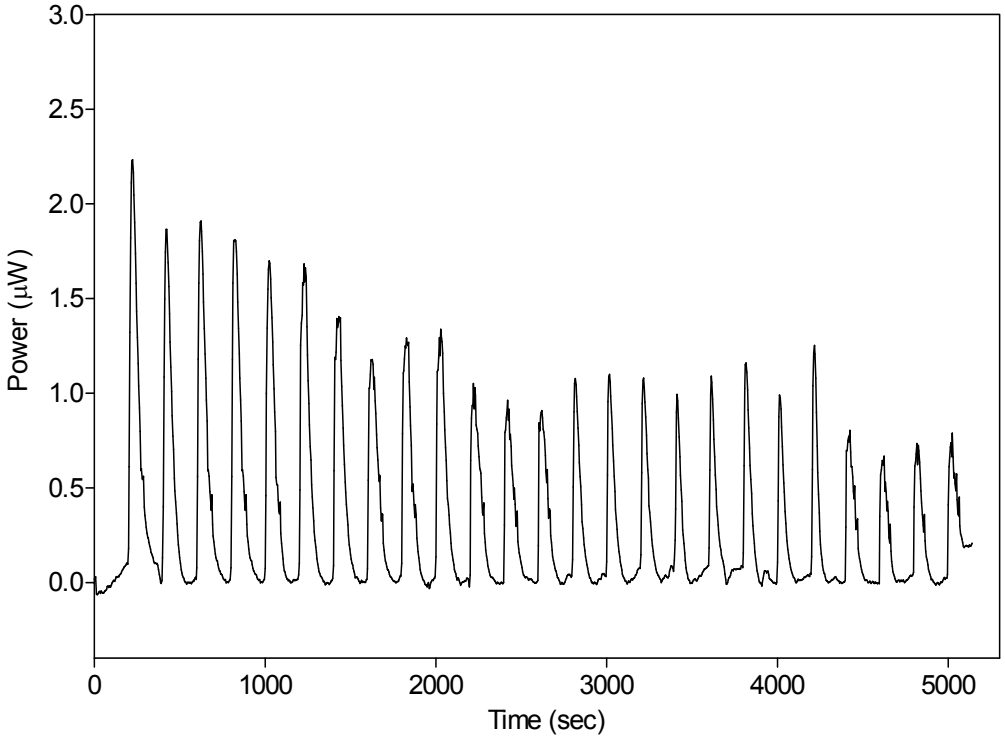

Figure 3.23. ITC Raw Data for Titration of Tubulin with Compound **56**.

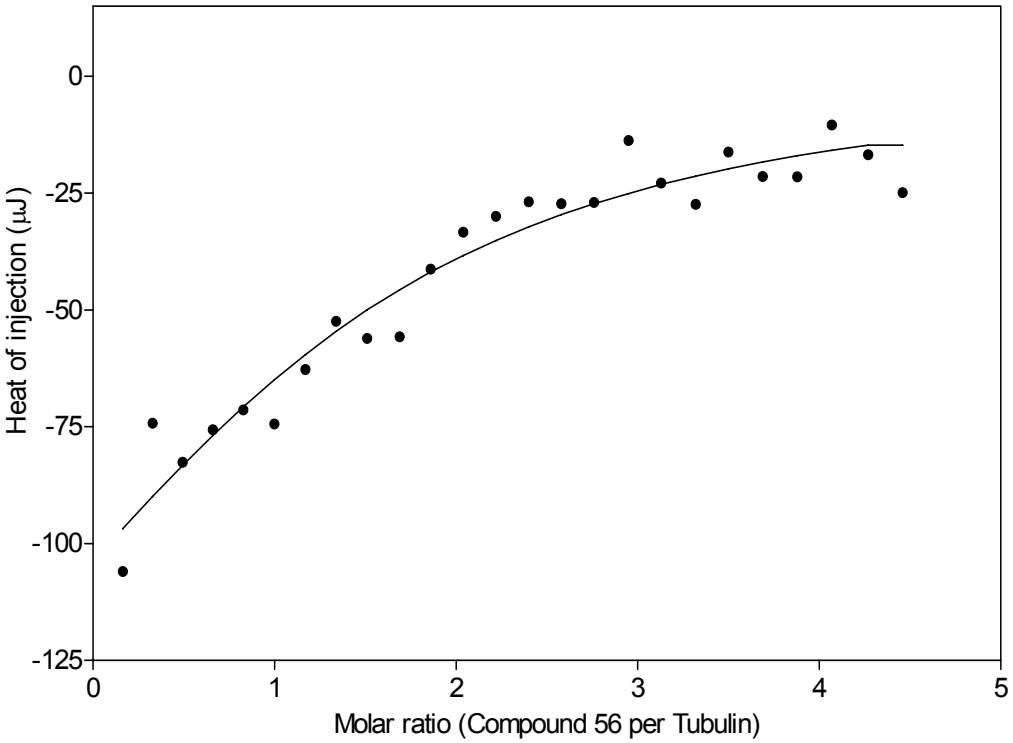

Figure 3.24. Heat Measured at each Injection versus Molar Ratio of Cumulative Compound **56** added per Tubulin.

However like its mono-aminosubstituted analog (compound **39**), the binding process of compound **56** to tubulin is not entropically driven. The calculated entropy of the interaction was -51.7 $Jmol^{-1}K^{-1}$ which was more than 2-fold the entropy observed in the interaction of compound **39** with tubulin. This unfavorable ΔS observed further confirmed the possibility of more conformational changes in the structures of both the ligand and the tubulin. The stoichiometry of this interaction was 1.3. The decrease in antitubulin polymerization potency (IC_{50} value of 2.9 μM) is directly related to the loss in binding affinity of compound **56** to tubulin. Not only did di-amino substitution of the CA-1 phenolic ring lead to reduced binding affinity of the analog to tubulin, it also led to unfavorable entropy which was reflected in the reduce potency of the ligand exhibited during inhibition of tubulin polymerization studies.

Binding Thermodynamics of Combretastatin A-4 to Tubulin

CA-4 (compound **2**, figure 3.25) inhibits polymerization of tubulin with an IC_{50} value of 1.2 μM. This is almost a 2.0-fold increase in anti-tubulin potency compared to compound **3** which has an IC_{50} value of 1.9 μM. Ligand binding to the colchicine binding site of tubulin by CA-4 was also studied by isothermal titration calorimetry. Titration experiments were performed in order to determine the binding constant (K_b) of the interaction between CA-4 and tubulin, the number of binding sites of CA-4 per mole of tubulin, and the bioenergetics ($\Delta G = \Delta H - T\Delta S$) associated with the reaction. Figure 3.26 shows ITC raw data for titration of tubulin (0.022mM) with 10.0μL injections of compound **2** (0.5mM) in PEM buffer (50mM, pH 7.0), containing GDP (0.1mM). Each

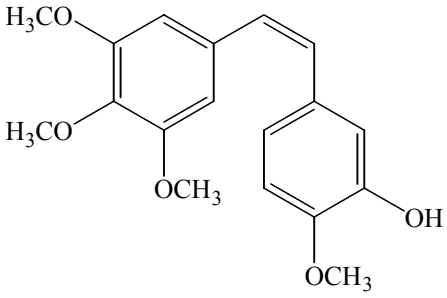

2

$K_b = 2.3 \times 10^4\ M^{-1}$

$IC_{50} = 1.2\ \mu M$

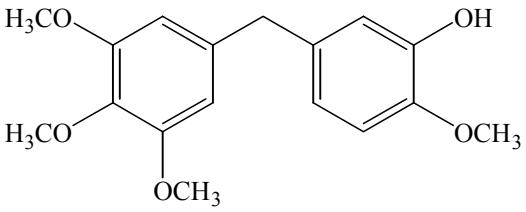

70

$K_b = 1.4 \times 10^4\ M^{-1}$

$IC_{50} = 3.3\ \mu M$

Figure 3.25. Structures of Compounds **2** and **70** Analyzed by ITC.

Table 3.4. Thermodynamic Data for Binding of Compounds **2 (CA-4)** and **70** to Tubulin.

Parameters	Independent Set of Multiple Binding Sites	
Compound	**(2)**	**(70)**
N	0.9	1.0
K (M^{-1})	2.3×10^4	1.4×10^4
$\Delta G°$ (kJ mol^{-1})	-24.8	-23.6
$\Delta H°$ (kJ mol^{-1})	-52.0	-44.7
$\Delta S°$ (J $mol^{-1}K^{-1}$)	-91.25	-70.7
$-T\Delta S°$ (kJ mol^{-1})	+27.2	+21.1

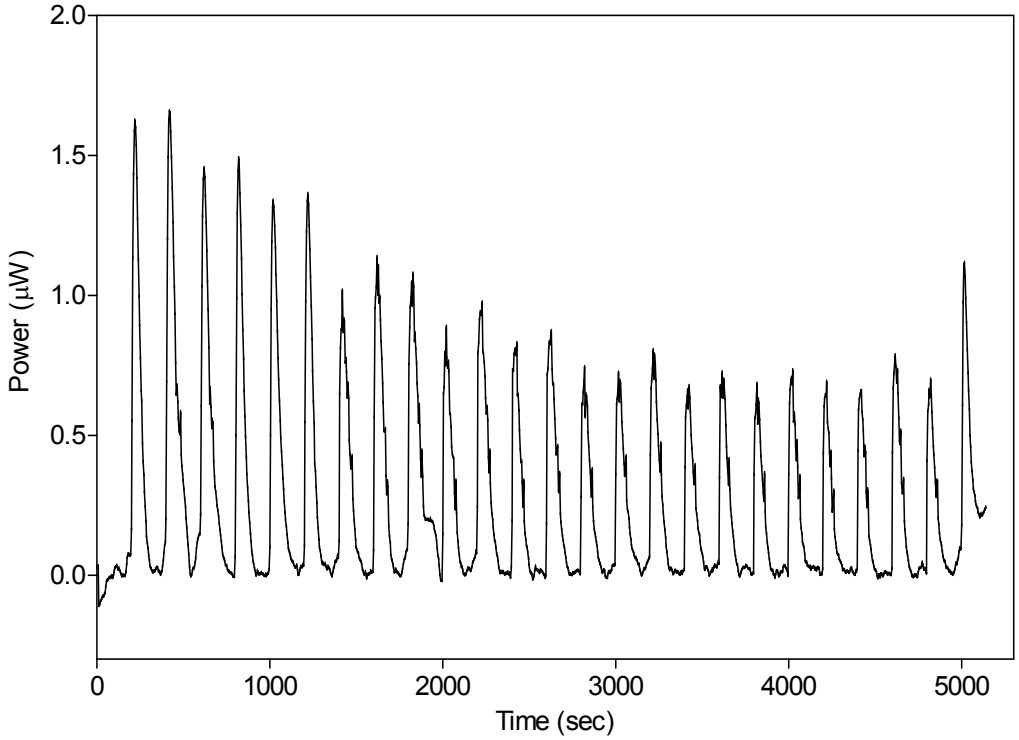

Figure 3.26. ITC Raw Data for Titration of Tubulin with CA-4 **(2).**

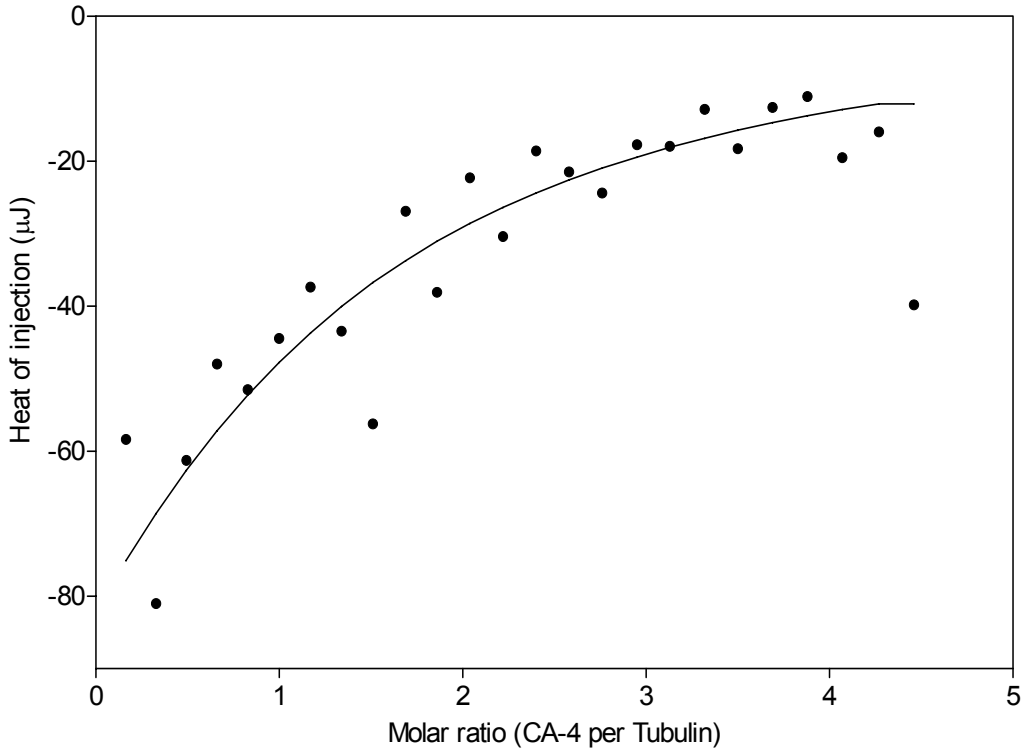

Figure 3.27. Heat Measured at each Injection versus Molar Ratio of Cumulative Compound **2** added per Tubulin.

peak corresponds to the shift of heat, arising from the change in molar ratio of CA-4 per tubulin before and after each injection into the ITC sample cell.

The exothermic heat measured at each injection was plotted against molar ratio of cumulative ligand added per tubulin in the sample cell (Figure 3.27). The net heat effect observed at each injection was obtained by subtracting the heat of dilution of the ligand in the buffer. ITC thermodynamic analysis showed decreased affinity of CA-4 to tubulin with a low binding constant, $K_{b,}$ of 2.3 x 10^4 M^{-1} and 0.9 binding sites. This corresponds to a Gibbs free energy of binding ($\Delta G = \Delta H - T\Delta S$) of -24.8 kJ mol^{-1} (Table 3.4). In addition, CA-4 binding to tubulin was enthalpically driven (-52.0 kJ mol^{-1}) due to strong hydrogen bond formation between the CA-4 hydroxyl group and the polar amino acid residues in the colchicine binding site.

*Binding Thermodynamics of Unbridged Stilbene Analog (**70**) to Tubulin*

Compound **70** (figure 3.25) was found to inhibit polymerization of tubulin with an IC_{50} value of 3.3 μM. This compound bears structural resemblance with CA-4 only that the ethene bridge separating the trimethoxyphenyl ring and the phenolic ring has been replaced by a methylene bridge. This leads to a 2.7-fold decrease in antitubulin potency compared to CA-4 which has an IC_{50} value of 1.2 μM.

Figure 3.28 shows the raw data from 25 successive ITC calorimetric titrations of tubulin with Compound **70** in power (μW) versus time (sec). The area under each peak is directly proportional to the heat produced after injection. The titration experiment involved addition of 10.0μl aliquots of compound **70** (0.5mM) per injection at 200 seconds intervals to tubulin (0.022mM) in PEM (50mM, pH 7.0) buffer with GDP (0.1mM) at 298 °K. The binding isotherm produced by plotting integrated peaks against

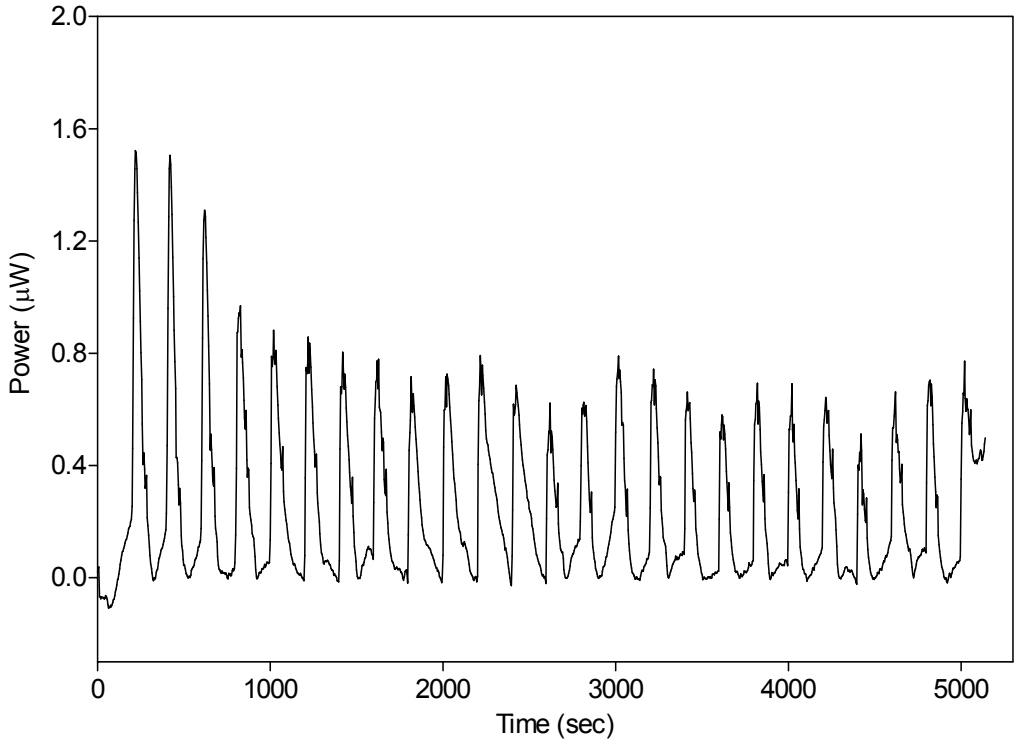

Figure 3.28. ITC Raw Data for Titration of Tubulin with Compound **70**.

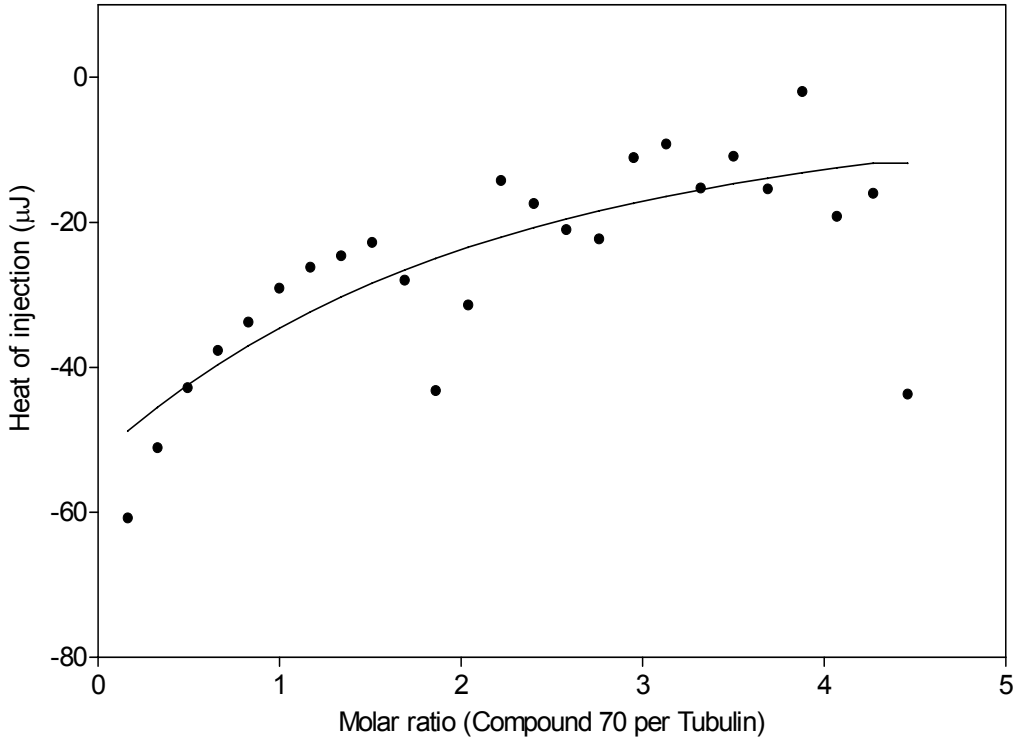

Figure 3.29. Heat Measured at each Injection versus Molar Ratio of Cumulative Compound **70** added per Tubulin.

the molar ratio of Compound **70** added to tubulin in the cell is shown in figure 3.29. Data was analyzed with BindWorks software according to a single–site model.

Like CA-4, ITC thermodynamic analysis of compound **70** showed reduced affinity to tubulin, binding tubulin with a binding affinity constant, $K_{b,}$ of 1.4 x 10^4 M^{-1} and 1.0 binding site. This corresponds to a Gibbs free energy of binding ($\Delta G = \Delta H - T\Delta S$) of -23.6 kJ mol^{-1} (Table 3.4). The binding of this stilbene to tubulin was highly favored by enthalpy (ΔH = -44.7 kJ mol^{-1}) and not favored by entropy (ΔS = -70.7 J $mol^{-1}K^{-1}$). This high enthalpy is characteristic of hydrogen bond formation and a conformational change in either the structure of compound **70** or tubulin heterodimer or both. The difference in antitubulin activity between CA-4 and compound **70** can be thermodynamically accounted for by the enthalpy difference (ΔH = -7.4 kJ mol^{-1}) observed when the two ligands bind tubulin which probably accounts for the enthalpic contribution of the ethene bridge.

*Binding Thermodynamics of a Dichloro-Substituted CA-4 Analog (**27**) to Tubulin*

Compound **27** (figure 3.30), a newly synthesized compound in which two methoxy groups in the A-ring of CA-4 were replaced by two chloride groups was also analyzed by ITC. This compound proved to be a good inhibitor of tubulin with an IC_{50} value of 1.7 μM as compared to CA-4 which has an IC_{50} value of 1.2 μM. Figure 3.31 shows ITC raw data for titration of tubulin (0.022mM) with 10.0μL injections of compound **27** (0.5mM) in PEM buffer (50mM, pH 7.0), containing GDP (0.1mM).

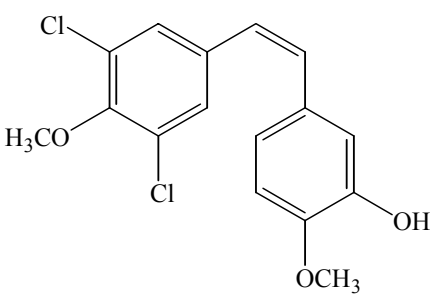

27

$K_b = 9.8 \times 10^5\ M^{-1}$

$IC_{50} = 1.7\ \mu M$

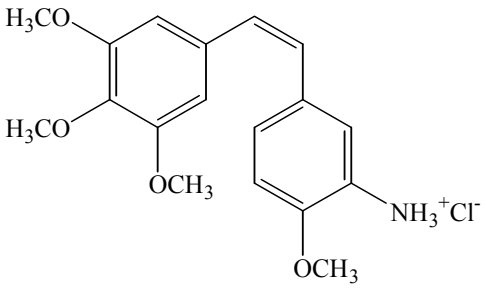

45

$K_b = 2.9 \times 10^5\ M^{-1}$

$IC_{50} = 1.3\ \mu M$

Figure 3.30. Structures of Compounds **27** and **45** Analyzed by ITC.

Table 3.5. Thermodynamics Data for Binding of Compounds **27** and **45** to Tubulin.

Parameters	Independent Set of Multiple Binding Sites	
Compound	**27**	**45**
N	2.1	0.6
K (M^{-1})	9.8×10^5	2.9×10^5
$\Delta G°$ (kJ mol^{-1})	-34.2	-31.1
$\Delta H°$ (kJ mol^{-1})	-2.6	-29.5
$\Delta S°$ (J $mol^{-1}K^{-1}$)	+106.2	+5.4
$-T\Delta S°$ (kJ mol^{-1})	-31.7	-1.6

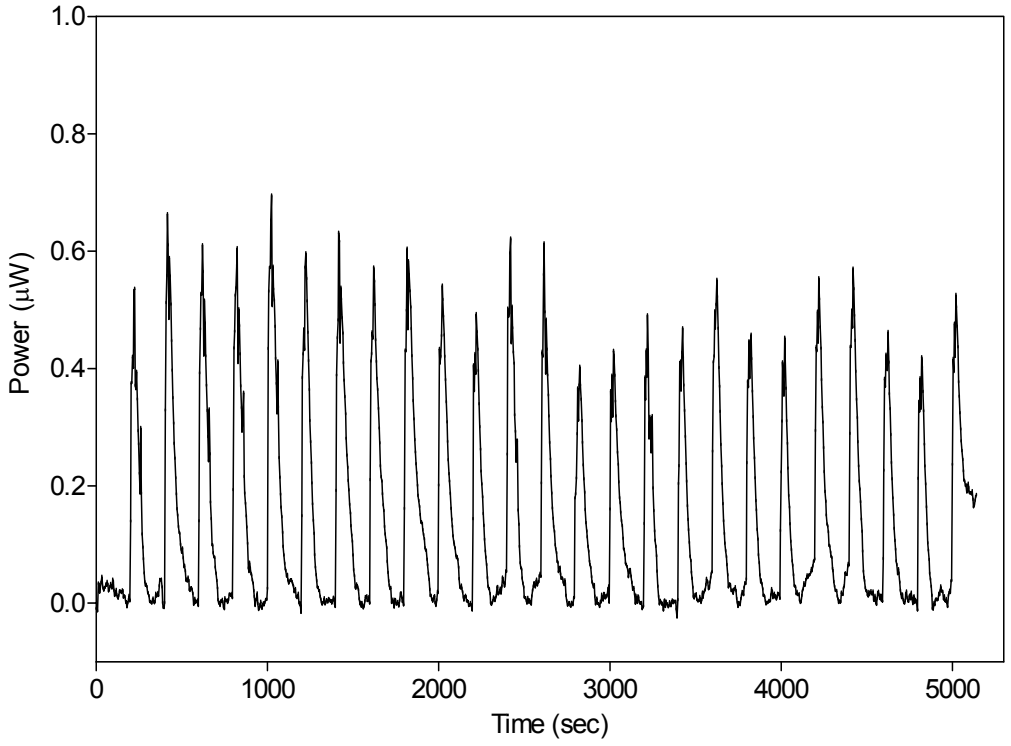

Figure 3.31. ITC Raw Data for Titration of Tubulin with Compound **27**.

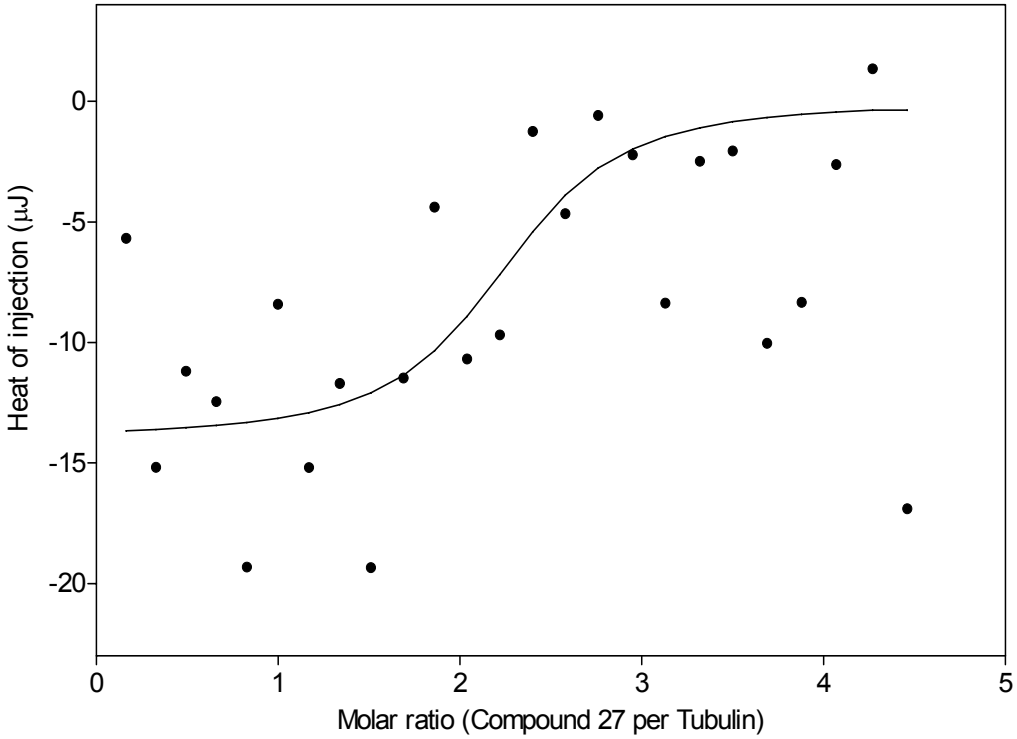

Figure 3.32. Heat Measured at each Injection versus Molar Ratio of Cumulative Compound **27** added per Tubulin.

The heat obtained by integrating the peaks was plotted against molar ratio of compound **27** per tubulin in the sample cell. The exothermic interaction of this compound with tubulin upon binding yielded a binding isotherm although more heat was still being produced upon ligand saturation (Figure 3.32).

ITC thermodynamic analysis showed that compound **27** binds to tubulin with a binding constant, $K_{b,}$ of 9.8 x 10^5 M^{-1}, which corresponds to a Gibbs free energy of binding ($\Delta G = \Delta H - T\Delta S$) of -34.2 kJ mol^{-1} (Table 3.5). This interaction was both entropically driven (ΔS = +106.2 J $mol^{-1}K^{-1}$) and highly favored by enthalpy (-34.2 kJ mol^{-1}). This kind of binding is usually characterized by favorable hydrogen bonding and hydrophobic interactions. The process of the binding of compound **27** is entropically driven. The calculated entropy of the interaction was +106.2 $Jmol^{-1}K^{-1}$. This favorable TΔS observed pointed to a thermodynamic profile of tight binding by the ligand on the tubulin binding site. The number of binding sites observed in this interaction was 2.1.

*Binding Energetics of a 3-Aminohydrochloride Substituted CA-4 Analog (**45**) to Tubulin*

ITC was also used to study the binding thermodynamics of compound **45** (Figure 3.30). Figure 3.35 represents the raw calorimetric data for successive titrations of tubulin with compound **45** as power (μW) versus time (seconds). The area under each peak was directly proportional to the heat produced by the interaction. The titration procedure involved addition of 10.0μl aliquots of compound **45** (0.5mM) per injection at 200 seconds intervals to tubulin (0.022mM) in PEM (50mM, pH 7.0) buffer with GDP (0.1mM) at 298°K.

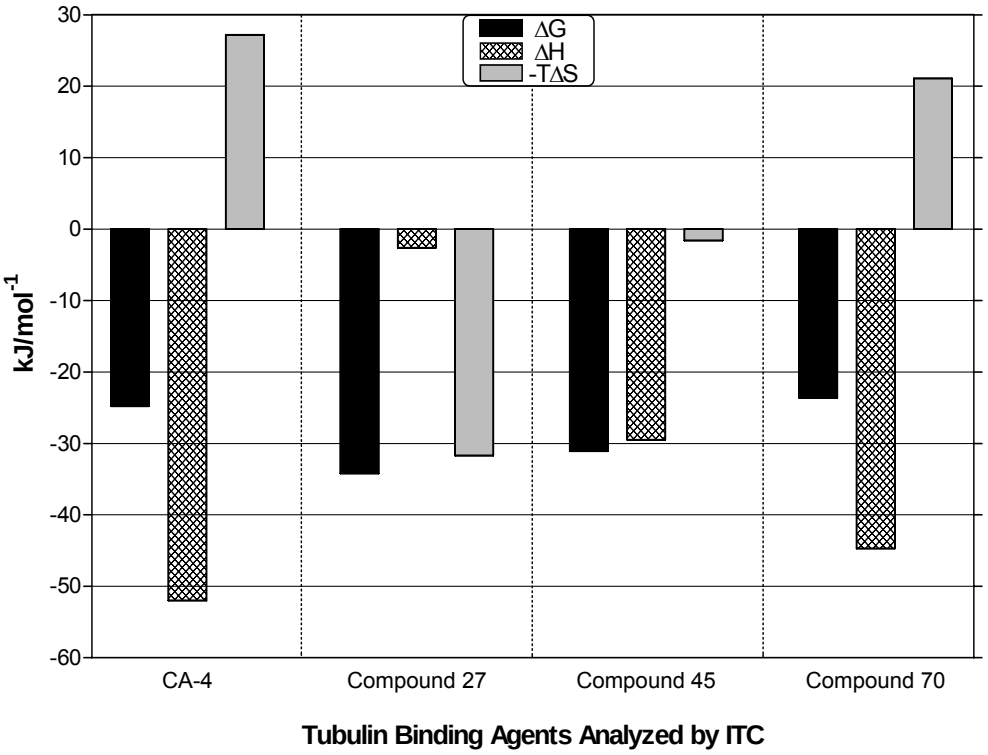

Figure 3.33. Thermodynamic Signatures of Binding of CA-4 Analogs to Tubulin.

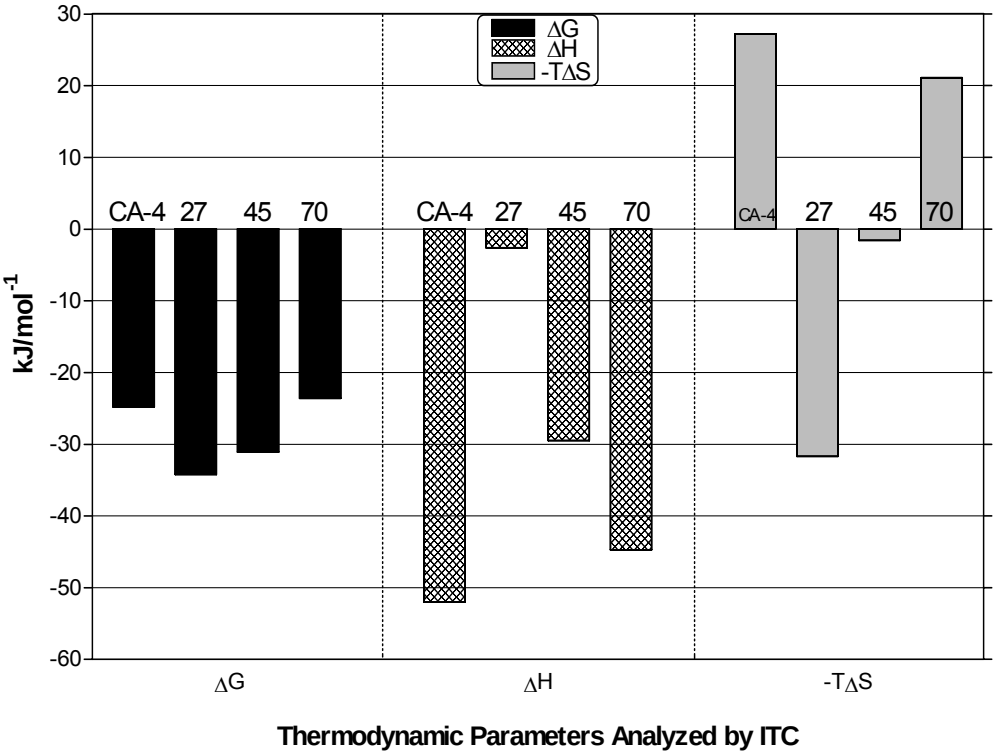

Figure 3.34. Thermodynamic Variations in Binding of CA-4 Analogs to Tubulin.

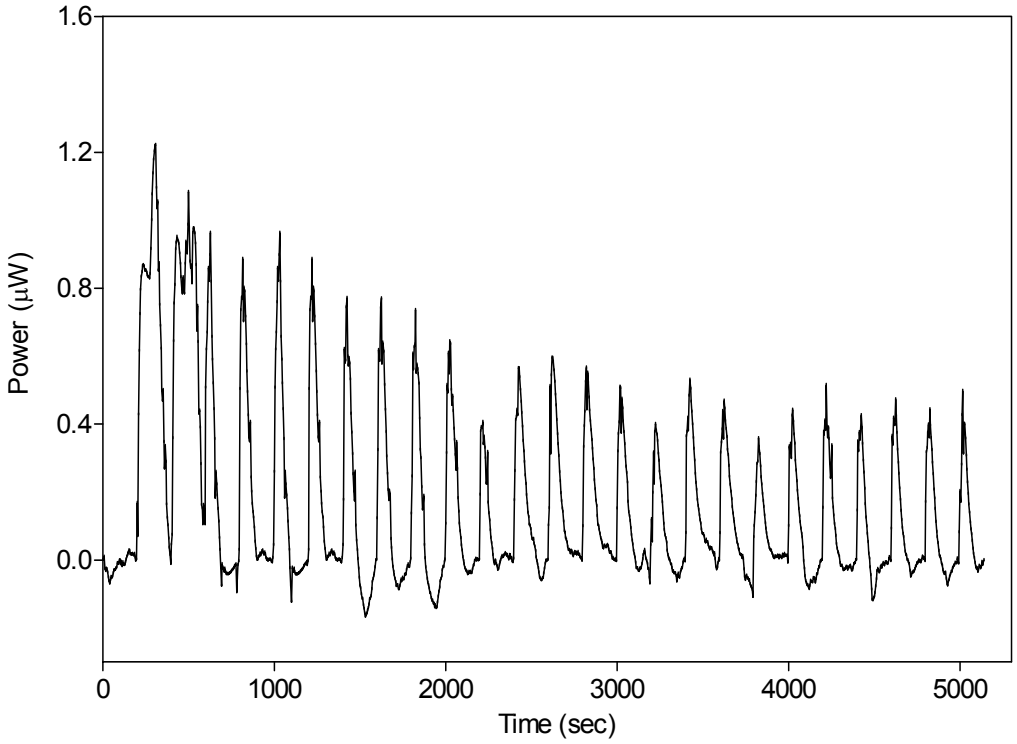

Figure 3.35. ITC Raw Data for Titration of Tubulin with Compound **45**.

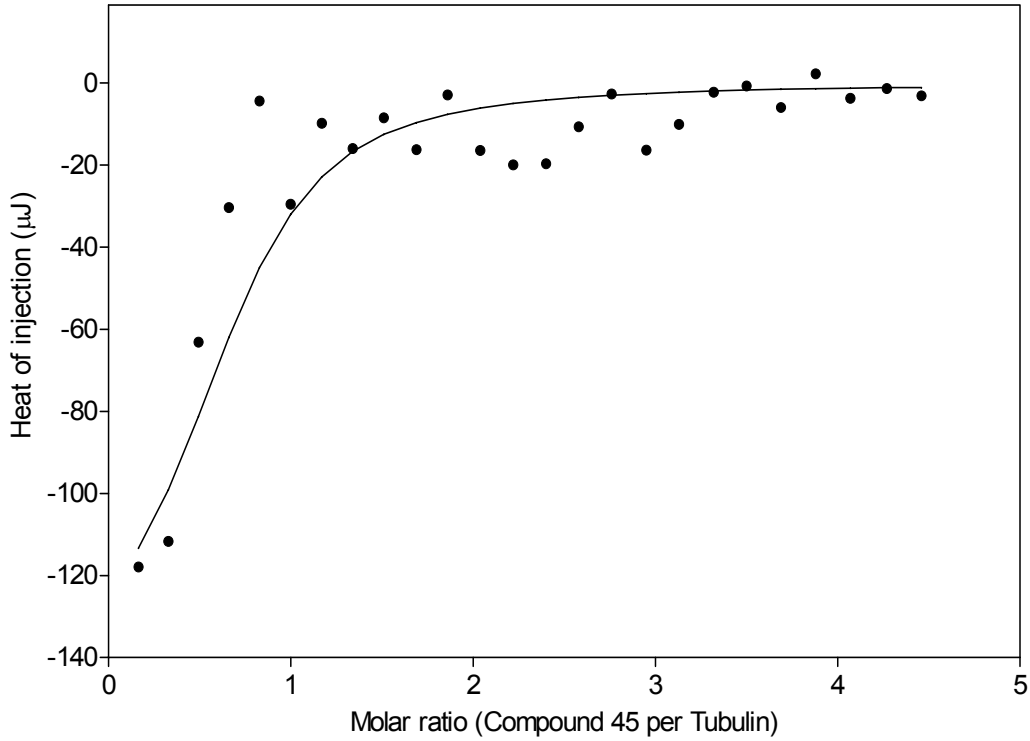

Figure 3.36. Heat Measured at each Injection versus Molar Ratio of Cumulative Compound **45** added per Tubulin.

Results from the experiment showed that the binding of compound **45** to tubulin was stoichiometric at constant temperature. High exothermic heat was produced at the beginning of the interaction of compound **45** with tubulin and then gradually showed a monatomic decrease in reaction heat produced upon additional ligand injection until saturation was reached. Figure 3.36 illustrates the binding isotherm produced by plotting heat obtained by integrating the peaks against the molar ratio of ligand to tubulin in the ITC cell. Data analysis was performed using BindWorks software supplied by CSC with the ITC equipment.

Clearly, the binding of compound **45** with tubulin is ethalpically driven and occurs through favorable hydrogen bonding and hydrophobic interactions. The large negative ΔH value reflects polar interaction through hydrogen bonding and Van der Waals contacts whereas the small positive ΔS reflected minimal hydrophobic contacts. Using the independent set of multiple binding sites, compound **45** was found to bind tubulin with a binding affinity ($6.7 \times 10^5\ M^{-1}$) and a favorable Gibbs energy of binding ($-31.1\ kJ\ mol^{-1}$) at 298°K. The thermodynamic parameters associated with the binding of compound **45** to tubulin are shown in Table 3.5. The binding of compound **45** to tubulin was also associated with high enthalpy change ($-29.5\ kJ\ mol^{-1}$) and a low positive entropy change ($-5.4\ Jmol^{-1}K^{-1}$). Compound **45** is a highly potent inhibitor of tubulin polymerization with an IC_{50} value of 1.3 μM. The binding of CA-4 to tubulin is characterized by good hydrogen bonding and a conformation change where as the binding of compound **45** favors hydrogen bonding and hydrophobic interactions. The molar binding ratio for the binding of compound **45** to tubulin was 0.6. When IC_{50} values

were plotted against the negative logarithm of binding constants, a clear hyperbolic relationship was observed (Figure 3.37).

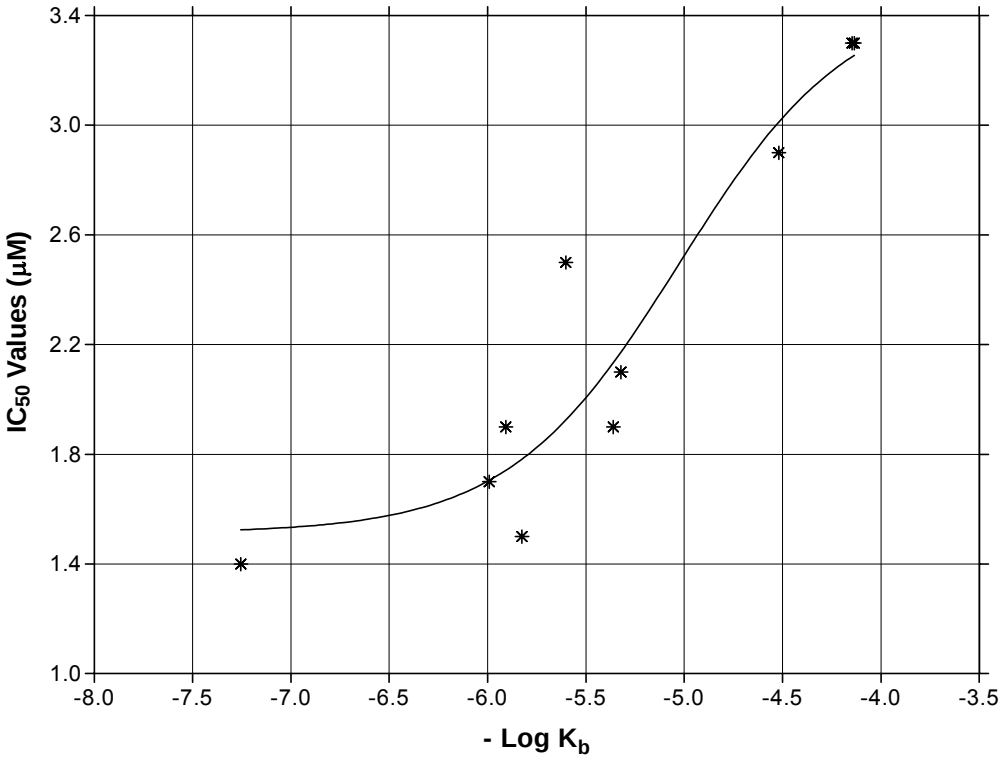

Figure 3.37. Relationship Between Binding Affinities and IC_{50} Values.

Binding Energetics of Colchicine to Tubulin

The thermodynamics of the binding of colchicine (compound **1**, figure 3.38) to tubulin were measured by isothermal titration calorimetry. Colchicine binds tightly to tubulin and therefore most conventional methods can not be used to determine its binding affinity. However Ramirez *et al*., 1996, using the data of Diaz and Andreu (1991), were able to calculate the binding affinity of colchicine to tubulin as $K_b = 1.6 \times 10^7\ M^{-1}$ at 37 ºC with a free energy of -37.7 $kJmol^{-1}$.

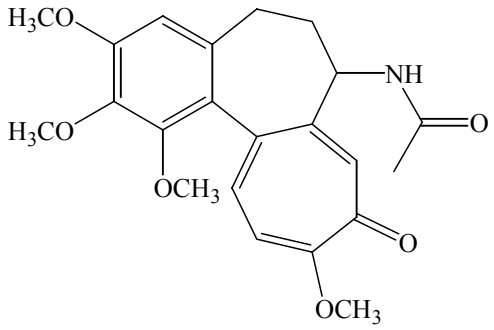

1

$K_b = 1.8 \times 10^7 M^{-1}$

$IC_{50} = 1.4$

Figure 3.38. Structure of Colchicine (**1**) Analyzed by ITC.

Table 3.6. Thermodynamics Data for Binding of Colchicine **(1)** to Tubulin.

Parameters	Independent Set of Multiple Binding Sites
Compound	**(1)**
N	2.3
K (M^{-1})	1.8×10^7
$\Delta G°$ (kJ mol^{-1})	-41.4
$\Delta H°$ (kJ mol^{-1})	-6.6
$\Delta S°$ (J $mol^{-1}K^{-1}$)	+116.7
$-T\Delta S°$ (kJ mol^{-1})	-34.8

Figure 3.39 shows ITC raw data for titration of tubulin (0.022mM) with 10.0 μL injections of colchicine (0.5mM) in PEM buffer (50mM, pH 7.0), containing GDP (0.1mM). The heat change obtained by integrating the peaks was plotted against molar ratio of cumulative colchicine added per tubulin in the sample cell (Figure 3.40). ITC thermodynamic analysis indicated that colchicine binds to tubulin with a binding constant, $K_{b,}$ of 1.8 x 10^7 M^{-1}, which corresponds to a Gibbs free energy of binding ($\Delta G = \Delta H - T\Delta S$) of -41.4 kJ mol^{-1} (Table 3.6). In addition the binding of colchicine to tubulin was found to be moderately favored by enthalpy (-6.6 kJ mol^{-1}) and highly favored by entropy (+116.7 $Jmol^{-1}K^{-1}$). Menendez *et al*., (1989) have reported the binding of colchicine to tubulin as favored by enthalpic (-21.0 $kJmol^{-1}$) and entropic (+71.4 $Jmol^{-1}K^{-1}$) contributions to the interaction. These very large entropy changes are known to arise from a combined increase in solvent entropy and a minimal loss of conformational entropy (Nezami *et al.*, 2002), since colchicine is hydrophobic and rigid and lacks the ability to adapt to changes in tubulin structure.

Colchicine binds to a single high affinity site of tubulin (Menendez *et al*., 1989). However ITC analysis showed that colchicine binds to tubulin with a stoichiometry of 2.3. This observation in the stoichoimetry and high-affinity binding of colchicine to tubulin has been accounted for by Andreu and Timasheff (1982) using a simple thermodynamic model of the non-cooperative binding of a bifunctional ligand to two independent subsites on the tubulin binding site. The model stipulates that the tropolone methyl ether ring of colchicine binds to one subsite by means of ring stacking and to some extent by hydrogen bonding whereas the trimethoxyphenyl ring binds hydrophobically with the other subsite (Perez-Ramirez *et al*., 1994).

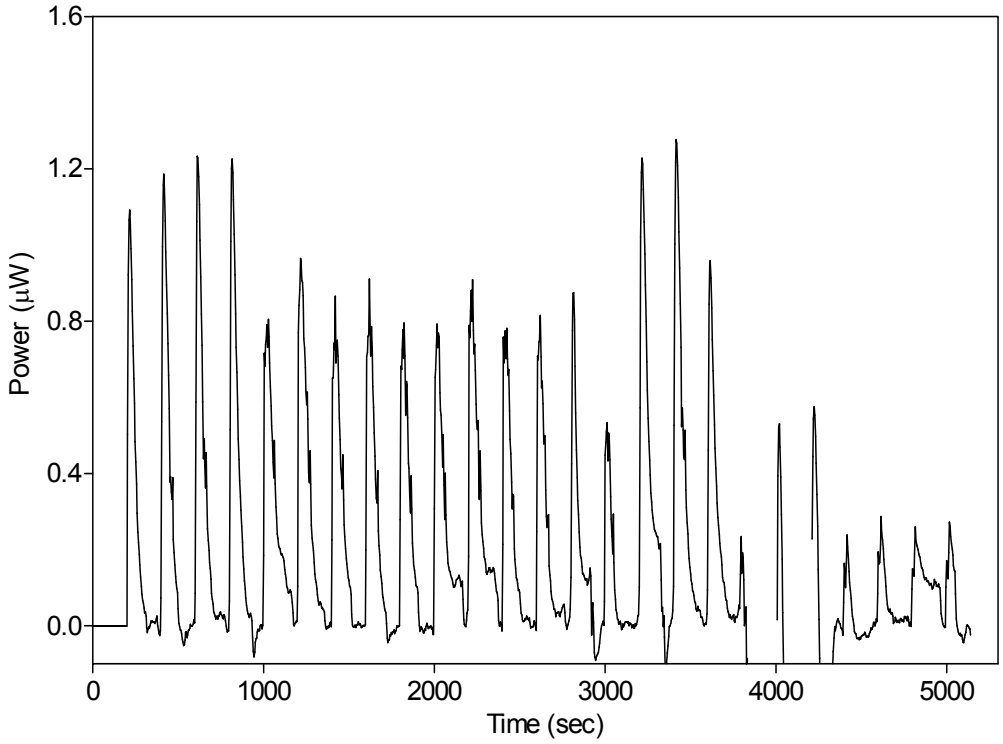

Figure 3.39. ITC Raw Data for Titration of Tubulin with Compound **1**.

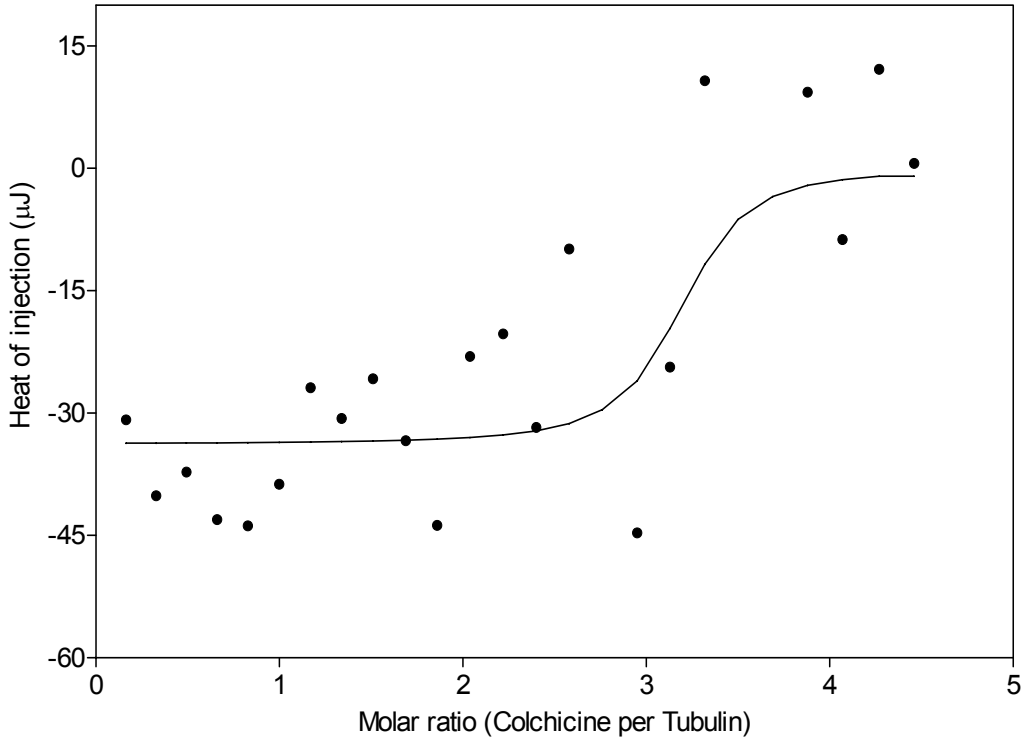

Figure 3.40. Heat Measured at each Injection versus Molar Ratio of Cumulative Colchicine added per Tubulin.

Conclusions

ITC is the only technique that can resolve the enthalpic and entropic components of binding affinity. Because the enthalpic and entropic components are related to structural parameters, they can be used as a guide in molecular design, as a way to validate structure-based computational predictions of binding energetics and in developing rigorous structure/energy correlations. With improved reliability, sensitivity and accuracy of ITC instrumentation, the method is gaining a more prominent role in molecular design in general and drug design in particular.

Figures 3.11 and 3.12 show the thermodynamic signatures of binding of CA-1 and compounds **12, 30** and **39**. The binding of compounds **CA-1, 12, 30** and **39** to tubulin are all driven by enthalpy with less entropic contribution to the interactions. The thermodynamic signatures observed for each of these compounds are reminiscent of favorable hydrogen bonding and hydrophobic interactions apart from compound **30** with a 2-nitrosubstitution in ring B that seemed to suggest minimal conformational change upon interaction. CA-1 and compounds **12, 30** and **39** possess at least one polar hydroxyl group in ring B and compound **39** has a polar amino group in position 2 of ring B. Hydrogen bonding is a result of optimal placement of hydrogen bond donor and acceptor groups on the drug and target, and is highly directional and specific. The hydrogen bonding derived from the thermodynamic signatures could be attributed to interactions between the oxygen atoms of these compounds with the polar side chains of amino acids Ser178, Lys350, Asn347, Thr351 and Thr179 that could be lying with in 3.5 Å distances from these molecules. Also the observed favorable hydrophobic interactions between these compounds and tubulin could be attributed to interactions between the methoxy groups of these compounds with the non-polar side chains of amino acids Cys 239, Val

349, Ala 248, Leu 253 and Val 313 that could be lying with in 3.5 Å distance of these molecules (Ravelli *et al*., 2004; figure 3.2). The binding of CA-1 is almost entirely driven by favorable enthalpy and to a less extent, entropy. Hydrogen bond formation and favorable van der Waals interactions between drug and target results in favorable enthalpy.

Figure 3.21 and 3.22 shows the thermodynamic signatures of tubulin binding with CA-1 and compounds **15**, **56** and colchicine. Like CA-1, the binding of compound **56** was enthalpy driven and this could be due to the presence of the highly polar amino groups in ring B. Thus favorable bonding occurs between these amino groups and the polar side chains of amino acid spurring the combretastatin binding pocket on tubulin. However, the entropic contribution to the interaction of this molecule with tubulin is minimal and as its thermodynamic signature suggests, the good hydrogen bonding that occurs upon interaction is also accompanied by a conformational change. This seems to suggest that hydrogen bond donors and receptors may be in close proximity in a crystal structure but may have little effect on binding affinity, due to conformational effects. The binding of compound **15** and colchicine were driven by entropy with less enthalpic contributions. Thus in case of these two compounds, hydrophobic effects could probably be much higher than the forces due to hydrogen bonding during their interactions with tubulin. As seen from figure 3.37, there was a direct correlation between the antitubulin activity and the binding affinity of a given particular inhibitor. Incorporation of additional non-polar groups is usually done to increase hydrophobic interactions between target and compound. However, hydrophobic interactions are non-specific compared to hydrogen bonding. Compounds with favorable enthalpy and entropy tend to have the

highest affinity, due to specific hydrogen bond formation and van der Waals interactions as well as hydrophobic interactions with the intended target.

Figures 3.33 and 3.34 show the thermodynamic signatures of binding of tubulin with CA-4, and its analogs; compounds **27**, **45** and **70**. Cleary the interactions of CA-4 and compounds **45** and **70** with tubulin are enthalpy driven whereas the binding of compound **27** is entropy driven. The interactions between CA-4 and compound **70** with tubulin are characterized by hydrogen bonding and conformational changes. A conformational change is inevitable if their B-rings have to fit in the colchicine binding pocket. The binding of compound **27** which bears a 3,5-dichlorosubstitution in ring A with tubulin is entropy driven with very minimal enthalpy contribution. Still, the polar to polar interactions of the functional groups of these compounds with the side chains of polar amino acids in the binding pocket could be responsible for the observed hydrogen bonding interactions. Information on the functional structure – activity studies of combretastatin A-4 and A-1 and their derivatives as inhibitors of microtubule assembly together with thermodynamic parameters of the interaction of these combretastatin analogs with tubulin using ITC will further the unending search for more potential and effective Vascular Targeting Agents (VTA) and drugs for pharmaceutical, diagnostic and research sectors.

APPENDICES

TABLE OF CONTENTS

Appendix A

Chapter Two: Inhibition of Tubulin Polymerization Graphs.

Appendix B

Chapter Three: ITC Blank Titrations

APPENDIX A

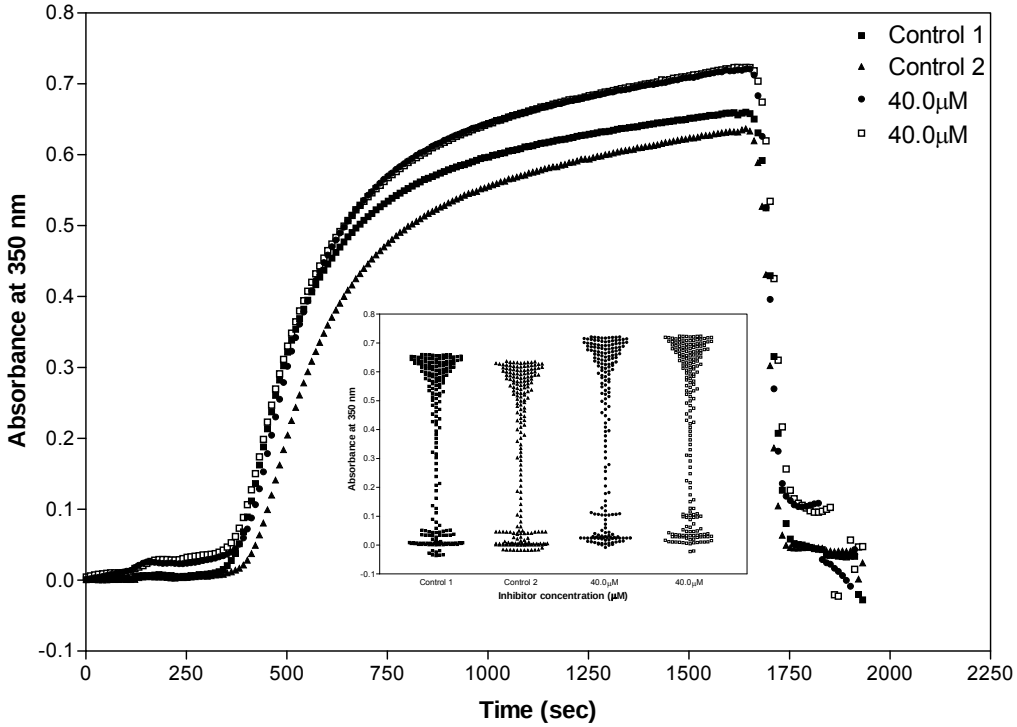

Figure A.2.1. Inhibition of Tubulin Polymerization by Compound **(4)** at 30ºC.

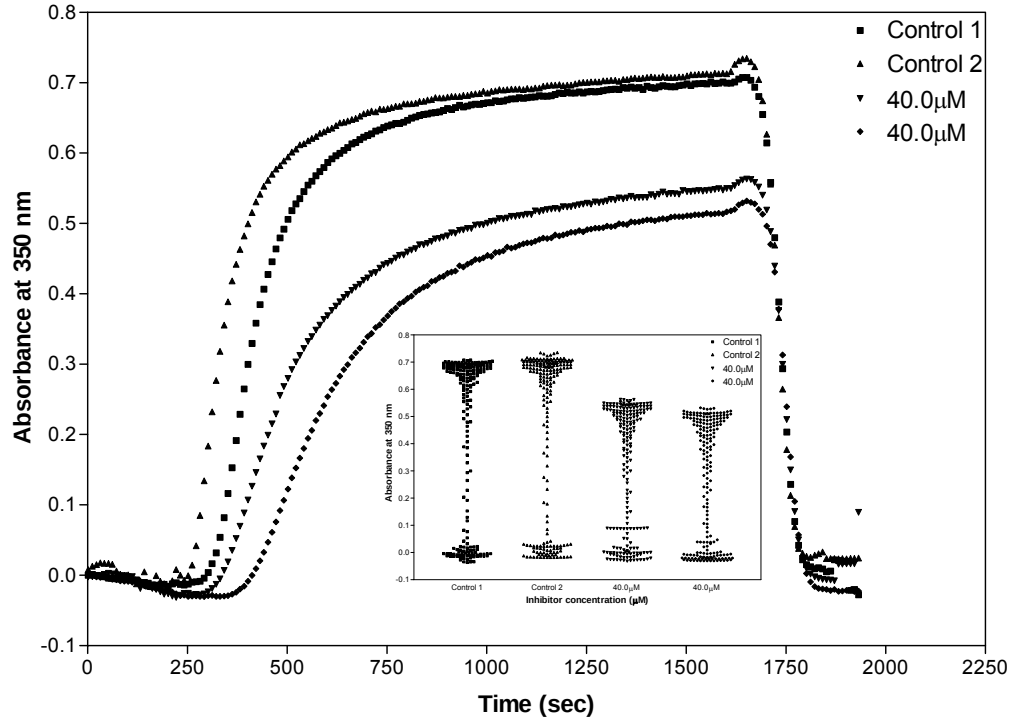

Figure A.2.2. Inhibition of Tubulin Polymerization by Compound **5** at 30ºC.

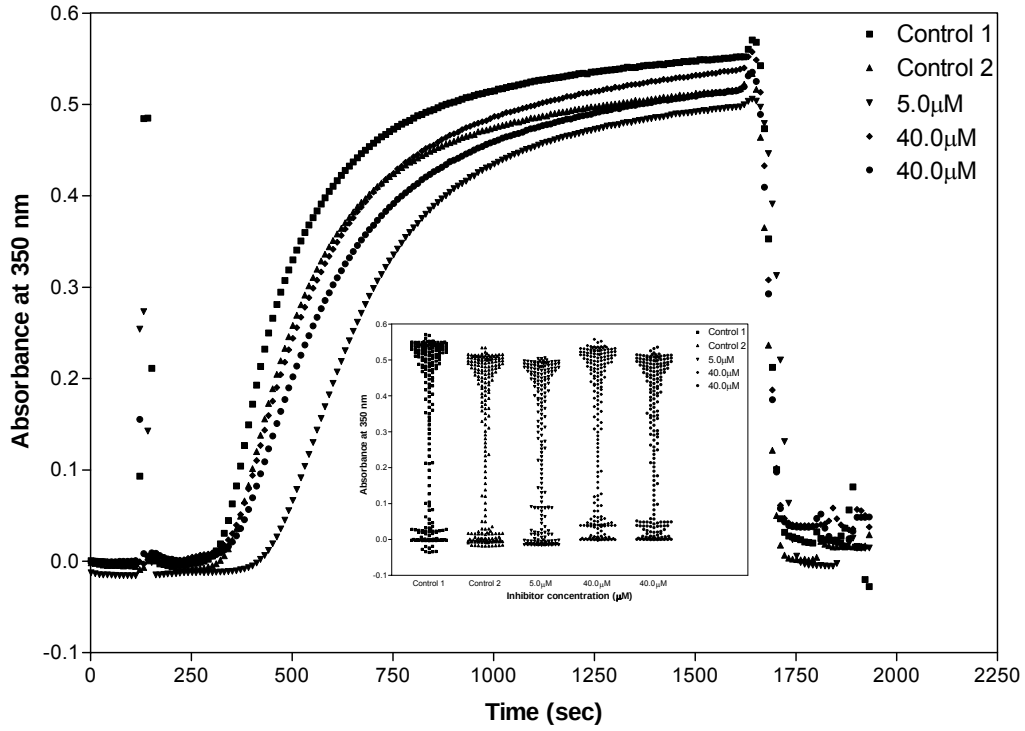

Figure A.2.3. Inhibition of Tubulin Polymerization by Compound **6** at 30ºC.

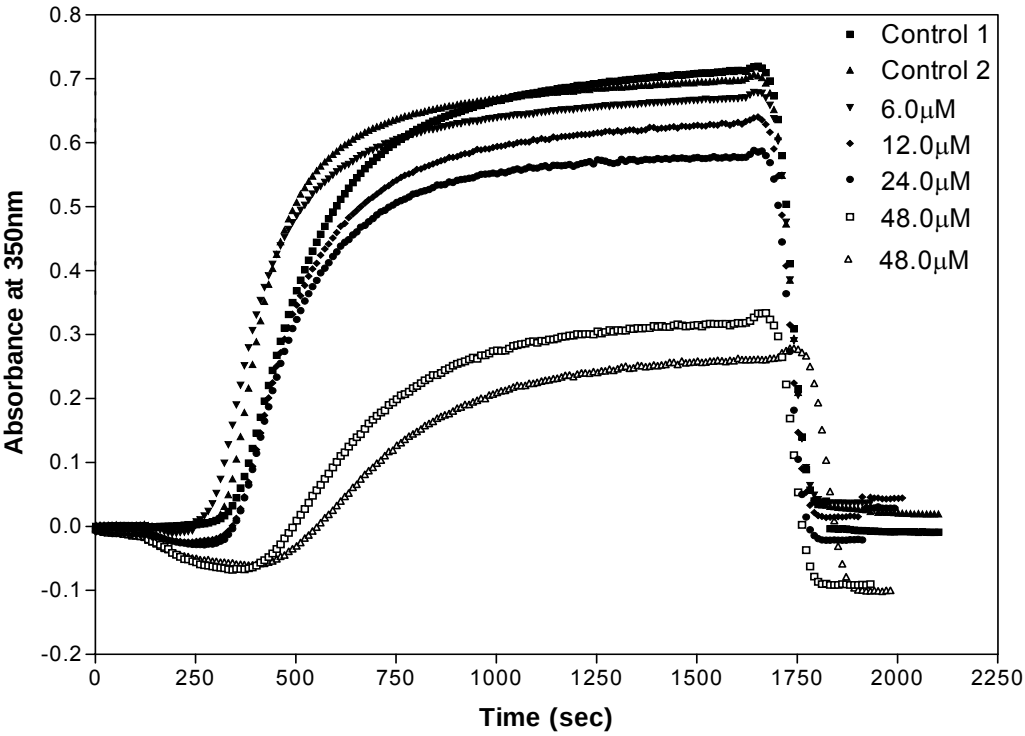

Figure A.2.4. Inhibition of Tubulin Polymerization by Compound **10** at 30ºC.

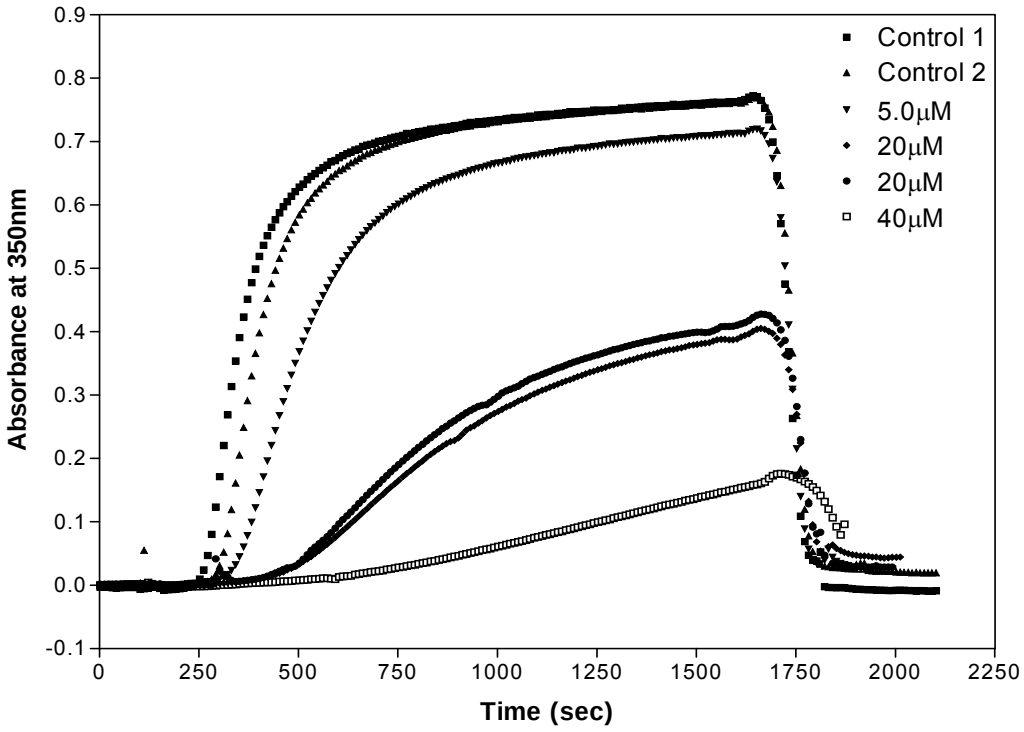

Figure A.2.5. Inhibition of Tubulin Polymerization by Compound **11** at 30ºC.

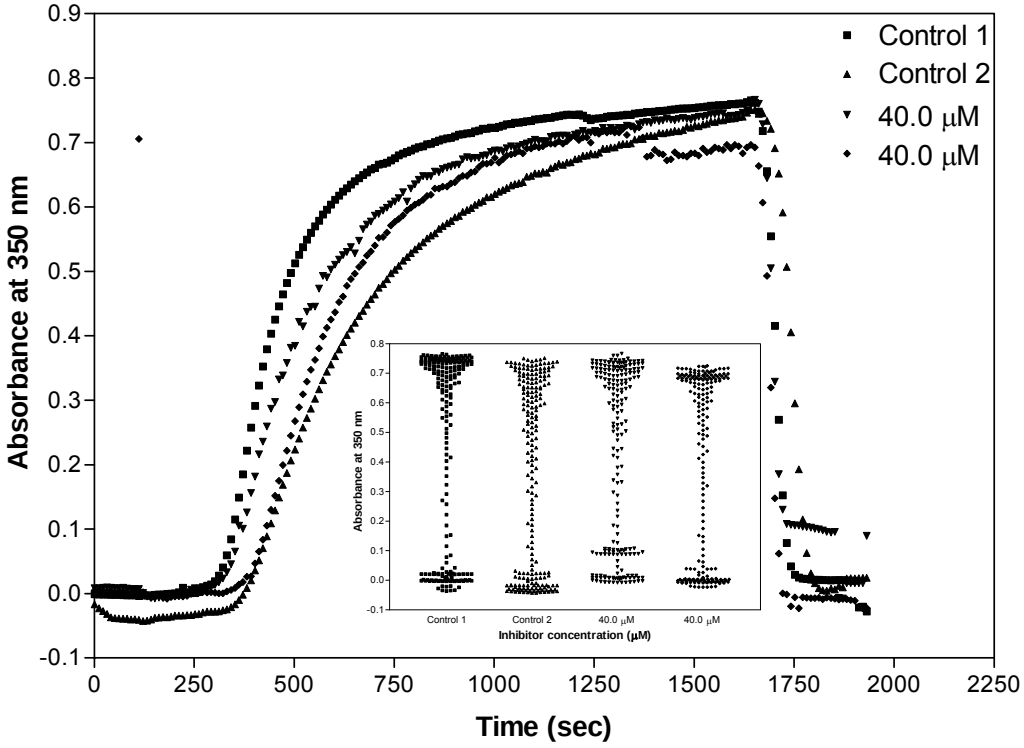

Figure A.2.6. Inhibition of Tubulin Polymerization by Compound **17** at 30ºC.

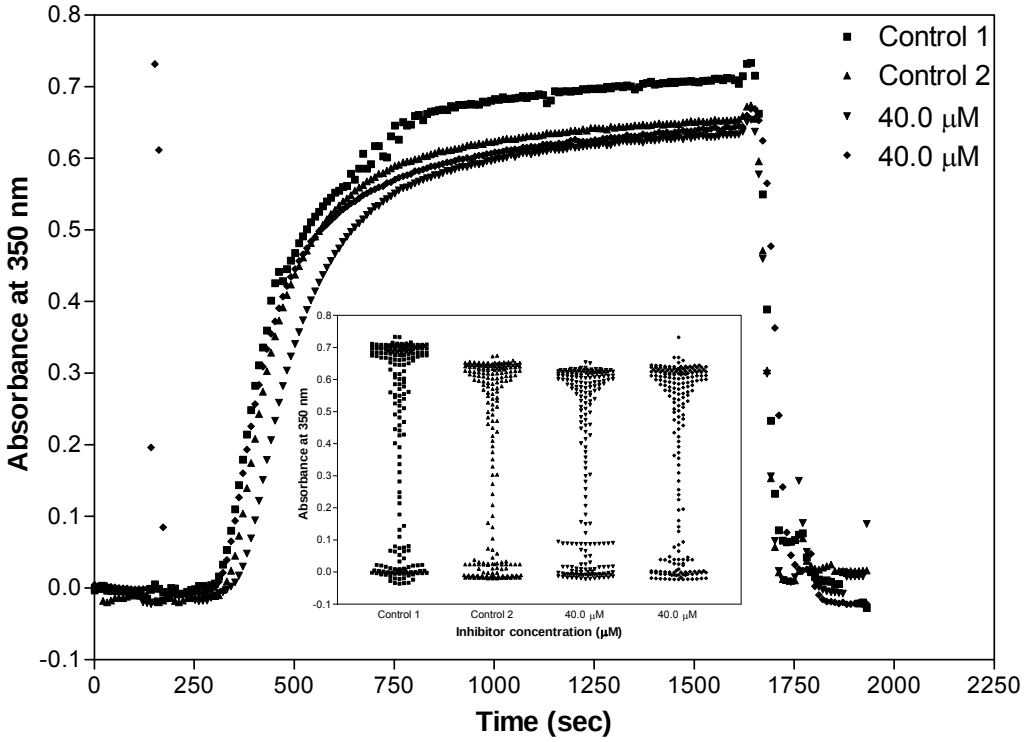

Figure A.2.7. Inhibition of Tubulin Polymerization by Compound **20** at 30ºC.

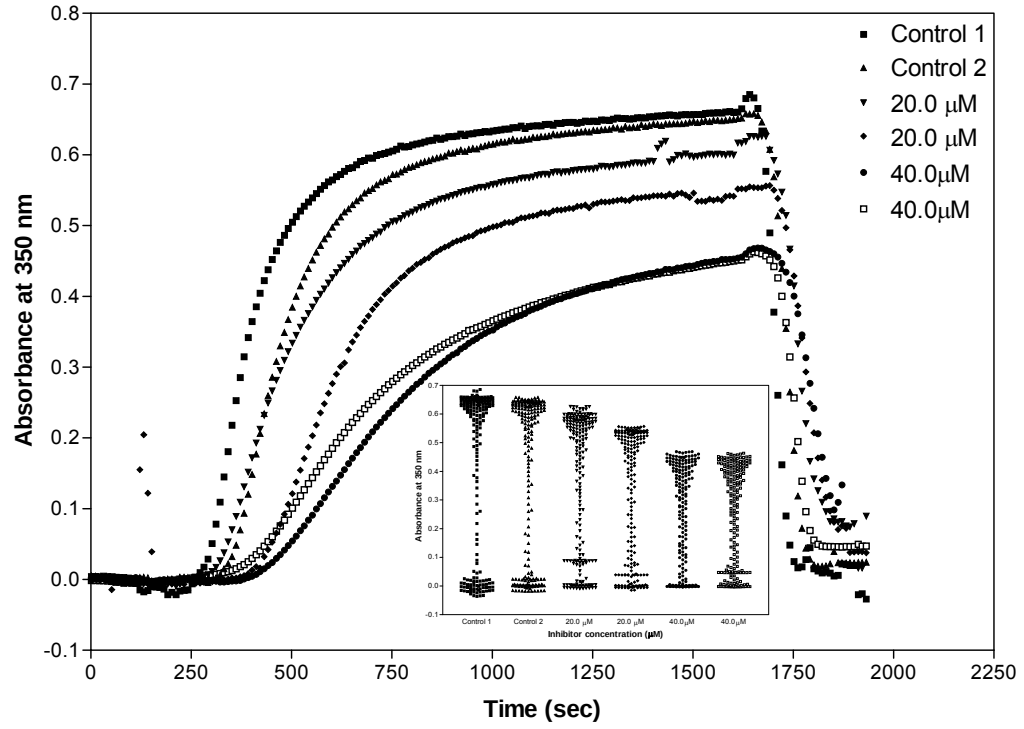

Figure A.2.8. Inhibition of Tubulin Polymerization by Compound **24** at 30ºC.

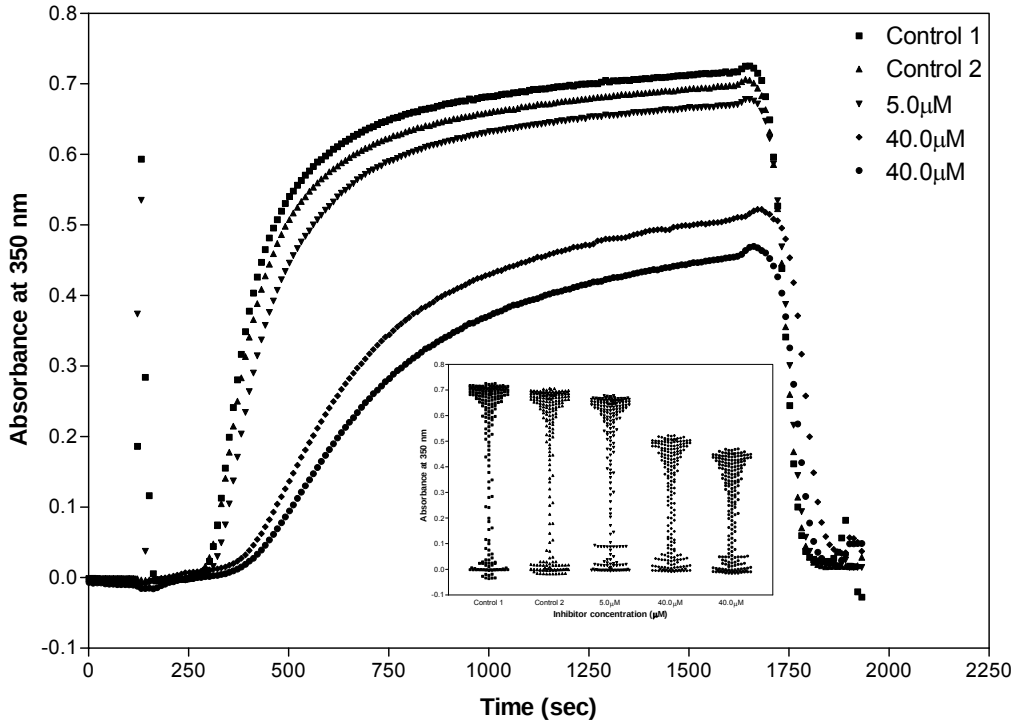

Figure A.2.9. Inhibition of Tubulin Polymerization by Compound **32** at 30ºC.

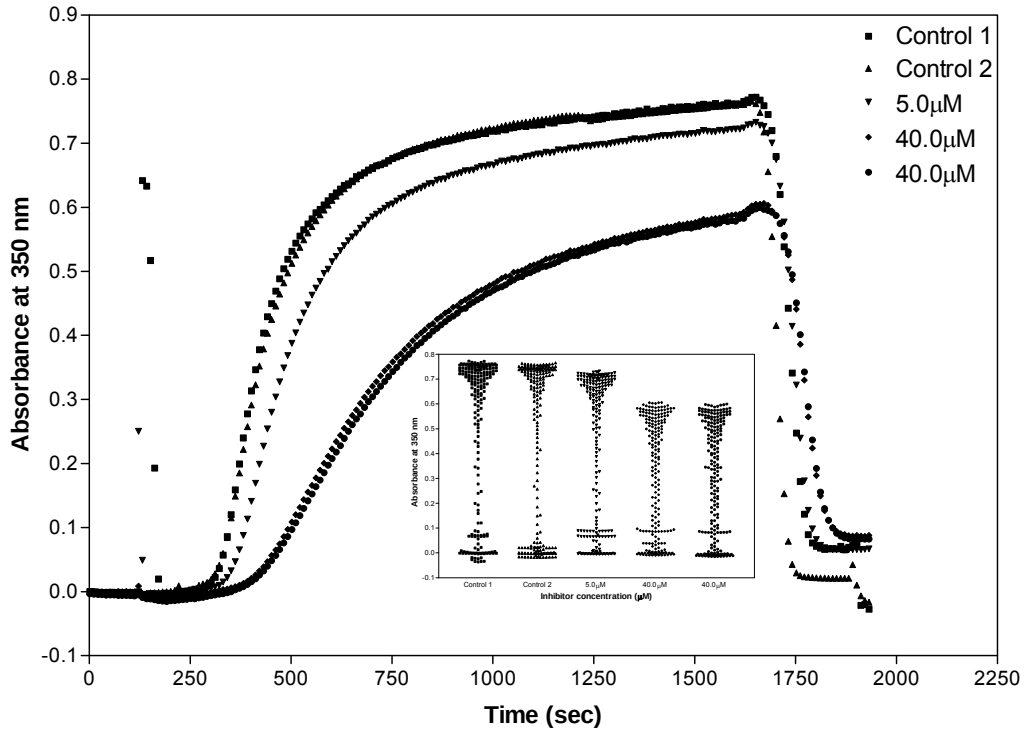

Figure A.2.10. Inhibition of Tubulin Polymerization by Compound (**33**) at 30ºC.

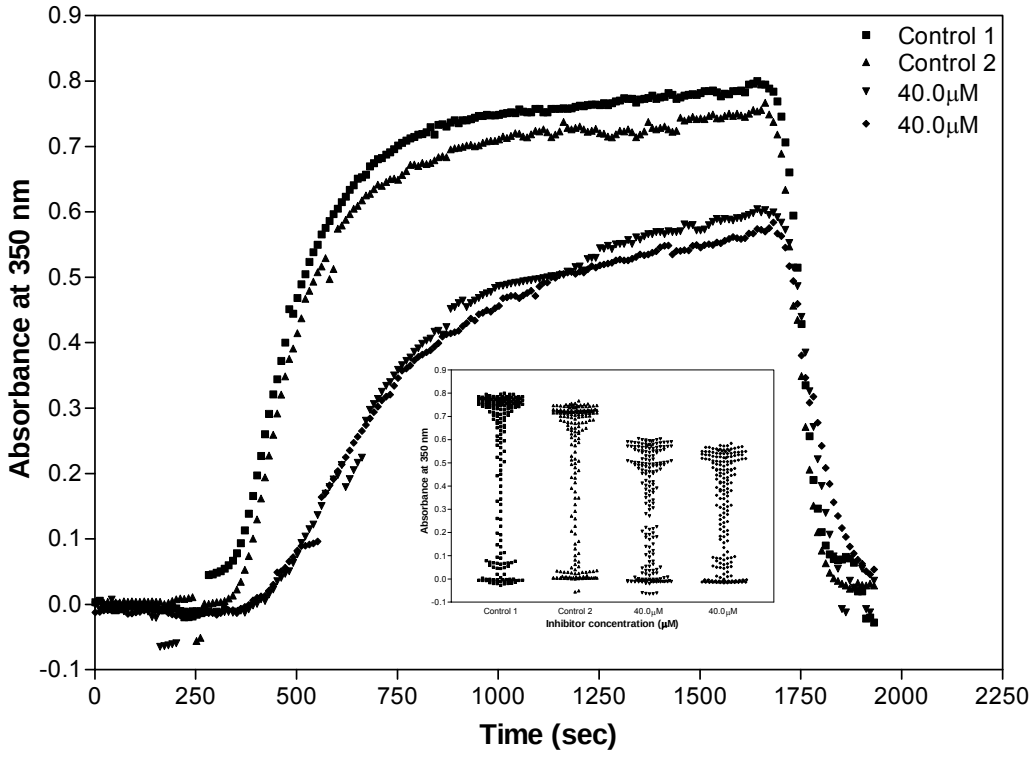

Figure A.2.11. Inhibition of Tubulin Polymerization by Compound **34** at 30ºC.

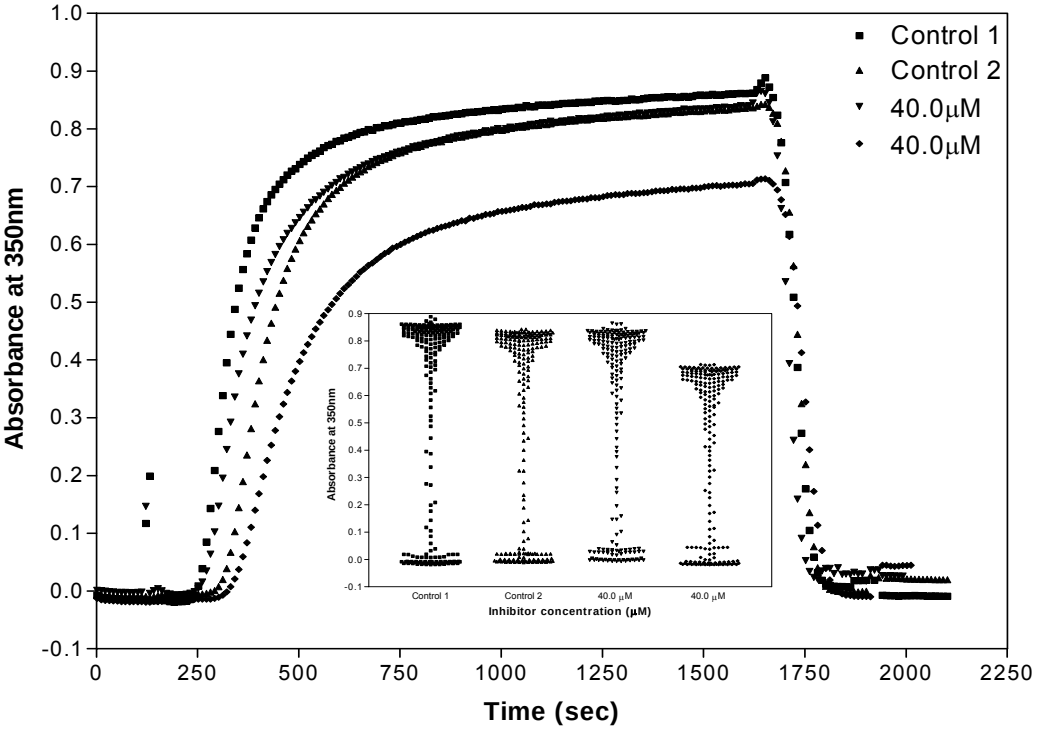

Figure A.2.12. Inhibition of Tubulin Polymerization by Compound **35** at 30ºC.

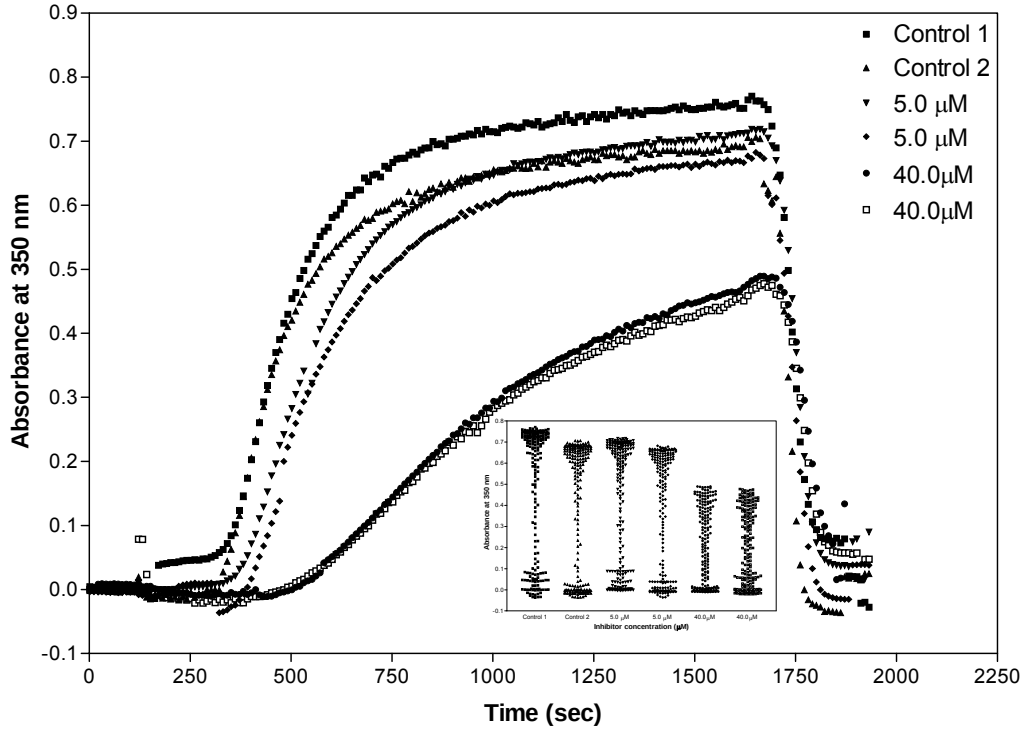

Figure A.2.13. Inhibition of Tubulin Polymerization by Compound **36** at 30ºC.

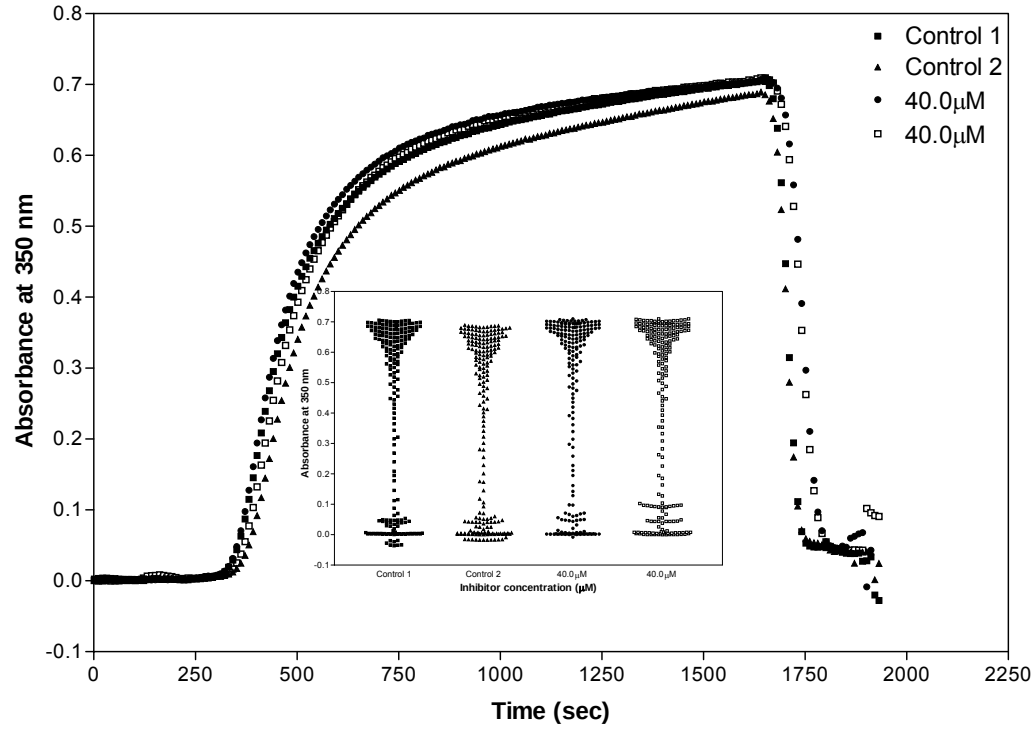

Figure A.2.14. Inhibition of Tubulin Polymerization by Compound **38** at 30ºC.

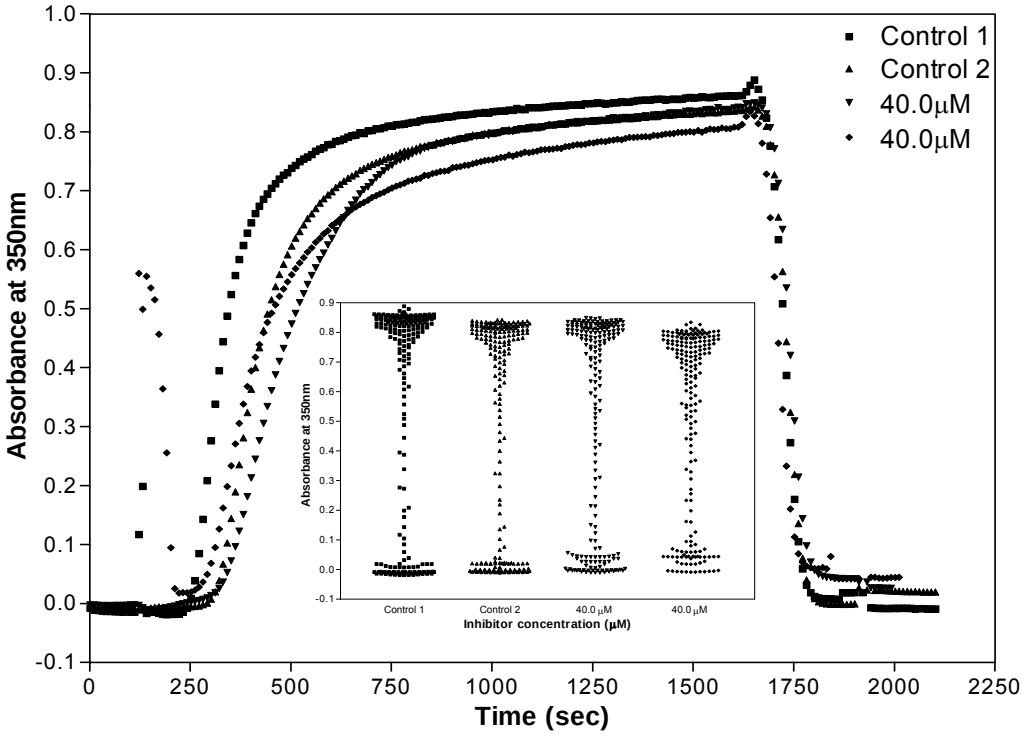

Figure A.2.15. Inhibition of Tubulin Polymerization by Compound **41** at 30ºC.

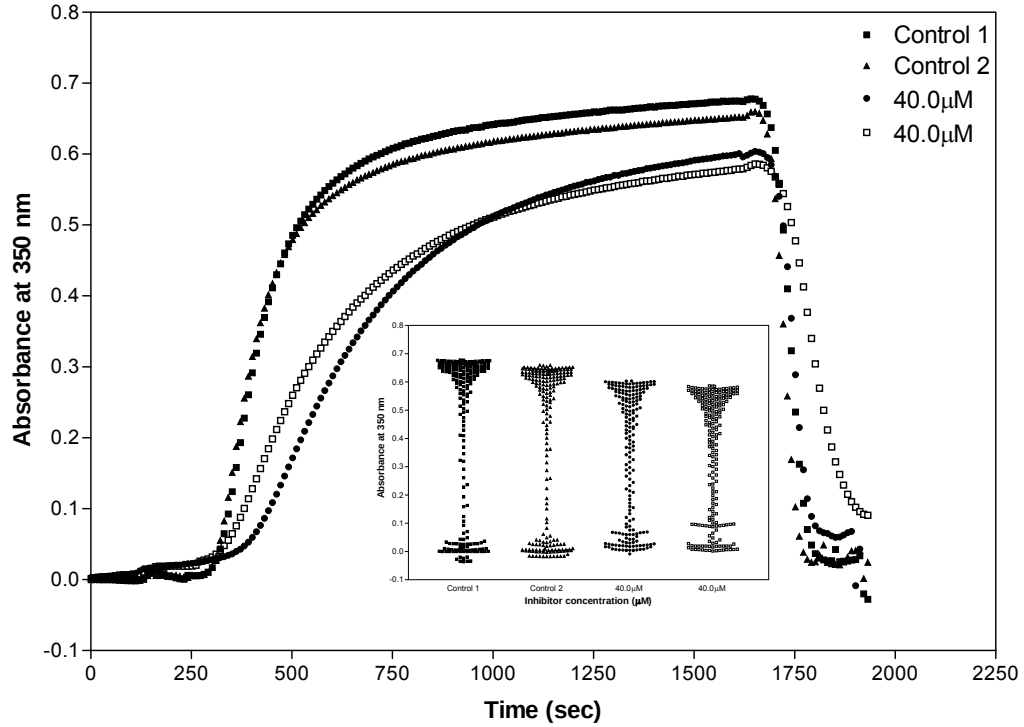

Figure A.2.16. Inhibition of Tubulin Polymerization by Compound **46** at 30ºC.

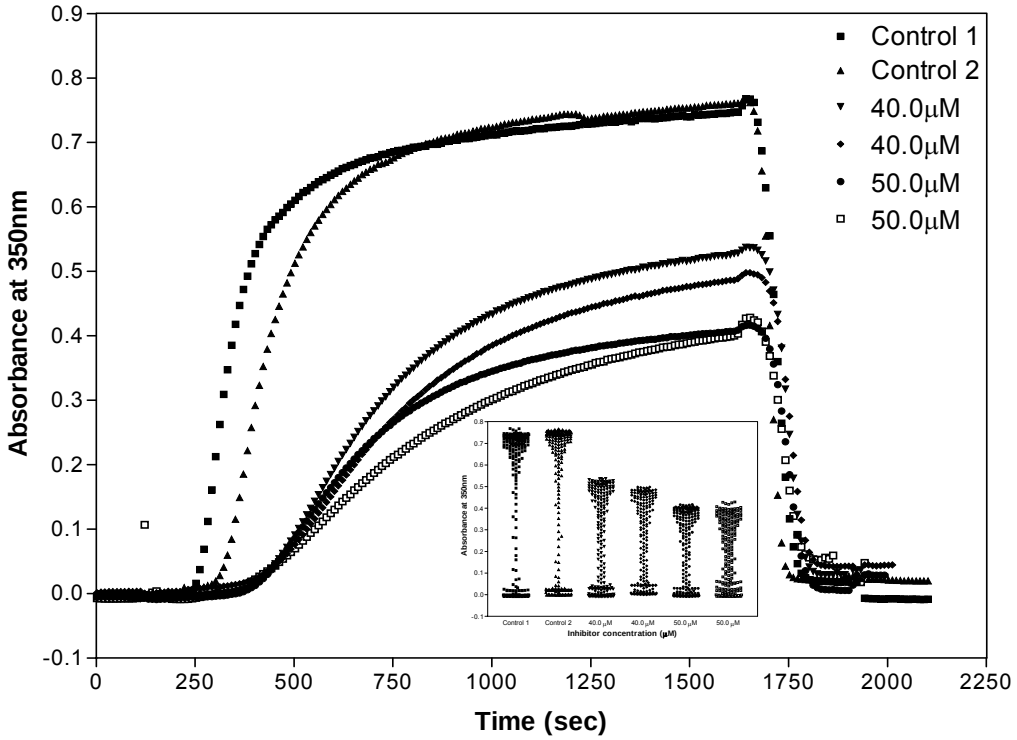

Figure A.2.17. Inhibition of Tubulin Polymerization by Compound **47** at 30ºC.

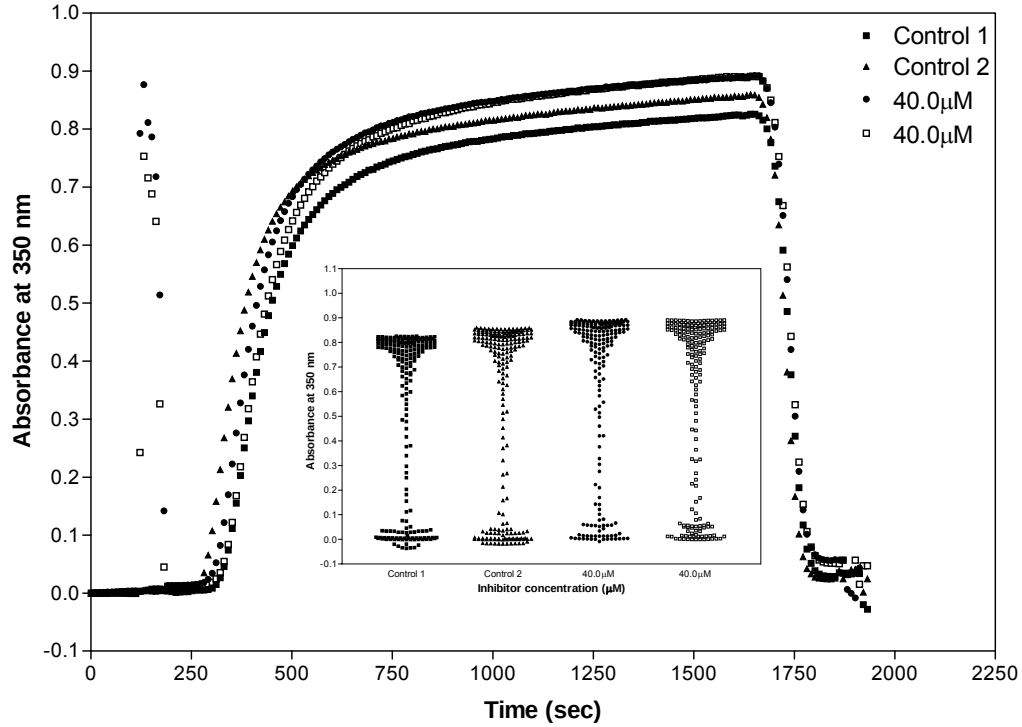

Figure A.2.18. Inhibition of Tubulin Polymerization by Compound **50** at 30ºC.

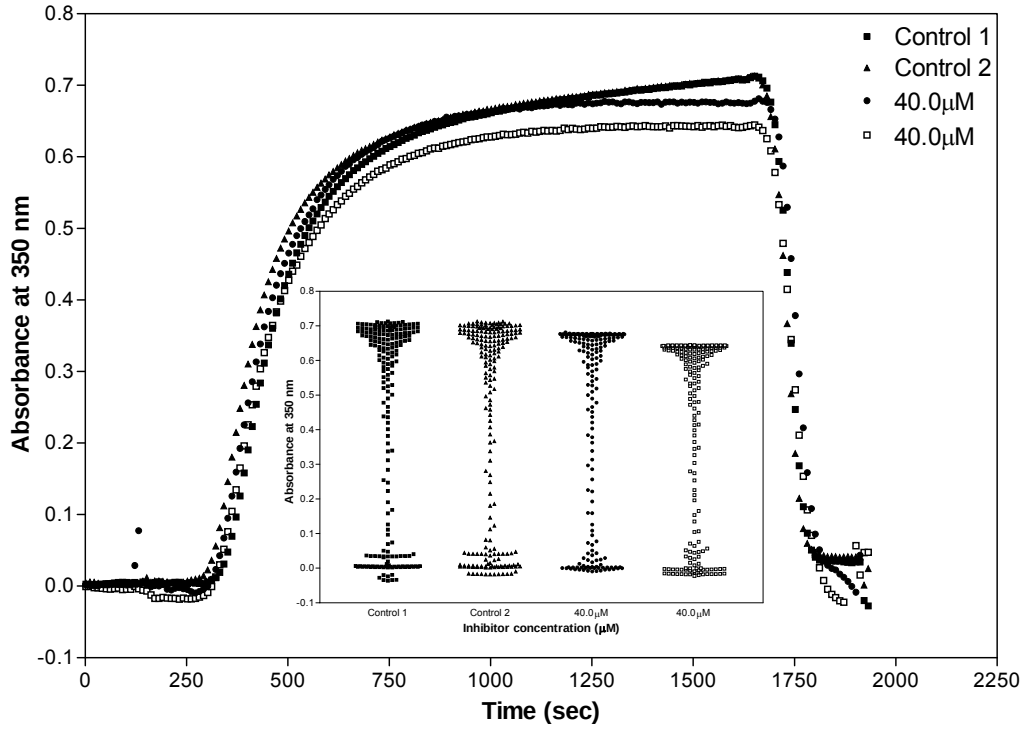

Figure A.2.19. Inhibition of Tubulin Polymerization by Compound **53** at 30ºC.

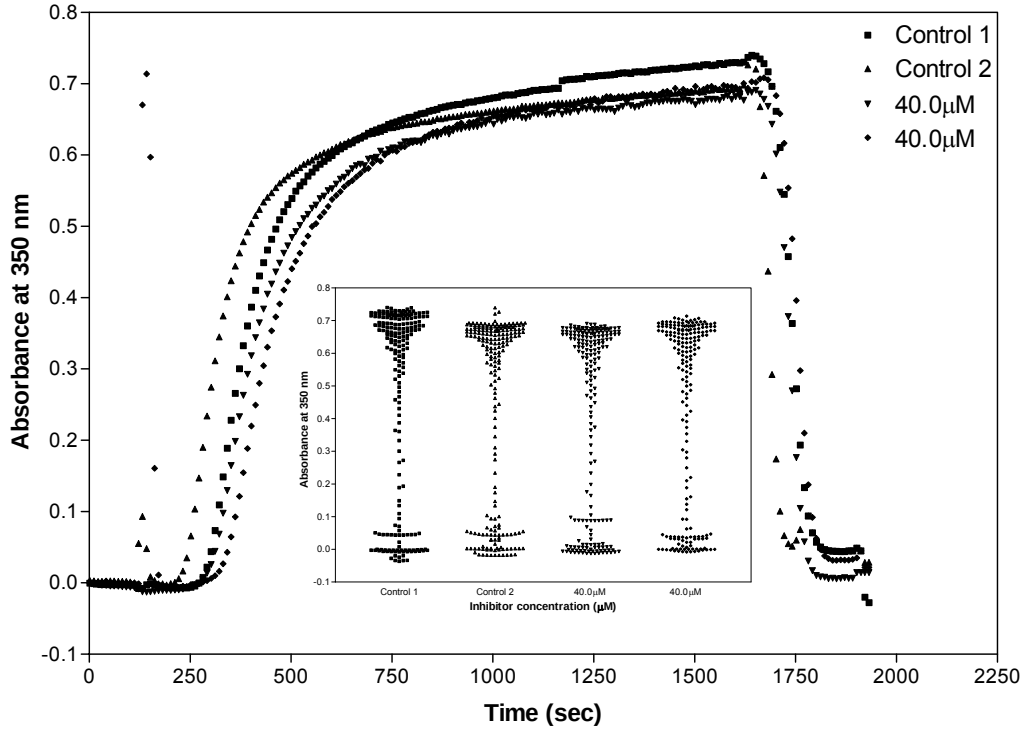

Figure A.2.20. Inhibition of Tubulin Polymerization by Compound **54** at 30ºC.

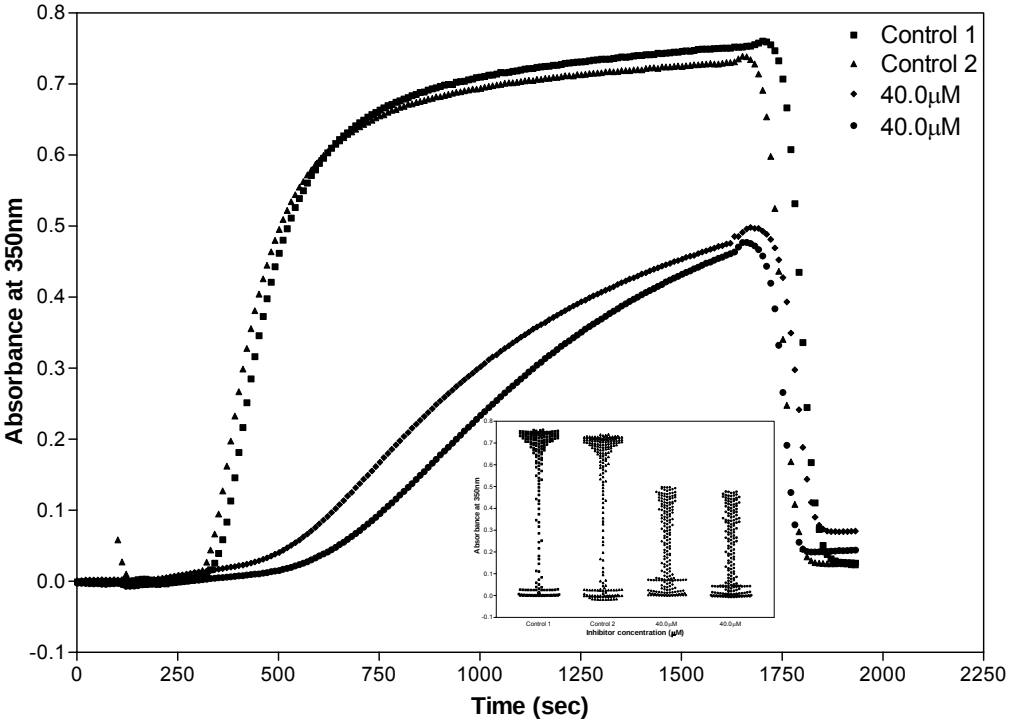

Figure A.2.21. Inhibition of Tubulin Polymerization by Compound **55** at 30ºC.

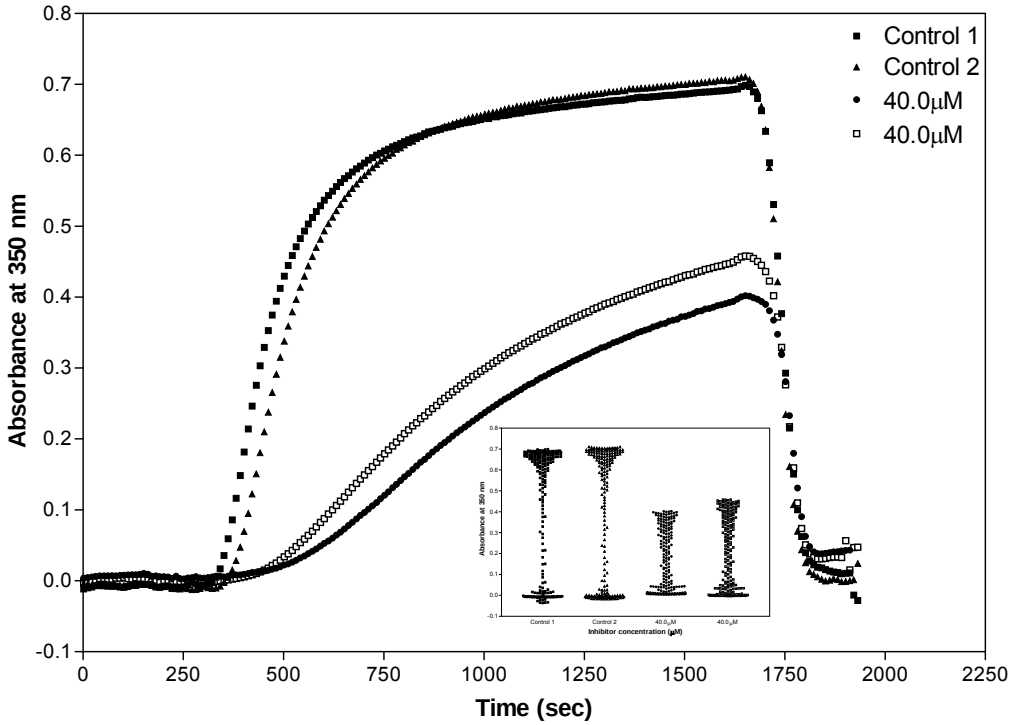

Figure A.2.22. Inhibition of Tubulin Polymerization by Compound **58** at 30ºC.

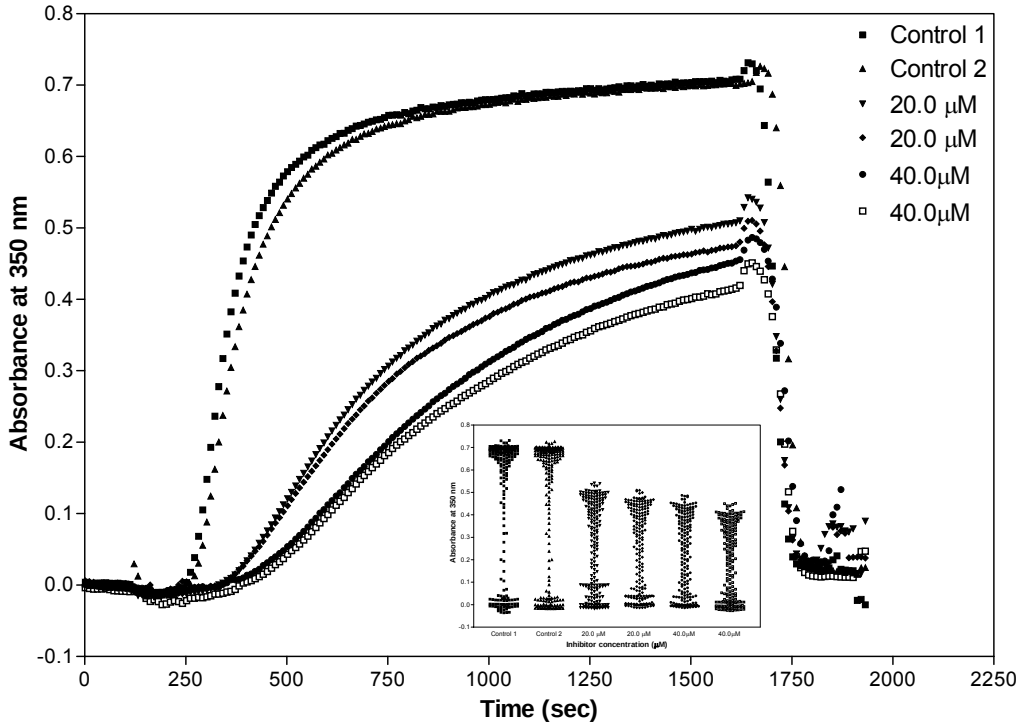

Figure A.2.23. Inhibition of Tubulin Polymerization by Compound **60** at 30ºC.

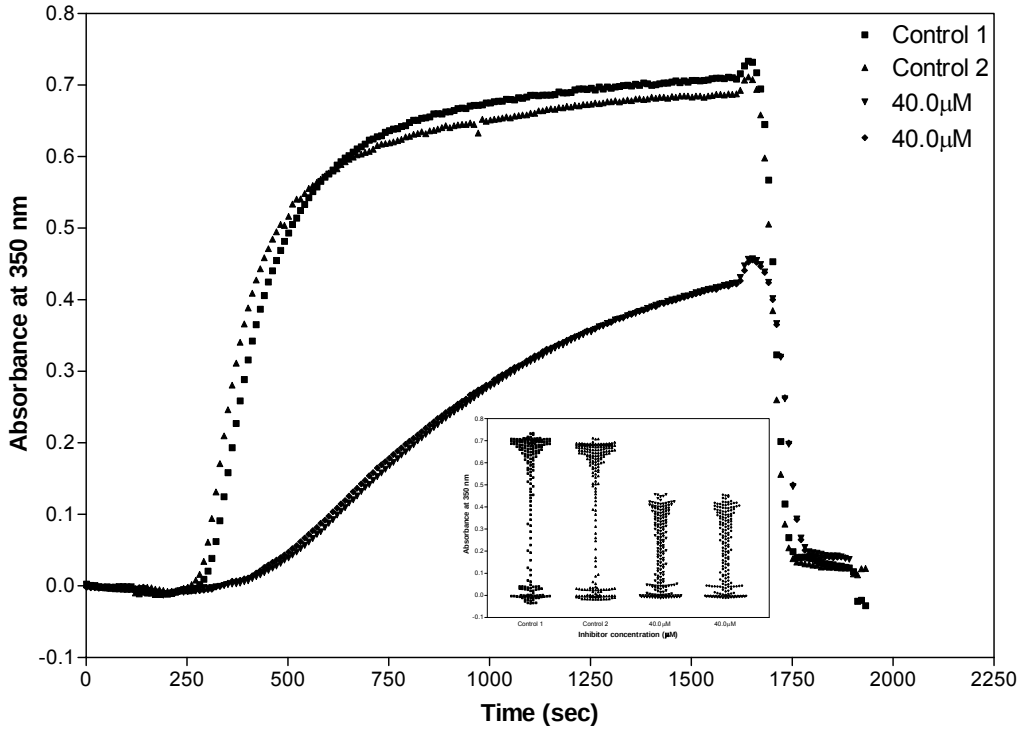

Figure A.2.24. Inhibition of Tubulin Polymerization by Compound **61** at 30ºC.

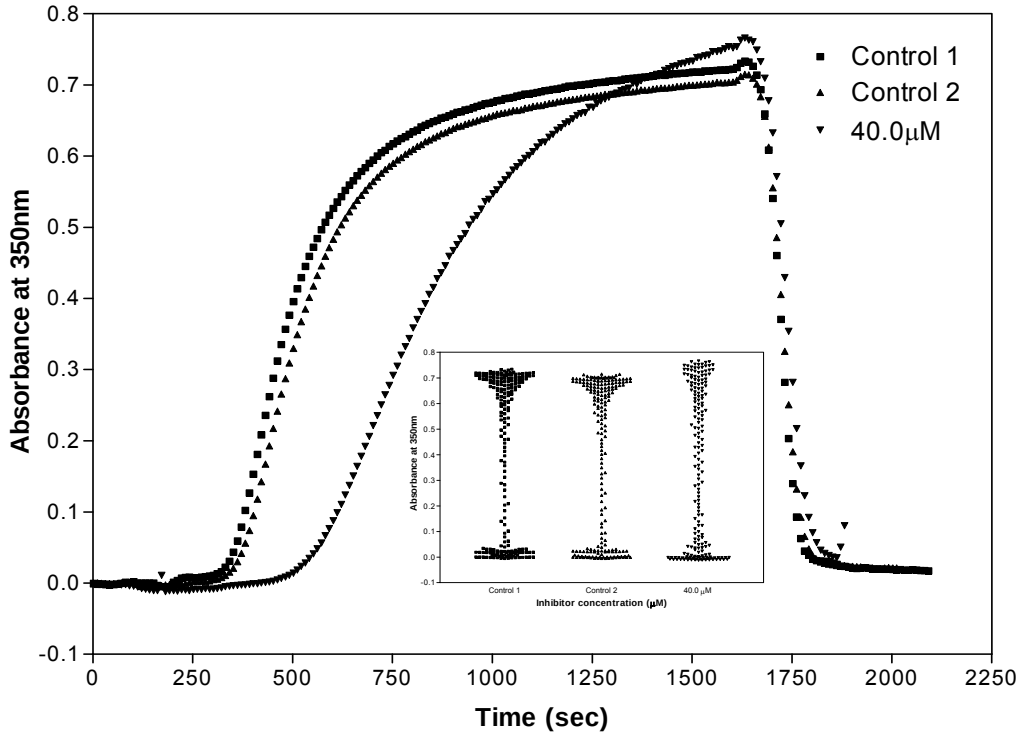

Figure A.2.25. Inhibition of Tubulin Polymerization by Compound **62** at 30ºC.

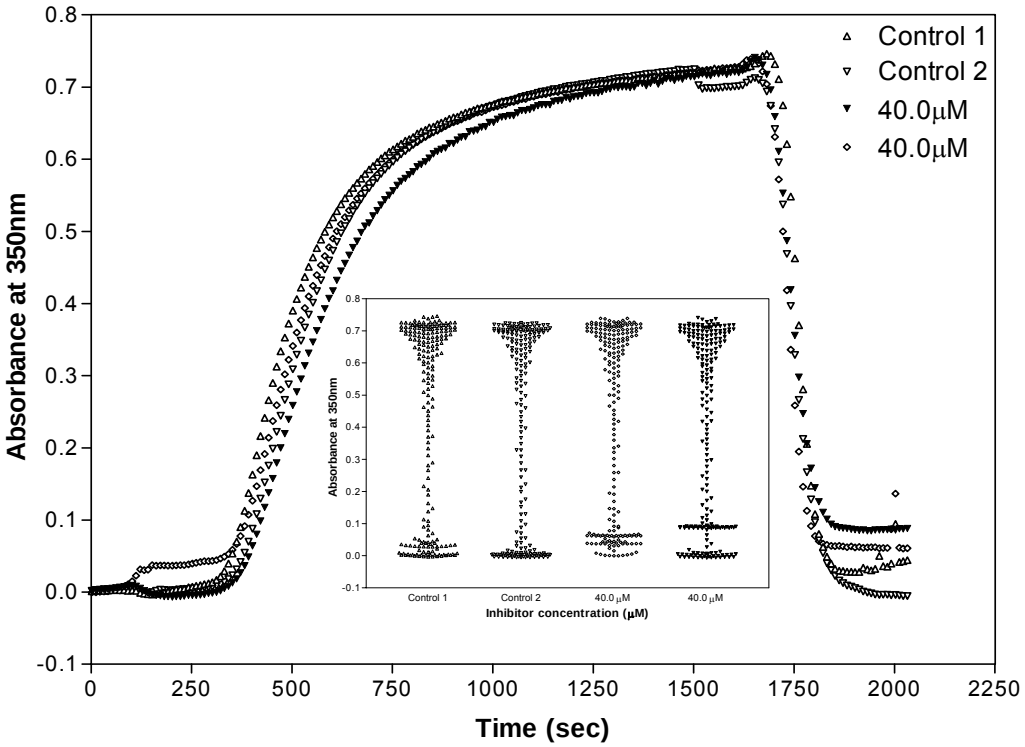

Figure A.2.26. Inhibition of Tubulin Polymerization by Compound **63** at 30ºC.

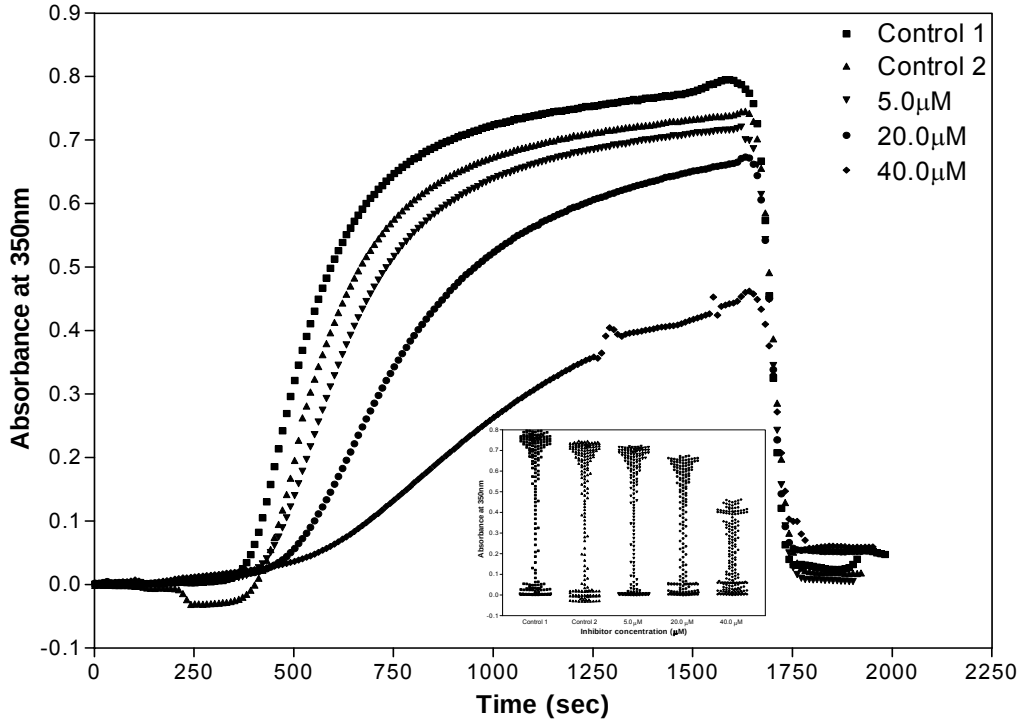

Figure A.2.27. Inhibition of Tubulin Polymerization by Compound **64** at 30ºC.

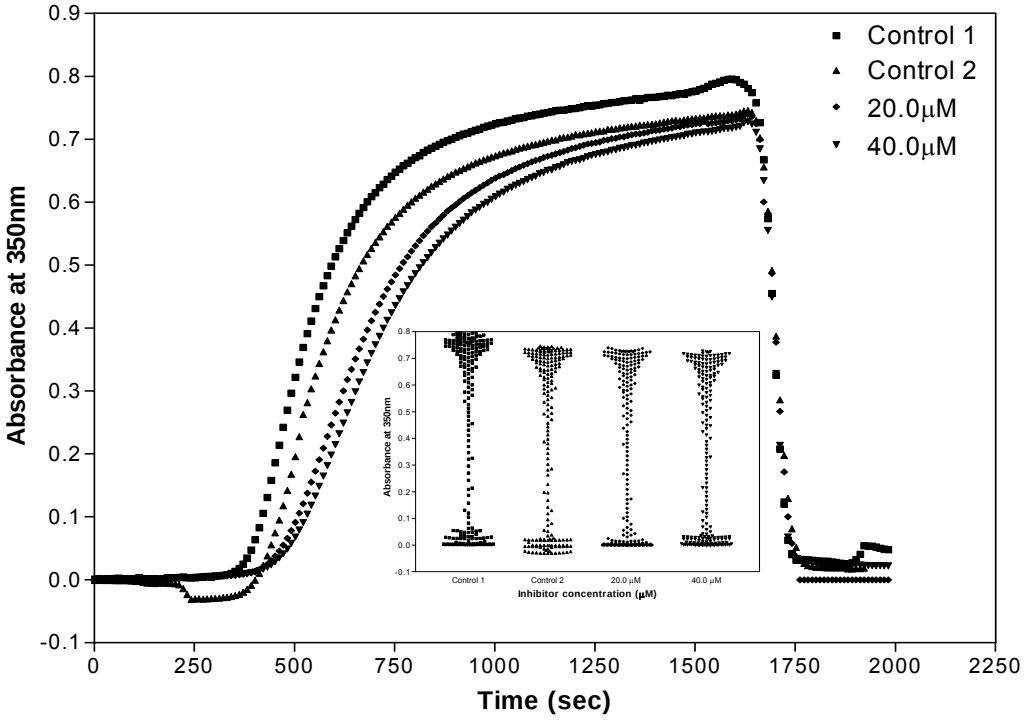

Figure A.2.28. Inhibition of Tubulin Polymerization by Compound **65** at 30ºC.

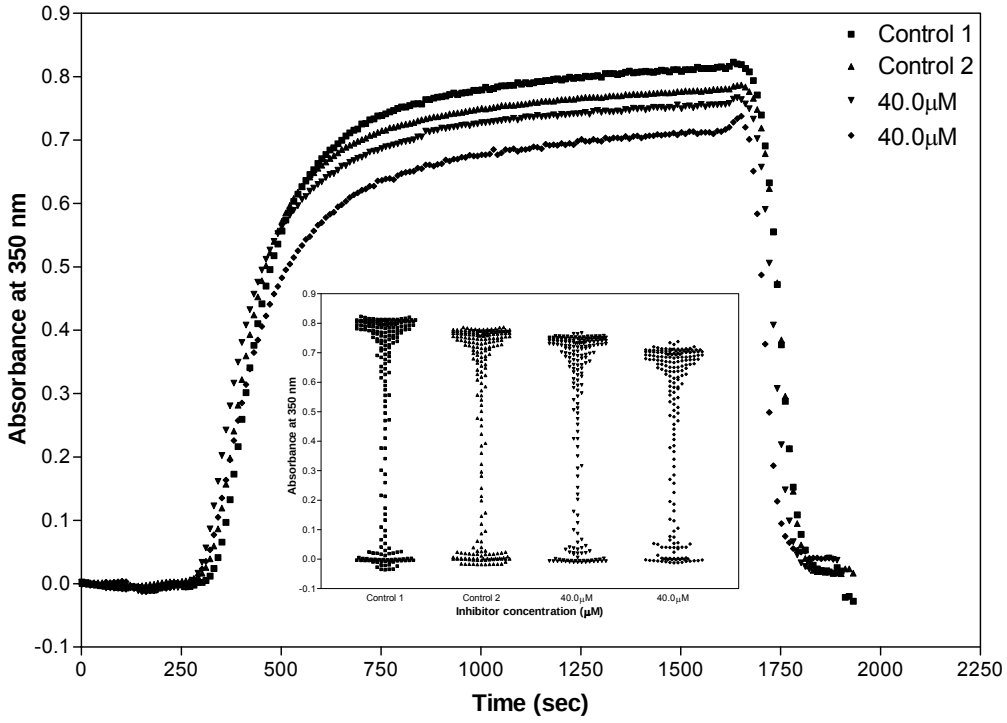

Figure A.2.29. Inhibition of Tubulin Polymerization by Compound **68** at 30ºC.

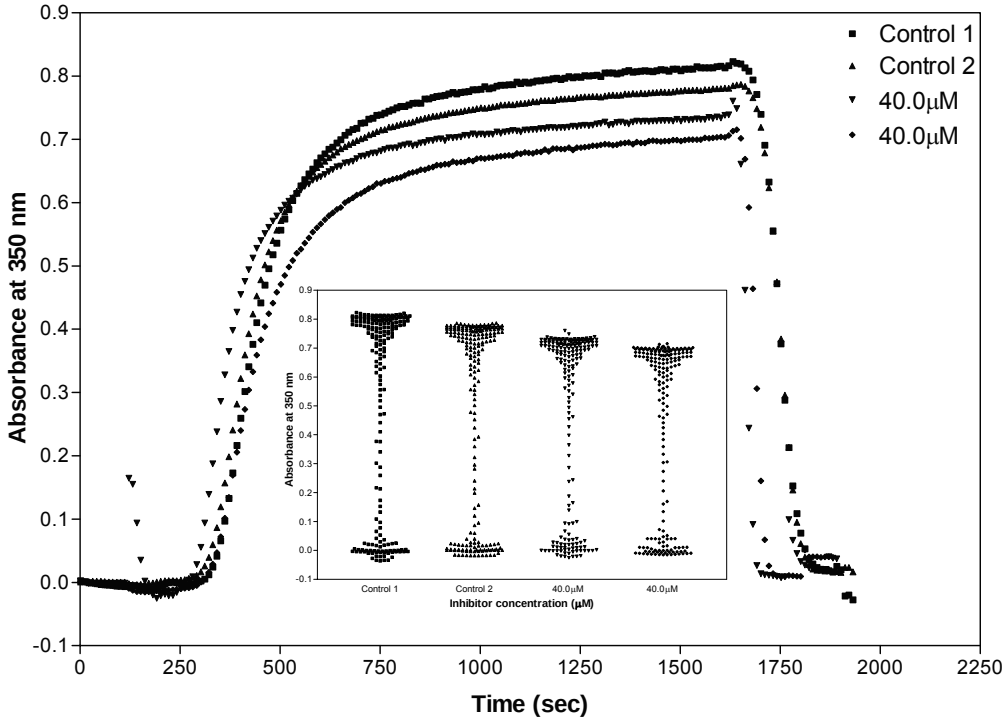

Figure A.2.30. Inhibition of Tubulin Polymerization by Compound **69** at 30ºC.

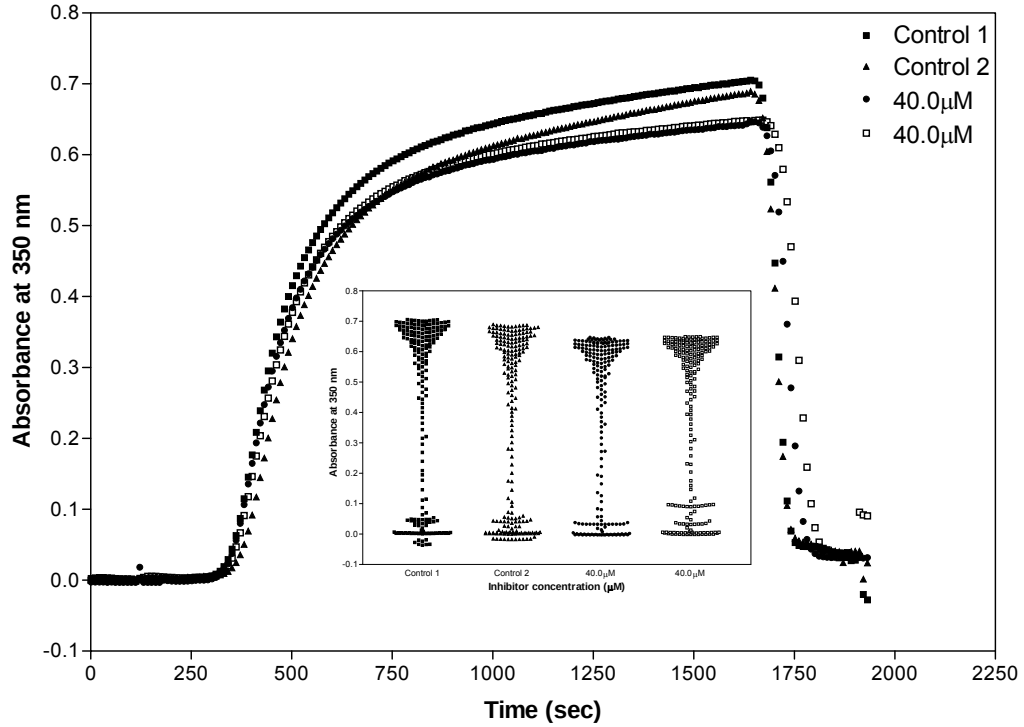

Figure A.2.31. Inhibition of Tubulin Polymerization by Compound **71** at 30ºC.

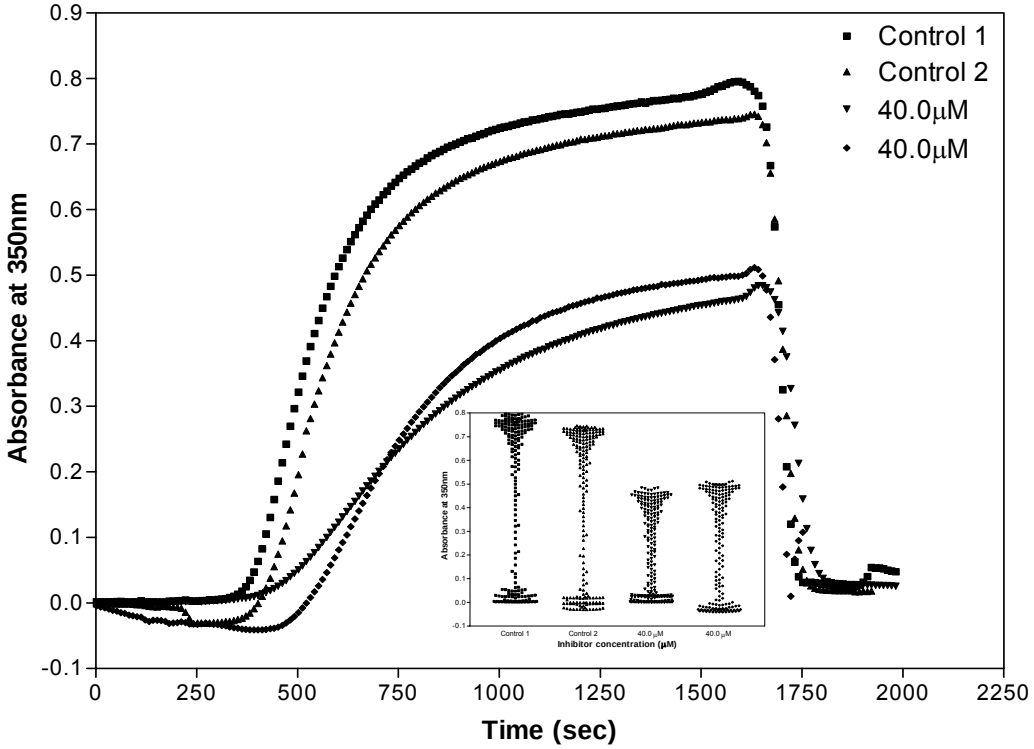

Figure A.2.32. Inhibition of Tubulin Polymerization by Compound **72** at 30ºC.

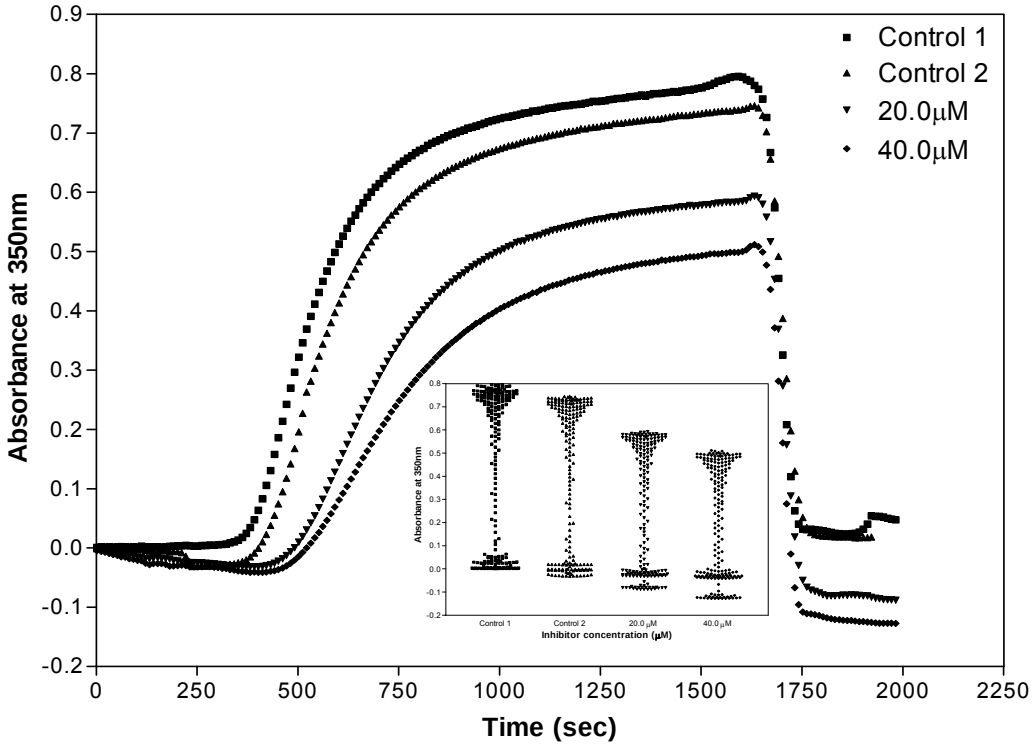

Figure A.2.33. Inhibition of Tubulin Polymerization by Compound **73** at 30ºC.

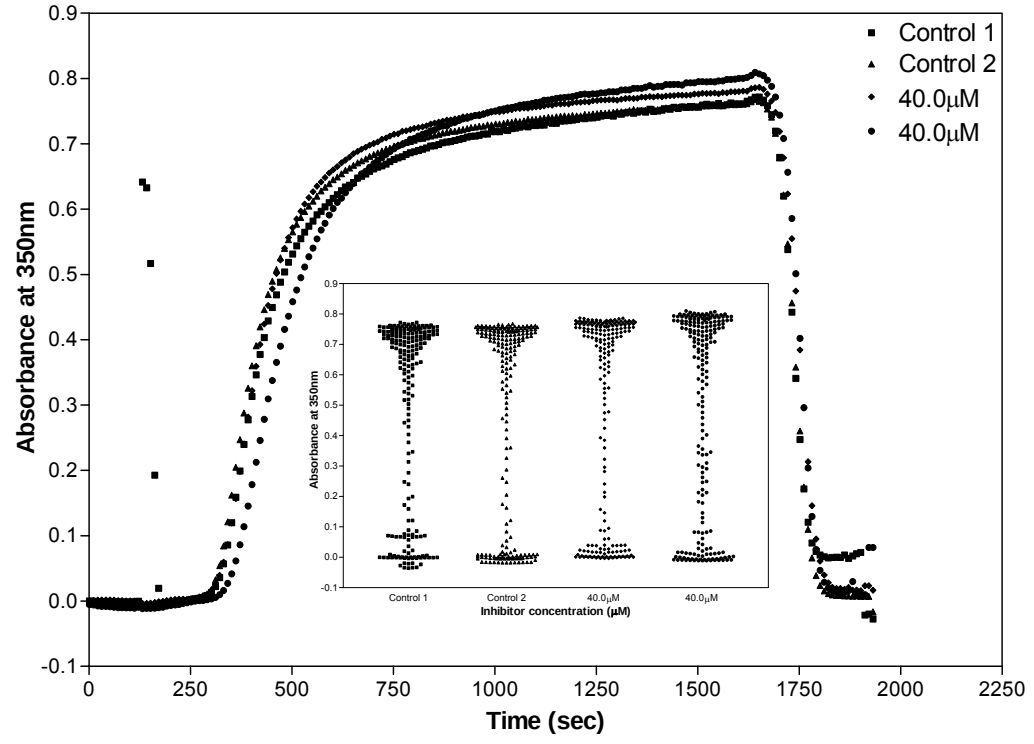

Figure A.2.34. Inhibition of Tubulin Polymerization by Compound **75** at 30ºC.

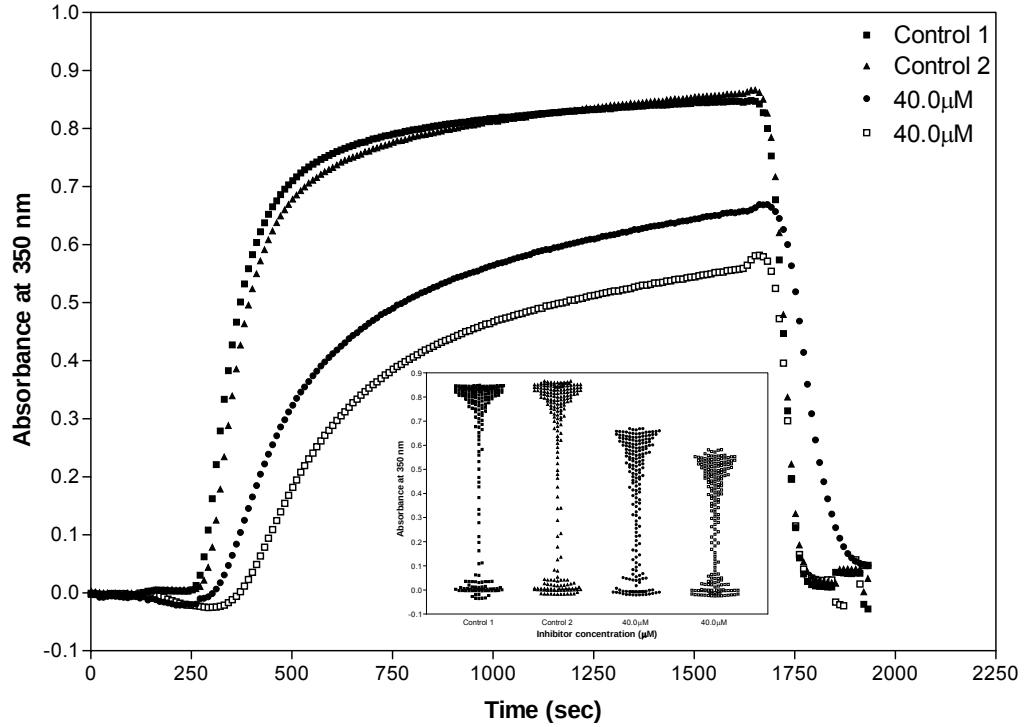

Figure A.2.35. Inhibition of Tubulin Polymerization by Compound **77** at 30ºC.

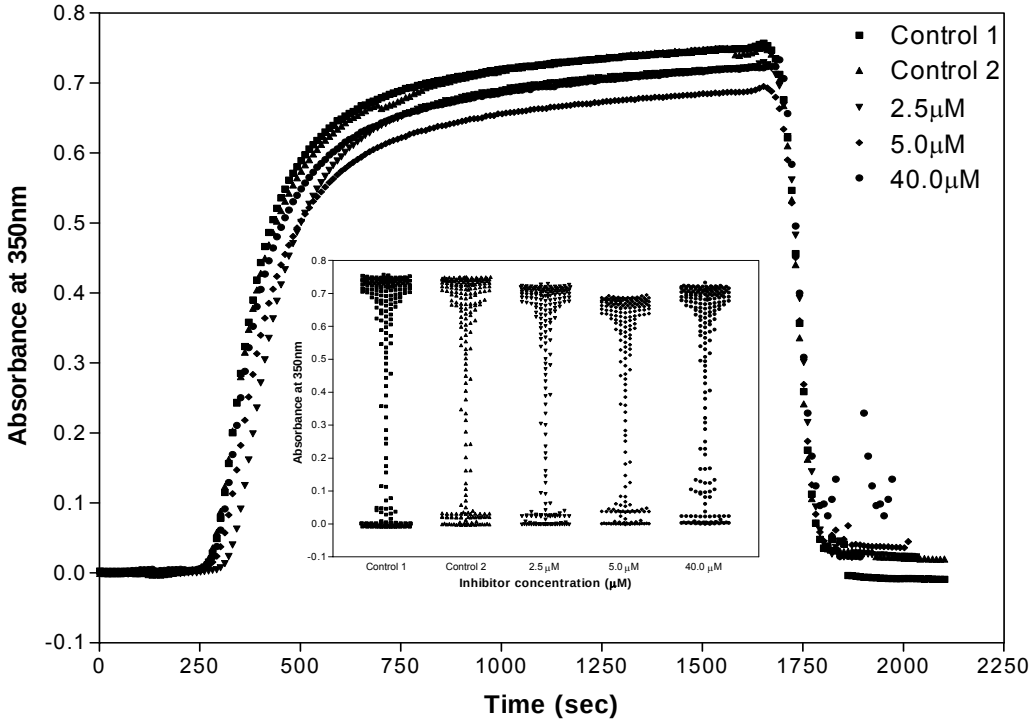

Figure A.2.36. Inhibition of Tubulin Polymerization by CA-4 Glucuronide **78** at 30ºC.

APPENDIX B

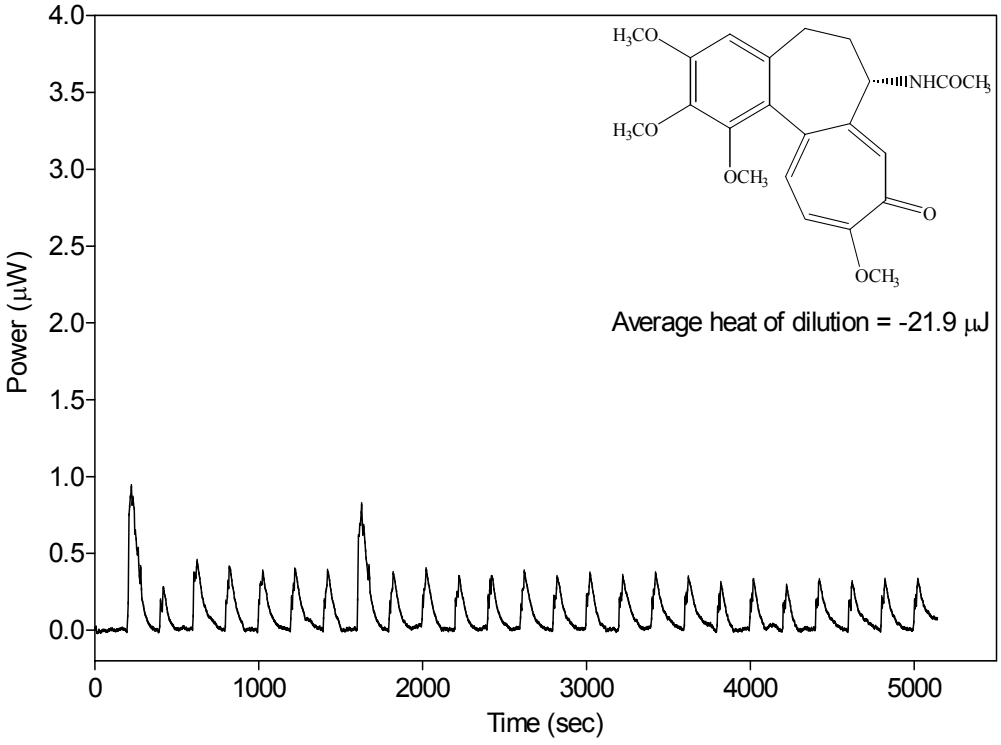

Figure B.3.1. ITC Blank Titration of Compound **1.**

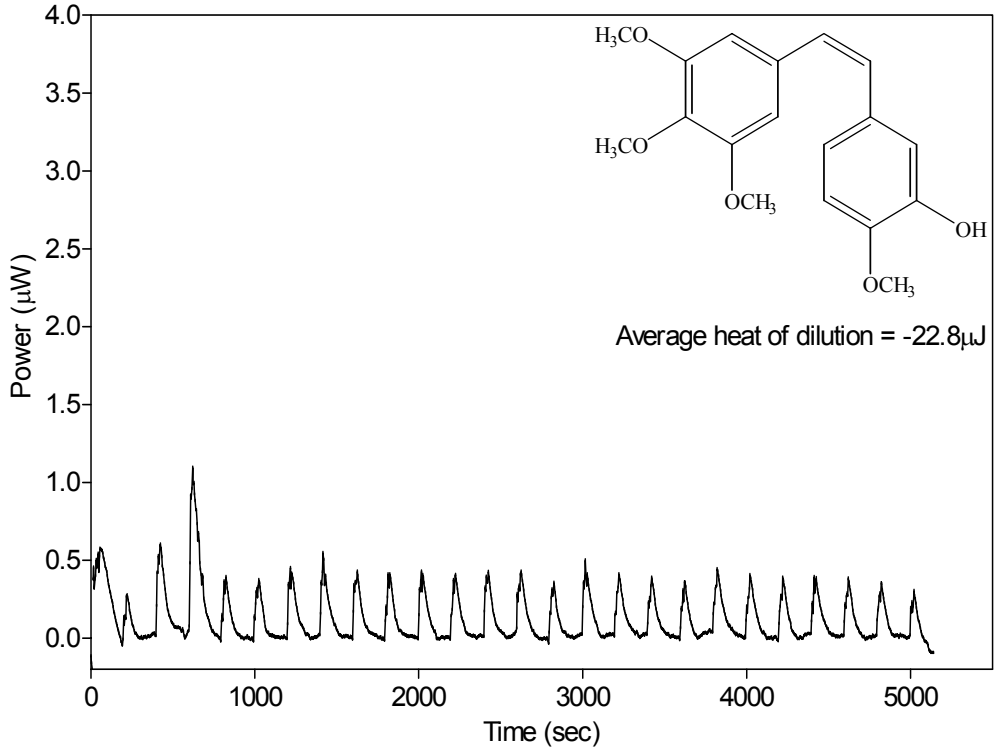

Figure B.3.2. ITC Blank Titration of Compound **2.**

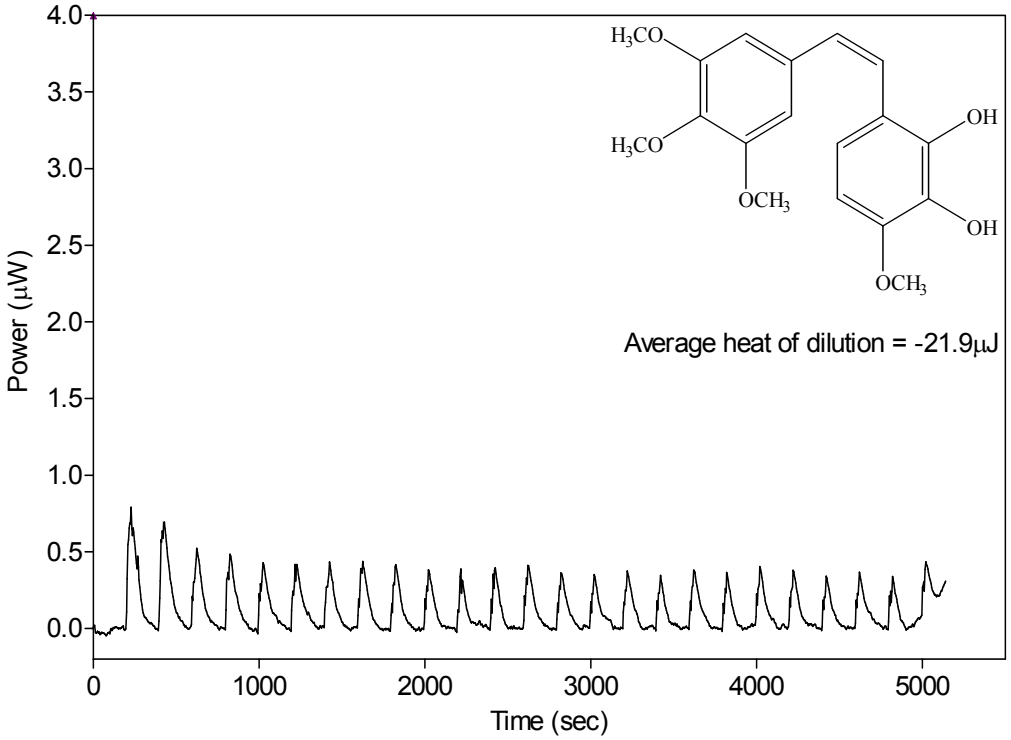

Figure B.3.3. ITC Blank Titration of Compound **3**.

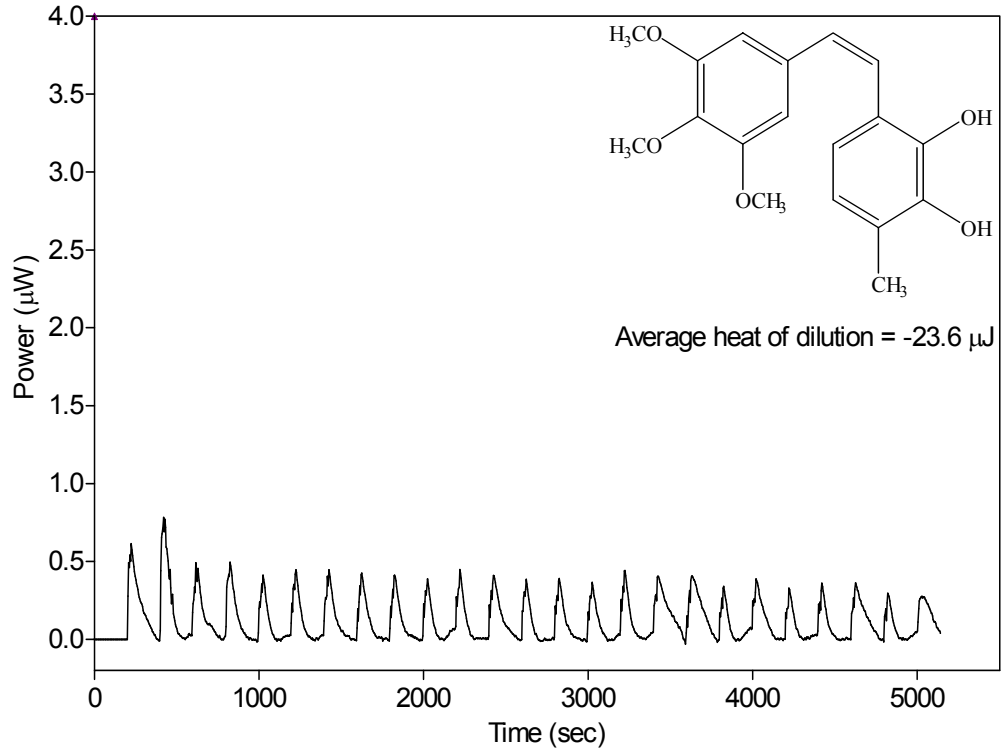

Figure B.3.4. ITC Blank titration of Compound **12.**

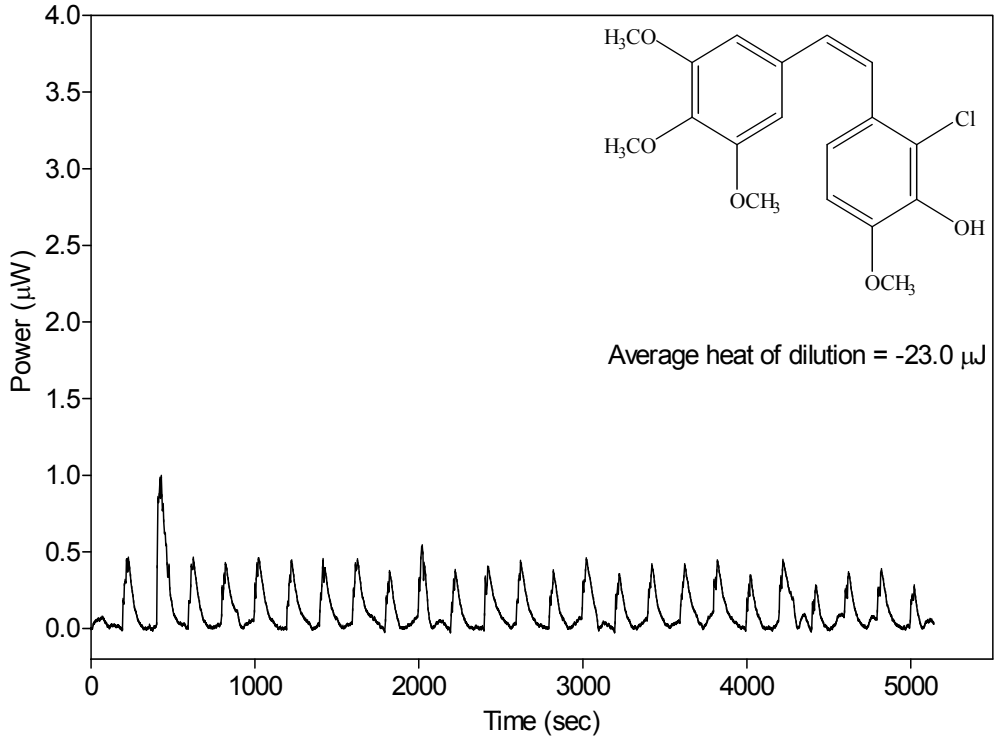

Figure B.3.5. ITC Blank titration of Compound **15.**

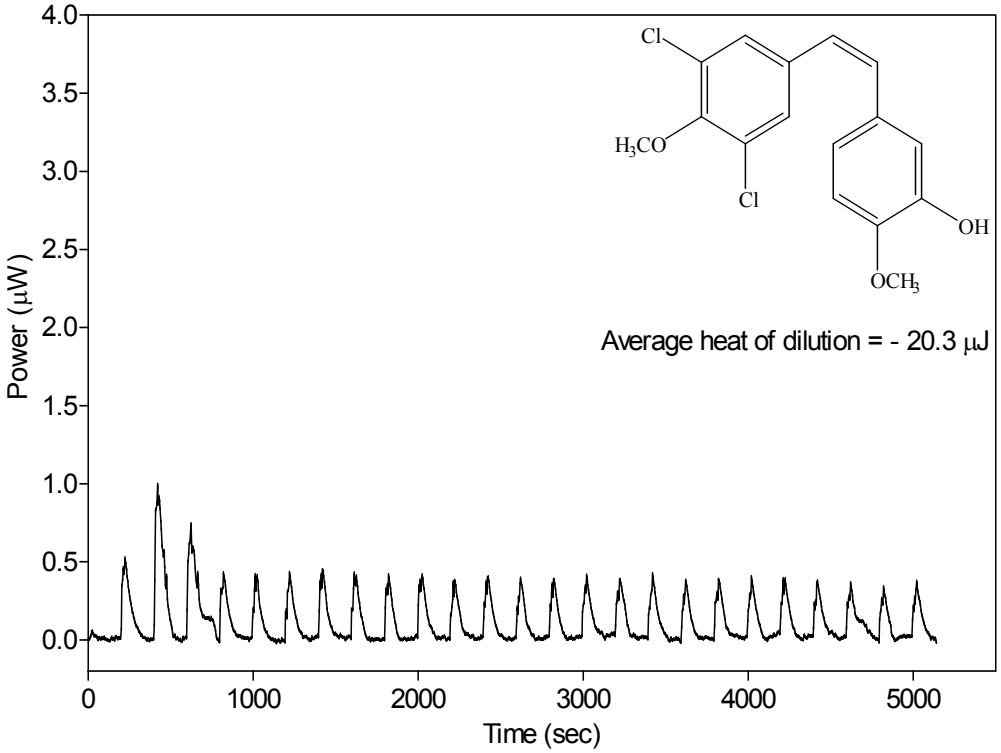

Figure B.3.6. ITC Blank Titration of Compound **27.**

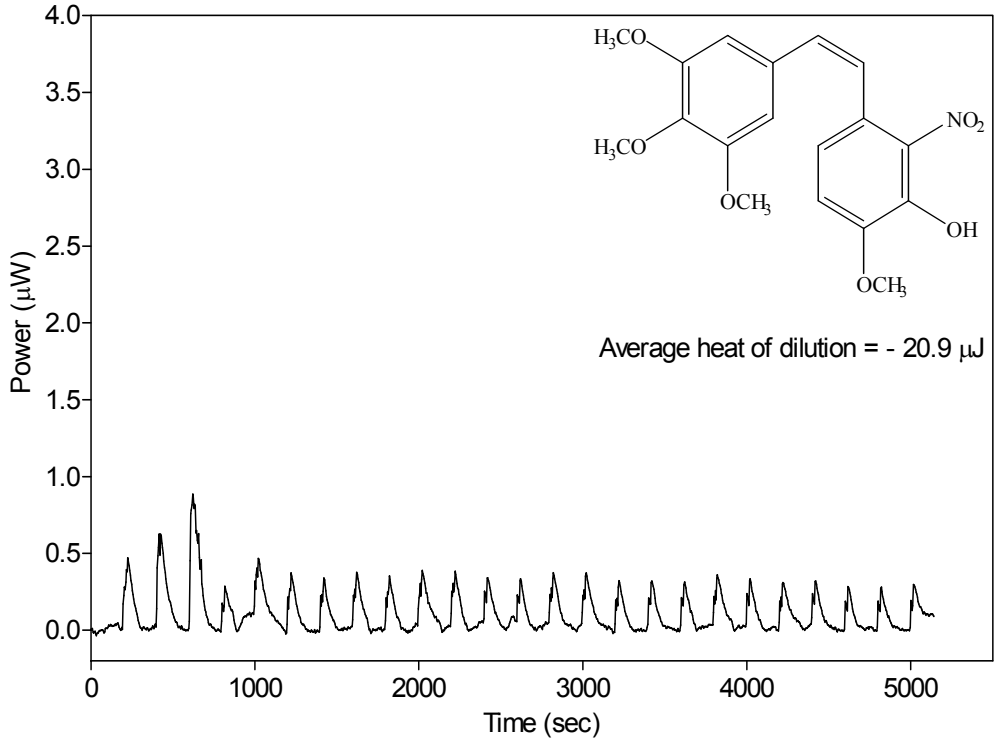

Figure B.3.7. ITC Blank Titration of Compound **30.**

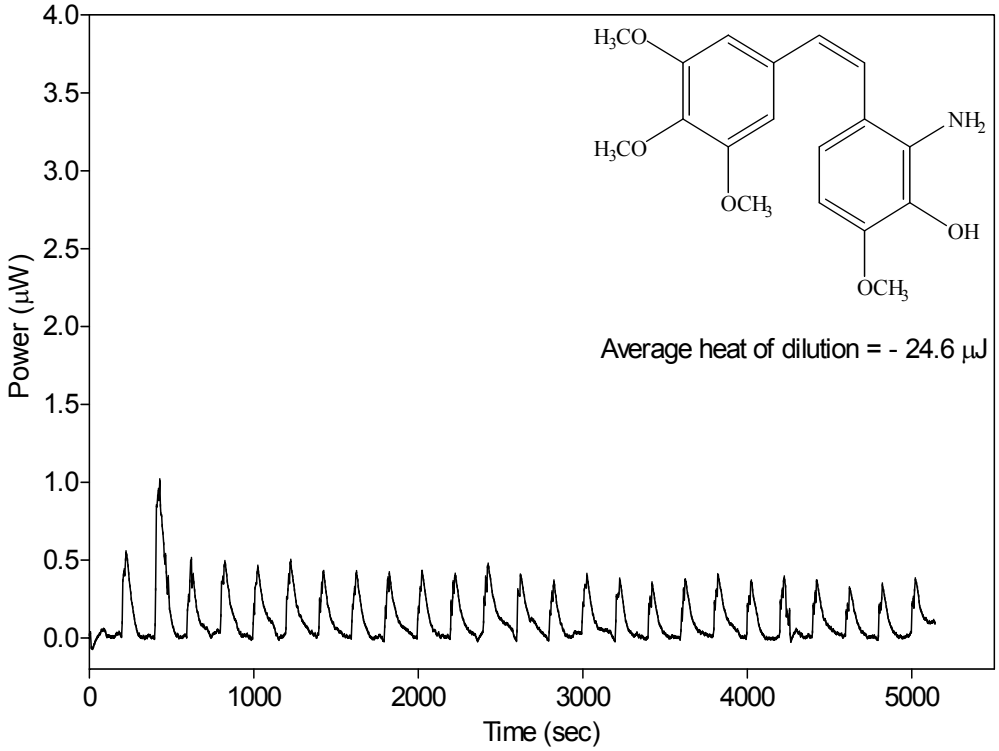

Figure B.3.8. ITC Blank Titration of Compound **39.**

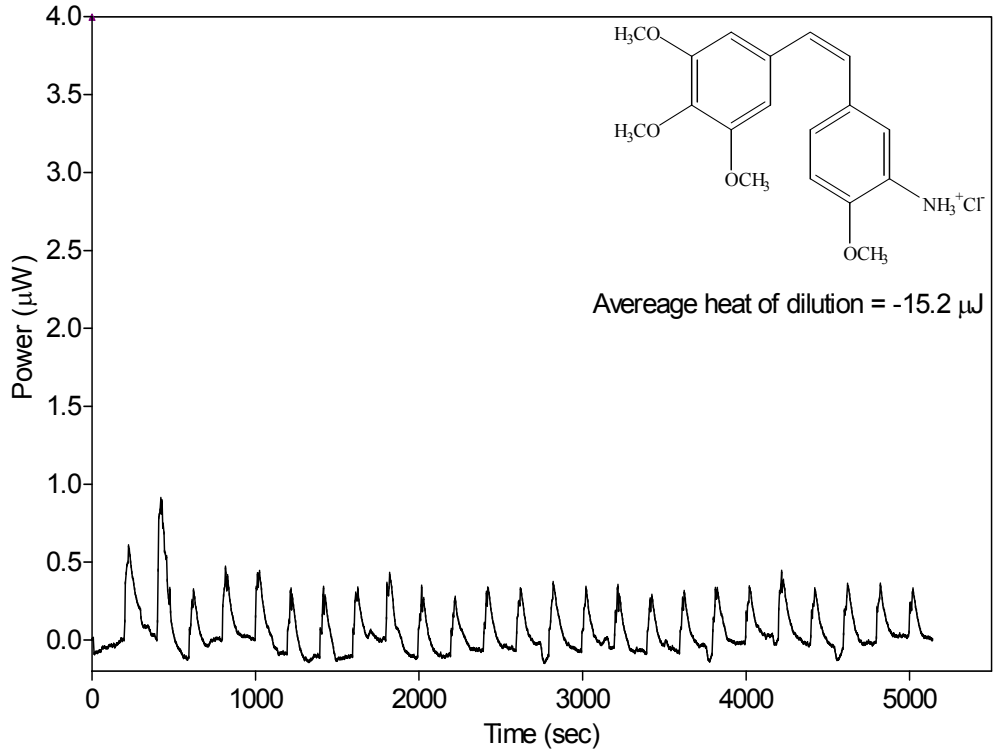

Figure B.3.9. ITC Blank Titration of Compound **45.**

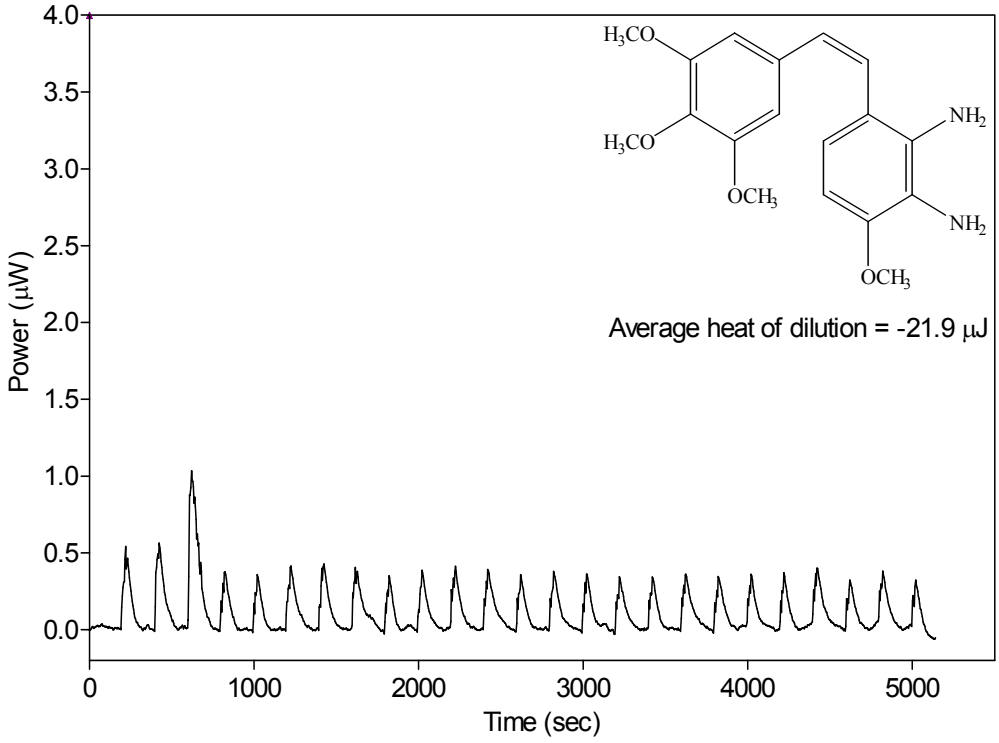

Figure B.3.10. ITC Blank Titration of Compound **56.**

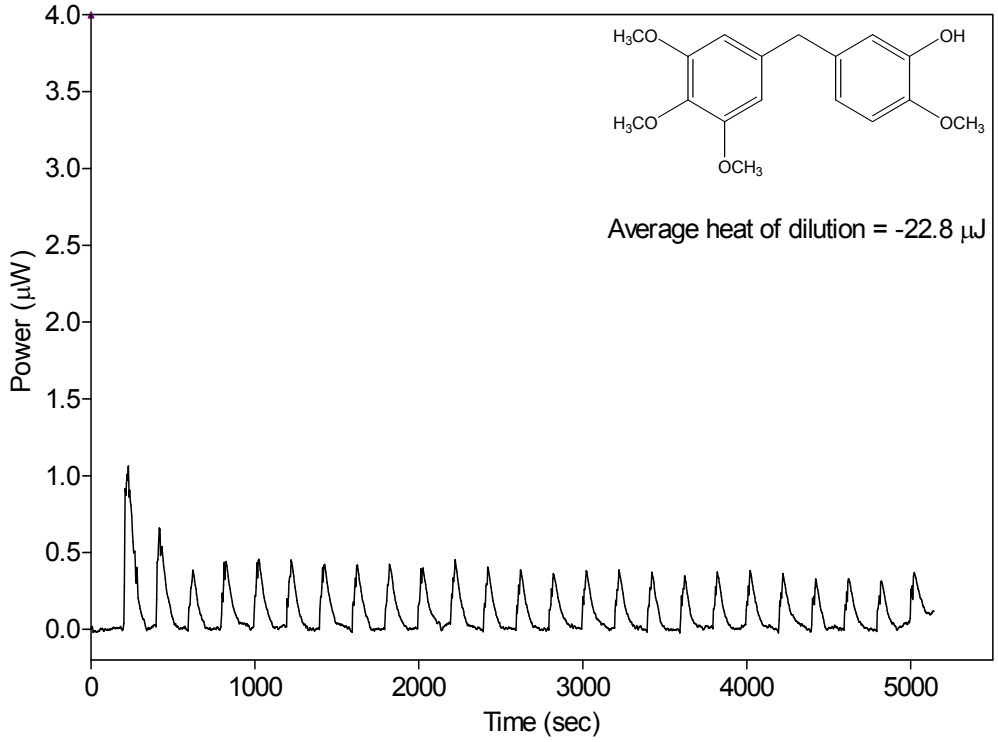

Figure B.3.11. ITC Blank Titration of Compound **70.**

REFERENCES

Ainsztein, A.M.; Purich, D.L. Stimulation of Tubulin Polymerization by MAP-2. *Journal of Biological Chemistry*, **1994**, 269, 28465-28471.

Aleksandrzak, K.; McGown, A.T.; Hadfield, J.A. Antitmitotic activity of diaryl compounds with structures resembling combretastatin A-4. *Anticancer Drugs*, **1998**, *9*, 545-550.

American Cancer Society. Cancer Statistics 2005. A presentation from the American Cancer Society, 2005. Data source from US Mortality Public Use Data Tape 2002, National center for Health Statistics, Center for Disease Control and Prevention, 2004, http://www.cancer.org.

Andrade, M.A.; Chacon, P.; Merelo, J.J.; Moran, F. Evaluation of secondary structure of proteins from UV circular dichroism spectra using an unsupervised learning neural network. *Protein Eng*. **1993**, *6*, 383–390.

Andreu, J.M.; Timasheff, S.N. Interaction of Tubulin with Single Ring Analogues of Tubulin. *Biochemistry*, **1982**, *21*, 534-543.

Andreu, J.M.; Gorbunoff, M.J.; Lee, J, C.; Timasheff, S.N. *Biochemistry*, **1984**, *23*, 1742-1752.

Andreu, J.M.; Timasheff, S.N. *Biochemistry*, **1982**, *21*, 6465-6476.

Arnaoutov, A.; Dasso, M. The Ran GTPase regulates kinetochore function. *Dev. Cell*, **2003**, *5*, 99-111

Atkins, P. Physical Chemistry, 6th ed. W.H. Freeman and Company, NewYork, **2000**.

Authorization to reproduce the X-ray crystal structure of tubulin was granted by Eva Nogales. Illustration was made using MDL Chime 2.6 SP6 program (Nogales *et al,* **1998**).

Bacher, G.; Beckers, T.; Emig, P.; Klenner, T.; Kutscher, B.; Nickel, B. New small molecule tubulin inhibitors. *Pure Appl. Chem.* **2001,** *73*, 1459-1464.

Baguley, B.C. Antivascular therapy of cancer: DMXAA. *Lancet Oncol.* **2003**, 4, 141-148.

Baguley, B.C.; Holaway, K.M.; Thomsen, L.L.; Zhuang, L.; Zwi, L.J. Inhibition of growth of colon 38 adenocarcinoma by vinblastine and colchicine: evidence for a vascular mechanism. *Eur. J. Cancer*, **1991**, *27*, 482-487.

Bai, R.; Pei, X.; Boye, O.; Getanunt, Z.; Grover. S. Identification of cysteine 354 of β-tubulin as part of the binding site of for the A ring of colchicine. *J. Biol. Chem*. **1996**, *271*,12639-12645.

Bai, R et al. Mapping the binding site of colchicinoids on β-tubulin. *J. Biol. Chem*. **2000**, *275*, 46443-46452.

Bai, R.; Pei, X.; Boye, O.; Getanunt, Z.; Grover. S. Identification of cysteine 354 of β-tubulin as part of the binding site of for the A ring of colchicine. *J. Biol. Chem*. **1996**, *271*, 12639-12645.

Banerjee, M.; Poddar, A.; Mitra, G.; Surolia, A.; Owa, T.; Bhattacharyya, B. Sulfonamide Drugs Binding to the Colchicine Site of Tubulin: Thermodynamic Analysis of the Drug-Tubulin Interactions by Isothermal Titration Calorimetry. *J. Med. Chem.* **2005**, *48*, 547-555.

Barbier, P.; Peyrot, V.; Dumortier, C.; D'Hoore, A.; Rener, G. A.; Engelborghs, Y. Kinetics of Association and Dissociation of Two Enantiomers, NSC 613863 (R)-(+) and NSC 613862 (S)-(-) (CI 980), to Tubulin. *Biochemistry,* **1996**, *35*, 2008-2015.

Blakey, D.C.; Westwood, F.R.; Warker, M.; et al. Antitumor activity of the novel vascular targeting agent ZD6126 in a panel of tumor models. *Clin. Cancer Res*. **2002**, *8*, 1974-1983.

Bokoch, G.M. Biology of the p21-activate kinases. *Annu. Rev. Biochem.* **2003**, *72*, 743-781.

Borisy, G.G.; Marcum, J.M.; Olmsted, J.B.; Murphy, D.B.; Johnson, K.A. Purification of tubulin and of high molecular weight proteinsfrom porcine brain and characterization of microtubule assembly i vitro. *Ann. NY Acad. Sci.* **1975**, *253*, 107-32.

Boyland E.; Boyland, M.E. Studies in tissue metabolism. IX. The action of colchicine and B.*typhosus* extract. Biochem. Journal, **1937**, *31*, 454-460.

Brewer, C.F.; Loike, J.D.; Horwitz, S.B.; Sternlicht, H.; Gensler, W.J. Conformational analysis of podophyllotoxin and its congeners. Structure-Activity Relationship in Microtubule Assembly. *J. Med.Chem*. **1979,** *22*, 215-221.

Caplow, M.; Ruhlen, R.L.; Shanks, J. The free energy of hydrolysis of a microtubule-bound nucleotide triphosphate is near zero: All the free energy is stored in the microtubule lattice. *J. Cell Biol.,* **1994**, *127*, 779-788.

Carlier, M.F. Control of actin dynamics. *Curr.Opin. Cell. Biol.,* **1998**, *10*, 45-51.

Chae, J, K.; Kim, I.; Lim, S.T.; Chung, M, J.; Kim, W.H.; Kim, H.G.; Ko, J, K.; Koh, G,Y. Coadministration of angiopoietin-1 and vascular endothelial growth factor enhances collateral vascularization. *Arterioscler. Thromb Vasc. Biol.* **2000**, *20* (12), 2573-2578.

Chakraborty, S.; Sarkar, N.; Bhattacharyya, B. Nucleotide-dependent bisANS binding to tubulin. *Biochim. Biophys. Acta.* **1999**, *1432*, 350–355.

Chaudhuri, A.R.; Seetharamalu, P.; Schwarz, P.M.; Hausheer,F.H.; Luduena, R. F. The interaction of the B-ring of Colchicine with α- Tubulin: A Novel Foot print Approach. *J. Mol. Biol*. **2000**, *303*, 679-692.

Chau, M.F.; Radeke, M.J.; de Ines, C.; Barasoain, I.; Kohlstaedt, L.A. *Biochemistry,* **1998**, *37*, 17692-703.

Chaudhuri, A.R.; Seetharamalu, P.; Schwarz, P.M.; Hausheer, F.H.; Luduena, R. F. The interaction of the B-ring of Colchicine with α- Tubulin: A Novel Foot print Approach. *J. Mol. Biol*. **2000**, *303*, 679-692.

Ching, L.M.; Joseph, W.R.; Crosier, K.E.; et al. Induction of tumor necrosis factor-α messenger RNA in human and murine cels by the flavone acetic analogue: 5,6, dimethylxanthenone-4-acetic acid (NSC64088). *Cancer Res*. **1994**, *54*, 870-872.

Ching, L.M.; Joseph, W.R.; Crosier, K.E.; et al. Induction of intratumoral tumor necrosis factor (TNF) synthesis and heamorrhagic necrosis by 5,6-dimethylxanthenone-4-acetic acid (DMXAA) in TNF knockout mice. *Cancer Res.* **1999**, *59*, 3304-3307.

Chretien, D.; Fuller, S.D.; Karsenti, E. Structure of growing microtubule ends. Two-dimensional sheets close into tubes at variable rates. *J. Cell. Biol*. **1995**, *129*, 1311-1328.

Cliff, M.J.; Gutierrez, A.; Ladbury, E.J. A survey of the year 2003 literature on applications of isothermal titration calorimetry. *J. Mol. Recognit.* **2004,** *17*, 513-523.

Cushman, M.; Nagarathnam D.; Gopal, H.M.; Chakraborti, A.K.; Lin C.M.; Hamel, E. Synthesis and Evaluation of Stilbene and Dihydrostilbene Derivatives as Potential Anticancer Agents that Inhibit Tubulin Polymerization. *J. Med. Chem.* **1991**, *34*, 2579-2588.

Cushman, M.; Nagarathnam, D.; Gopal, D.; He, H.M.; Lin, C.M.; Hamel, E. Synthesis and Evaluation of analogues of (Z)-1-(4-Methoxyphenyl)-2-(3,4,5-trimethoxyphenyl)-ethene as potential Cytotoxic and Antimitotic Agents. *J. Med. Chem.* **1992**, *35*, 2293-2306.

Daub, H.; Gevaert, K.; Vandekerekhove, J.; Sobel, A.; Hall, A. Rac/Cdc42 and p65PAK regulate the microtubule-destabilization protein stathmin through phosphorylation at serine 16. *J. Biol. Chem*. **2001**, *276*, 1677-1680.

David-Pfeuty, T.; Erickson, H.P.; Pantaloni, D. Guanosine triphosphatase activity of tubulin associated with microtubule assembly. *Proc. Natl. Acad. Sci. USA*, **1977**, *74*, 5372-5376.

Davis A.; Sage C.R.; Dougherty C.A.; Farrell K.W. Microtubule dynamics modulated by guanosine triphosphate hydrolysis activity of β-tubulin. *Science*, **1994**, *264*, 839-842.

Denekamp, J. Vasculature as a target for tumor therapy. *Prog. Appl. Microcirc.* **1984,** *4*, 28-38.

Denekamp, J. Angiogenesis, neovascular proliferation and vascular pathophysiology as targets for cancer therapy. *Br. J. Radiology*, **1993**, *66*, 181-196.

Denekamp, J.; Hill, S.A.; Hobson, B. Vascular occlusion and tumor cell death. *Eur. J. Cancer Clin. Oncl.* **1983**, *19***,** 271-175.

Desai, A.; Mitchison, T.J. Microtubule Polymerization Dynamics. *Annu. Rev.Cell Dev. Biol.* **1997***, 13*, 83-117.

De Tar, D.F. Suggested preliminary standards for calibration of optical rotatory dispersion and circular dichroism instruments. *Anal. Chem*. **1969**, *41*, 1406–8.

Diaz, J.F.; Andreu, J.M. *J. Biol. Chem.* **1991**, *266*, 2890 - 2896.

Downing, K.H. Structural Basis for the Interaction of Tubulin with Proteins and Drugs that affects Microtubule Dynamics. *Annu. Rev. Cell Dev. Biol.* **2000**, *16*, 89-11.

Doyle, M.L. Characterization of binding interactions by Isothermal Calorimetry. *Curr. Opin. Biotechnol*. **1997**, *8*, 31-35.

Drewes, G.; Ebneth, A.; Mandelkow, E.M. *Trends Biochem. Sci* **1998**, *23*, 307-311.

Dumortier, C.; Gorbunoff, M.J.; Andreu, J.M.; Engelborghs, Y. Alterations of Rings B and C of Colchicine are Cumulative in Overall Binding to Tubulin but Modify each Kinetic Step. *Biochemistry*, **1996**, *35*, 15900-15906.

Endo, A.; Nagashima, K.; Kurose, H.; Mochizuki, S.; Matsuda, M.; Mochizuki N. Sphinosine 1-phosphate induces membrane ruffling and increases motility of human umbilical vein endothelial cells via vascular endothelial growth factor receptor and CrkII. *J. Biol. Chem*. **2002**, *277* (26), 23747-54.

Erickson, H.P. Microtubule surface lattice and subunit structure and observations on reassembly. *J. Cell Biol.* **1974**, *60*, 153-167.

Ettienne-Manneville, S.; Hall, A. Rho GTPases in cell biology. *Nature* **2002**, *420*, 629-635.

Freire, E.; Mayorga, O.L.; Straume, M. Isothermal titration calorimetry. *Anal. Chem*. **1990**, *62*, 950A-959A.

Garland, D.L. *Biochemistry*, **1978**, *178*, 4266-4272.

Gaukroger K.; Hadfield A.J.; Lawrence, N.J.; Nolan, S.; McGown, A.T. Structural requirements for the interaction of combretastatins with tubulin: How important is the trimethoxy unit?. *Org. Biomol. Chem*., **2003,** *1*, 3033-3037.

Giannakakou, P.; Gussio R.; Nogales E.; Downing K.H.; Zaharevitz D. A common pharmacophore for epothilone and taxol: Molecular basis for the drug-resistance conferred by tubulin mutations in human cancer cells. *Proc. Natl. Acad. Sci*. **2000**, USA *97*, 2904-9.

Gupta, S.; Chakraborty, S.; Poddar, A.; Sarkar, N.; Das, K.P.; Bhattacharyya, B. BisANS Binding to Tubulin: Isothermal Titration Calorimetry and the Site-specific Proteolysis Reveal the GTP-induced Structural Stability of Tubulin. *Proteins:* **2003**, *50*, 283-289.

Gwaltney, S.L.; Imade, H.M.; Barr, K.J.; Qun, L.; Gehrke, L.; Credo, R.B., Warner, R.B.; Lee, J.Y.; Kovar, P.; Wang, J.; Nukkala, M.A.; Zielinski, N.A.; Frost, D.; Ng, S.; Sham, H.L. Novel sulfonate analogs of combretastatin A-4: potent anti-mitotic agents. *Bioorg. Med. Chem. Lett.* **2001**, *11*, 871-874.

Hahnfeldt, P.; Panigrahy, D.; Folkman, J., et al. Tumor development under angiogenic signaling: a dynamical theory of tumor growth, treatment response, and postvascular dormancy. *Cancer Res*. **1999**, *59*, 4770-4775.

Hamel E. Antimitotic natural products and their interactions with tubulin. *Med. Res. Rev*. **1996**, *16*, 207-31.

Hamel E. Interaction of tubulin with small ligands. In Microtubule proteins Avila J. Boca Raton: *CRC Press*, **1990**, 89-191.

Hamel. E.; Lin, C.M. Separation of active tubulin and Microtubule-Associated Proteins by ultracentrifugation and Isolation of a component causing the formation of Microtubule Bundles. *Biochemistry*, **1984**, *23*, 4173-4184.

Hamel, E.; Sackett, D.L.; Vourloumis, D.; Nicolaou, K.C. *Biochemistry,* **1999**, *38*, 5490-5498.

Harrisson, C. M. H.; Page, B. M.; Keir, H. M. *Nature,* **1976**, *260*, 470-476.

Hill, S.A.; Logernan, S.J.; Denekamp, J.; Chaplin D.J. Vinca alkaloids: anti-vascular effects in murine tumor. *Eur. J. Cancer.* **1993**, *9*, 1320-1324.

Hill, S.A.; Sampson, L.E.; Chaplin D.J. Anti-vascular approaches to solid tumor therapy: evaluation and vinblastine and flavone acetic acid. *Int. J. Cancer,* **1995**, *63*, 119-123.

Hill, S.A.; Williams, K.B.; Denekamp, J. Vascular collapse after flavone acetic acid: a possible mechanism of its anti-tumor action. *Eur. J. Cancer Clin. Oncol.* **1989**, *25*, 1419-1424.

Holdgate, G.A. Making cool drugs hot: isothermal titration calorimetry as binding energetics. *Biotechniques*, **2001**, *31*, 164-170.

Holwell, S. E.; Cooper, P. A.; Grosios, K.; Lippert, J. W.; Pettit, G. R.; Shnyder, S. D.; Bibby, M. C. Combretastatin A-1 phosphate a novel tubulin-binding agent with *in vivo* anti vascular effects in experimental tumours. *Anticancer Res*. **2002**, *22:* 707-711.

Honnappa, S.; Cutting, B.; Jahnke, W.; Seelig, J.; Steinmetz, M.O. Thermodynamics of the Op18/Stathmin-Tubulin Interaction. *J. Biol. Chem.,* **2003**, *278*, 38926-38934.

Hori, K.; Saito, S.; Nihei, Y.; Suzuki, M.; Sato, Y. Antitumor effects due to irreversible stoppage of tumor tissue blood flow: evaluation of a novel combretastatin A-4 derivative, AC7700. *Jpn. J. Cancer Res.* **1999**, *90*, 1026-1038.

Hori, K.; Saito, S.; Sato, Y. A novel combretastatin A-4 derivative, AC7700, strongly stanches tumor blood flow and inhibits growth of tumors developing in various tissues and organs. *Br. J. Cancer*, **2002**, *86*, 1604-1614.

Hori, K.; Saito, S.; Sato, Y.; Kubota, K. Stoppage of blood flow in 3-methylcholanthrene-induced primary tumor due to a novel combretastatin A-4 derivative, AC7700, and its antitumor effect. *Med. Sci. Monit.* **2001**, *7*, 26-33.

Howell, B.; Larsson, N.; Gullberg, M.; Cassimeris, L. *Mol. Biol. Cell,* **1999**, *10*, 105-18.

Hyams, J.S.; Lloyd, C.W. Microtubules, Wiley-Liss, New York.
Jayaram B. and Haley B. E. *J. Biol. Chem.* **1994**, *269*, 3233-3242.
John Wiley and Sons, Inc. 259-296.

Hyman, A.A.; Salser, S.; Drechsel, D.N.; Unwin, N.; Mitchison, T.J. Role of GTP hydrolysis in microtubule dynamics: information from a slowly hydrolysable analogue, GMPCPP. *Mol. Biol. Cell*, **1992**, *3*, 1155-1167.

Jordan, A.; Hadfield, A. J.; Lawrence, N.J.; McGown, A.T. Tubulin as a target for the anticancer drugs: Agents which interact with the mitotic spindle. John Wiley and Sons, Inc., **1998**, 259-296.

Jordan, M.A.; Leslie, W. Microtubules as a Target for Anticancer. *Nature Reviews / cancer*, **2004**, *4*, 253-266.

Kabsch, G.; Vandekerckhove, J. Structure and function of action. *Annu. Rev. Biophys. Biomol*.. **1992**, *21*, 49-76.

Kanthou, C.; Tozer, G.M. The tumor vascular targeting agent combretastatin A-4-phosphate induces reorganization of the actin cytoskeleton and early membrane blebbing in human endothelial cells. *Blood,* **2002**, *99*, 2060-2069.

Kanthou, C.; Greco, O.; Stratford, A.; Cook, I.; Knight, R.; Benzakour, O.; Tozer, G. The Tubulin-Binding Agent Combretastatin A-4-Phosphate arrests endothelial cells in Mitosis and induces mitotic cell death. *Journal of pathology*, **2004**, *165*, 1401-1411.

Koenigbauer, M.J. Pharmaceutical applications of microcalorimetry. *Pharm. Res.,* **1994**, *11*, 777-783.

Krishnamurthy, G.; Cheng, W.; Lo,M.; Aulabaugh, A.; Razinkov, V.; Ding, W.; Loganzo, F.; Zask, A.; Ellestad, G. Biophysical Characterization of the Interaction of HTI-286 with Tubulin Heterodimer and Microtubules. *Biochemistry*, **2003**, *42*, 13484-13495.

Kuntziger, T.; Gavet, O.; Manceau, V.; Sobel, A.; Bornens, M. Stathmin/Op18 phosphorylation is regulated by microtubules assembly. *Mol. Biol. Cell*, **2001**, *12*, 437-448.

Kuriyama, R.; Keryer, G.; Borisy, G.G. The mitotic spindle of Chinese hamster ovary cells isolated in taxol containing medium. *J. cell Sci.* **1984**, *66*, 265-76.

Lamberir, A.; Engelborghs, Y. *J. Biol. Chem*. **1981**, *256*, 3279-3282.

Laurine, E.; Lafitte, D.; Gregoire, C.; Seree, E.; Loret, E.; Douillard, S.; Michel, B.; Briand, C.; Verdier, J.M. Specific Binding of Dehydroepiandrosterone to the N Terminus of the Microtubule-associated Protein MAP2. *J. Biol. Chem.* **2003**, *278*, 29979-29986.

Lawler S. *Curr. Biol.* **1998**, *8*, 212-214.

Lin, C.M.; Singh, S.B.; Chu, P.S.; Dempsy, R.O.; Salmon, S.E.; Pettit, G.R. *Molecular Pharmacology,* **1988**, *34*, 200-208.

Little, M.; Seehaus, T. Comparative analysis of tubulin sequences. *Biochem. Physiol*. **1988**, *90B*, 655-670.

Lowe, J; Amos, L.A. Crystal structure of the bacterial cell-division protein FtsZ. *Nature*, **1998**, 203-206.

Ludford, R.J. Factors determining the action of colchicine on tumor growth. *Br. J. cancer*, **1948**, *2*, 75-86.

Luduena, R.F.; Roach, M.C. Tubulin sulfhydryl groups as probes and targets for antimitotic and antimicrobial agents. *Pharmac. Ther.* **1991**, *49*, 133-152.

MacNeal, R.K.; Purich, D.L. Stoichiometry and role of GTP hydrolysis in bovine neurotubule assembly. *J. Biol. Chem.* **1978**, *253*, 4683-4387.

Manavalan, P.; Johnson, W.C. *Anal. Biochem*. **1987**, *167*, 76 – 85.

Mandelkow, E.; Mandelkow, E-M. Microtubules and microtubules-associated proteins. Current Opinion in Cell Biology, **1995**, *7*, 72-81.

Mandelkow, E.M.; Schultheiss, R.; Rapp, R.; Mueller, M.; Mandelkow, E. On the surface lattice of microtubules: helix starts, protofilament number, seam and handedness. *J. Cell Biol*, **1986**, *102*, 1067-1073.

Manning, D. Evidence mounts to receptor-independent activation of heterotrimeric G proteins normally in vivo: positioning of the mitotic spindle in *C. elegans. Science STKE* pe35, **2003**.

Maucuer, A.; Moreau, J.;Mechali, J.; Sobel, A. A stathmin Gene family; phylogenetic conservation and developmental regulation in *Xenopus*. *J. Biol. Chem*., **1993**, *268*, 16420-16429.

McGown, A.T.; Fox, B.W. Structural and biochemical comparison of the anti-mitotic agents colchicine, combretastatin A-4 and amphethinile. *Anti-Cancer Drug Des*. **1989**, *3*, 249-254.

Menendez, M.; Laynez, Jose.; Medrano, J.; Andreu., J.M. A thermodynamic Study of the Interaction of Tubulin with Colchicine Site Ligands. *J. Biol. Chem.***1989**, *264*, 16367-16371.

Meniscus Educational Institute, Meniscus limited, granted the permission to download Figures from Horizons, V*ascular Targeting*, **2002,** Vol. *3*, No. 2 *http://www.meniscus.com/horizons/* .

Mickey, B.; Howard, J. Rigidity of microtubules is increased by stabilizing agents. *J. Cell Biol.,* **1995**, *130*, 909-917.

MicroCal^{TM} . Isothermal Titration Calorimetry and Drug Design. ITC Application note. Ultrasensitive Calorimetry for the life sciences, **2003**, 1 -3.

Modlich, U.; Pugh, C.W.; Bicknell, R. Increasing endothelial cell specific expression by the use of heterologous hypoxic and cytokine-inducible enhancers. *Gene Ther*., **2000**, *7*, 896-902.

Monk, A.K.; Rogelio, E.S.; Mallinath, B.H.; Mugabe, B.E.; Ackley, F.; Studerus, S.W; Edvardsen, K.; Trawick, L.M.; Garner, M.C.; Rhodes, M.R.; Pettit, G.R.; Pinney, K.G. Design, Synthesis, and Biological Evaluation of Combretastatin Nitrogen Containing Derivatives as Inhibitors of Tubulin Assembly and Vascular Disrupting Agents, **2005**. (Manuscript in Press).

Mugabe, B. E.; Rogelio, S.; Monk, A.K.; Mallinath, B.H.; Wehbe, H.; Trawick, L.M.; Garner, M.C.; Pinney, K.G. Application of Isothermal Titration Calorimetry in Thermodynamic Studies on the Binding of Combretastatin A-1 and A-4 Analogs to Tubulin, **2005.** (Manuscript in Press).

National Center for Bioctechnology Information; National Library of Medicine, National Institutes of Health. http://www.ncbi.nlm.nih.gov.

Nezami, A.; Kimura, T.; Hidaka, K.; Kiso, A., Liu, J.; Kiso,Y.; Goldberg, D.E.; Freire, E. High-affinity inhibition of a family of *Plasmodium falciparum* protease by a designed adaptive inhibitor. *Biochemistry,* **2003**, *42*, 8459-8464.

Nezami, A.; Luque, I.; Kimura, T.; Kiso, Y.; Freire, E. Identification and Characterization of allophenylnorstatime-based inhibitors of plasmepsin II, and malarial target. *Biochemistry,* **2002**, *41*, 2273-2280.

Nihei, Y.; Suzuki, M.; Okano, A.; Tsuji, T.; Akiyama, Y.; Tsuruo, T.; Saito, S.; Hori, K.; Sato, Y. Evaluation of Antivascular and Antimitotic Effects of Tubulin Binding Agents in Solid Tumor Therapy. *Jpn.. J. Cancer. Res.* **1999**, *90*, 1387-1395.

Nogales, E. Structural Insights into Microtubule Function. *Annu. Rev.* **2000**, *69*, 277-302.

Nogales, E.; Whittaker, M.; Milligan, R.A.; Downing, K.H. High-resolution model of the microtubule. *Cell*, **1999**, *96*, 79-88.

Nogales, E.; Wolf, G.S.; Downing ,K.H. Structure of the αβ tubulins dimmer by electron crystallography. *Nature,* **1998**, *391*, 199-203.

Ohtaka, H.; Schön, A.; Freire, E. Multidrug resistance to HIV-1 protease inhibition requires cooperative coupling between distal mutations. *Biochemistry,* **2003**, *42*, 13659-13666.

Ohtaka, H.; Velazquez-Campoy, A.; Xie, D.; Freire, E. Overcoming drug resistance in HIV-1 chemotherapy: The binding thermodynamics of amprenavir and TMC-126 to wild-type and drug-resistant mutants of the HIV-1 protease. *Protein Sci*. **2002**, *11*, 1908-1916.

Ohsumi, K.; Nakagawa, R.; Fuduka, Y.; Hatanaka, T.; Morinaga, Y.; Nihei, Y.; Ohishi, K.; Sua, Y.; Akiyama, Y.; Tsuji, T. Novel combretastatin analogues effective against murine solid tumors, design and structure-activity relationships. *J. Med. Chem*. **1998**, *41*, 3022-3032.

Olmsted, J. B.; Borisy, G.G. Microtubules. *Ann. Rev. Biochem,* **1973**, *42***,** 507-40.

Owa, T.; Okauchi,T.; Yoshimatsu, K.; Sugi, N.H.; Ozawa, Y.; Nagasu, T.; Koyanagi, N.; Okabe, T.; Kitoh, K.; Yoshino, H. A focused compound library of novel *N*-(7-indolyl)benzenesulfonamides for the discovery of potent cell cycle inhibitors. *Bioorg. Med. Chem. Lett.,* **2000**, *10,* 1223-1226.

Owa, T.; Yokoi, A.; Yamazaki, K.; Yoshimatsu, K.; Yamori, T.; Nagasu, T. Array-based structure and gene expression relationship study of antitumor sulfonamides including N-[2-[(4-hydroxyphenyl)amino]-3-pyridinyl]-4-methoxybenzenesulfonamide and N-(3-chloro-7-indolyl)-1,4-benzenedisulfonamide. *J. Med. Chem.,* **2002**, *45*, 4913-4922.

Owa, T.; Yoshino, H.; Okauchi, T.; Yoshimatsu, K.; Ozawa, Y.; Sugi, N.H.; Nagasu, T.; Koyanagi, N.; Kitoh, K. Discovery of novel antitumor sulfonamides targeting G1 phase of the cell cycle. *J. Med. Chem.,* **1999**, *42*, 3789-3799.

Pal, D.; Mahapatra, P.; Manna, T.; Chakrabarti, P.; Bhattacharyya, Banerjee, A.; Basu, G.; Roy, S. Conformational Properties of α-Tubulin Tail Peptide: Implications for Tail-Body Interaction. *Biochemistry*, **2001**, *40*, 15512-15519.

Perez-Ramirez, B.; Andreu , M.J.; Gorbunoff J.M.; Timasheff, S.N. Stoichiometric and Substoichiometric Inhibition of Tubulin Self-Assembly by Colchicine Analogues. *Biochemistry,* **1996**, *35*, 3277-3285.

Perez-Ramirez, B.; Shearwin, K.E.; Timasheff, S.N. The Colchicine-Induced GTPase Activity of Tubulin: State of the Product. Activation by Microtubule-Promoting Cosolvents. *Biochemistry,* **1994**, *33*, 6253-6261.

Perczel, A.; Hollosi, M.; Tusnady, G.; Fasman, G D. Convex constraint analysis: a natural deconvolution of circular dichroism curves of proteins. *Protein Eng*. **1991**, *4*, 669 – 679.

Pettit, G.R.; Singh, S.B. Isolation, structure and synthesis of combretastatins A-2, A-3, and B-2. *Can. J. Chem.* **1987**, *65*, 2390-2396.

Pettit, G.R.; Singh, S.B.; Hamel, L.; Lin, C.M.; Alberts, D.S.; Garcia-Kendall, D. Isolation and structure of the strong cell growth and tubulin inhibitor combretastatin A-4. *Experientia*, **1989**, *45*, 209-211.

Pettit, G.R.; Singh, S.B.; Hamel, L.; Lin, C.M.; Alberts, D.S.; Garcia-Kendall, D. Antineoplastic agents 322. Synthesis of combretastaatin A-4 prodrugs. *Anticancer drug design.* **1995**, *10*, 299-309.

Pettit, G.R.; Toki, B.; Herald, D.L.; et al. Antineoplastic agents. 379. Synthesis of phenstatin phosphate. *J. Med. Chem*. **1998**, *41*, 1688-1695.

Philpott, M.; Baguley, B.C.; Ching L.M. Induction of tumor necrosis factor-α by single and repeated doses of the antitumor agent 5,6-dimethylxanthenone-4-acetic acid. *Cancer Chemother. Pharmacol*. **1995**, *36*, 143-148.

Pinney, K.G.; Bounds, A.D.; Dingerman, K.M.; Mocharla., V.P.; Pettit, G.R.; Bai R.; Hamel, E. *Bioorg. Med Chem. Lett.* **1999**, *9*, 1081.

Pinney, K.G; Mejia, M.P.; Villalobos, V.M.; Rosenquist, B.E.; Pettit, G.R.; Verdier-Pinard, P.; Hamel, E. Synthesis and Biological Evaluation of Aryl Azide Derivatives of Combretastatin A-4 as Molecular Probes for Tubulin. *Bioorg. Med. Chem*. **2000**, *8*, 2417-2425.

Raftopoulou, M.; Hall, A. Cell migration: Rho GTPases lead the way. *Dev. Biol*. **2004**, *265*, 23-32.

Ravelli, B.G.; Gigant, B.; Curmi, P.A.; Jourdain, I.; Lachkar, S.; Sobel, A.; Knossow, M. Insight into tubulin regulation from a complex with colchicines and a stathmin-like domain. *Nature*, **2004**, *428*, 198-202.

Remedios dos,C.G.; Chhabra, D.; Kekic, M.; Desova, I.V.; Tsubakihara, M.; Berry, D.A.; Nosworthy, N.J. Actin binding proteins: regulation of cytoskeletal microfilaments. *Physiol. Rev*., **2003**, *83*, 433-473

Rithner, C.D.; Bushweller, C.H.; Gensler, W.J.; Hoogasian, S. Dynamic Nuclear magnetic Resonance and Emperical Force Field Studies of podophyllotoxin. *J. Org. Chem.* **1983**, *48*, 1491-1495.

Rogelio, E,S.; Mallinath, B.H.; Monk, A.K.; Mugabe, B.E.; Ackley, F.; Edvardsen, K.; Trawick, L.M.; Garner, M.C.; Pinney, K.G. Design, Synthesis and Biological Evaluation of Nitrogen Substituted CA-1 Stilbene Analogues as Potential Vascular Targeting Agents, **2005**. (Manuscript in Press).

Sackett, D.L. Podophyllotoxin, steganicin and combretastatin: natural products that bind at the colchicine site of tubulin. *Pharmacol*. *Ther.* **1993**, *59*, 163-228.

Sherline, P.; Schiavone, K. Immunofluorescence localization of proteins of high molecular weight along intracellular microtubules. *Science*, **1977**, *198*:1038-40.

Schön, A.; Ingaramo, M.M.; Freire, E. The binding of HIV-1 protease inhibitors to human serum proteins. *Biophys. Chem.* **2003**, *105*, 221-230.

Schweigerer L. Antiangiogenesis as a novel therapeutic concept in pediatric oncology. *J. Mol. Med.* **1995**, *73*, 497-508.

Seed, L.; Slaughter, D.P.; Limarzi, L.R. Effect of colchicine on human carcinoma. Surgery, **1940**, *7*, 696-709.

Siemann, D.W. Vascular Targeting Agents. *Horizons in Cancer Therapeutics:* From bench to Bedside, **2002**, Vol. *3*, No 2, 4-15. Dr. Siemann grated me the permission to reproduce figure 2.17.

Siemann, D.W.; Rojiani, A.M. Enhancement of radiation therapy by the novel vascular targeting agent ZD6126. *Int. L .Radiat. Oncol. Biol. Phys.* **2002**, *53*, 164-171.

Sloboda, R.D.; Rudolph, S.A.; Rosenbaum, J.L.; Greengard, P. Cyclic AMP-dependent endogenous phosphorylation of a microtubule associated protein. *Proc. Natl. Acad. Sci. USA,* **1975**, *72*, 177-81.

Smith, G.P.; Calveley, S.B.; Smith, M.J.; Baguley, B.C. Flavone acetic acid (NSC 347512) induces haemorrhagic necrosis of mouse colon 26 and 38 tumors. *Eur. J. Cancer Clin. Oncol.* **1987**, *23*, 1209-1211.

Spiegelman, B.M.; Penningroth, S.M.; Kirschner, M.W. Turnover of tubulin and the N-site GTP in Chinese hamster ovary cells. *Cell*, **1977**, *12*, 587-600.

Starnes, C.O. Coley's toxins in perspective. *Nature*, **1992**, *357*, 11-12.

Suprenant, K.A.; Dentler, W.L. Association between endocrine pancreatic secretory granules and in vitro assembled microtubules is dependent upon microtubule associated proteins. *J. Cell. Biol*. **1982**, *93*, 164-74.

Takashi, R.; Tonomura, Y.; Morales M.F. 4,4'-Bis (1-anilinonaphthalene 8-sulfonate) (bis-ANS): a new probe of the active site of myosin. *Proc Natl AcadSci USA*; **1977**, *74*, 2334-2338.

Tannock, I.F. Population kinetics of carcinoma cells, capillary endothelial cells, and fibroblasts in a transplanted mouse mammary tumor. *Cancer Res*. **1970**, *30*, 2470-2477.

Thorpe, P.E. Vascular Targeting Agents as Cancer Therapeutics. *Clinical Cancer Research,* **2004**, *10*, 415-427.

Tomioka, K.; Ishiguro,T.; Mizuguchi, H.; Komeshima, N.; Koga, K.; Tsukagoshi, S.; Tsuruo, T.; Tanida, S.; Kishi,T. Stereoselective reactions. XVII. Absolute structure-cytotoxic activity relationships of steganacin congeners and analogs. *J. Med. Chem*. **1991**, *34*, 54-57.

Tozer, G.M.; Kanthou, C.; Baguley, B.C. Disrupting tumor blood vessels. *Nat. Rev. Cancer*, **2005**, *5*, 423-435.

Tozer, G.M.; Prise, V.E.; Wilson, J. Mechanisms associated with tumor vascular shut-down induced by combretastatin A-4 phosphate: Intravital microscopy and measurement of vascular permeability. *Cancer Res*. **2001**, *61*, 6413-6422.

Tozer, G.M.; Kanthou, C.; Parkins, C, S.; Hill, S.A. The biology of the combretastatins as tumor vascular targeting agents. *International Journal of Experimental Pathology*, **2002**, *83*, 21-38.

Tozer, G.M.; Bicknell, R. Therapeutic Targeting of the Tumor Vasculature. *Seminars in Radiation Oncology*, **2004**, *14*, 222-232.

Tran, P.T.; Joshi, P.; Salmon, E.D. How tubulin subunits are lost from the shortening end of microtubules. *J. Struct. Biol.* **1997**, In press.

Trepel, M.; Grifman, M.; Weitzmanm M.D., *et al*. Molecular adaptors for vascular-targeted adenoviral gene delivery. *Hum. Gene. Ther.* **2000**, *11*, 1971-1981.

Trepel, M.; Arap, W.; Pasqualini R. Exploring vascular heterogeneity for gene therapy targeting. *Gene Ther*. **2000**, *7*, 2059-2060.

Uppuluri S.; Knipling L.; Sackett D.L; Wolff J. *Proc Natl Acad Sci USA*, **1993**, *90*, 11598-11602.

Vaillant, A.R.; Muller R.; Langkopf, A.; Brown D.L. Characterization of the Microtubule-binding Domain of Microtubule-associated Protein 1A and its effects on Microtubule Dynamics. *Journal of Biological Chemistry*, **1998**, *273*, 13973-13981.

Veenendaal, L.M.; Jin, H.; Ran, S.; *et al*. P*roc. Natl. Acad. Sci.* **2002**, *99*, 7866-7871.

Velazquez-Campoy, A.; Kiso, Y.; Freire, E. The binding energetic of first- and second-generation HIV-1 protease inhibitors: Implications for drug design. *Arch. Biochem. Biophys.* **2001**, *390*, 169-175.

Velazquez-Campoy, A.; Vega, S.; Freire, E. Amplification of the effects of drug resistance mutations by background polymorphisms in HIV-1 protease from African subtypes. *Biochemistry,* **2002**, *41*, 8613-8619.

Velazquez-Campoy, A.; Todd, M.J.; Freire, E. HIV-1 protease inhibitors: Enthalpic versus entropic optimization of the binding affinity. *Biochemistry,* **2000**, *39*, 2201-2207.

Velazquez-Campoy, A.; Vega, S.; Freire, E. Amplification of the effects of drug resistance mutations by background polymorphisms in HIV-1 protease from African subtypes. *Biochemistry*, **2002**, *41*, 8613-8619.

Verdier-Pinard, P.; Lai,J.-Y.; Yoo, H.-D.; Yu, J.; Marquez, B.; Nagle, D.G.; Nambu, M.; White, J.D.; Falck, J. R.; Gerwick, W.H.; Day, B.W.; Hamel, E. Structure-Activity Analysis of the Interaction of Curacin A, the Potent Colchicine Site Antimitotic Agent, with Tubulin and Effects of Analogs on the Growth of MCF-7 Breast Cancer Cells. *Mol. Pharmacol*. **1998**, *53*: 62-76.

Verin, A.D. et al. Microtubule disassembly increases endothelial cell barrier dysfunction: role of MLC phosphorylation. *Am. J. Physiol. Lung Cell. Mol. Physiol.* **2001**, *281*, L565-L574.

Voet, D.; Voet G.J. Biochemistry. Second edition, John Wiley and Sons, Inc. **1995**, 1274 -1276.

Von Angerer, E. Current Opinion in Drug Discovery and Development, **2000**, *3*, 575-584.

Walczak, C.E.; Mitchison T.J.; Desai, A. *Cell*, **1996**, *84*, 37-47.

Walker, R.A.; O'Brien, E.T.; Pryer, N.K.; Soboeiro, M.F.; Voter, W.A.; Erickson, H.P. Salmon, E.D. Dynamic instability of individual microtubules analyzed by video light microscopy: rate constants and transition frequencies. J. *Cell. Biol*., **1988**, 1437-1448.

Wang, L.; Woods, K.W.; Li,Q.; Barr, K.J.; McCroskey, R.W.; Hannick, S.M.; Gherke, L.; Credo, B.R.; Hui, Y.; Marsh, K.; Warner R.; Lee, J.Y.; Zielinski-Mozng, N.; Frost, D.; Rosenberg, S.H.; Sham, H.L. *J. Med. Chem.* **2002**, *45*, 1697-1711.

Ward, W.H.J.; Holdgate, G.A. (2001). Isothermal titration calorimetry in drug discovery. *Prog. Med.* ***Chem***. **38**, 309-376.

Weingarten, M.; Lockwood, A.; Hwo, S.; Kirschner, M. A protein factor essential for microtubule assembly. *Proc. Natl. acad. Sci. USA,* **1975**, *72*, 1858-1862.

Weis, K. *Curr. Opin. Cell Biol*. **2002**, *14*, 328-335.

Wilson, L.; Bamburg, J,R.; Mizel, S.B.; Grisham, L.M.; Creswell, K.M. Interaction of drugs with microtubule proteins. *Fed.Proc*.**1974**, *33*, 158-166.

Wilson, L.; Bryan, J. *Adv. Cell. Mol. Biol*. **1974**, *3*, 21-72.

Wilson.L ; Jordan M.A. Microtubule dynamics: Taking aim at a moving target. *Chem. Biol*. **1995**, *2*, 569 – 573.

Wiseman, T.; Williston, S.; Brandts, J.F.; Lin, L.N. Rapid measurement of binding constants and heats of binding using a new titration calorimeter. *Anal. Biochem*. **1989**, *179*, 131-137.

Woglum, W.H. A critic of tumor resistance. *J. Cancer Res*. **1923**, *7*, 283-311.

Woods, J.A.; Hadfield, J.A.; Pettit, G.R.; Fox, B.W.; McGown, A.T. The interaction with tubulin of a series of stilbenes based on combretastatin A-4. *Br. J. Cancer*, **1995**, *71*, 705-711.

Yamaguchi, R.; Newport, J. *Cell,* **2003**, *113*, 115-125.

Yang, J.T.; Chuen, C.W.; Martinez, H. M. Calculation of protein conformation from circular dichroism. *Methods Enzymol*. **1986**, *130*, 208-269.

Ye, L.H et al. Myosin Light Chain-kinase of smooth muscle stimulates myosin ATPase activity without phosphorylating myosin light chain. *Proc. Natl. Acad. Sci. USA*, **1999**, *96*, 6666-6671.

Zavala, F.; Guenard D.; Robin J. P.; Brown E. *J. Med. Chem*., **1980**, *23*, 546-549.

Zheng, Y. G-Protein Control of Microtubule Assembly. *Annu. Rev. Cell Dev. Biol,* **2005**, *20*, 867-94. Granted permission to reproduce figures 2.3 and 2.4.

Zwi, L.J.; Baguley, B.C.; Gavin, J.B.; Wilson, W.R. *J. Natl. Cancer Inst.* **1989**, *81*, 1005-1013.